Final Report

DSE 2: SPEAR

Delft University of Technology

TU Delft

Final Report

by

DSE 2: SPEAR

Patrick N. Albert	*4833295*
Stijn L.J. de Vries	*4558081*
David A. Hartong	*4771117*
Job P.Q. Hoyng	*4664299*
Alexander A.C. van den Heiligenberg	*4805798*
Jesse J.A. van der Toorn	*4846648*
Wieger R. Verbeek	*4675150*

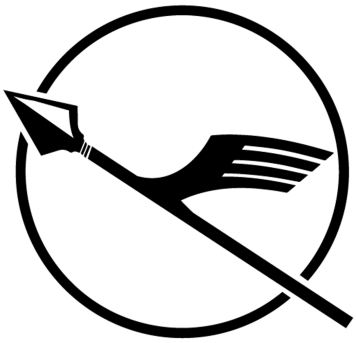

SPEAR

Sailplane Pioneering Emission-free Aerial Recreation

In partial fulfillment of the requirements for the degree of

Bachelor of Science
Faculty of Aerospace Engineering

Date of Submission

25 January 2022

Tutors: Ir. M.J. Schuurman
Ir. J.A. Melkert
J.A.P. Leijtens
M.M. Doole

TU Delft Delft University of Technology

Preface

This report was written by seven BSc Aerospace Engineering students for their Design Synthesis Exercise (DSE), the concluding project of the bachelor program. Assigned as Group 2, the team was tasked to conceptualize a design for a sailplane capable of taking off and landing on water for Trans Maldivian Airways (TMA) in the Maldives.

It is assumed the reader has a basic understanding of aerospace engineering, project management, and systems engineering. Terms that lie outside of this scope are clarified in the text.

We would like to thank our tutors, Ir. M. J. Schuurman, Ir. J. A. Melkert, J. A. P. Leijtens, and M. M. Doole, as well as our TA, L. Motinelli, for their fantastic feedback and assistance.

Delft, 25 January 2021
P. N. Albert, S. L. J. de Vries, D. A. Hartong, J. P. Q. Hoyng,
A. A. C. van den Heiligenberg, J. J. A. van der Toorn, W. R. Verbeek

Summary

"We cannot wait for speeches, when the sea is rising around us all the time" is what Simon Kofe (Foreign Minister of Tuvalu, a small island nation in the Pacific) stated at the recent United Nations Climate Change Conference in Glasgow.[1] Immediate action and innovation in reducing the global carbon footprint is required such that small island nations do not drown. The Maldives, like Tuvalu, is an island nation that is equally on the front line in threat of rising sea levels due to climate change.

Given this imminent crisis, Trans Maldivian Airways (TMA) has sought to invest in sustainable ecotourism, with the potential introduction of an emission free sailplane to their fleet. TMA has tasked the team of seven engineers listed as authors of this report to conceptualize the design of an emission-free sailplane capable of take-off and landing on water.

Following a market analysis it was realized that there is an opening for a water sailplane that provides short flights for sight-seeing in high-end tourist destinations nearby bodies of water. Competition for such a service exists in the form of a regular aircraft, helicopter, and sailboat. In the Maldives specifically, there was an estimated market size of $46.75\,\$$ million based on the service obtainable market. In agreement with the client, this was thus determined to be the use case of the aircraft.

Having determined a definitive use case the most feasible design options were considered for five subsystems of the aircraft: the wing configuration, empennage configuration, flotation device, air propulsion, and water propulsion. Following a trade-off of the subsystems concerning safety, performance, maintainability, and autonomy a preliminary concept was concluded. This was a water sailplane with a high wing, T-tail, floats, on-board air propulsion, and no water propulsion. The concept was designed in detail in the final design phase.

During the final design phase the aircraft fuselage was determined to have the same tadpole shape that conventional sailplanes make use of for aerodynamic purposes. Accommodating a pilot in the front and two passengers in the back it has a maximum width of $1.26\,\mathrm{m}$, height of $1.38\,\mathrm{m}$ and length of $10.5\,\mathrm{m}$. The wing made use of a FX 62-K-153/20 airfoil for its desirable C_L and good performance with contamination by water. The final wing design made use of a Schuemann wing planform with a surface area of $23.7\,\mathrm{m}^2$ and span of $24.5\,\mathrm{m}$. Off-the-shelf components were used for the propulsion system, with the REB-90 electric motor used, and a lithium polymer battery pack due to its shapeability. Both components were developed by MGM COMPRO. E-glass was used for the majority of the aircraft structure, with structures that required local stiffening making use of carbon fiber. A render of the final design is visible in Figure 1:

[1] https://www.oxfamamerica.org/explore/stories/four-powerful-quotes-from-cop26/ [Accessed: 18 Jan 2022]

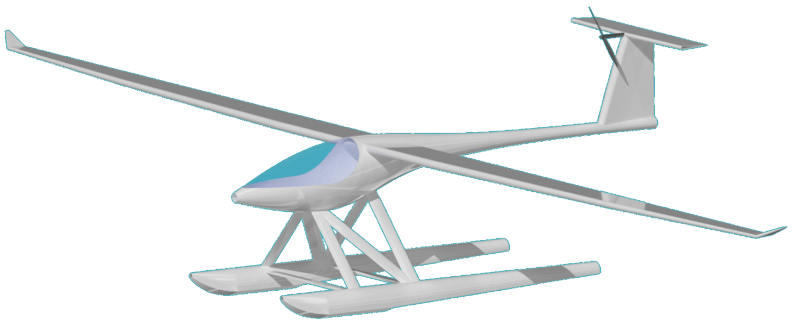

Figure 1: CATIA render of the final design

In the final iteration of the aircraft design it was determined to have a maximum take-off weight (MTOW) of $1071\,\mathrm{kg}$. Key performance characteristics of the aircraft were its lift-to-drag ratio, rate of descent, climb rate, stall speed, and cruise speed. They are summarized in Table 1:

Table 1: Key performance characterstics

Performance characteristic	Value	Unit
Lift-to-drag ratio	34.75	–
Descent rate	0.8	m/s
Climb rate	4	m/s
Stall speed	72	km/hr
Cruise speed	97.2	km/hr

To verify the robustness of the conceptual design a sensitivity test was performed. With this analysis the sensitivity of the design to a number of parameters was tested, and determined whether requirements are still met within a satisfactory margin. Four parameters were tested for their sensitivity: the stall speed, take-off distance, minimum descent rate, and total energy required for the propulsion unit. Each was investigated with respect to uncertainty in the MTOW, an underestimation of the drag, an overestimation of the lift, and energy density overestimation of the batteries. Of all tests the sensitivity of the take-off distance and total energy required was most sensitive to a the uncertainty of the MTOW, with a $32.9\,\%$ and $19.4\,\%$ increase to a $15\,\%$ increase in MTOW. However in general, the sensitivity analysis showed that the four parameters remained within the margin that was budgeted.

In a financial analysis it was determined the cost per aircraft was $414\,419\,\$$, given that 60 aircraft could be produced over 5 years. Operational costs were also estimated to be $41\,493\,\$$ annually. While this may appear as a low value, it was based on Maldivian wages for maintenance and crew personnel and that the aircraft makes only 274 flight hours annually.

Sustainability was a key aspect during the conceptual design of the aircraft. While the aircraft produces no emissions during operation - as the propulsion system is electric - there remain gray emissions from the electricity production. For the Maldives this is particularly the case since they rely heavily on imported oil for energy production, although have begun an energy transition to more sustainable sources such as solar and tidal since the 2004 Indian Ocean tsunami.[2] With a life cycle analysis of the aircraft's structural components the recycling of the materials used was investigated.

[2]https://www.adb.org/sites/default/files/publication/654021/renewables-roadmap-energy-sector-maldives.pdf [Accessed: 24 Jan 2022]

Nomenclature

Abbreviations

AHP	Analytic Hierarchy Process
APE	Absolute Percentage Error
BLDC	Brushless Direct Current
C.G.	Centre of Gravity
CAA	Civil Aviation Authority
CB	Center of Buoyancy
CER	Cost Estimation Relationship
CFD	Computational Fluid Dynamics
COVID-19	Coronavirus Disease 2019
CS	Certification Specification
DAPCA	Development and Procurement Costs of Aircraft
DSE	Design Synthesis Exercise
EASA	European Aviation Safety Agency
EV	Electric Vehicle
EW	Empty Weight
FAA	Federal Aviation Administration
FBD	Free Body Diagram
FBS	Functional Breakdown Structure
FEM	Finite Element Method
FFD	Functional Flow Diagram
FFF	Fused Filament Fabrication
FL	Flight Level
IM	Intermediate Modulus
ISA	International Standard Atmosphere
LCC	Life Cycle Cost
MAC	Mean Aerodynamic Chord
MC	Metacenter
MNS	Mission Need Statement
MTOW	Maximum Take-Off Weight
OEW	Operational Empty Weight
PD&D	Project Design & Development Logic
PESTELE	Political, Economical, Social, Technological, Environmental, Legal, and Ethical
POS	Project Objective Statement
PRSU	Propeller Speed Reduction Unit
RAMS	Reliability, Availability, Maintainability and Safety
RCM	Requirement Compliance Matrix
RPM	Rotations Per Minute
RPS	Rotations Per Second
SAM	Serviceable Available Market
SDG	United Nations Sustainable Development Goal
SDIN	Small Developing Island Nations
SM	Stability Margin
SMART	Specific, Measurable, Attainable, Realistic, Time-bound
SOM	Serviceable Obtainable Market
STOL	Short Take-Off and Landing
SWOT	Strength, Weaknesses, Opportunities and Threats
TAM	Total Addressable Market
TMA	Trans Maldivian Airways
UHS	Ultra High Strength
UN	United Nations
US	United States
V&V	Verification & Validation
VFR	Visual Flight Rules
WS	Water Sailplane

Symbols

α	Angle of attack
α_T	Thrust angle of attack
β	Angle of dead rise
β	Mach number parameter
γ	Flight path angle
γ_d	Glide angle
η_{bat}	Battery efficiency
η_i	Ideal propeller efficiency
η_{mot}	Motor efficiency
η_p	Propeller efficiency
η_v	Viscous profile efficiency

θ	Pitch angle
θ_b	Heel angle
κ	Ratio of two-dimensional lift curve slope to 2π
Λ	Wing sweep
λ	Taper ratio
$\Lambda_{C/2}$	Sweepback of mid-chord
Λ_{LE}	Sweep angle at the leading edge
μ	Aerodynamic roll angle
ρ	Density
ρ_W	Water density
Φ	Bank angle
A	Aspect ratio
a	Wing lift curve slope
A_{prop}	Propeller area
A_{sp}	Spinner area
AR	Aspect ratio
B_{fl}	Float width
b_w	Main wing span
$c.g.$	Center of Gravity
C_1	Taper ratio correction factor
C_f	Skin friction coefficient
C_m	Moment coefficient
C_{D_0}	Zero-lift drag coefficient
C_{D_f}	Skin friction drag coefficient
C_{D_i}	Induced drag coefficient
$C_{D_{misc}}$	Miscellaneous or additive drag coefficient
C_{D_o}	Pressure drag coefficient
C_{D_W}	Wave drag coefficient
C_D	Total drag coefficient
C_{L_α}	Slope of the lift curve
C_L	Aircraft lift coefficient
C_{m_α}	Slope of the pitching moment coefficient curve
$\frac{d\varepsilon}{d\alpha}$	Downwash gradient
D	Drag
D_{fus}	Fuselage diameter
D_{prop}	Propeller diameter
e	Oswald efficiency factor
E°	Standard Reduction Potential
E_{bat}	Battery energy
E_{climb}	Energy required for climb
$E_{takeoff}$	Energy required for take-off
f	Fineness ratio
F_{buoy}	Buoyancy force
FF	Form factor
g	Acceleration due to gravity
GM	Metacentric Height
H_e	Energy height
h_{fl}	Float height
h_{MC_L}	Longitudinal Metacentric Height
h_{MC_T}	Transverse Metacentric Height
H_{max}	Service Ceiling Altitude
I	Current
I_y	Moment of inertia around y-axis (pitch)
IF	Interference factor
K_1	Empirical hull station weighing factor
K_p	Propeller constant
L	Lift
l_m	Mean geometric chord
L_t	Tail length
L_{fl}	Float length
L_{fus}	Fuselage length
M	Mach number
m	Mass
n	Load factor
N_{en}	Number of engines
n_{rot}	Rotational rate
N_z	Ultimate load factor
P	Power
P_{br}	Brake power
P_{mot}	Motor power
q_{cr}	Dynamic pressure at cruise
R	Turn radius
r_x	Ratio of distance
RC	Climb Rate

RD	Descent rate
Re	Reynolds number
S	Area
s_m	Safety margin
s_{fl}	Float center-to-center spacing
S_{ht}	Horizontal wing surface area
s_{TO}	Take-off distance
S_{vt}	Vertical wing weight
S_{wet}	Wetted surface area
S_w	Main wing surface area
t/c	Thickness to chord ratio
T	Thrust
T_π	Time for $180°$ coordinated turn
T_{net}	Net Forward Force
T_{static}	Static Thrust
U	Energy Density
U	Gust velocity
$\bar{V}_h$	Horizontal tail volume coefficient
$\bar{V}_v$	Vertical tail volume coefficient
$\frac{V_h}{V}$	Speed ratio horizontal tail/main wing
V	Airspeed
V_A	Design maneuvering speed
V_a	Approach Speed
V_B	Design Gust Speed
V_D	Design Dive Speed
V_d	Volume of displaced water
V_{LOF}	Lift-Off Speed
V_{mcg}	Minimum Control Speed on Ground
V_{RA}	Rough Air Speed
V_{S_0}	Stall Speed Landing Config.
V_{stall}	Stall speed
$V_{tip_{helical}}$	Propeller tip speed
$V_{tip_{static}}$	Static propeller tip speed
W/P	Power Loading
W/S	Wing Loading
W	Weight
w	Induced airspeed
$W_{avionics}$	Avionics group weight
W_{bat}	Battery weight
W_{dg}	Design gross weight
W_{elec}	Electric systems group weight
W_{fctrl}	Flight control group weight
W_{floats}	Floats weight
W_{furn}	Furnishing group weight
W_{fus}	Fuselage group weight
W_{fw}	Fuel weight in wing
W_{gb}	Gearbox weight
W_{ht}	Horizontal wing group weight
$W_{hydraulics}$	Hydraulic systems group weight
W_{mc}	Motor controller weight
W_{mot}	Motor weight
W_{prop}	Propulsion group weight
W_{vt}	Vertical wing group weight
W_w	Wing group weight
$\bar{x}$	x location w.r.t. the MAC
$\frac{X_0}{C}$	Location of fictitious turbulent boundary layer
$\frac{X_{tr}}{C}$	Transition point from laminar to turbulent boundary layer
X_a	Aerodynamic X-axis
X_b	Body X-axis
Z_a	Aerodynamic Z-axis
Z_e	Earth Z-axis

Contents

1. Introduction

To remain a competitive tourist destination the Maldives must provide innovative solutions to attract new visitors. With this in mind, Trans Maldivian Airways (TMA) provided a group of seven BSc Aerospace Engineers of the TU Delft with the task of conceptualizing the design of a sailplane capable of taking off from and landing on water. The project is the capstone of their bachelor degree, and was completed in a time frame of 10 weeks. As a result of the task, the team concluded the following Mission Need Statement (MNS):

Conceptualize and design a sustainable, emission-free sailplane capable of taking off from and landing on water.

With the MNS as a broad framework, the team generated a more concrete Project Objective Statement (POS). It was concluded through a discussion with the client, negotiating initial requirements that were posed. Here it was agreed that the design would focus on the design of a water sailplane with the use case of aerial recreation for two passengers and one pilot. This was agreed on the basis that the design of a full-scale transport glider, intending to replace TMA's fleet of Twin Otters, was too ambitious for an aircraft type that has never been produced. As a result, the POS became:

Conceptualize and design a sustainable, emission-free sailplane capable of taking-off from and landing on water, for aerial recreation opportunities of two passengers and one pilot for TMA, by seven students in ten weeks.

The project was divided into four phases: the Project Plan, Baseline, Midterm, and Final. In the first phase, the project logistics were planned, assigning each group member a management and technical function. Additionally, planning was detailed until the third phase of the project, and initial contact was made with the client to discuss the framework of the project. The second phase was mainly highlighted a market analysis, functional and requirement analysis, and concept generation following a design options discovery. In the third phase, a preliminary concept was chosen through a diligent trade-off of design options. This phase also created a planning for the detailed design phase that follows. The final phase concerned itself with a preliminary detailed design of the aircraft.

Overall, this report aim is to conclude the feasibility of the aircraft conceptualized. As a result, the structure of the report is split into four parts. The first provides the project overview consisting of a market analysis, functional analysis, sustainable development strategies, a technical risk assessment, the requirements, and a summary of the concept overview concluded from the Midterm with a Class I weight estimation. Following this, the second part presents the methodology of the detailed design. This consisted of verification and validation procedures, and design tools, with their methodology, of the aircraft components and their performance. The second part concludes with a Class II Weight estimation. The third part of the report presents the final design of the aircraft following multiple design iterations, and the reliability, availability, maintainability, and safety (RAMS) characteristics. The technical resource budget tracking, sensitivity analysis, and requirement compliance are also discussed. The fourth and final part of the report discusses the operations of the aircraft. This consists of operations and logistics, a financial analysis, the project development logic and plan, and conclusions and recommendations for further study.

Project Overview

2. Market Analysis

This chapter presents the market analysis of the water sailplane, a market analysis is vital to understand client and market conditions. Allowing for a strategic design and minimization of risk. Firstly, Section 2.1 will present the insights obtained from the Maldives market analysis. Following that,Section 2.2 and Section 2.3 respectively include a stakeholder identification and strength, weaknesses, opportunities and threats (SWOT) analysis from the insights obtained in the market overview. Then, Section 2.4 entails the determination of the business and use case of the aircraft. With a determined business case, an analysis of the business case was done in Section 2.5. Section 2.6 introduces the calculation of the market size. Finally, Section 2.7 presents an overview of other markets of interest for the use of the water sailplane.

2.1. Maldives Market Overview

This section presents an overview of the tourism market in the Maldives. The overview of the market is done with a PESTELE analysis. This is a framework used to analyze the macro-environmental factors that have an impact on an organization.[1] This framework was chosen for the analysis as an understanding of the business environment in its broadest sense of the word, minimizing the chance of a component, and therefore risk and requirement, being missed. Note that, the footnote considers the same major points, with the exception of ethics. Ethics were included in the analysis to cover the sustainability aspect of the market analysis. Finally, the seven lenses with which the market is researched provide an informational overview. The SWOT analysis presented in Section 2.3 picks out the stakeholders and relevant risks that the research provided.

2.1.1. Political

The political overview of the Maldives is provided in terms of the government structure, diplomatic ties, monetary and fiscal policy, and a summary of key indices describing the political environment. Precise risks from this research are extracted and analyzed in Section 2.3.

The Maldives is a presidential republic with an executive, judicial, and legislative branch The island nation adopted its most recent constitution in 2008; which provides the legal foundation for the existence of the nation, its government structure, and sets out the rights and duties that citizens receive.[2] An Islamic (sharia) legal system is in place, with English common law being incorporated primarily in commercial aspects.

Within their diplomatic ties, the Maldives are vocal in their stance on fighting climate change, as they are one of the many countries to be hit hardest.[3] Additionally, the nation is part of numerous international agreements, and many nations - such as the U.S. - provide aid in the promotion of the tourist industry.[4]

According to the Heritage Foundation the Maldives score 53.2 out of 100 points (2019) in terms of economic autonomy from government intervention.[5] Additionally, in 2021 the nation was assigned a country risk rating of C (on a scale from A - E) by Coface - meaning it has a ”very uncertain political and economic outlook and a business environment with many troublesome weaknesses can have a significant impact on corporate payment

[1] https://libguides.library.usyd.edu.au/c.php?g=508107&p=5994242 [Accessed: 25 Nov 2021]
[2] https://globaledge.msu.edu/countries/maldives/government [Accessed: 25 Nov 2021]
[3] https://www.gov.mv/en/organisations [Accessed: 25 Nov 2021]
[4] https://www.tourism.gov.mv/dms/document/9b617c2e4c27d7e169024d5f11579971.pdf [Accessed: 17 Nov 2021]
[5] https://www.heritage.org/index/ranking [Accessed: 25 Nov 2021]

behavior".[6] While these indices paint a relatively unstable landscape in the Maldives, the tourist industry is the most dominant sector in the economy making it less affected. This makes the Ministry of Tourism (as well as of transport and civil aviation), key governmental agencies. Further information on the tourist industry is outlined in greater detail in the sub-section below.

2.1.2. Economical

The focus of this sub-section lies within the economical landscape of the Maldives. Particularly the tourism industry - as this is the most relevant for the product - while also transitioning to the role of TMA. As with the previous sub-section, the research is described with the key points highlighted in the SWOT analysis later in the chapter.

The Maldivian economy relies most heavily on the tourism and fishing industry, respectively. Tourism contributes more than 25% to the annual GDP of the Maldives, with more than 1.7 million tourists visiting the island before prior to the COVID-19 crisis.

Within the tourist industry, aerial transport plays a large role due to it being an island nation. There are three registered air carriers (as of 2020), nine airports - with Velana International Airport the main hub on Malé - allowing an annual passenger traffic of 1,147,247 in 2018. Of the three airlines Trans Maldivian Airways (TMA) is the largest for the purpose of tourist transportation.[7] Despite the current infrastructure, growth in the tourism sector must go into compromise with the fragile nature that surrounds the nation, therefore requiring a sustainable approach.

Trans Maldivian Airways is, with a fleet of 57 de Havilland Twin Otters, the largest seaplane operator in the world. TMA flies to 115 resorts, transporting over 1,000,000 passengers per year.[8] The airline provides the following services: photo flights, resort transfers, private charters, excursions and emergency evacuation flights. Many of the destination resorts tend to be high-end, with the Maldives being "primarily positioned towards the attraction of high-net-worth luxury segments".[9] High-end tourism is the main stimulus for the increase in wealth and growth.[10] As such, the client profile of TMA is high net worth tourists seeking transport from the Velana International Airport to their resort (and back), or for leisure such as an excursion or tour. During research, it was noted that data regarding the revenue or profit of the airline cannot be found in the public domain as the company is privately owned by the Carlyle group.[11] [8]

2.1.3. Social

The social lens of the Maldivian market is provided in this sub-section. It provides an overview of demographics (nation and tourists), media and communication, and tourist buying behavior. A focus is once again provided on these facets in the tourism industry.

Tourists make up a significant portion of the population, therefore also contributing to the societal ambiance. Additionally, their consumer behavior and reasons for being there are largely relevant to the product. The main roles for customer satisfaction were destination image (26.3%), and coastal tourism (27.9%). Furthermore, there is a high retention of repeated visits with 29% of total arrivals in 2013 being there for a second or more time. Further conclusions were that price did not have a significant impact on customer experience, further supporting that the Maldives is a high-end destination. However, political instability, personal safety, and security have a significant impact on tourists' willingness to travel to the Maldives. [1]

2.1.4. Technological

This subsection describes the current technological infrastructure, and developments in the Maldives, with a focus on aviation. As stated previously, there are three registered air carriers (as of 2020) - none of which have helicopters in their fleet. This due their lower reliability compared to water planes, and their history of crashes in the Maldives.[12][13] The entire fleet of TMA consists of the de Havilland Canada DHC-6 Twin Otter. In the meeting with the client, it was mentioned that the older generation (from the 1970s and 1980s) proved more durable and reliable than the new generation (from the 2000s). A detailed discussion of the Twin Otter is presented below.

The de Havilland Canada DHC-6 Twin Otter

In a client meeting, it was explained that the de Havilland Canada DHC-6 Twin Otter aircraft is still in use due to its rigid design, allowing high maneuverability, durability, safety, and easy maintainability. Particularly

[6] https://www.coface.com/Economic-Studies-and-Country-Risks [Accessed: 25 Nov 2021]
[7] https://www.cia.gov/the-world-factbook/countries/maldives/ [Accessed: 17 Nov 2021]
[8] https://www.transmaldivian.com/ [Accessed: 17 Nov 2021]
[9] http://www.the-businessreport.com/article/maldives-tourism-competition-investors-globe-mmprc/ [Accessed: 25 Nov 2021]
[10] https://www.worldbank.org/en/country/maldives/overview#1 [Accessed: 17 Nov, 2021]
[11] https://www.reuters.com/article/us-trans-maldivian-m-a-carlyle-group-idUSKCN2E73T8 [Accessed: 18 Nov 2021]
[12] https://aviation-safety.net/wikibase/30774 [Accessed: 25 Nov 2021]
[13] https://apnews.com/article/fdf6b6ab949b4722840c4b4032642a48 [Accessed: 25 Nov 2021]

those made in the 1970s are the favored product of TMA. A Twin Otter can carry up to 20 passengers without luggage.[14] The old generation has a largely analog flight deck, allowing it to be durable in the harsh environmental conditions - while the newer generations incorporated more electronic devices (which have proven to be troublesome in TMA's experience).

The investigation into the technology of zero emission water sailplane would be groundbreaking technology as there are no current certified models of water sailplanes capable of performing this. However, this does pose the challenge of there being no recent reference designs.

2.1.5. Environmental

Being an archipelago nation of just under 1,200 islands made up of a chain of 26 atolls, the Maldives is one of the most geographically scattered countries. The Maldives lies in the tropic band, and thus experiences stable high temperatures between $25\,^{\circ}\mathrm{C}$ to $30\,^{\circ}\mathrm{C}$. Two major seasons are experienced: a dry season (January to April) and a monsoon rain season (May to December). During the dry season, there is consistent sunlight and higher temperatures, while the monsoon season results in increased rainfall, up to $250\,\mathrm{mm}$ per month.[15] Wind speeds are mild, averaging $5\,\mathrm{m\,s^{-1}}$. Hence during the dry season tourism is the highest.

It should be noted that with the humid air, found in the Maldives lowers the appearance of thermals, which are used by gliders to fly for a longer duration. This is due to the fact that the specific heat capacity of humid air is greater than dry air, meaning it will take more energy to heat the air. Furthermore, the presence of mainly homogeneous ground, and the sea, also has a negative effect on the existence of thermals. Thermals are formed due to the uneven heating by the radiation of the sun. If the ground is fully homogeneous, then the probability of uneven heating is greatly reduced.[16]

Note, however, that as a result of climate change the climate of the Maldives has become much more dynamic and unpredictable. The two seasons have become increasingly blurred, with 71% of the inhabitants having reported perceived shifts in weather patterns in the past 10-15 years in 2013. Only 8% observed no change. [2]

2.1.6. Legal

This section discusses the laws and regulations that affect the market such as safety regulations. The Civil Aviation Authority (CAA) was founded in 2007 by the Maldivian government to administer and develop regulations with regards to the development of aviation in a safe, orderly and economical manner. In 2007 the governmental body immediately introduced the Maldivian Civil Aviation Regulations (MCAR), the regulations they embody can be found in the following footnote.[17] The regulation is aimed to be integrated with international regulations from EASA.

From a client meeting it became clear that TMA has an exemption to fly at an altitude of 500 feet to provide a more scenic view of the Maldives. Furthermore, TMA only flies at VFR, this means that the aircraft TMA operates are intended to fly in visual meteorological operations.[18] Further regulations regarding sustainability will be discussed in the following section.

Once a new aircraft has been developed, it must obtain certification to determine the airworthiness of the aircraft. Sailplanes and powered sailplanes are specified in the EASA CS-22 documents. However this limits the aircraft to two passengers including the pilot. Should the aircraft contain more than two passengers, different a certification applies. Then the requirements set by EASA CS-23 would be applicable, even as a sailplane. [3, 4]

2.1.7. Ethical

This section presents the ethical environment of the Maldives, and the effect it may have on the product being designed by the team. The ethical environment is assessed for sustainability. Due to climate change, the Maldives is under threat of flooding with the islands having an average elevation of only $1.6\,\mathrm{m}$ above sea level, with over 80% of the islands being less than $1\,\mathrm{m}$ above sea level.[19] Given the current rates of global warming and rising sea levels, the Maldives is at risk of becoming uninhabitable by the end of the century, and has thus placed an enormous emphasis on sustainable tourism.[20]

Due to these threats the Maldivian government has set multiple goals and efforts. The first of them is net-zero emissions by 2030.[21] Furthermore, efforts are made to contribute to sustainable development goal (SDG) 13. The UN SDGs are seventeen goals adopted by the members of the UN in their fight against global poverty.

[14] https://www.baesystems.com/en/heritage/de-havilland-canada-dhc-6-twin-otter [Accessed: 18 Nov 2021]
[15] http://worldweather.wmo.int/en/city.html?cityId=228 [Accessed: 10 Nov 2021]
[16] https://www.boldmethod.com/learn-to-fly/weather/how-thermals-work/ [Accessed: 26 Nov 2021]
[17] https://www.caa.gov.mv/rules-and-regulations/maldivian-civil-aviation-regulations-(mcar) [Accessed: 26 Nov 2021]
[18] https://atpflightschool.com/become-a-pilot/flight-training/vfr-ifr-flight-rules.html [Accessed: 26 Nov 2021]
[19] https://www.theguardian.com/environment/2008/nov/11/climatechange-endangered-habitats-maldives [Accessed: 10 Jan 2022]
[20] https://abcnews.go.com/International/facing-dire-sea-level-rise-threat-maldives-turns/story?id=80929487 [Accessed: 09 Nov 2021]
[21] https://www.worldbank.org/en/news/feature/2021/07/12/towards-a-sustainable-net-zero-future-in-maldives [Accessed: 25 Nov 2021]

SDG 13 is stated as follows: Take urgent action to combat climate change and its impacts.[22] The Maldives government has formed a regulatory entity for contributing to sustainability goals, the environmental protection agency (EPA). Their activities consists of protection, conservation and management of the environment and biodiversity.[23] TMA would contribute to the SDGs by adding an emission free aircraft to their fleet.

2.2. Stakeholder Identification

In this section a stakeholder identification on the water sailplane is performed. A stakeholder, according to the NASA Systems Engineering Handbook, is a group or individual who is affected by or is accountable to an extent for the outcome of a system. This primarily includes customers and other interested parties, such as those affected by the product from production to use [5]. Identifying the stakeholders is essential for understanding which parties are involved in the project and what boundaries the project has. The framework of classification that was applied for stakeholder identification is the interest influence matrix [6], which can be seen in Table 2.1. The application of the chosen method divided the stakeholders into four categories based on the amount of influence and interest. From the PESTELE analysis in Section 2.1, the following stakeholders are identified:

Table 2.1: Stakeholder Identification

	High Interest	**Low Interest**
High Influence	Trans Maldivian Airways Project Tutor	EASA Maldivian Ministry of Transport and Civil Aviation
Low Influence	Maldivian Ministry of Tourism Tourists DSE committee	Velana International Airport EPA Resorts

2.3. SWOT Analysis

In this section a SWOT analysis is presented for the market and the product respectively, to have a perspective on a macro to micro scale. From these weaknesses and threats, risks are identified and further investigated in Chapter 5. From the market overview, in Section 2.1, the following strengths, weaknesses, opportunities and threats are identified:

Table 2.2: SWOT analysis market

	Helpful	Harmful
Internal	**Strengths** S1. TMA is a market leader (pricing power) S2. TMA is one of the largest companies in the economy S3. Unique environment drives interest in air touring S4. Tourists have a large presence on social media S5. Nation has strong diplomatic ties S6. Tourism is the nation's most dominant sector S7. English is widely spoken (easy communication with locals) S8. High retention of repeated tourists	**Weaknesses** W1. Instability of TMA as client (airlines are highly leveraged) W2. TMA is privately owned (opaque market, hard to find financial information) W3. Difficulty delivery of the product due to remote and dispersed location W4. Presence of thermals due to environmental factors

[22] https://maldives.un.org/en/sdgs/13 [Accessed: 25 Nov 2021]
[23] https://en.epa.gov.mv/about [Accessed: 25 Nov 2021]

Table 2.2 continued from previous page

	Helpful	Harmful
External	**Opportunities** O1. Deal with USA to increase tourism O2. Eco-tourism is in an upwards trend O3. Customers are high net worth individuals with great influence in world O4. Large incentive to bounce back tourist industry post COVID-19 crisis	**Threats** T1. Climate change (more unpredictable weather patterns) T2. The Maldives loses tourism to competitors T3. Tourism is highly sensitive to adverse global events (e.g. COVID) T4. Instability in government (low ratings in indices) T5. Social tensions due to controversial government

Table 2.3 presents a SWOT analysis of the product.

Table 2.3: SWOT analysis product

	Helpful	Harmful
Internal	**Strengths** S1. No direct competitors due to niche product S2. Innovative idea that the client is enthusiastic about S3. High marketability (sustainability hype and large social media presence of tourists and locals) S4. The product produces less noise than other forms of aviation	**Weaknesses** W1. Few reference designs W2. Technological immaturity in Maldives W3. Certification Specifications are unclear for three passenger gliders
External	**Opportunities** O1. Potential use in many other tourist destinations O2. Exemption flight Altitude TMA	**Threats** T1. Harsh climate (salt water) T2. Air regulation change (Maldives or EASA)

2.4. Business Case

This section outlines the business case and the use case of the product. To identify the business case and the use case which are the most optimal to successfully penetrate the market, firstly the needs of customer and clients will be identified. Then a use case will be presented, based on the results found in the SWOT analysis. Finally, this use case will provide a unique selling point.

2.4.1. Use Case

A need is defined as a non technical user requirement, which constraints the use of the product. User requirements **TL-USER-PERF-03** and **TL-USER-PERF-04**, were subject to change due to compromise with the client during status meetings when considering their feasibility. They are also further described in detail in Appendix A. Synthesizing these needs together with the SWOT analysis, it was concluded - in agreement with the client - that the water sailplane shall be a proof of concept for recreational purposes. This would provide the largest competitive advantage for the product. Examples of the use case could be a romantic (honeymoon) flight, or the unique thrill of aerobatic maneuvers in a sailplane aircraft. This is supported for the following reasons:

The Twin Otter is fitted to provide transfers of large groups of tourists between resorts, whereas sailplanes have only experimentally been flown with three persons including the pilot and the concept of a water sailplane has not been fully developed. The combination of these two factors makes designing a water sailplane able to compete with the transport of large groups of tourists not technically viable within time and resources available to the group.

On top of that, the operational costs would largely increase even if it was technically achievable to transport half the passenger amount of the Twin Otter. Additionally, it would disturb the operational efficiency TMA benefits from currently, with their homogeneous fleet of Twin Otters. This results in a water sailplane for transportation to be too great of a financial risk for the airline.

The competitive advantage for a water sailplane lies in the other services TMA provides with the Twin Otter, namely the photo tours and private charters. The Twin Otter is able to provide these services with less quality than a sailplane could. Where the Twin Otter is noisy, has small windows and has limitations in aerobatics. Where on the other hand a sailplane is quiet, can do aerobatics, and provides better visibility. The use of a water sailplane for recreation and entertainment provides a new experience of the Maldives, which is very marketable due to being new, green, romantic and quiet. Furthermore, if the proof of concept succeeds further research could be implemented towards scaling the model up for larger scale tourist transport. The unique selling point is summarized by the following sentence: ”A new experience of the Maldives.” This use case was proposed during the status meeting and accepted by the client, making the user requirements **TL-USER-PERF-04:** and **TL-USER-OPER:04:** no longer applicable.

2.5. Competitor Landscape

This section discusses the competitor analysis. It provides insights on how competing products with a similar use case as discussed in Section 2.4 compare to the water sailplane. There are few water sailplanes that exist, therefore similar products were used. These were found to be helicopters, sailing boats and Twin Otter tours. The is made with respect to: cost, user experience, operability, and reliability. For all selling points, except cost, coarse scoring is applied. Table 2.4 presents the scoring of the water sailplane with respect to the three competitors with motivation for the scores provided below the table:

Table 2.4: Competitor analysis

	Water sailplane	**Helicopter tours**	**Sailing tours**	**Twin Otter tours**
Cost	TBD	1500-2500 USD per charter	150-300 USD per half day	2000-3000 USD per hour
User experience	$++$	$+$	$\sim$	$\sim$
Operability	$+$	$\sim$	$+$	$++$
Reliability	$++$	$--$	$++$	$+$

Coarse Scoring: $++$ excellent, $+$ good, $\sim$ mediocre, $-$ poor, $--$ horrific

Water sailplane

After the use case was presented in the client meeting, the client made clear that safety and reliability have the utmost priority in design. Hence, these high ratings have been applied to be seen as an endeavor to maintain a competitive advantage over the other tours methods. A figure for the cost is presented in Chapter 27

Helicopter tours

The cost estimation for helicopter tours is based on similar tours in Sri Lanka[24], as helicopters in the Maldives are a rare occurrence and no information on pricing could be found. The user experience is rated high as there is a wide and high view in the helicopter of the atolls. However, noise will still be present. The operability of the helicopter is rated neutral as there is a large volume of helicopters worldwide so parts will be widely available, but a helicopter requires many hours of maintenance. The reliability of helicopters is rated horrific relative to the other competitors, this is done as the helicopter consists of many moving parts which can be affected by corrosion. There is also a history of helicopter crashes in the Maldives.[25]

Sailing tours

Although a sailing tour was found to be quiet, it does not provide an up top overview of the islands and is thus rated lower for user experience. The operability of the sailing tours was rated good as the island was originally designed for the infrastructure of boats. However, providing a large sailboat with a new coating is operationally intensive as it would have to be taken out of the water for maintenance. Finally, a sailing boat is rated highly for reliability as it is very safe relative to the other methods of transport.

Twin Otter tours

The user experience for the Twin Otter was rated neutral as a high view of the Maldives is provided, but the field of view is small inside the airplane relative to the helicopter and water sailplane. Furthermore, the aircraft

[24]https://www.resort98acres.com/things-to-do/helicopter-rides.html [Accessed: 25 Nov 2021]
[25]https://apnews.com/article/fdf6b6ab949b4722840c4b4032642a48 [Accessed: 25 Nov 2021]

generates a lot of noise further reducing the experience. The operability of the Twin Otter was rated very high as the client already operates this aircraft, hence operational efforts for the means of transportation. Performing operational activities for touring would thus have a low impact. The reliability of the aircraft was rated high, the plane is built to be very rigid and durable.

2.6. Market Size

This section covers the calculation of the market size. The calculation is based on the Total Addressable Market (TAM), Serviceable Available Market (SAM), and Serviceable Obtainable Market (SOM) framework.

2.6.1. Total Addressable Market

To estimate the market size for this product the number of target customers was determined. Data required for this estimation is not public knowledge, hence a conservative estimation has been made. As stated previously, the airline transports over one million passengers per year. To remain conservative in our estimation it was rounded down to one million passengers to account for the transportation of individuals unrelated to tourism.

$$\text{Total Addressable Market} \approx 10^6 \text{ people} \tag{2.1}$$

2.6.2. Serviceable Available Market

Activities such as a private charter, photo tours, and excursions are in a higher price class than other touristic activities, such as scuba diving and a spa. The latter is in a range of 50-150 USD and the commercial rate for private flights range between 2000-3000 USD per hour. Despite the Maldives being a high-end tourist destination, there remain few that could afford such an activity. To estimate how many visitors could afford this, the amount of resorts costing 1000 USD or more per night were found with respect to the total amount of resorts. Of of the 115 locations TMA flies to, 45 meet this price. It is assumed that the passengers are uniformly distributed over the resort, and so a factor of $\frac{45}{115}$ can be seen in Equation (2.2):

$$\text{Serviceable Available Market} \approx 10^6 \cdot \frac{45}{115} \approx 374000 \text{ people} \tag{2.2}$$

2.6.3. Serviceable Obtainable Market

Not all of the customers in the serviceable available market will convert to a sale of the service. Hence a penetration rate of 5% has been applied to accommodate for this, leading to an estimated 18,700 target customers as seen in Equation (2.3).

$$\text{Serviceable Obtainable Market} \approx 10^6 \cdot \frac{45}{115} \approx 18700 \text{ people} \tag{2.3}$$

Finally, to find the market size, the volume and value must be found. It is assumed each target customer will only use the service once. For an approximation of the value, a rate of 2500 USD per hour is assumed, given that private charters cost an equivalent amount. Additionally, it is assumed that the activity takes up to an hour with pre-flight instructions included. This resulted in the following market size:

$$\text{Market Size} \approx 18\,700 \cdot 2500 \approx 46\,750\,000 \text{ USD} \tag{2.4}$$

The estimation for the market size does not take into account the added value of providing a new and sustainable way of experiencing the Maldives. Eco-tourism shows immense growth[26], hence the market size estimation should be seen as a lower bound value, as these unaccounted factors are not quantifiable, but would produce a net positive effect.

2.7. Target Markets

Two components are key in identifying other target markets for this product: locations with high-end tourists - given the high cost associated with the product - and the market should geographically be located near bodies of water. The latter flows logically since the aircraft is designed to take-off and land on water. To find these markets touristic locations were filtered for their highest average price per day, and per location examined to see whether it had large bodies of water. This resulted in the following, but not limited to, list future markets in which the product was deemed viable:

[26] https://www.einnews.com/pr_news/548404192/ecotourism-market-size-is-projected-to-reach-333-8-billion-by-2027-registering-a-cagr-of-14-3-from-2021-2027 [Accessed: 17 Nov 2021]

1. Grand Cayman, Cayman Islands
2. Abu Dhabi, United Arab Emirates
3. Dubai, United Arab Emirates
4. The Antilles
5. Seychelles
6. Bora Bora, French Polynesia
7. Fiji
8. British Virgin Islands
9. Miami, United States
10. The Greek Islands
11. Hawaii, United States
12. Monaco

A final consideration that is relevant for the market analysis is the amount of aircraft that can be sold. In a meeting with the client, they deemed it feasible to buy 20 aircraft. Given the large list of future markets that could be penetrated above, it would be reasonable to assume that a similar amount of aircraft could be sold in two other locations. This makes a reasonable estimate of 60 aircraft to be sold in five years.

3. Functional Analysis

The water sailplane has to fulfill multiple functions in various phases from production to retirement. All these functions should be incorporated in the design of it. In order to discover what these functions are, a functional analysis was performed, which is described in this chapter. This analysis contains a Functional Breakdown Structure, covered in Section 3.1, and a Functional Flow Diagram, discussed in Section 3.2.

3.1. Functional Breakdown Structure

In the Functional Breakdown Structure (FBS), which is shown as Figure 3.1 on page 11, all functions of the water sailplane were categorized into three groups. Each group stands for a different phase that the aircraft goes through in its 'life'. The following phases were evaluated in the FBS:

- Production
- Operation
- Retirement

The production of the water sailplane covers the gathering of (sustainable) resources and the manufacturing of parts and components, as well as the assembly, testing, and delivery of the aircraft. The operational phase includes all functions related to the use of the water sailplane, so all pre-/post-flight operations, and safety, reliability and maintainability functions. Lastly, the disassembly of the aircraft into all its components and parts, and the reusability or recyclability of these, belongs to the retirement of the aircraft.

3.2. Functional Flow Diagram

The Functional Flow Diagram (FFD) shows the order in which the functions, described in the Functional Breakdown Structure, occur. It also shows the relation between different functions, for this reason 'and'- and 'or'-blocks were created. The FFD can be seen as Figure 3.2 on page 12.

3.3. Function Origin

As mentioned previously, the functions of the water sailplane were identified during this analysis. However, not all functions match those from regular aircraft. The market analysis, risk mitigation and requirements all influenced the three phases the aircraft goes through. Therefore, in this section the origin of some of the identified functions in the FBS and FFD are explained.

Functions Connected to the Market Analysis

Several functions flowed from the market analysis in Chapter 2 that would increase the chances of dealing with potential competitors. These functions include taking off from and landing on water (3.3 and 3.7).

Functions Connected to the Risk Mitigation

In order to cope with some of the risks defined in Chapter 5 some functions had to be added to the Functional Breakdown Structure and the Functional Flow Diagram. This involved ensuring the quality of the water sailplane by performing quality control and tests. These functions were the following: 2.1.3, 2.2.4, 2.3.3, 2.4.8 and 2.5.2. Considering the testing of the aircraft 2.6 was included in the functional analysis.

Functions Connected to the Requirements

In case of the requirements the opposite was the case, multiple requirements flowed out of the functional analysis. The incorporation of recycled and recyclable materials and parts (2.1.2, 2.2.1, 4.4.1 and 4.4.4) for example, as well as the usage of off the shelf parts and components (2.2.3, 2.3.2 and 2.4.5) provided several requirements for the production and retirement of the water sailplane. Operational functions that had an influence on the requirements were landing on and taking off from water (3.3 and 3.7).

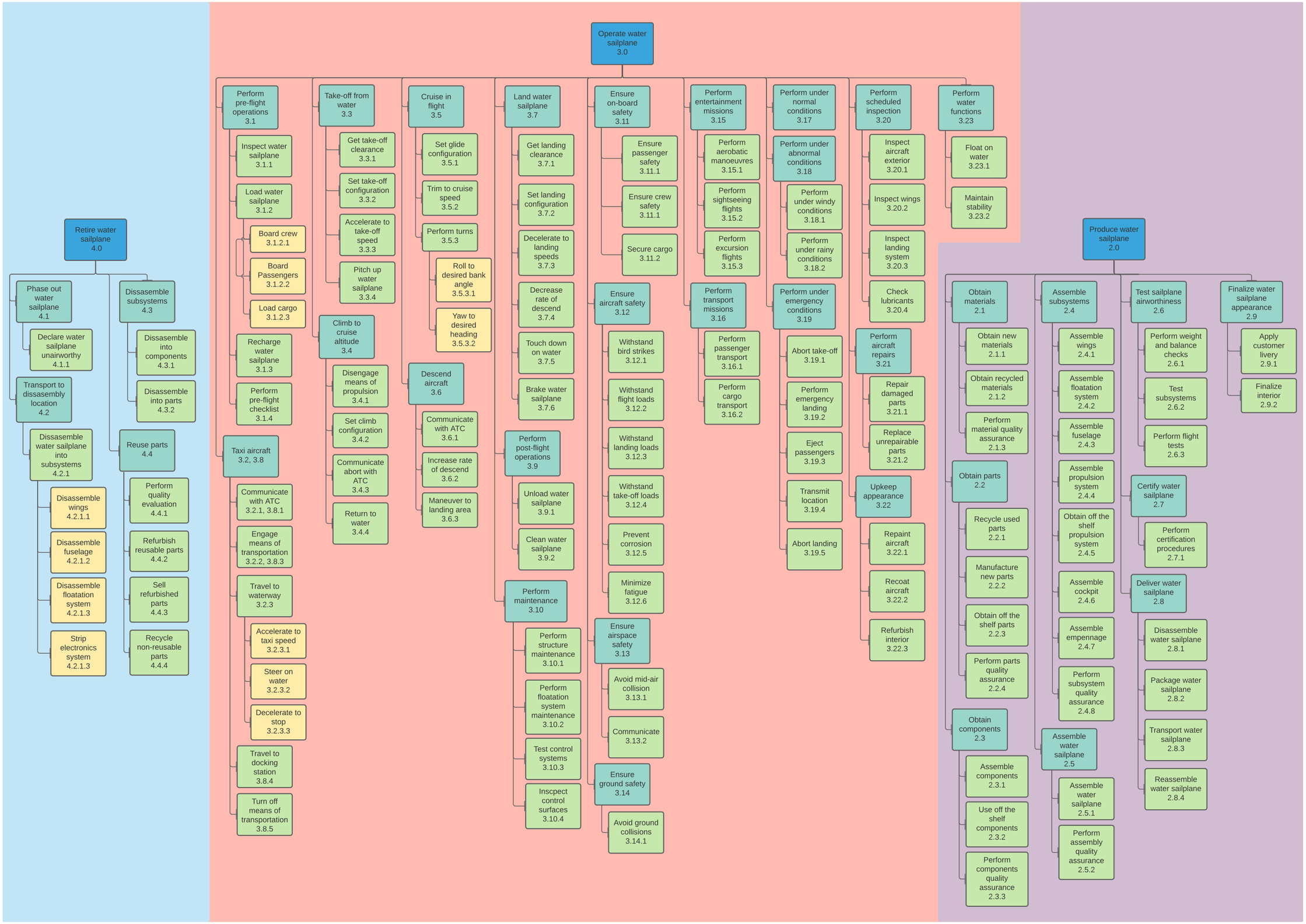

Figure 3.1: Functional Breakdown Structure

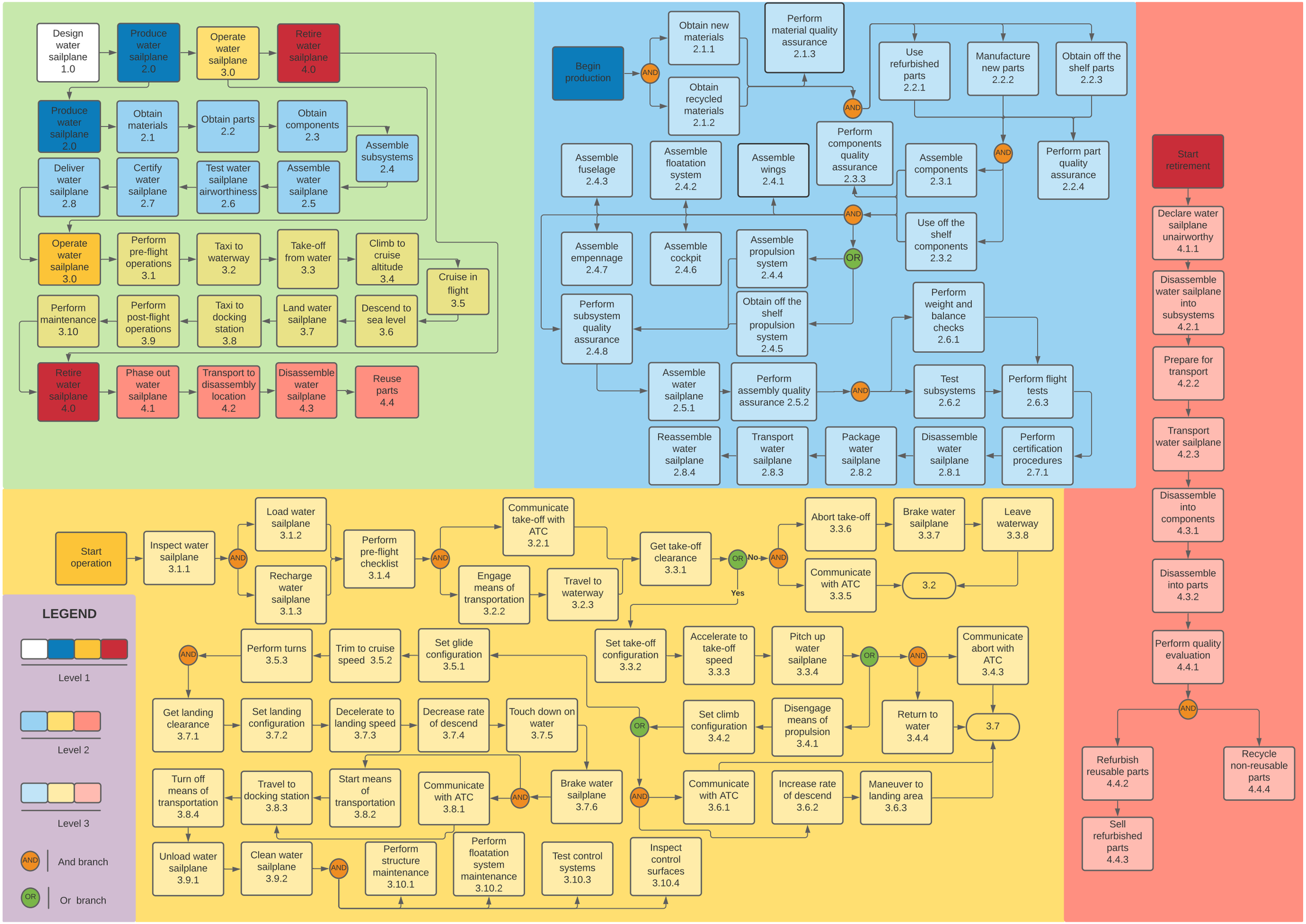

Figure 3.2: Functional Flow Diagram

4. Sustainability Development Strategy

Nowadays sustainability has one of the highest priorities in modern society, therefore the UN have adopted 17 Sustainable Development Goals (SDG's).[1] These were developed to improve the global environmental, economic and social sustainability. Moreover, the Maldives, for which this water sailplane is being designed, are in danger of the rising sea levels due to the changing climate. Therefore, it is of utmost importance to include a sustainable development strategy for the design of the water sailplane. In Chapter 4 the three facets of the sustainability development strategy are discussed. These include the environmental, economic and social sustainability, which are elaborated upon in Section 4.1, Section 4.2, and Section 4.3 respectively. Lastly, the control over the developed strategy is explained in Section 4.4, which gives a more in-depth view on the responsibilities and check-ups for this sustainability development strategy.

4.1. Environmental Sustainability

Environmental sustainability plays an important role in the design of the water sailplane. First of all because the Maldives are in danger of the rising sea levels, but also because this was in the client's interest. Chapter 6 presents multiple requirements that consider the environmental sustainability of the water sailplane. REQ-WS-SUST-01 and REQ-WS-SUST-09 were the two driving requirements, which considered zero-emissions of the aircraft and eliminating the usage of harmful materials for the marine environment [7]. The design phases in which environmental sustainability was specifically included, were the trade-off and the detailed design phase. Their evaluation is presented in Section 4.1.1 and Section 4.1.2, respectively. With regard to the production phase of the aircraft two methods were considered through which waste and emissions could be minimized. This is shown in Section 4.1.3.

As a side note, the generation of electricity which is needed to produce and operate the aircraft was considered as well. Solar and hydro power were concluded to be the main energy sources to obtain this electric energy, because of the surplus of sunlight and water in the Maldives. However, this lies out of the control of the design team, hence no further analysis was provided in this section.

4.1.1. Trade-off

During the trade-off process environmental sustainability was implicitly included in the aerodynamic drag and hydrodynamic resistance. An increase in drag would require more power, consequently more energy. Therefore, it was concluded that the performance of the water sailplane reflects on the contribution to the environment by minimizing the aerodynamic and water drag.

4.1.2. Material Selection in the Detailed Design Phase

The material choice can have a significant influence on the environment. Chapter 10 performed an evaluation of the material selection in manufacturing, operational and end-of-life phases of the water sailplane. During the selection process only composites were considered due to their low specific weight.

4.1.3. Minimization of Waste and Emissions during Production

During the production of the water sailplane significant gains can be made with regard to environmental sustainability. By implementing the philosophy of lean-thinking waste can be minimized and the highest level of effectiveness can be achieved [8]. As a result, this would reduce both wasted material and energy. Some requirements were established for sustainability of the production phase, which can be seen in Chapter 6.

4.2. Economic Sustainability

Economic sustainability is the term for contributing to the support of long-term economic growth.[2] It should be obvious that the water sailplane has to comply with this sustainable aspect. Two ways in which the aircraft could contribute to economic growth are by minimizing costs and by opening up job opportunities. For the cost several requirements were defined, which can be seen in Chapter 6. REQ-WS-COST-01, REQ-WS-COST-02 and REQ-WS-COST-03 include the maximum price for the aircraft itself, the training costs and the operational costs, respectively. The implementation of economic sustainability in the trade-off is explained in Section 4.2.1. Thereafter solutions on the consideration of cost reduction in the detailed design phase are elaborated upon in

[1] https://sdgs.un.org/goals [Accessed: 6 Dec 2021]

[2] https://sustainability.umw.edu/areas-of-sustainability/economic-sustainability/ [Accessed: 6 Dec 2021]

Section 4.2.2. Section 4.2.3 presents the minimization of cost by making use of the philosophy of lean-thinking during the production phase of the aircraft. And lastly, the profitable areas that could open up because of the water sailplane are shown in Section 4.2.4.

4.2.1. Economic Sustainability in the Trade-off

During the trade-off the criteria of autonomy and maintainability accounted for the economic sustainability of the water sailplane. The autonomy affects the number of flights that are possible to perform with one aircraft. The more autonomous the water sailplane is, the less time is required to prepare it for the next operation and vice versa. More flights create more revenue, which is good for the economic sustainability. Reducing the cost also benefits the economy of the water sailplane. This could be achieved by designing an aircraft that is easy to maintain, hence maintenance cost decrease.

4.2.2. Cost Reduction in Detailed Design Phase

Cost reduction was also the main priority in the detailed design phase of the aircraft. Both the material selection and the pilot training were two areas with beneficial opportunities. Cost reduction was accounted for during the material selection by looking at the cost, weight and strength of the material type. For example, by choosing a material with high cost, but low weight and high strength characteristics could still be more beneficial to cost reduction than the other way around. In this way not only the short term, but also the long term costs were considered.

In the other area, pilot training, cost could be minimized by designing the aircraft interior to look like that of a DHC-6 Twin Otter. TMA's pilots are used to flying these seaplanes, hence the transition to operating a water sailplane becomes easier. Therefore, less time has to be spent on pilot training saving costs.

4.2.3. Minimizing Production Cost

The philosophy of lean-thinking in the production phase also benefits the economical sustainability. Lean-thinking results in less waste and higher effectiveness [3], hence less material is used during production as well as hours spent. These two aspects could reduce the production cost significantly.

4.2.4. Profitable Areas

Through the realization of the water sailplane a new tourist attraction is created. This original way of experiencing the beautiful landscapes of the Maldives would be a huge advantage for the tourism sector. Hence, a new source of income is created for TMA. Furthermore, the tourist attraction generate a new wave of tourist coming to the nation, all increasing expenditures in the local economy.

4.3. Social Sustainability

Social sustainability focuses on the impact that businesses have on people.[4] The design team plays a part in three social relationships, which include the client (TMA), the customers and the Maldivian society. It is of utmost importance that these relationships remain intact and therefore a strategy has been developed, which identifies the fields of impact and provides solutions to keep all parties satisfied. At first a strategy is provided in Section 4.3.1 that describes how the team ensures the contentment of the client. Thereafter, all measures that will be taken by the team to provide the best possible customer experience are stated in Section 4.3.2. And lastly, in Section 4.3.3 is stated in which way is dealt with other residents.

4.3.1. Satisfied Client

The relationship with the client was the most important driver for the design team as he provided the money to facilitate their work. The basis of this relationship was built on close contact. This included providing information on important decisions and design changes. By doing so, the client was given the opportunity to reflect on these from his point of view. The client meetings ensured that both parties were on the same page throughout the entire design process. Furthermore, it was of great importance that requirements set by the client were met, and that if this could not be achieved he was informed as soon as possible.

4.3.2. Tourist Experience

The purpose of the water sailplane is to serve as a tourist attraction by providing an unforgettable experience of the Maldivian landscapes. By complying with customer requirements regarding the viewing experience of the passengers, REQ-WS-COMF-02 - REQ-WS-COMF-04 in Chapter 6, the best possible flight tour should

[3] https://www.leanproduction.com/essence-of-lean/ [Accessed: 6 Dec 2021]
[4] https://www.unglobalcompact.org/what-is-gc/our-work/social [Accessed: 6 Dec 2021]

be provided [7]. These requirements were taken into account in designing the fuselage as well as in the wing placement.

4.3.3. The Resorts

Something that lies beyond the scope of the design team, but is relevant for the resorts and TMA, is the interference of the new tourist attraction with other on-going activities. The realization of the water sailplane for recreational purposes should not spoil the views of other residents and should not be in the way of other attractions. This would disrupt the experience of the guests.

4.4. Sustainability Control

To ensure that the sustainability development strategy described above was complied with, team members were appointed who carried that responsibility. They were responsible for performing check-ups for each aspect to make sure that the strategy was followed correctly. Table 4.1 shows the responsible person per department, the task and the frequency of the check-ups. Note that only the sustainability aspects were considered that were within the control of the design team.

Table 4.1: Sustainability control

Sustainability department:	**Responsible:**	**Responsible for:**	**Management**
Environmental	Sustainability Manager	Calculations on performance	During trade-off & design Phase
		Material selection	Weekly
Economic	Sustainability Manager	Autonomy & maintainability	During trade-off and detailed design
		Material selection	Weekly
	Product Manager	Delivery of tourist attraction	Biweekly
		Training footprint	Twice during design phase
Social	Product Manager	Satisfaction of the client	Every client meeting
		Customer comfort	Biweekly

5. Technical Risk Assessment

One of the most essential steps during the detailed design phase is the technical risk assessment. With this assessment technical risk are identified and mitigated. Much of this chapter is derived from the risk assessment in the Midterm report [7]. In this chapter, firstly, a strengths weaknesses, opportunities, and threats (SWOT), analysis is performed in Section 5.1 to help identify the risks. After this, the risks are analyzed in Section 5.2 and are shown in a risk map in Section 5.3. Then the risks mitigation can be seen in Section 5.4 and lastly, a contingency plan is described in Section 5.5.

5.1. SWOT Analysis

The SWOT analysis is used to identify both the internal and external elements, either helpful or harmful. Identification of these elements assist in the identification of risks as well as realizing which elements might demand extra attention. The SWOT analysis can be seen in Table 5.1. The numbers in front of the strengths, weaknesses, opportunities, and threats are used to identify them.

Table 5.1: SWOT Analysis

	Helpful	Harmful
Internal	**Strengths** S1. Stable high-wing design S2. Good visibility due to high-wing design S3. Maintenance more easily due to floats and high-wing S4. Emission free	**Weaknesses** W1. Floats not aerodynamic W2. High weight due to floats W3. High weight due to propulsion system W4. High weight due to batteries W5. Propulsion system too little power W6. Battery charge time very long W7. Battery capacity small
External	**Opportunities** O1. Possibility to land and take-off near sandbanks O2. Maintenance similar to Twin-Otter O3. Little extra infrastructure required	**Threats** T1. Salt water and electric motor T2. Descent ratio not sufficient T3. Leakage in floats T4. Electricity not available T5. Exceeding cost budget T6. Engine failure

5.2. Risk Analysis

The risks that were identified are described in Table 5.3. Here each of the risks is given a risk ID. All these risks are divided into categories. These categories are Production (P), Technical (T), Financial (F), Organizational (OR), Operational (OP), Safety (S), Market (M), and Sustainability (SUS).

In Table 5.3 the second column describes the risk, and the section where the risk is identified is given in brackets. The midterm report is denoted with (MR) [7]. If no section is given, the risk is identified by a discussion with the team. The third column gives the effect of these risks. The fourth, fifth, and sixth columns rank the likelihood, impact, and risk factors respectively. The likelihood and impact are ranked using Table 5.2, with likelihood given as a probability, and impact as a decrease in the ability to perform the mission. The risk factor is the product of the probability and impact score, resulting in a number from 0 to 25. In Section 5.3 the risk factor will be explained further. Note a column is included to present the risk mitigation strategies and the effect it has on the risk factor. These will be described in Section 5.4

Table 5.2: Ranking the likelihood and impact of risks in ascending order

Score	Likelihood (Probability of the Risk)	Impact (Performance)
1	Rarely (<5%)	Minor (Performance is not influenced)
2	Unlikely (5-25%)	Significant (Performance is decreased by <25%)
3	Occasional (25-75%)	Severe (Performance is decreased by 25-50%)
4	Likely (75-95%)	Major (Performance is decreased by 50-75%)
5	Almost certain (>95%)	Catastrophic (Performance is decreased by >75%)

Table 5.3: Technical Risks including their risk ID, description, effect, likelihood (L), impact (I), risk factor (RF), mitigation strategy, discussed in Section 5.4, and the L,I and RF after applying the mitigation strategies.

Risk ID	Description	Effect	L	I	RF	Mitigation	L	I	RF
R-T-01	Poor aerodynamics due to floats (MR)	Descent rate too high	5	3	15	M-01	4	2	8
R-T-02	Poor hydrodynamic design of the floats (MR)	Often incidents during landing and take-off	4	2	8	M-02	3	2	6
R-T-03	High weight due to floats (MR)	Descent rate too high	4	3	12	M-03	3	2	6
R-T-04	High weight due to propulsion system (MR)	Descent rate too high	4	4	16	M-03	3	3	9
R-T-05	Insufficient propulsion power (SWOT, W5)	Unable to self-launch	5	4	20	M-04 M-07	4	3	12
R-T-06	Insufficient battery capacity (SWOT, W7)	Little range	4	4	16	M-04 M-07	4	3	12

Table 5.3 – continued from previous page

Risk ID	Description	Effect	L	I	RF	Mitigation	L	I	RF
R-OP-01	Corrosion in structure due to harsh environment (SWOT, T1)	Structural integrity degraded	3	3	9	M-06	2	3	6
R-OP-02	Engine failure (MR)	Emergency landing required	2	4	8	-	2	4	8
R-OP-03	Floatation device landing/take-off failure (MR)	Uncontrolled landing/ take-off	4	3	12	M-5	2	3	6
R-OP-04	Sailplane not emission free (MR)	Final design is not as sustainable as originally intended	2	4	8	-	2	4	8
R-OP-05	Control subsystem failure	Sailplane becomes uncontrollable	3	4	12	M-11	2	4	8
R-OP-06	Sailplane is unstable	Control system needed	3	4	12	M-09	2	3	6
R-OP-07	Sailplane is uncontrollable	Little maneuverability	3	4	12	M-09	2	3	6
R-OP-08	Infrastructure not fit for sailplane (sec. 4.1.2)	High operational costs	3	2	6	-	3	2	6
R-OP-09	Much maintenance needed for sailplane (sec. 4.2.1)	High operational costs	3	2	6	-	3	2	6
R-OR-01	Verification and Validation not done correctly (MR)	Detailed design becomes unfeasible	4	2	8	-	4	2	8
R-OR-02	Wrong aerodynamic estimations (MR)	Trade-off done incorrectly	3	4	12	M-01	2	3	6
R-OR-03	Wrong/forgotten requirements	Sailplane is wrongly designed	2	4	8	-	2	4	8
R-OR-04	Few reference designs (MR)	Unrealistic design developed	2	4	8	-	2	4	8
R-F-01	Cost budget exceeded (MR)	Product unable to be deployed	2	5	10	M-10	1	5	5
R-S-01	Customers do not feel safe in sailplane (MR)	Less customers will use the sailplane	2	4	8	M-03	1	4	4
R-M-01	Market analysis is over estimated (MR)	Few interested clients	2	5	10	M-12	1	4	4
R-SUS-01	Client is not satisfied (sec. 4.3.1)	No continuation of the project	2	5	10	M-12	1	5	5
R-SUS-02	Sailplane is not comfortable (sec. 4.3.2)	Bad customer review	2	3	4	-	2	3	4
R-P-01	Production delay	Delivery date not met	2	3	6	-	2	3	6

5.3. Risk Map

A visualization of the presented risks is provided in a risk map in Figure 5.1a. This map has the likelihood on the vertical axis and the impact on the horizontal axis. Both are defined as an integer number from one to five as described in Table 5.2. A color scheme is added to help visualize the severity of the risk. This color scheme is described in Table 5.4. In this table, the cell color in the severity column corresponds to the color in the risk map. A short description is given as to the management of each of the different severities. The risks which have a risk factor of above ten are required to be mitigated, which is presented in Section 5.4.

Table 5.4: Risk factor classification

Risk factor	Severity	Responsible	Management
1-3	Insignificant	Risk Manager	Once every three weeks
4-6	Minor	Risk Manager	Once every two weeks
7-9	Controllable	Risk Manager	Once every week
10-14	Dangerous	Risk Manager	Twice a week
15-25	Extreme	Risk Manager	On a daily basis

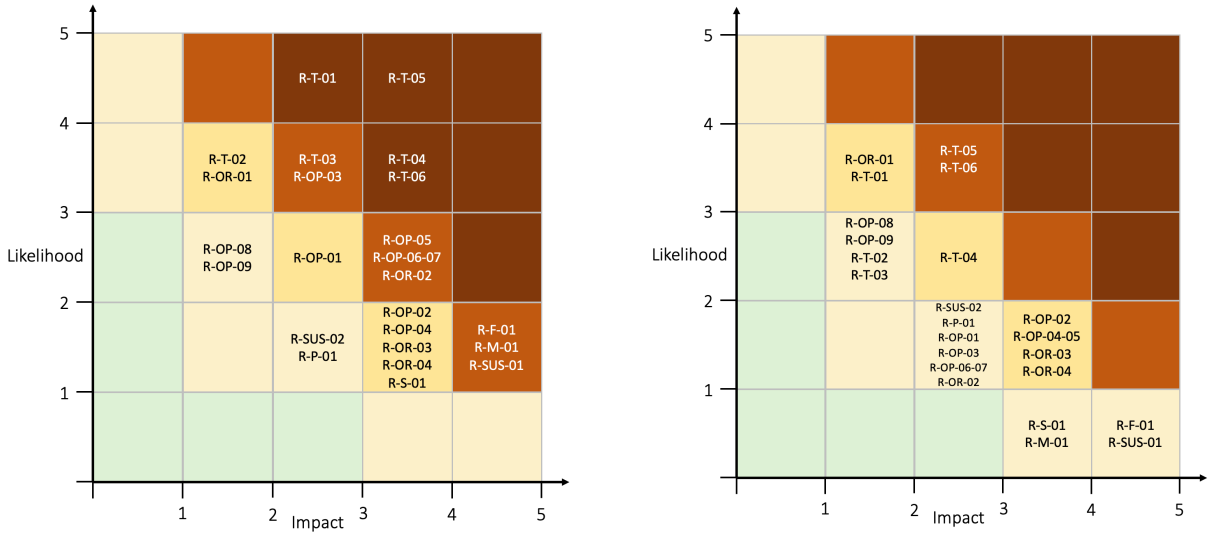

(a) Risk map

(b) Risk map after mitigation

Figure 5.1: Risk map before and after mitigation strategy has been applied

5.4. Risk Mitigation

From the risk map, it became clear that several risks are unacceptable and need to be addressed. These risks have a risk factor of ten or higher. Unacceptable risks are mitigated using the mitigation strategies described in Table 5.5. Here the mitigation's ID, description of the mitigation strategy, the team member responsible for the strategy, and the risk being addressed by the strategy are present. In the mitigation column in Table 5.3 the mitigation strategies which are relevant for the corresponding risk are mentioned. The three columns right of this mitigation column score the new likelihood, impact, and risk factor of the risk after the mitigation strategy has been applied. Important to mention is that all the risks, even the ones which are not mitigated, are managed in the manner described in the management column in Table 5.4.

Table 5.5: Mitigation strategy with a description, team member responsible and the risk which is being addressed with the mitigation strategy

Mitigation ID	Description	Team member responsible	Risk addressed
M-01	Meet with aerodynamics specialist	Aerodynamics Engineer	R-T-01, R-OR-02
M-02	Meet with hydrodynamics specialist	Hydrodynamics Engineer	R-T-02
M-03	Perform Verification and Validation in early stage	Quality Control manager	R-T-03, R-T-04, R-S-01
M-04	Meet with water planes specialist	Project leader	R-T-04
M-05	Meet with structures specialist	Structural Engineer	R-OP-03
M-06	Meet with materials specialist	Materials Engineer	R-OP-01
M-07	Meet with propulsion specialist	Propulsion Engineer	R-T-05, R-OP-02
M-08	Sustainability manager makes sure the emissions during the operation are minimized	Sustainability manager	R-OP-04
M-09	Perform control and stability analysis	Control and Stability Engineer	R-OP-06, R-OP-07, R-OP-09
M-10	Keep budgeting of subsystems up to date	System Engineer, Product Manager	R-F-01
M-11	Regular maintenance on all subsystems	System engineer	R-OP-05
M-12	Regular meeting with client	Project Leader	R-M-01, R-SUS-01

These mitigated risks are again put into a risk map to visualize the severity of the risks. This map can be seen in Figure 5.1b. Although most risks are mitigated to an acceptable level, two remain unacceptable. This risk is R-T-05 and R-T-06. For these risks, a contingency plan is needed. This plan will be described in Section 5.5.

5.5. Contingency Plan

A contingency plan has been made since two risks lie in the dangerous or extreme severity zone even after the mitigation strategy has been applied. These risks are R-T-05 and R-T-06 which are insufficient propulsion power and insufficient battery capacity respectively. These risks are present due to the propulsion system.

There is much uncertainty regarding the capability of the plane taking off from water as there can exist a rapid snowball effect of an increase in weight requiring more batteries and thus weight. The contingency plan is a preparation for the situation where the propulsion system is not a feasible design. The contingency strategy consists of precautions, which are stated in Table 5.6.

Table 5.6: Label and strategy of the contingency with the team member responsible and the relevant risk being addressed

Label	Contingency Strategy	Responsibility	Risk addressed
C-1	Design the plane to be launched using a winch or an aero tow. This design ensures that if the propulsion system does not have enough thrust or the battery does not have enough capacity to take-off from water, the winch can be used for the launch, and the propulsion system can be used as a sustainer.	Structural engineer	R-T-05, R-T-06

As a further note, if the propulsion system does have sufficient power and battery capacity, then the winch launch could still be used to increase the range. For example the water sailplane could be winch launched then fly to a sandbank and fly back on its own power since the battery was unused during the first take-off.

6. Requirements

To provide a framework for how the design will fulfill the mission, it is necessary to generate requirements. These requirements will provide a reference for how each system should be designed and what parameters it must achieve to fulfill the mission goal. Section 6.1 presents the requirements that have come directly from the stakeholder, and presents the wishes of the client within an engineering context. From there, it is possible to combine the stakeholder requirements with aspects from the Market Analysis, Functional Analysis, Sustainability Development Strategy, Technical Risk Assessment, and regulations, and obtain system requirements. Through the requirement discovery tree, the full list of system requirements is obtained. The system requirements are elaborated upon in Section 6.2.

6.1. Stakeholder Requirements

The top level user requirements have been processed to the stakeholder (SH) requirements in accordance with the client meetings with TMA and represent the client wishes for the design of the water sailplane (WS). Although technically all requirements should be SMART (specific, measurable, attainable, realistic, time-bound), the stakeholder requirements are not. They represent the direct wishes of TMA, with as few changes as possible. The system requirements in the following sections are SMART and go into more detail than the stakeholder requirements. The third column indicates whether the requirement is *Driving*, *Key*, or *Killer*. Killer requirements drive the design beyond an optimum point, sacrificing other areas and were modified or removed. Driving requirements have a large influence on the final design, while Key requirements are simply important to achieving the mission.

Some stakeholder requirements require contextualization:

- **SH-03:** From client meetings it became clear that the weather in the Maldives is difficult to predict and can rapidly change from blue skies to gusty storms. This drives the design to be able to cope with the changing weather conditions.
- **SH-05-06:** The client needs an aircraft that is continuously operable while not down for maintenance. This requires the aircraft to be inspectable and maintainable on water.

- **SH-07:** TMA desires that their fleet is operative most of the time, and with the limited resources they have at hand, maintenance cannot occur too often. Therefore, they need a maintenance interval of at least 8 weeks.
- **SH-09:** With the initial client demands, this was first deemed as a killer requirement. After a client meeting the requirement was reformulated to its current state, which turned it into a driving requirement. The wave height follows from historical data of the average wave height in the Maldives around atolls [9].
- **SH-12:** A noise level of higher than $70\,\mathrm{dB}$ can feel uncomfortable after prolonged exposure.[1] Therefore an interior noise level budget of $70\,\mathrm{dB}$ at cruise is set.
- **SH-16:** The client wants to offer sightseeing tours for 2 passengers at a time. This requirement is driving the design, as it is unconventional and has a substantial impact on sizing.

Table 6.1: List of stakeholder requirements

Identifier	Requirement	Type
REQ-WS-SH-01	The WS shall perform sightseeing flights for tourists	Driving
REQ-WS-SH-02	The WS shall have no accidents leading to physical harm	Driving
REQ-WS-SH-03	The WS shall be able to land in changeable weather conditions	Driving
REQ-WS-SH-04	The WS shall have analog avionics	Key
REQ-WS-SH-05	The WS shall be inspectable on water	Driving
REQ-WS-SH-06	The WS shall be maintainable on water	Key
REQ-WS-SH-07	The WS shall have 8 weeks between required maintenance	Driving
REQ-WS-SH-08	The WS shall be corrosion resistant	Driving
REQ-WS-SH-09	The WS shall be able to land on high waves of $0.3\,\mathrm{m}$	Driving
REQ-WS-SH-10	The WS shall have a total price of $500\,000\,\mathrm{USD}$, including pilot training costs	Key
REQ-WS-SH-11	The WS shall have operational costs of $25\,000\,\mathrm{USD}$ per month	Key
REQ-WS-SH-12	The WS shall not have an interior noise level higher than $70\,\mathrm{dB}$	Driving
REQ-WS-SH-13	The WS shall have a luxurious interior	Driving
REQ-WS-SH-14	The WS shall perform aerobatic maneuvers	Key
REQ-WS-SH-15	The WS shall not cause motion sickness during flights	Driving
REQ-WS-SH-16	The WS shall have an occupancy of 2 passengers and 1 pilot	Driving

6.2. System Requirements

The system requirements have been grouped by: Water operations, Aerodynamics, Operational, Stability, Controllability, Payload, Aerodynamics, Power, Structural, Cost, Logistics, Safety, Regulations, Sustainability, Comfort and Reliability. The system requirements are more elaborate than any requirements specified by the client and are used to ensure engineering decisions are made in compliance with market research and the intended functions of the water sailplane.

In total, 63 system requirements were defined, however, not all requirements could be addressed during this stage of the design phase. Therefore only 39 requirements were covered, where each requirement is presented at the beginning of the relevant chapters. All requirements will be summarized in Chapter 26.

[1] https://www.cdc.gov/nceh/hearing_loss/what_noises_cause_hearing_loss.html [Accessed: 25 Nov 2021]

7. Trade-off Summary and Concept Overview

Following the requirement analysis design options and eventually preliminary concepts were developed in the initial stages of the project. This chapter summarizes the initial concept options in Section 7.1, the trade-off methodology and results in Section 7.2 with a Class I weight estimation of the preliminary concept.

7.1. Initial Concepts

To generate concepts the team first had a brainstorming session to consider design options for five subsystems: the empennage configuration, flotation device, wing configuration, air propulsion system, and water propulsion system. For brevity, the complete set of design options is not included in this report.

Following the list of design options, those deemed most unrealistic were excluded from the concept generation. Eventually, three concept options were concluded based on the combination of subsystem options listed int the previous paragraph. They are summarized in Table 7.1:

Table 7.1: Concept overview

Concept	Empennage	Flotation	Wing	Air propulsion	Water propulsion
Concept 1	T-tail	Flying boat	High	Sustainer	None
Concept 2	V-tail	Catamaran	High	None	Motor
Concept 3	Cruciform	Floats	Mid	Self-launch	None

7.2. Trade-off Method and Results

In order to reach a final concept a trade-off of individual subsystem options was made, rather than of global concepts. The reasoning for this method was that there is no existing water sailplane design to generate a well supported concept. As a result of this limitation, there was a reasonable risk of a well performing subsystem being overlooked in a poorly configured concept.

7.2.1. Method

Four subsystems were considered in the tradeoff: the flotation device, propulsion method, wing configuration, and empennage configuration. Each had various options within the subsystem, summarized by Table 7.2:

Table 7.2: Overview of design options per subsystem

Empennage	Flotation	Wing	Air-prop	Water-prop
T-tail	Floats	Mid	Self-launch	None
Cruciform	Flying boat	High	Sustainer	Motor
V-tail	Catamaran		None	

Each option, in turn, was evaluated concerning a number of criteria. Criteria were established with the client demands in mind and confirmed their satisfaction by presenting them in a meeting. Weights were attributed to each of the criteria by an Analytical Hierarchy Process (AHP) method, as they are not of equal importance. A summary of the criteria, their definition, and respective weights are provided in the list below:

- **Safety (40%):** The minimization of risk - where risk is quantified by the probability times impact
- **Performance (35%):** The evaluation of hydro and aerial performance in terms aerodynamic drag, hydrodynamic stability, hydrodynamic resistance, and glide time.
  - **Glide time (40%)**

  - **Aerodynamic drag (35%)**
  - **Hydrostatic stability (10%)**
  - **Hydrodynamic resistance (10%)**

- **Maintainability and inspectability (20%):** The energy that is required to maintain and inspect the aircraft or its subsystem to keep it operable.
- **Autonomy (15%):** The ability of the aircraft to perform its operations without the use of systems outside of its own structure.

Note that the performance category was split into four additional categories with their own respective weights in order to provide a more detailed analysis of each subsystem.

7.2.2. Results

Using the methodology presented in Section 7.2.1 concluded that the best performing concept would make use of: a self-launching air propulsion system, floats as the flotation device, a high wing configuration, T-tail, and no water propulsion. This was verified with a sensitivity test, which for brevity is not included in the report. Figure 7.1 shows a sketch of the concept:

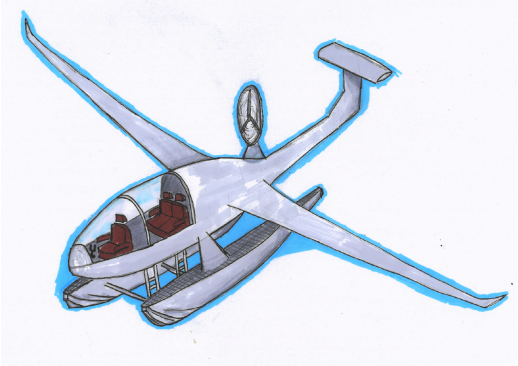

Figure 7.1: Preliminary concept following trade-off

With the final preliminary concept decided upon a Class I weight estimation was made. This relied on the statistical regression of sailplanes for the aircraft body and floatplanes to estimate the floats. The result provided an estimation of $962\,\mathrm{kg}$, and is the starting point for the design in Part II.

II

Initial Design

8. Verification & Validation Procedures

Throughout the project, design tools were developed in Excel and Python to design and analyze the performance of the water sailplane. To determine confidence on the level of correctness, each of these tools had to be verified. To determine the usefulness of the tools their validity had to be assessed. This chapter explains the procedures that were used in order to both verify and validate the results obtained from the developed tools. Section 8.1 will discuss the unit and system tests planned to verify the tools used during the DSE. Following that, Section 8.2 will discuss the validation methods that were performed, as well as validation methods that could be used after the DSE project to further validate the results obtained from the design and analysis tools.

8.1. Verification

Verification is essential to ensure the simulated model accurately describes the physical system that it simulates. The simulated model can consist of multiple tools which each have to be verified. This consists of both ensuring no errors are present in the model, for example coding errors, and that the results fall within an expected range. This section discusses the unit and system tests that were performed after design tools were developed.

8.1.1. Unit Testing

Unit testing was performed by testing individual components or building blocks of a certain tool, to ensure each component performs its task within the tool correctly. Seven different unit tests were performed. Each of these tests was given a unique label to effectively show the results in the following design chapters. A short description of each test is given below. For all tests, it holds that they were only applied to tools where this was relevant.

Unit Tests:

UT 00: Zero Test - Insert the number '0' as an input, and ensure tools adequately handle this input.

UT 01: Compile Test - Run the tool to ensure a code compiles and encounters no syntax errors

UT 02: Sign Test - Change the sign of an input, and verify the output changes sign accordingly.

UT 03: Relation Test - Change an input (e.g. double it), and verify that an output changes according to the expected relation (e.g. for a quadratic relation doubling the input should quadruple the output).

UT 04: Discretization Test - Plot the discretization error, and ensure the error is below an accepted limit

UT 05: Unit Conversion Test - Manually perform unit conversion calculations to check these are correctly performed.

UT 06: Unit Matching Test - Verify that an output is in the expected units (e.g. a force should be outputted in N or $\mathrm{kg\,m\,s^{-2}}$

8.1.2. System Testing

System testing was done to check that the combination of the components of a tool did not introduce additional errors and that the relationships between the components were accurately implemented. Furthermore, system tests were performed to analyze if the developed tool produced the results it was made for and if these were within reasonable accuracy levels.

The unit tests described previously could also be performed on system level and are not described again here. Only the two unique system tests are described below. For this reason these test labels start at 7, as the system test corresponding to a unit test would simply be called **ST XX**.

System Tests:

ST 07: **Assumption Testing** - Verify that an assumption made in developing a tool does not produce incorrect or inaccurate results by comparing it to the results of a (simple) case that does not use this assumption

ST 08: **Analytical Comparison** - Compare the results from the numerical model to an analytical calculation (e.g. manually calculate the lift at a certain velocity and check the numerical model produces a similar result)

ST 09: **Domain Test** - Input a range of values outside of the domain the tool is developed for, and check it does not continue operating normally

ST 10: **Model Comparison** - Compare the results obtained from the developed tool to another model found in literature (e.g. plot the results and check if the shape and range of the plot is comparable to a graph in a book representing the same system)

8.2. Validation

Validation was done to determine the predictive capability of a model for its intended use by comparing the model outcome to existing data. This was be done for all the results presented in the final report. Four validation procedures were determined and are described below. Due to the limited time available for the DSE project, it was not possible to perform the last two validation procedures. For completion they are, however, still mentioned in this section. In Chapter 29 it is shown when these validation procedures would be performed after the DSE project.

Validation Procedures:

VP 01: **Parameter Validation** - Compare the resulting design parameters to parameters from existing aircraft (e.g. wing span and MTOW)

VP 02: **Analysis Validation** - Compare the results obtained from an analysis to existing (experimental) data from literature (e.g. compare estimated glide performance to flight test data)

VP 03: **Advanced Model Validation** - Use advanced models and tools like Finite Element Methods (FEM) and Computational Fluid Dynamic analysis (CFD) to validate results obtained from the less advanced tools used in the conceptual design phase

VP 04: **Testing Validation** - Validate results by performing small- and full-scale prototype testing (e.g. wing bending, wind tunnel, tank towing & flight tests)

8.3. V&V Procedure

As each respective aircraft subsystem undergoes various calculations throughout the design phase, each design tool must undergo verification and validation tests to ensure that the results are reliable and reflective of the requirements.

Simple verification tests can be quickly tested and thus, only the results will be displayed in a tabular form as exemplified by Table 8.1. More complex tests, such as **UT 04** or **ST 08** may be accompanied by a graph to display the results or show relative differences.

More in-depth verification or validation tests such as **ST 07** or **VT 01** will be accompanied by an in-depth explanation, and may also include results in either graphical or tabular form to showcase the impact of the assumption on the final result.

Table 8.1: Example of typical presentation of unit and system tests

ID	Parameter	Input	Pass Condition	Test Result	Pass or Fail	Comments
UT 02	V	$-$	$+$	$-$	Fail	Mistake found. Missing brackets
UT 02	V	$+$	$+$	$+$	Pass	
UT 06	$T(V)$		N	$\mathrm{kg\,m\,s^{-1}}$	Pass	
ST 06	P_a		W	$\mathrm{kg\,m^2\,s^{-3}}$	Pass	

9. Design Tools

In this chapter, several tools are highlighted that were used for the start of the design of the water sailplane. In Section 9.1 the determined mission profile for the water sailplane is highlighted. Section 9.2 covers the wing and power loading diagrams that were used to determine a design point, and Section 9.3 shows the flight envelope diagrams that were used to determine the load factors the water sailplane would be designed with.

9.1. Mission Profile

Before starting the design of the water sailplane, a mission profile needed to be defined. The requirement relevant for the mission profile can be seen in Table 9.1. The client wished for the water sailplane to be able to perform gliding flights of 15 minutes. It was however decided to design the water sailplane to be able to glide for 30 minutes. This way, if the design would end up having a lower performance than designed for, the wish of the client would still be exceeded, or in case of a higher performance drop, still meet the wishes of the client. The mission profile that made for the water sailplane is shown in Figure 9.1:

Table 9.1: Mission profile requirements

Identifier	Requirement
REQ-WS-FLPE-AER-04	The WS shall have a service ceiling H_{max} of FL100

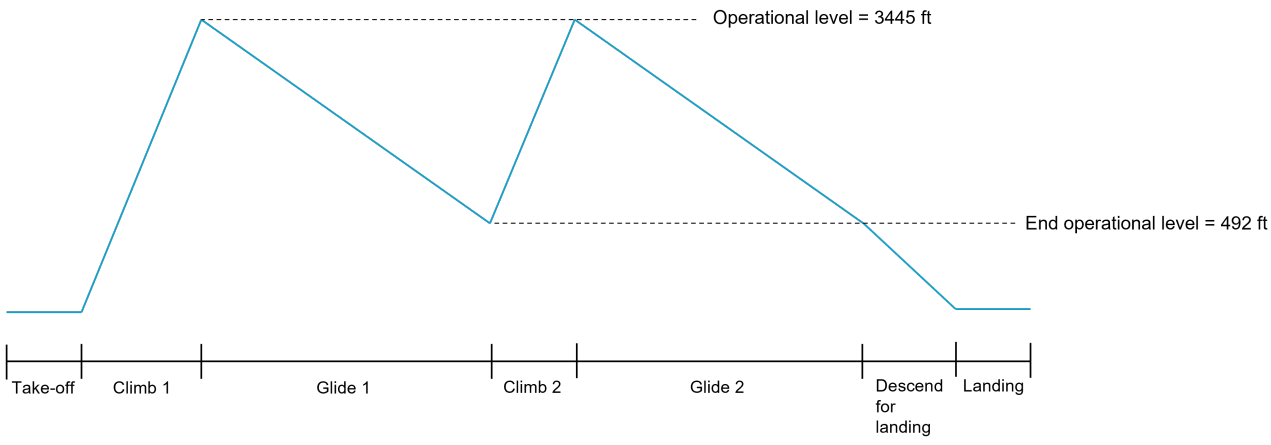

4

Figure 9.1: Mission Profile

Because the gliding flights would be scenic tours of the Maldives, it is preferred to fly relatively low. However, the water sailplane would have to start gliding at a sufficient enough height to glide for the desired 30 minutes.

Assuming the descent rate requirement of $1\,\mathrm{m\,s^{-1}}$ would be met, it was determined that the water sailplane would climb to an operational level of $3445\,\mathrm{ft}$ after take-off, then glide to a height of $492\,\mathrm{ft}$ over a duration of 15 minutes. When this height is reached, the water sailplane climbs to the operational level once again, to then glide for another 15 minutes, after which the descent for landing is initiated.

9.2. Wing Loading - Power Loading Diagram

To obtain an initial design point, a wing loading versus power loading diagram is constructed. This diagram relates the wing surface area and the brake power of the aircraft based on their ratio to the weight of the aircraft. The wing loading (W/S) determines the required size of the wing surface area, while the power loading (W/P) determines the brake power required from the aircraft.

Both the wing loading and power loading requirements come from an analysis of the various flight conditions of the aircraft. By relating the two variables, a feasible design space is found, which can then be used as the initial design point. The requirements relevant for the wing loading can be seen in Table 9.2.

Table 9.2: Wing loading requirements

Identifier	Requirement
REQ-WS-WATO-07	The WS shall have a water take-off distance of $400\,\mathrm{m}$
REQ-WS-WATO-08	The WS shall have a water landing distance of $300\,\mathrm{m}$
REQ-WS-WATO-13	The WS shall have a V_{LOF} of $1.3 \cdot V_{s1}\ \mathrm{m\,s^{-1}}$ at MTOW
REQ-WS-WATO-14	The WS shall have a V_a of $1.3 \cdot V_{s1}\ \mathrm{m\,s^{-1}}$ at MTOW
REQ-WS-FLPE-AER-01	The WS shall achieve a climb rate of $4\,\mathrm{m\,s^{-1}}$
REQ-WS-FLPE-OPL-01	The WS shall have a V_{S_0} of $80\,\mathrm{km\,h^{-1}}$ in landing configuration
REQ-WS-FLPE-PAY-12	The WS shall have a MTOW of $1250\,\mathrm{kg}$

9.2.1. Assumptions & Initial Design Parameters

To obtain an initial design point, several assumptions were made to simplify calculations and thereby provide ballpark estimates of the aircraft constraints. For all the following sizing procedures, the following assumptions were made, where **IS** is short for Initial Sizing assumptions.

IS 01: Symmetric flight assumption. This assumes the aircraft is flying horizontally and that there are no net lateral forces. Thus the aircraft does not experience sideslip, yaw or roll.

IS 02: Steady flight assumption. This implies the aircraft's flight path and velocity are constant. This dramatically simplified the analysis, which at this stage of the design process is acceptable.

IS 03: Zero thrust angle of attack. This assumes the thrust vector coincides with the velocity vector. As the propulsion system has not been designed, this is an unknown and thus this assumption must be made.

IS 04: Small angle approximation for the flight path. This assumes that throughout any non-horizontal flight phase such as climb or landing, the flight path angle (γ) is small enough that $\cos\gamma \approx 1$.

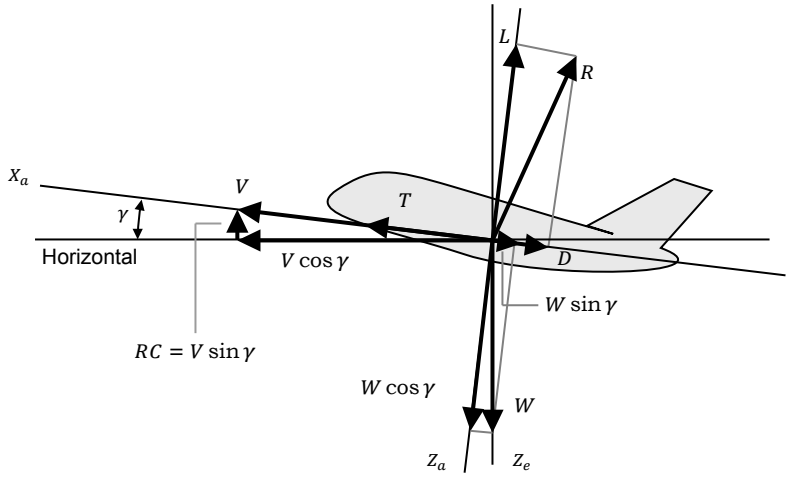

Figure 9.2: Diagram of an aircraft assuming steady symmetric flight

In order to perform the various calculations required for the sizing, some values were assumed or given a range. Two primary free variables were the maximum lift coefficient ($C_{L_{max}}$) and the wing aspect ratio (A). These values were assumed based on reference data of various sailplanes resulting in the ranges displayed in Table 9.3

Table 9.3: Initial design parameters for lift coefficient and aspect ratio

Lift Coefficient		**Aspect Ratio**	
$C_{L_{max1}}$	1.4	A_1	24
$C_{L_{max2}}$	1.5	A_2	27
$C_{L_{max3}}$	1.6	A_3	30

9.2.2. Sizing for Stall Speed

Given the above assumptions, sizing for the stall speed becomes a function of only the wing loading, as it has no relation to the power loading. Assuming steady horizontal flight, then the vertical forces are in equilibrium hence the lift must be equal to the weight of the aircraft. By expanding the equation for lift, the weight and wing surface area can be related, yielding equation Equation (9.2). [10]

From requirement **REQ-WS-FLPE-OPL-01**, a maximum stall speed of $80\,\mathrm{km\,h^{-1}}$ is defined [3]. As low speed operations are desirable for the design and mission profile, an initial design stall speed of $60\,\mathrm{km\,h^{-1}}$ or equivalently $16.67\,\mathrm{m\,s^{-1}}$ was chosen. As cruise conditions are limiting in terms of wing loading, an air density at an altitude of $1050\,\mathrm{m}$ was used.

$$W = L = C_L \frac{1}{2}\rho V^2 S \tag{9.1}$$

$$(W/S) = C_{L_{max_{clean}}} \frac{1}{2}\rho V_{s1}^2 \tag{9.2}$$

9.2.3. Sizing for Take-Off Performance

The sizing for take-off is dependent on the take-off distance, where the take-off distance is defined as the total distance covered from the initial acceleration until the aircraft reaches a screen height of $50\,\mathrm{ft}$ or approximately $15.2\,\mathrm{m}$ [11]. The take-off distance is proportional to a take-off parameter (TOP), defined by Equation (9.3) [10]. However, as the empirical formulas used assume take-off from land, some corrections must be applied. As there are no reference water sailplanes, an initial estimate of the water take-off distance was based on the take-off distance of the DHC-6 Twin Otter. A Twin Otter has a take-off distance of approximately $600\,\mathrm{m}$.[1] It was assumed that all possible locations where the water sailplane would be utilized would be a location that was also served by TMA's current fleet of Twin Otters. To build some margin for sandbank's or lagoon visits, a water take-off distance of $400\,\mathrm{m}$ was used.

$$s_{TO} \propto TOP = \left(\frac{W}{S}\right)\left(\frac{W}{P}\right)\frac{\rho_0}{\rho}\frac{1}{C_{L_{TO}}} \tag{9.3}$$

[1] https://teamjas.com/twin-otter-on-floats/ [Accessed: 21 Dec 2021]

According to Mees, a seaplane has a water take-off distance between 1.1 and 1.5 times greater than an equivalently configured landplane when at sea level [12]. By applying this upper bound factor, the equivalent land take-off distance would approximately equal $267\,\mathrm{m}$. By applying this distance to an empirical relation provided by Raymer, a take-off parameter (TOP) of $100\,\mathrm{lbf^2\,ft^{-2}\,hp^{-1}}$ is obtained, which is converted to a final TOP of $28.56\,\mathrm{N^2\,m^{-2}\,W^{-1}}$.

As the aircraft will be operating in the Maldives, it is assumed that it will take-off from sea level pressure, and thus the air density ratio ρ/ρ_0 is assumed to equal 1. To obtain an initial estimate for the take-off lift coefficient, the relation defined by Roskam is used, presented as Equation (9.4). By rearranging Equation (9.3), the wing loading can be related to the power loading resulting in Equation (9.5).

$$C_{L_{TO}} = \frac{C_{L_{max}}}{1.21} \tag{9.4}$$

$$(W/P) = \frac{TOP \cdot C_{L_{TO}}}{(W/S)} \tag{9.5}$$

9.2.4. Sizing for Landing

Sizing for landing was based on approach conditions. As defined by requirement **REQ-WS-WATO-14**, the aircraft shall have an approach speed of $1.3V_{s1}$. Landing assumed sea level conditions, and the same $C_{L_{max}}$ values specified in Table 9.3. Furthermore, it was assumed the aircraft would use battery electric motors, and thus the landing weight would be equal to the maximum take-off weight. By applying the same expansion, where it is assumed the lift is equal to the weight, expression Equation (9.6) was obtained.

$$(W/S) = C_{L_{max_{land}}} \frac{1}{2} \rho V_{land}^2 \tag{9.6}$$

9.2.5. Sizing for Cruise

To obtain a relation between the wing loading and power loading for cruise conditions, it is assumed that the aircraft is flying at steady, stable horizontal flight conditions. While it is not expected that the aircraft will operate at a constant altitude during operations, as defined by the mission profile in Section 9.1, ensuring the aircraft is capable of cruising if necessary will ensure the design point does not omit aircraft capabilities.

Assuming steady, stable horizontal flight, then it follows that the aircraft is in equilibrium. Therefore the drag force is equal to the thrust force and thus the power available must equal the power required. Note that this assumes the thrust vector is parallel to the drag vector.

$$P_a = P_r \tag{9.7}$$

$$P_a = \eta_p P_{br} \tag{9.8}$$

$$P_r = DV \tag{9.9}$$

By expansion of the relation, it is possible to relate the wing loading to the brake power of the aircraft. Note, however, that the power generated by the aircraft decreases when at higher altitudes, as the air becomes thinner, and thus an altitude compensation factor must be applied. Furthermore, it is assumed that the aircraft is not at full thrust during cruising conditions and thus a power setting fraction ($P_{setting}$) is applied.

$$P_{cruise} = P_{TO} \left(\frac{\rho}{\rho_0} \right)^{0.75} \tag{9.10}$$

$$\frac{\rho}{\rho_0} = \left(1 + \frac{\lambda h}{T_0} \right)^{-\left(\frac{g_0}{R\lambda}+1\right)} \tag{9.11}$$

Combining the various expressions yields Equation (9.12), which can then plot the relation between wing loading and power loading. As various parameters such as C_{D_0}, η_p, e are unknown, these were based on typical values for CS-23 seaplane aircraft. This was done on the basis that the aircraft would make use of floats and thus seaplane aircraft were seen as more comparable than reference sailplanes. A summary of the initial parameters used is available in Table 9.4.

Table 9.4: Initial parameters used to perform sizing

Parameter	Value	Parameter	Value
$h\ [m]$	1000	$P_{setting}$	0.9
C_{D_0}	0.028	η_p	0.8
e	0.78		

$$(W/P) = P_{setting}\eta_p \left(\frac{\rho}{\rho_0}\right)^{0.75} \left(\frac{C_{D_0}\frac{1}{2}\rho V^3}{(W/S)} + \left(\frac{W}{S}\right)\frac{2}{\pi Ae\rho V}\right)^{-1} \tag{9.12}$$

9.2.6. Sizing for Climb Rate

Based on the assumptions **IS 01-IS 04**, the following equilibrium equation can be created for the aircraft's relative horizontal components.

$$T = D + W\sin\gamma \tag{9.13}$$

$$\sin\gamma = \frac{T-D}{W} \approx \gamma \tag{9.14}$$

Given the expression for the climb rate (RC), and the expression for power available and power required, then the climb rate can be expressed in terms of the power available and the power required, as seen in Equation (9.15).

$$RC = \frac{P_a}{W} - \frac{P_r}{W} \tag{9.15}$$

By expanding terms, the climb rate equation can be reformulated to Equation (9.16).

$$RC = \frac{n_p P_{br}}{W} - \frac{\sqrt{(W/S)}\sqrt{2}}{\frac{C_L^{1.5}}{C_D}\sqrt{\rho}} \tag{9.16}$$

To maximize the climb rate, the ratio $\frac{C_L^{1.5}}{C_D}$ must be maximized [10]. This ratio is maximized when the following two conditions are met:

$$C_{L_{RC_{max}}} = \sqrt{3C_{D_0}\pi Ae} \tag{9.17}$$

$$C_{D_{RC_{max}}} = 4C_{D_0} \tag{9.18}$$

Evaluating these expressions it is possible to substitute and rearrange Equation (9.16) to yield Equation (9.19). A climb rate of $4\,\mathrm{m\,s^{-1}}$ was chosen as the desired climb rate. The remaining unknowns are the same as for the cruise condition and visible in Table 9.4.

$$(W/P) = \frac{n_p}{RC + \frac{\sqrt{(W/S)}\sqrt{\frac{2}{\rho}}}{1.345\frac{(Ae)^{0.75}}{C_{D_0}^{0.25}}}} \tag{9.19}$$

9.2.7. Sizing for Climb Gradient

Applying the same assumptions for the climb rate, it follows that the climb gradient can be expressed as Equation (9.20).

$$\frac{RC}{V} = \sin\gamma \approx \gamma = \frac{P_a - P_r}{WV} \tag{9.20}$$

Performing a similar set of expansions of the expression yields Equation (9.21)

$$\gamma = \eta_p \frac{P_{br}}{W\frac{1}{\sqrt{\frac{W}{S}\frac{2}{\rho}\frac{1}{C_L}}}} - \frac{C_D}{C_L} \tag{9.21}$$

Optimizing the above function, however, results in a C_L value very close to $C_{L_{max}}$. Therefore, a safety margin is built in resulting in the C_L values equaling $C_{L_{max}} - 0.2$. Rearranging the equation results in Equation (9.22). A climb gradient of 0.144 was used based on the ratio of the desired climb rate to the cruise speed of $27.78\,\mathrm{m\,s^{-1}}$

$$(W/P) = \frac{n_p}{\sqrt{(W/S)}\left(\gamma + \frac{C_D}{C_L}\right)\sqrt{\frac{2}{\rho}\frac{1}{C_L}}} \tag{9.22}$$

9.2.8. Feasible Design Space & Initial Design Point

By plotting the various functions outlined, a wing loading - power loading diagram can be constructed. Using the initial design parameters from Table 9.3, various lines for each sizing condition could be plotted showing how each condition changes based on the design parameters. As can be seen in Figure 9.3, the lines create restrictions as a specified wing loading and power loading is required to meet each sizing condition. These restrictions outline the feasible design space, shown in green.

To optimize the design while ensuring compliance with each of the sizing conditions, the top right corner of the feasible design space is chosen. This maximizes the wing loading and the power loading resulting in the smallest possible wing surface area and brake power.

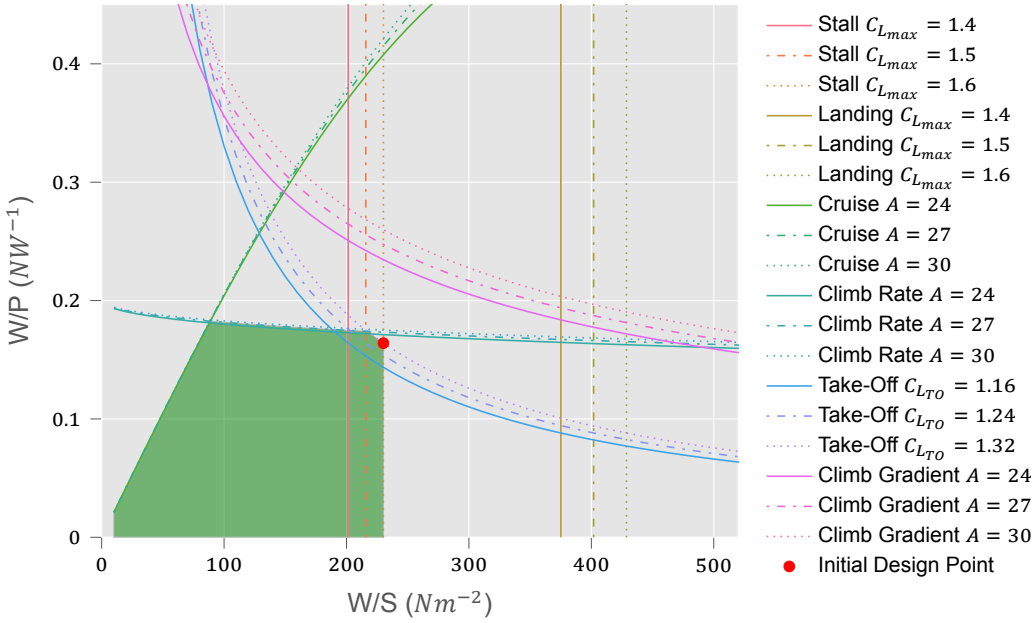

Figure 9.3: Complete Wing Loading - Power Loading Diagram with the feasible design space shown in green for $A = 27$ and $C_{L_{max}} = 1.6$

As can be seen in Figure 9.3, the top right corner is cut out due to the take-off condition. As a result, the rightmost vertex is chosen instead, as this would minimize wing surface area. It was determined that minimizing wing surface area would be more important than minimizing the brake power of the aircraft, as the additional weight and drag of a larger wing would have a more severe impact on flight performance than a slightly heavier electric motor.

Therefore an initial design point was chosen with $W/S = 230.155$ and $W/P = 0.164$. Using the initial MTOW value of $962\,\mathrm{kg}$ a wing surface area of $40.990\,\mathrm{m}^2$ was found with a brake power of $57.49\,\mathrm{kW}$. Note that this plot would be iterated throughout the design process.

9.3. Flight Envelope

With the use of a flight envelope, the operation limits of the aircraft are found. Such a flight envelope is often represented by a V-n graph in which the horizontal axis denotes the airspeed (V), and the vertical axis denotes the load factor (n). When an aircraft exceeds the limits of its flight envelope structural damage to the sailplane may occur. The V-n graph consists of two envelopes, which are the maneuvering and gust envelope. These are explained in the following sections. Due to the time restraints of this project only the clean flying configuration is explored. The requirement relevant for the flight envelope are can be seen in Table 9.5.

Table 9.5: Flight envelope requirements

Identifier	Requirement
REQ-WS-FLPE-OPL-08	The WS shall fly with a gust wind of $15\,\mathrm{m\,s^{-1}}$ acting normal to the flight path at the design gust speed V_B
REQ-WS-FLPE-OPL-09	The WS shall fly with a gust wind of $7.5\,\mathrm{m\,s^{-1}}$ acting normal to the flight path at the maximum design speed V_D
REQ-WS-REGS-01	The WS shall comply with EASA CS-22 regulations

Table 9.5 – continued from previous page

Identifier	Requirement
REQ-WS-REGS-03	The WS shall comply with relevant EASA CS-23 regulations
REQ-WS-FLPE-PAB-01	The WS shall perform select aerobatic maneuvers under the Utility category of the CS-22 airworthiness regulations

9.3.1. Maneuvering Envelope

Firstly, the maneuvering envelope is calculated using the method described in [3]. From the CS-22 requirements the load factors seen in Table 9.6 are found. However, the highest positive load factor is changed because after multiple iterations the load factor of 5,3 was unable to be reached. Thus from the CS-23 requirements, the positive load factor was used. This load factor is 4.4. Here V is some trivial velocity faster than V_{stall} yet slower than V_A. V_A is the Design Maneuvering Speed and V_D is the Design Maximum Speed. The V_A is calculated using Equation (9.23), with n_{V_a} being 4.4 and the V_{stall} being the stall speed. V_D Is found using Equation (9.24), with $\frac{W}{S}$ in $\mathrm{daN/m^2}$ and C_{Dmin} being the lowest possible drag coefficient of the sailplane. These two variables were estimated, using an iterative process, to be 43.42 and 0.03195 respectively.

Table 9.6: Limit maneuvering load factors

Velocity	Load Factor	
	Positive	Negative
V	-	-2.65
V_A	4.4	-
V_D	4	-1.5

$$V_a = V_{S1}\sqrt{n_{V_a}} \tag{9.23}$$

$$V_D = 18\sqrt[3]{\frac{W}{S}\frac{1}{C_{Dmin}}} \tag{9.24}$$

With the aforementioned load factors and equations, the maneuver load diagram was made. On the horizontal axis, the velocity ranges from zero to V_D and on the vertical axis the load factor ranges from 4.4 to -2.65 as stated in Table 9.6. The positive load factor is calculated using Equation (9.25) and the negative load factor with the same equation but with $-n$ instead of n. The air density ρ was assumed to be constant. The $C_{l_{max}}$ with high lift devices is 1.8145.

$$n = \frac{1}{2}\rho C_{l_{max}} V \tag{9.25}$$

This resulted in the maneuvering envelope which can be seen in Figure 9.4a. V_A was found to be $42.61\,\mathrm{m/s}$ and V_D $64.85\,\mathrm{m/s}$. Notice the straight lines from V_A to V_D. This is stems from the requirements in CS-22[3]. The magnitude of the limit maneuvering load factors is lower at V_D than it is at V_A. Also, notice the speed were the maneuvering envelope is one g is the stall speed, which is $20.32\,\mathrm{m/s}$. Lastly, the highest negative load factor is reached at $33\,\mathrm{m/s}$, this V can be seen in Table 9.6.

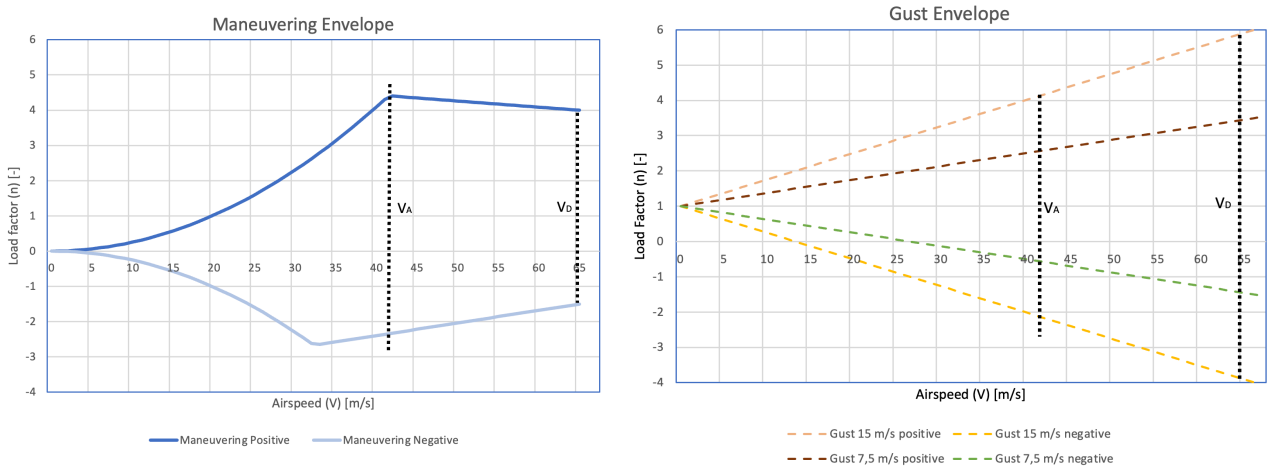

(a) Maneuvering Envelop

(b) Gust Envelope

Figure 9.4: Maneuvering and Gust Envelope

9.3.2. Gust Envelope

Secondly, the gust envelope was calculated using the method described in the certification specification for sailplanes [3]. From this the gusts speeds, which the sailplane must be able to withstand, are obtained. These are $15\,\mathrm{m/s}$ for the V_A and $7.5\,\mathrm{m/s}$ for the V_D. The gust load factors are computed with the use of Equation (9.26).

$$n = 1 \pm \left[\frac{\frac{k}{2}\rho_0 UVa}{\frac{mg}{S}} \right] \qquad with, \qquad k = \frac{0.96\frac{\mu}{H/l_m}}{0.475\frac{\mu}{H/l_m}} \tag{9.26}$$

μ and H defined as,

$$\mu = \frac{2\frac{m}{S}}{\rho l_m a} \qquad and, \qquad H = (12.17 + 0.191\mu) l_m \tag{9.27}$$

The mean geometric chord of the wing (l_m) is $1.02\,\mathrm{m}$. The mass (m) and surface area of the main wing (S) were estimated to be $1051.2\,\mathrm{kg}$ and $23.74\,\mathrm{m}^2$ respectively. Lastly the slope of the wing lift curve (a) was calculated with Equation (9.28)[14]. With the aspect ratio (AR) of 26.4 a slope of the wing lift curve of 5.82 is found.

$$C_{L\alpha} = \frac{2\pi * AR}{2 + \sqrt{AR^2 + 4}} \tag{9.28}$$

This resulted in Figure 9.4b, where the gust speeds can be seen. Both gust speeds result in a positive and a negative gust load factor. Notice that, V_A and V_D are also included in the figure. The resulting maximum gust load factors are;

Table 9.7: Gust load factors

Gust speed	Velocity	Load Factor	
		Positive	Negative
15	V_A	4.2	-2.2
7.5	V_D	3.5	-1.5

Finally, it was checked if the values found in Figure 9.4b do not exceed Equation (9.29). As this is stated in the CS-22[3].

$$n = 1.25\left(\frac{V}{V_{S1}}\right)^2 \tag{9.29}$$

9.3.3. Load Diagram

As a final step the two envelopes are combined. By doing so the maximum load factors are found. The flight envelope can be seen in Figure 9.5. The maximum load factors can be seen in Table 9.8.

Table 9.8: Maximum Load Factors

Velocity	**Load Factor**	
	Positive	Negative
V_A	4.4	-3.0
V_D	4.3	-1.5

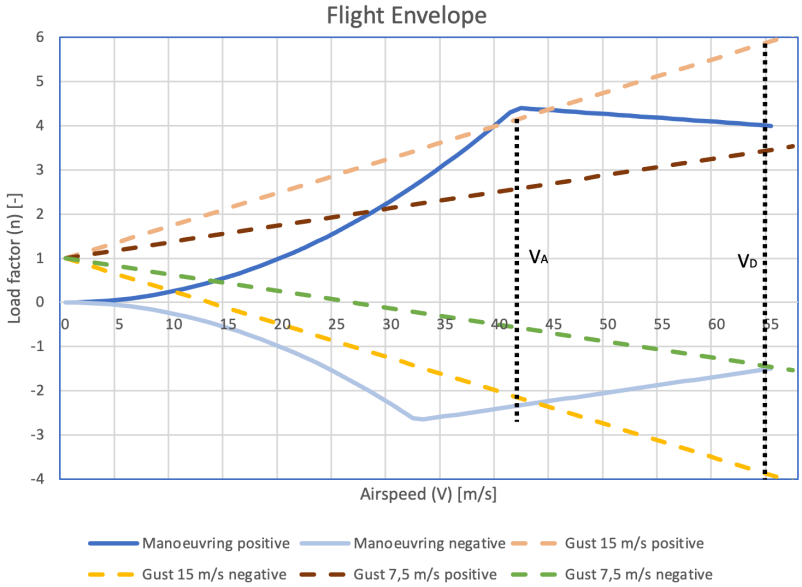

Figure 9.5: Flight Envelope

9.3.4. Verification & Validation

The method described in Chapter 8 was validated and verified. The software used for the calculations of the flight envelope tool is Excel and has to be verified and validated to ensure correctness and usefulness of the tools. Firstly, the verification is performed in sec. 14.2.9 where after the validation is performed in sec. 14.2.9.

Verification

For the verification of the Excel program, a number of unit and system tests are performed. The verification results are presented below, with a summary in Table 9.9.

- **Unit tests** All unit tests from **UT00-UT06** are passed, thus no irregularities were found in the Excel program. The results can be seen in Table 14.8. No discretization error was calculated as no function of a continuous variable was represented by a finite number.
- **System tests** AN analytical comparison is added Table 14.8.

Table 9.9: Unit and system tests for the flight envelope

ID	Parameter	Input	Pass Condition	Test Result	Pass or Fail	Comments
UT 00	ρ	0	All loads=0	0	Pass	-
UT 02	g	–	Flipped gust loads	Flipped	Pass	-
UT 03	$Vstall$	$*2$	n not exceed is multiplied by 4	Multiplied by 4	Pass	-
UT 05	W	1051 kg	10 310 N	10 310 N	Pass	-
UT 06	n		-	$\frac{m/s}{m/s}$	Pass	-
ST 08	n not exceed	10 m/s	$n = 0.303$	0.303	Pass	-

Validation

For the validation the procedures described in Section 8.2 can be used. Validation procedure **VP02** can be performed by comparing the flight envelope generated by excel to the flight envelope stated in EASA[3]. The flight envelope form EASA can be seen in Section 9.3.4. From the figure it is clear that the flight envelope generated by excel heavily corresponds to the flight envelope described by EASA. Therefor the excel tool is validated. However some more complete validation procedures could be performed in the future such as **VP03** and **VP04**.

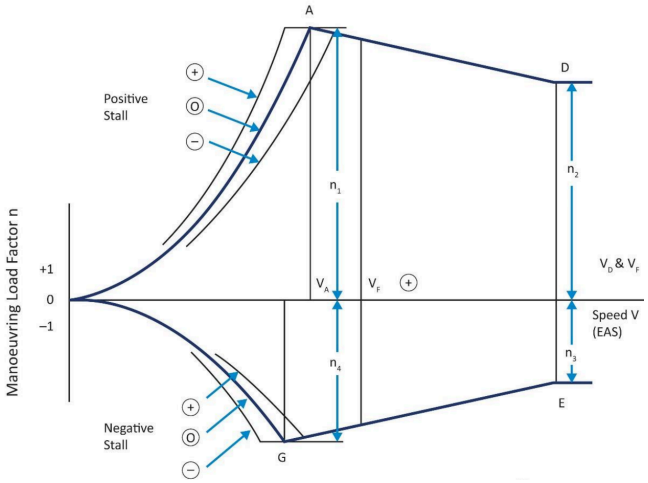

Figure 9.6: Maneuvering envelope

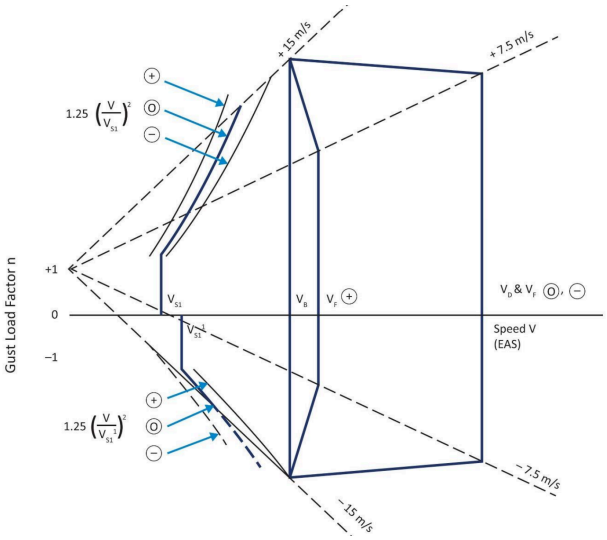

Figure 9.7: Gust envelope

10. Material Selection

A driving requirement of the aircraft design was the sustainability of the material used in the aircraft. This makes the material selection process an important design choice that must be made with care. This chapter presents the material options in Section 10.1 and the method with which they were evaluated with respect to one another in Section 10.2. Here after the end of life strategy and sustainability are presented in Section 10.3. Additionally, it is important to note that this is the material selection for the exterior of the aircraft. The requirements relevant for the material selection can be seen in Table 10.1.

Table 10.1: Material requirements

Identifier	Requirement
REQ-WS-SUST-05	80% of the WS materials shall be recyclable
REQ-WS-STRC-03	The WS shall be resistant to wet corrosion ($E^\circ > 0.4$)

10.1. Material Options

Historically, the first sailplanes were made of wood, fabric, and later metals and composites. The latter remains the preferred material choice as it allows more laminar flow as single parts can be manufactured with less assembly than metals. Moreover, composites are lightweight materials [15]. Furthermore, floats in floatplanes are commonly made of composite materials, again due to the enhanced laminar flow characteristics and low specific weight. Therefore, in the preliminary material selection process only composite materials were considered.

Within the realm of composites, several fibers were considered in an epoxy resin: high strength intermediate modulus (IM) carbon, basalt, E-glass, and aramid (Kevlar 49). As the aircraft deals with loads in multiple directions, the properties for these fibers were for quasi-isotropic composites. Quasi-isotropic composites refer to those where the fiber directions are laid up such that they have the same percentage of fiber layers in every $180/n$ degrees, where $n \geq 3$ [16].

Table 10.2 presents a list of materials options with their properties. The properties for the basalt fiber epoxy composite was found from Plappert et al [17], and for the rest from Myer and Zweben [16].

Table 10.2: List of candidate materials with material properties, where all of have a fiber volume fraction, V_f, of 60 % (all properties are for quasi-isotropic composites)

Material	E GPa	G GPa	σ_{ult} MPa	τ_{ult} MPa	ρ kg/dm^3	Price \$/kg
UHS(IM) carbon (PAN)	63	21	1350	410	1.6	116
Basalt	20.3	3.3	441	50.5	2.0	5.6
E-glass	23	9	550	250	2.1	5.1
Kevlar 49	29	11	460	65	1.4	23

10.2. Trade-off Method

Having established the material options and found their relative properties, a method was determined on how to choose the best material for the best use. By looking at different aircraft systems such as wing, fuselage, empennage and floats, the critical load cases for each of these systems were identified. These critical load cases are:

- **Wing:** During flight, the most dominant loads the wing experiences are normal stresses due to bending and shear stresses due to torsion and shear forces.
- **Fuselage:** The most critical load case occurs during the landing. As the impact on the water creates high point loads on the fuselage due to the struts between the fuselage and floats. Also, the fuselage needs to carry loads of the wings, empennage, and propulsion system.
- **Empennage:** During flight, the most dominant loads the empennage experiences are normal stresses due to bending and shear stresses due to torsion and shear forces.
- **Floats:** The most critical load case occurs during the landing. This is due to the normal stresses in the struts between the floats and the fuselage.

Note that for the fuselage canopy, no material trade-off will be made, as it will be made of Plexiglas. This is due to it being the standard material that all sailplanes use. [1] Furthermore, the canopy design is outside the scope of this research.

[1] https://www.plexiglas.de/en/applications/clear-view-for-glider-pilots [Accessed: 22 Dec 2021]

The trade-off is performed with several criteria established to evaluate the material by using specific indices for the type of loading they describe [18]. Furthermore, the material performance was also evaluated for the price and the energy required to produce the fibers. Manufacturability was not considered as all options use an epoxy matrix, which use the same method. Additionally, fatigue was not considered relevant for this aircraft, as it will be operated significantly less than a commercial aircraft. The complete list of criteria are provided below:

1. $\frac{E^{1/2}}{\rho}$: Beam supporting a certain load that minimizes deflection with a free area end is as light as possible, and for a column that can support without buckling.
2. $\frac{E^{1/2}}{\rho\$}$: Beam that minimizes cost and weight under bending.
3. $\frac{\sigma_{ult}^{2/3}}{\rho}$: Index for a beam that is strong and light.
4. $\frac{\sigma_{ult}^{2/3}}{\rho\$}$: Index for a beam that is strong and light and minimizes cost.
5. $\frac{\tau_{ult}}{\rho}$: Material that is strong in shear and lightweight.
6. $\frac{\tau_{ult}}{\rho\$}$: Material that is strong in shear, lightweight, and minimizes cost.
7. $\frac{G}{\rho}$: Material that is torsionally stiff and lightweight.
8. $\frac{G}{\rho\$}$: Material that is torsionally stiff, lightweight, and minimizes cost.
9. Energy: The environmental impact in the production of a fiber in $\mathrm{MJ/kg}$.

For brevity the scoring of each material is not included in the report. It was concluded, however, that E-glass was the preferred material choice for the majority of the structures. This is particularly due to its significantly lower energy footprint than Kevlar 49 and carbon fiber. However it was also noted that for the wing structure carbon fiber will be used due to its significantly better stiffness and strength properties over E-glass. For further structures that require better properties, this can be achieved by increasing local stiffening or redesigning with a stiffer material.

10.3. End of Life Strategy and Sustainability

At the end of life of the aircraft it will be sought to recycle as much of the aircraft structure as possible to remain sustainable. Given that sophisticated composite structures are relatively modern materials, developments in their recycling capabilities are not as mature as with metals. Furthermore, the materials considered are all use thermoset resins, which are not reusable as thermoplastics are. Given that the aircraft will make use of carbon fiber for the wing and struts, and E-glass for the remainder of the structure their recyclability will be considered.

E-glass composite waste poses an environmental problem as it is non-biodegradable. Particularly since being introduced as a material for wind turbines, which are now being decommissioned. However, research has been done to establish a method to recycle E-glass from such turbines to reuse the material in a Fused Filament Fabrication (FFF) process in 3D printing [19]. Results showed that $60\,\%$ of the original material could be printed by the process of grinding the material down and creating pellets. Further, the final 3D printed product did not result in significant reductions in the original material properties. Additional possibilities of recycling E-glass include reusing it for the purpose of mixing concrete [20].

Recycling of carbon fiber composites typically consist of three methods. The first consists of a mechanical breakdown of the product, grinding or shredding it into small pieces and segregating the scrap into portions rich in fiber and portions rich in the matrix. A second method, the most widespread, is a thermal process that decomposes organic molecules into the atmosphere. Mechanical properties with this method only degrade by about $70\text{-}80\,\%$, although it produces hazardous gases and leaves char on the carbon fibers. The third process is a chemical process that decomposes the resin. While properties are about $90\,\%$ of the virgin product, the cost of the reactants used is significant and again hazardous gases are produced. [21]. Effective applications for recycled carbon fibers are to use them in the molds for carbon fiber composite productions. The advantage of this is that the mold has a very similar thermal expansion as the product, decreasing the tension between the mold and the part during cooling. [22]

As only the structural elements have been investigated for recycling purposes, it is assumed that these are the recyclable elements of the aircraft. Further investigation would be required on how to recycle elements such as the interior, propulsion unit (battery and motor), and electronics. As a result of only structural elements being recycled $67\,\%$ of the total aircraft weight is recyclable.

11. Wing Design

The wing design is one of the most important aspects of an aircraft. It essentially makes or breaks a design and decides whether the water sailplane will be an aircraft or a boat. The wing is a complex structure, thus good emphasis must be put on the design of it.

The first step was selecting a good wing planform, which is described in Section 11.1. Thereafter, an airfoil selection was performed. This is shown in Section 11.2. Section 11.3 presents the lift analysis of the wing. Finally, the preliminary wing structure can be seen in Section 11.4.

11.1. Planform Design

In this section the design of the wing planform is discussed. The planform was designed by looking at the aspect ratio and wing shape. The determination of the aspect ratio is presented in Section 11.1.1. Section 11.1.2 describes the chosen wing shape.

11.1.1. Aspect Ratio

An important characteristic of any wing is the aspect ratio, as it describes the slenderness of a wing. It is defined by Equation (11.1).

The aspect ratio of a wing has a significant effect on the induced drag of a wing, as can be seen in Equation (11.2), the equation for the induced drag coefficient [23].

$$AR = \frac{b^2}{S} \tag{11.1}$$

$$C_{D_i} = \frac{C_L^2}{\pi ARe} \tag{11.2}$$

Here e is the Oswald efficiency factor of the wing. Sailplane wings typically have high aspect ratios, ranging from 10 to as high as 40 [24]. These high aspect ratios have the goal to minimize the induced drag of the wing, allowing for long range and/or endurance flights.

A first estimate of the aspect ratio of the water sailplane was made using data from reference sailplanes. The aspect ratios of different 1- and 2-seater powered sailplanes were plotted against their MTOW. Linear regression was done for both the 1- and 2-seater sailplane data. It can be seen that the relation for the 2-seater sailplanes shifts down compared to the 1-seater sailplanes. The same trend in AR and MTOW behavior was assumed to be true between the 2- and 3-seater configuration. Therefore, the averages of the AR and MTOW of the 1- and 2-seater sailplanes were used to find the difference in aspect ratio and maximum take-off weight. By adding this to the data for the 2-seater, the linear regression for a sailplane with three occupants was approximated. Using the first estimate of the MTOW an initial AR of 30 was set for the wings of the water sailplane.

After this initial AR was set, a different method to determine the initial AR was found, based on the maximum Lift-to-Drag-ratio (L/D) of unpowered and powered sailplanes [14]. A desired L/D ratio for the water sailplane was determined using equations from Ruijgrok [11]. For gliding flight, Equations 11.3 - 11.6 hold.

$$L - W\cos\gamma = 0 \tag{11.3}$$

$$\gamma_d = -\gamma \tag{11.4}$$

$$\tan\gamma_d = \frac{RD}{V_{cr}} \tag{11.5}$$

$$\tan\gamma_d = \frac{C_D}{C_L} = \frac{D}{L} \tag{11.6}$$

With these equations, Equation (11.7) was derived, relating the L/D ratio to the cruise speed and descent rate.

$$\frac{L}{D} = \frac{V_{cr}}{RD} \tag{11.7}$$

Gudmundsson also related the maximum L/D ratio to the AR of powered sailplanes with Equation (11.8), which was rewritten to Equation (11.9).

$$L/D_{max} = 1.7405 \cdot AR - 0.443 \tag{11.8}$$

$$AR = \frac{L/D_{max} + 0.443}{1.7405} \tag{11.9}$$

Using this method a more accurate AR was obtained than by following the sailplane data extrapolation.

11.1.2. Wing Shape

Initially, it was decided that the leading edge would have an elliptical shape, and the trailing edge would be straight. This was suggested by sailplane design expert Loek Boermans. This would ensure an elliptical lift distribution over the wing, which is a desired situation, while allowing simple construction of flaps. However, later in the design process it was decided to slightly modify the shape, so that the wing fell under the category of Schuemann planforms [14]. This planform in theory also provides a near elliptical lift distribution over the wing, but allows for easier construction. Furthermore, it was also a lot easier to analyze this wing shape. Figure 11.1 shows the differences between the two planforms, and their relevant dimensions.

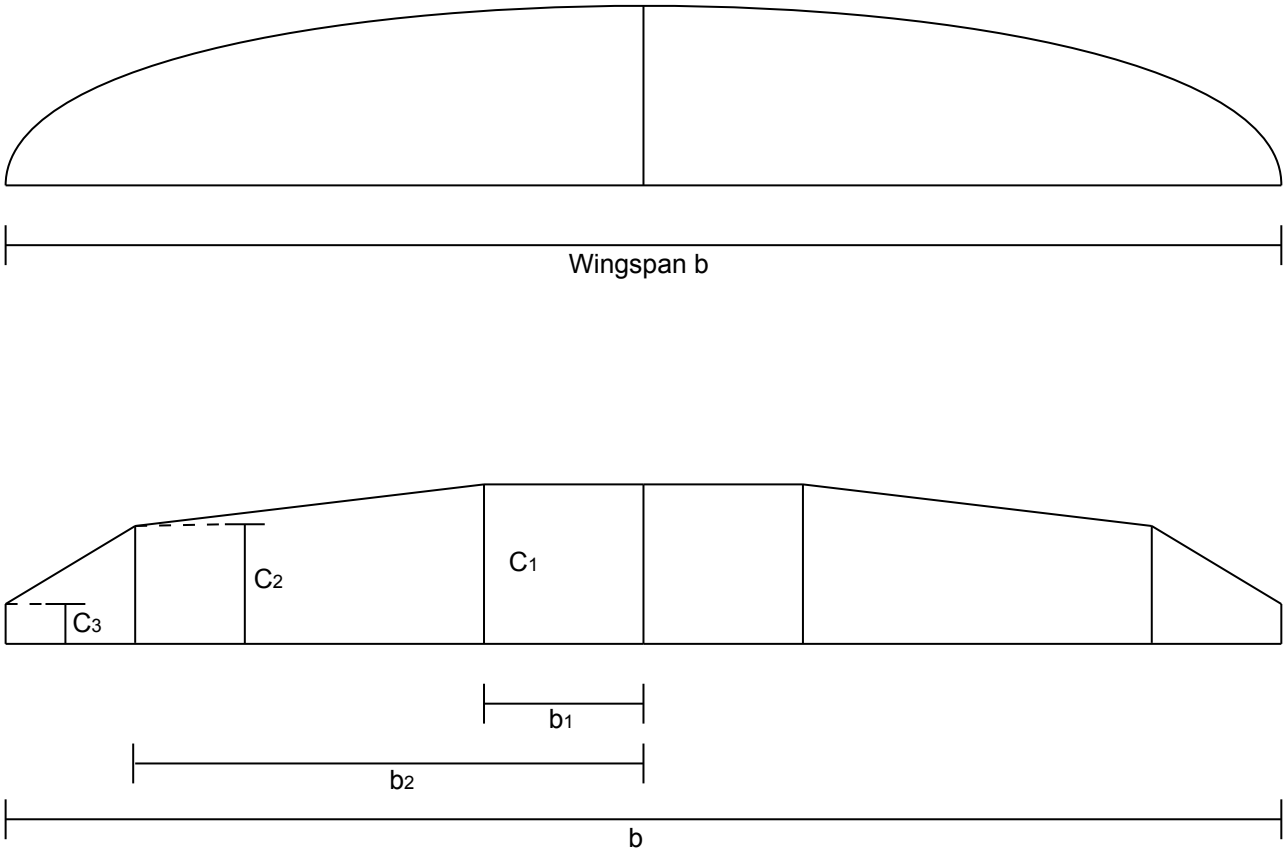

Figure 11.1: Elliptical and Schuemann wing planform

The surface area of this wing planform is given by Equation (11.10):

$$S = (b_1 + b_2)\, C_1 + \left(\frac{b}{2} - b_1\right) C_2 + \left(\frac{b}{2} - b_2\right) C_3 \tag{11.10}$$

11.2. Airfoil Selection

The selection of an airfoil is essential in order to meet the mission profile of the water sailplane. The critical conditions were identified for which a selection procedure was established, which was done in Section 11.2.1. The airfoils that were evaluated in the trade-off are presented in Section 11.2.2. Section 11.2.3 shows the trade-off procedure.

11.2.1. Selection Procedure

Before the selection procedure of water sailplane's airfoil started, the important characteristics, that had to be met, were determined. As the water sailplane will serve as a touristic attraction by performing scenic tours, the quality of these tours will depend on the delivered experience.

Therefore, it was concluded that the aircraft's operations should be performed at low speeds, so that the passengers can absorb the beautiful surroundings of the Maldives. Furthermore, as the aircraft will take-off and land on water, contamination of the wing should not severely decrease the performance of the water sailplane. Besides that, take-off was expected to be the most critical phase of the mission due to the water

resistance. Therefore, STOL was seen as favorable. Finally, a high glide time was concluded to benefit the customer experience as was assumed that repeatably climbing and descending is uncomfortable. These critical conditions were translated into airfoil characteristics, which were used to perform the trade-off. An overview is provided in Table 11.1.

The weights of each trade criterion was determined using the AHP method and can also be seen in Table 11.1. The trade-off method used for selecting the airfoil was the Weighted Sum Method.

Table 11.1: Critical mission aspects with their corresponding trade-off criteria and weights.

Critical Aspects	Trade Criterion	Weight
Low speed	Drag behavior at high lift coefficients	0.47
Take-off	High maximum lift coefficient	0.53

11.2.2. Airfoils

An initial selection of airfoils was established to limit the amount of airfoils in the trade-off. Through literature research it was concluded that a thickness-to-chord ratio around $12\,\%$ results in good stall characteristics. These ratios cause smooth trailing edge stall, which is easier to operate on [14].

Three Wortmann airfoils, with varying t/c and flap locations, were determined to be suitable for the mission of our aircraft. The FX 62-K-131/17 and FX 67-K-150/17 were selected from literature [24]. However, the FX 62-K-153/20 was advised by sailplane aerodynamics expert Loek Boermans during a meeting. He stated that this airfoil had great characteristics regarding wing contamination due to water. This was considered to be very favorable.

11.2.3. Airfoil Trade-Off

The three airfoils were evaluated in Javafoil at an estimated Reynolds number of $1.5E^6$. The $C_{l_{max}}$ was determined for each airfoil as well as the drag at high lift coefficients, since the water sailplane will operate at low speeds. To evaluate the drag objectively for each airfoil the C_d was looked up at a C_l of 1.2. A scale was established for the criteria and consequently a score was given. These can be seen in Table 11.2 and Table 11.3, respectively.

Table 11.2: The scaling of the airfoil criteria.

Scale	Drag	$C_{l_{max}}$
5	< 0.01	> 2.0
4	0.01 - 0.02	1.5 - 2.0
3	0.02 - 0.03	1.0 - 1.5
2	0.03 - 0.04	0.5 - 1.0
1	> 0.04	< 0.5

Table 11.3: The trade-off table of the airfoil selection.

Airfoil	C_d	$C_{l_{max}}$	Drag score [Weight: 0.43]	$C_{l_{max}}$ score [Weight: 0.57]	Weighted Sum
FX 62-K-131/17	0.103	2.26	1	5	3.28
FX 67-K-150/17	0.016	1.28	4	3	3.43
FX 62-K-153/20	0.004	1.61	5	4	4.43

The most suitable airfoil was concluded to be the recommendation of Loek Boermans, the FX 62-K-153/20. As mentioned before this airfoil does not experience severe performance reduction as a result of water contamination, this strengthens the confidence in the outcome.

11.3. Aerodynamic Lift Analysis

After the airfoil selection, the analysis on the lift of the wing was initiated. From this aerodynamic lift analysis important parameters of the water sailplane became available, which determined the performance behavior

of the aircraft. The $C_{L\alpha}$ was calculated as well as the maximum lift coefficient. For the latter two situations were evaluated, the first being the $C_{L_{max}}$ in clean configuration and the second was estimated with the use of high lift devices. Firstly, the assumptions made during the analysis are stated in Section 11.3.1. Section 11.3.2 covers the approximation of the wing's lift slope. The maximum lift coefficients of the wing are evaluated in Section 11.3.3 and Section 11.3.4. Finally, verification of the used code and assumptions was performed, presented in Section 11.3.5.

The outcome of the lift analysis can be found in Chapter 20.

11.3.1. Assumptions

Several assumptions were made to simplify calculations for the used method. An overview of these assumptions is presented below.

LA 01: Incompressible flow. This implies that the density of the flow over the wing is assumed to be constant.

LA 02: Flaperons. Assuming that the aileron functions as a flap as well the maximum lift coefficient increases due to an increase in flapped wing area.

LA 03: Maximum flap deflection of $30°$. The maximum lift coefficient with flaps was determined at the aforementioned deflection angle. This angle was chosen as for plain flaps a higher deflection typically does not benefit the lift anymore without paying the price in the drag [14].

LA 04: Flap free wing area over fuselage. This assumption implies that no flaps are present at the wing area covering the fuselage.

11.3.2. The Lift Slope

The linear part of the lift curve is called the lift curve slope. The value of this for the wing differs from that of the airfoil, which was obtained via Javafoil. The lift of the 3D-wing decreases with respect to the 2D-airfoil, as well as the slope of the so-called linear part of the lift curve. Therefore, in order to start performing calculations on the lift of the wing, the C_{L_α} needed to be estimated. Equation (11.11) was used to calculate the C_{L_α}. The lift curve slope of the airfoil was taken into account in this equation through κ, in which it is compared to the lift slope of an elliptical wing. [25]

$$C_{L_\alpha} = \frac{2\pi \cdot AR}{2 + \sqrt{(\frac{AR \cdot \beta}{\kappa})^2 \cdot (1 + \frac{\tan \Lambda_{C/2}{}^2}{\beta^2}) + 4}} \tag{11.11}$$

11.3.3. Maximum Lift Coefficient of the Wing

As was mentioned in Section 11.2, it was expected that the maximum lift coefficient of the wing would play an important factor for taking-off. Therefore, a value for the $C_{L_{max}}$ needed to be determined. The maximum lift coefficient was estimated by means of the USAF DATCOM Method 2. This method is deemed valid for aircraft with a high aspect ratio. To check whether this requirement was true for the water sailplane, an empirical relation was used. This relation of high AR aircraft can be seen in Equation (11.12). The taper ratio correction factor was determined by Equation (11.13). Using these two expressions it was concluded that the water sailplane indeed qualified as a high aspect ratio aircraft. [26]

$$AR > \frac{4}{(C_1 + 1) \cdot \cos \Lambda_{LE}} \tag{11.12}$$

$$C_1 = \frac{1}{2} \cdot \sin\left(\pi \cdot (1 - \lambda)^{1.5 + 0.8 \cdot \sin^{0.4}(\pi \cdot (1-\lambda)^2)}\right) \tag{11.13}$$

The next step in obtaining the wing's $C_{L_{max}}$ was determining its $C_{L_{max}}/C_{l_{max}}$ ratio, which was found to be equal to 0.9 for wings without sweep. By means of Equation (11.14) the maximum lift coefficient was obtained. The mach number correction factor was determined to be zero due to the low subsonic Mach number at stall. [26]

$$C_{L_{max}} = \frac{C_{L_{max}}}{C_{l_{max}}} \cdot C_{l_{max}} + \Delta C_{L_{max}} \tag{11.14}$$

11.3.4. $C_{L_{max}}$ with High Lift Devices

In order to minimize the take-off distance from water a higher $C_{L_{max}}$ is beneficial, as the required take-off speed decreases. Through the implementation of high lift devices the maximum lift coefficient can increase significantly dependent on the covered area, the flap chord and deflection angle. A trailing edge high lift device was selected for this purpose, which effects are explained.

As the selected airfoil FX 62-K-153/20 from itself contains a plain flap, this flap configuration was chosen [27]. An advantage of the plain flap is that the drag increase resulting from deflection is relatively low. Furthermore, it is a rather simple high-lift surface as it only uses rotation. Nevertheless, the plain flap has its drawbacks, such as a relatively low $C_{l_{max}}$ increase when deflected [14].

With the type of flap configuration known, the analysis of the maximum lift coefficient was initiated. In Section 11.1 the wing planform is shown, which states that the wing consists of multi-panels. In essence the flaperons cover the total wing, with the exception of the area over the fuselage and the clearance from the wingtip. The $C_{L_{max}}$ was calculated using the same method as described in Section 11.3.3, but now the $C_{l_{max}}$ was used with the flaps deflected. This value was obtained using Javafoil. Equation (11.15) shows the relation that was used to determine the $C_{L_{max}}$ for the wing with high lift devices [14]. As can be seen a distinction was made between the wing areas containing the flaps and vice versa.

$$C_{L_{max}} = \frac{0.9}{S_{ref}} \cdot (C_l \cdot (S_1 + S_4) + C_{l_{max_{flap}}} \cdot (S_2 \cdot \cos\Lambda_{hingeline_2} + S_3 \cdot \cos\Lambda_{hingeline_3})) \tag{11.15}$$

11.3.5. Verification

The verification of the aerodynamic lift analysis consists of both verification of assumptions as well as verification of the code. The assumption verification proves the validity of the use of these assumptions. The code verification provides an insight in the correctness of the use relations.

11.3.6. Assumption Verification

Incompressible flow

Item **DE 01:** assumed a constant density of flow. This assumption is valid for Mach number < 0.3 [28]. Calculating the Mach number for the water sailplane flying at cruise speed at sea level, proved that this assumption was implemented properly, which can be seen in Equation (15.16).

$$M = \frac{V_{cruise}}{c} = \frac{V_{cruise}}{\sqrt{\gamma \cdot R \cdot T}} = \frac{27.8}{\sqrt{1.4 \cdot 287 \cdot 288.15}} = 0.08 \tag{11.16}$$

Maximum deflection

Item **LA 03:** stated that the benefits of deflections higher than $30°$ would not outweigh the increase drag anymore. This assumption was verified using Javafoil in which the $C_{l_{max}}$ and its corresponding C_d of the airfoil were evaluated at deflections of 25, 30 and 35 degrees. The results of this are shown Table 11.4. From this data it can indeed be concluded that the drag coefficient of the airfoil increases abruptly at $35°$. Hence, this assumption was deemed valid.

Table 11.4: Verification of Item **LA 03:**.

δ_f	$C_{l_{max}}$	C_d
25	2.27	0.033
30	2.49	0.039
35	2.66	0.048

11.3.7. Code Verification

A numerical code was used for the calculations of the lift analysis. However, to ensure that no errors were present in this code, a code verification was performed. The system of codes was verified based on several unit tests described in Chapter 8. Table 11.5 shows which unit tests were used for verifying the code and what the results were.

Table 11.5: Results of the code verification of the lift analysis.

Unit test	Number of errors	Result
UT 00	0	PASS
UT 00	0	PASS
UT 00	0	PASS

11.4. Preliminary Structural Design

This section presents the methodology with which the preliminary wing structure was designed. Designing the wing structure began by considering the load requirements that the wing to withstand. These are listed below in Table 11.6:

Table 11.6: Requirements for the wing structure

Identifier	Requirement
REQ-WS-STRC-13	The wing structure must withstand a positive load factor of 4.4 with a safety factor of 1.5
REQ-WS-STRC-14	The wing structure must withstand a negative load factor of -2.65 with a safety factor of 1.5

11.4.1. Methodology and Assumptions

In order to perform a preliminary structural analysis of the wing, it was initially simplified to a wingbox beam model. This was designed based on the geometric constraints of the chosen airfoil's cross-section, and drawing a rectangular box with spars that maximized the area within. Figure 11.2 shows the model with the width and height of the wingbox as a proportion of the airfoil chord and maximum height given:

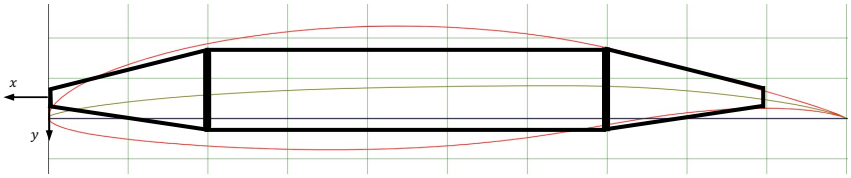

Figure 11.2: Model of the wing structure as a wingbox beam model within the geometric constraints of the FX 62-K-153/20 airfoil

The structure was further simplified into an idealized structure with booms. In total the model from Figure 11.2 eight booms: one at each corner of the model. The area of a boom was calculated with the following equations:

$$B_1 = \frac{t_{skin} b_{skin}}{6}\left(1 + \frac{\sigma_2}{\sigma_1}\right) \tag{11.17}$$

$$B_2 = \frac{t_{skin} b_{skin}}{6}\left(1 + \frac{\sigma_1}{\sigma_2}\right) \tag{11.18}$$

Where B_i is the area of the given boom, t_{skin} the thickness of the skin between consecutive booms, b_{skin} the length of the skin between consecutive booms, and σ_i the stress carried by the i^{th} boom. The ratio of stresses could be simplified by simply considering the ratio of heights between consecutive booms. The idealized structure of Figure 11.2 is shown in Figure 11.3:

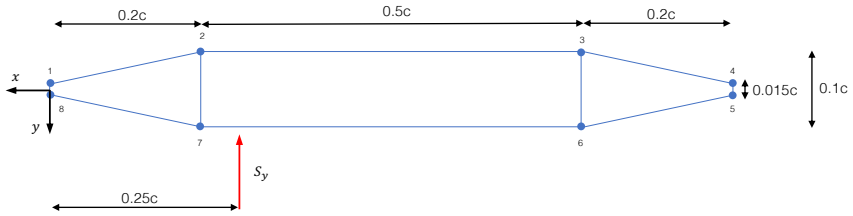

Figure 11.3: Idealized structure of the wingbox with lengths and coordinate system labeled

Note that, the dimensions of the idealized structure are in terms of the chord, meaning that it changes along the span given that the The coordinate system indicated in the drawing (with the z-axis coming out of the page) is used and remained consistent with calculations. Additionally, the sign convention had forces positive in the axis direction shown, and moments positive if they caused tension in the positive quadrant and negative if it caused compression in the positive quadrant.

As was shown in Figure 11.2 the wing has already been simplified to a rectangular wingbox model. In addition to this one, a number of other assumptions were made. These are listed below with reasoning as to why they were made, and their effect on the structural analysis:

SWD 01 The wingbox is rectangular. By this assumption the wingbox is modeled in an area contained by the wing's airfoil. This assumption results in an underestimation of the wing's moment of area, making the design conservative.

SWD 02 Idealized structure of wingbox. Creating booms and idealizing the structure underestimates the structure's stiffness. However, shear stresses are underestimated given that they are assumed to be constant in the sections between booms.

SWD 03 The structural wing weight is rejected. With respect to the aerodynamic load, the wing weight is negligible. By neglected it in the analysis, again, the calculations are conservative.

SWD 04 The drag force is neglected. A drag force would result in a bending moment about the y-axis. Given that the wingbox has a longer width than height it will be stiffer in this direction. Therefore it is more critical to analyze the lift load over the drag load.

SWD 05 Fixed supports at the root. At the root of the wing there is a fixed support leading to point reaction forces in the y- and z-direction, and a reaction moment. This results in a statically determinant model.

SWD 06 Thin walled assumption. With this assumption the stiffness calculation will be conservative. It is valid given that the largest thickness of an element is at least 10 times smaller than the smallest general dimensions (in this case the height of the wingbox).

SWD 07 It will be assumed that the lift force has a perfectly elliptical distribution. Therefore the equation is in the form:

$$L(z) = C\sqrt{1-\left(\frac{2z}{b}\right)^2} \tag{11.19}$$

Where b is the wingspan, and C a constant determined by the load case, defined in the following section.

SWD 08 Lift force acts at $0.25c$. This assumption translates to the rectangular wingbox as the lift acting at the first quarter of the rectangle's length. Therefore there is an additional resultant torque that the wingbox must be designed for.

SWD 09 Open sections do not carry torsional loads Elements such as stringers will be assumed to carry no torsional loads due to their significantly lower torsional stiffness compared the skin and spars. The assumptions results in a conservative representation of the wingbox's torsional stiffness.

SWD 10 The materials are considered isotropic. Despite the composite material properties listed being for quasi-isotropic composites, they are not truly so. Composites tend to be stronger in tension rather than compression, resulting in an underestimation of the compressive forces.

11.4.2. Internal Loading of the Wing

The first step of structural analysis was determining the internal loading of the wing. This process began by first drawing all of the forces acting on the wing as per the assumptions presented in the previous subsection. Figure 11.4 shows the free body diagram (FBD) of the half wing with the relevant coordinate system indicated:

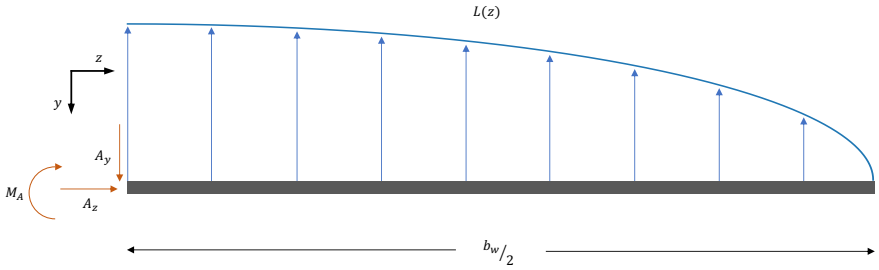

Figure 11.4: Free body diagram of the wingbox all relevant forces, reaction forces, and coordinates labeled

For the analysis two critical loading cases were considered: the largest lift force upwards, with a load factor of 4.4, and the largest lift force downwards, with a load factor of -2.65. As a result the total lift, equal to the integral of the elliptical lift, with these load factors was evaluated by:

$$\int_{-b/2}^{b/2} L(z)\, dz = n_{max} \cdot g \cdot MTOW \tag{11.20}$$

With this equation the constant C, which was shown previously in Equation (11.19), can be solved. This was done by evaluating the elliptical lift equation with a definite integral from $-b/2$ to $b/2$, and solving for C. As there is an analytical solution to the elliptical lift equation, solving for C is precise and given by:

$$C = \frac{4\, n_{max} \cdot g \cdot MTOW}{\pi b} \tag{11.21}$$

With the equation for the lift known the internal loading diagrams of the wingbox were created. These represent internal shear, moment, and torque at any given point along the wing. Mathematically the shear diagram is the integral of wing loading, and the moment about the z-axis the moment of the shear loading of the wing. For clarity this is provided in the following equations:

$$V(z) = \int_{b/2}^{z} L(z)\, dz \tag{11.22}$$

$$M_x(z) = \int_{b/2}^{z} V(z)\, dz \tag{11.23}$$

Note that both equations are integrating from the tip of the model wing to a given z location along the span. An additional internal torque about the z-axis is also provided as a result of the wing loading acting at $0.25c$. With these equations, and Equation (11.19), the following internal load diagrams are created:

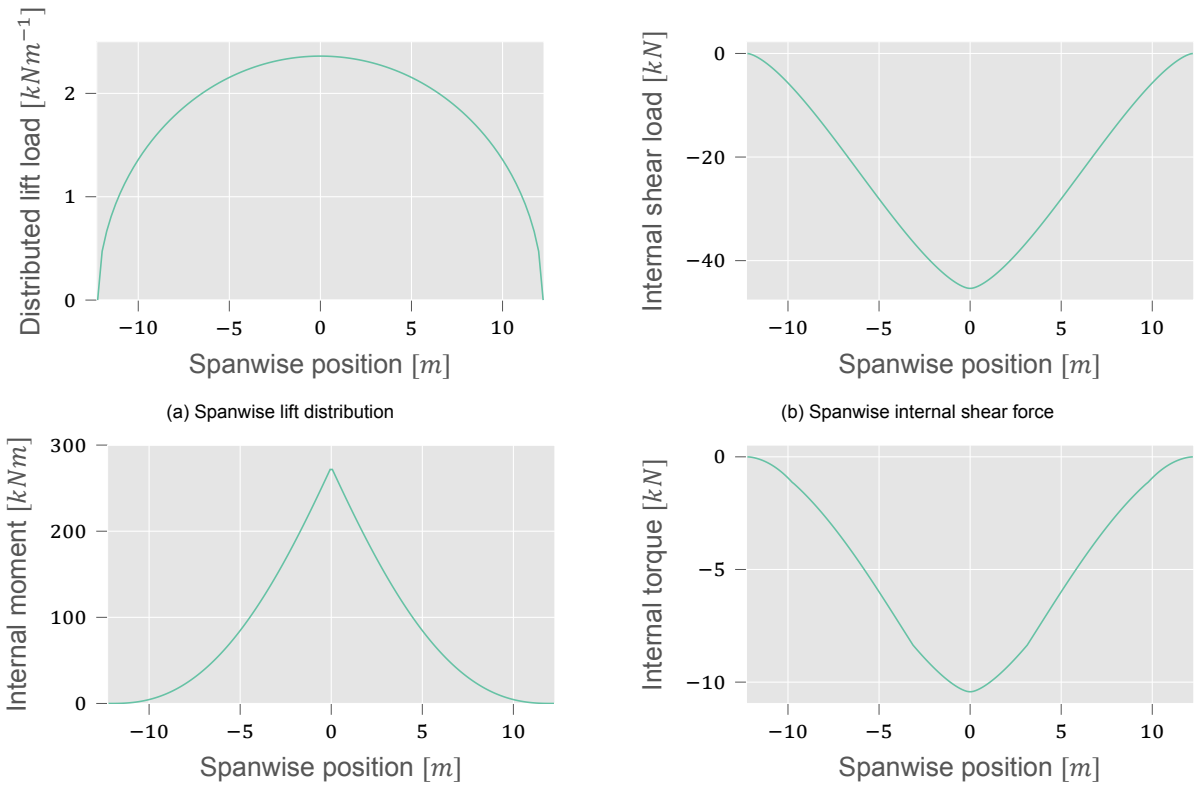

(a) Spanwise lift distribution

(b) Spanwise internal shear force

(c) Spanwise internal moment

(d) Spanwise internal torque

Figure 11.5: Loading and internal loading diagram of the wing with respect to the spanwise position, where the origin is the center of the wing

From Figure 11.5 it can be seen that the most critical loads occur at the root of the wing, as the highest internal bending moment, shear force, and torque occur. Given that the loads are large, the material choice for the wing was ultra high strength (UHS) intermediate modulus (IM) carbon fiber in an epoxy resin matrix. Additionally, given that composite materials do not have a yield strength a safety factor of 1.5 is applied in order to account for errors in the calculation, and manufacturing errors of the material causing a lower ultimate strength.

Table 11.7: Material properties of UHS(IM) carbon fiber with and without a safety factor applied

Safety factor applied	E GPa	G GPa	$\sigma_{ult_{ten}}$ MPa	$\sigma_{ult_{com}}$ MPa	τ_{ult} MPa	ρ kg/dm^3	Price \$/kg
No	63	21	1350	580	410	1.6	116
Yes	n/a	n/a	900	386	273	n/a	n/a

11.4.3. Stress Calculations

When analyzing the wing structure the normal stress, shear stress, and buckling stress of the skin and spar were considered most critical for the design. Normal stresses were evaluated with a simplified version of the generalized stress equation. It was simplified given that there is only a bending moment around the x-axis, and that I_{xy} equals zero due to the double symmetry of the model. This provided the following equation:

$$\sigma_z = \frac{M_x y}{I_{xx}} \tag{11.24}$$

Where M_x is the bending moment about the x-axis, y the vertical distance from the neutral axis, and I_{xx} the moment of inertia. Note that y was always taken as the furthest distance from the neutral axis, $0.05c$ in the case of the wingbox model.

Shear stresses due to shear forces were computed by making a cut in each of the three individual cells of the wingbox model, and evaluating the shear flow contribution of each boom. At the location of the virtual cut the shear flow was equal to zero, due to the free edge, and the additional shear flow contribution by every following boom was given by:

$$\Delta q_{bi} = -\frac{V_y}{I_{xx}} B_i y_i \tag{11.25}$$

The shear flow distribution with the virtual cut of each section then became its shear flow contribution added to those of the booms prior to it. Finally the total base shear, when accounting for the redundant shear q_{s0} as a result of the cut, was given by:

$$q_s = q_b + q_{s0} = -\frac{V_y}{I_{xx}} \sum_{i=1}^{n} B_i y_i + q_{s0} \tag{11.26}$$

However q_{s0} is still unknown for all three cells. Therefore a compatibility equation is introduced where the angle of twist of the cross section is computed. Given that the shear acts at the shear center the twist equals zero, and this will be the case for each individual cell. As a result the angle of twist was computed with the following equation:

$$\left(\frac{d\theta}{dz}\right)_i = \frac{1}{2A_i} \oint \frac{(q_{bi} + q_{s0})\, ds}{t_i G_i} \tag{11.27}$$

Where A_i is the enclosed area of each cell, t_i the thickness of the relevant segment, and G_i the shear modulus of the material. The final step of the calculation was to determine moment equivalence of the shear force, and the internal shear flows. This resulted in a four by four matrix which could be solved to find the final shear flow distribution, also accounting for the fact that the shear force acts at $0.25c$.

The final critical stress that was considered was skin buckling, to determine the amount of stringers required. Stringers essentially 'segment' the skin into smaller dimensions causing the critical buckling stress to increase. The stringer spacing was determined by rearranging Equation (11.28) to solve for the sheet width b, where the stress σ_{cr} was equal to 1.5 times the maximum normal stress of the wingbox at a given spanwise location. As both the chord and the maximum normal stress decrease from the root to the tip the number of stringers along the span decreased. This was computed by splitting the wing span into 10 equal segments and determining the number of stringers required on the top and bottom sheet at these locations.

$$\sigma_{cr} = C \frac{\pi^2 E}{12(1-\nu^2)} \left(\frac{t}{b}\right)^2 \tag{11.28}$$

In Equation (11.28) C is a constant depending on how the skin is supported (assumed to be equal to 4 with simple supports on all edges), E is the Young's modulus, ν the Poisson ratio, t the thickness of the skin, and b the plate width. Note that the rib spacing was determined from literature to be optimized at a spacing of $32\,\mathrm{in}$ $(81.28\,\mathrm{cm})$ in order to ensure that the aerodynamic shape of the wing is retained [29]. With this spacing 30 ribs are required in total for the whole wingspan.

Given the theory of how stresses were computed, the wingbox could be designed with the following free variables: skin thickness, spar thickness, and number of stringers. The iteration of the design was done with these steps:

1. Compute the required moment of inertia of the cross section such that the maximum normal stress does not exceed $\sigma_{ult}/1.5$
2. Compute the shear flow distribution and ensure that the skin and spar thickness at all locations results in a shear stress less than $\tau_{ult}/1.5$
3. Determine the number of stringers required such that the skin does not buckle. This is done by ensuring that $\sigma_{cr} > 1.5\ \sigma_z$, where σ_z is the maximum normal stress as a result of the bending moment.
4. Compute the new moment of inertia with the given amount of stringers, and check whether the number of stringers could be decreased given that the moment of inertia has increased with stringers added

11.4.4. Verification and Validation

In order to verify the code of the wingbox structural design a number of unit tests and system tests were established to determine the robustness of the code. Additional code debugging was initially performed to ensure that there were no simple errors in the code, such as incorrect variables in equations. The following list presents the verification tests that were completed:

WSTR-ST 01 Verifying thin walled assumption
With this test the largest thickness, t_{sp} was divided by the smallest overall wingbox geometry, $0.015c$, in order to check that the ratio of $t_{sp}/0.015c < 0.1$. The test resulted in a ratio of 0.16, making the assumption invalid. As a result the moment of inertia of the wingbox is underestimated by neglecting the thickness terms. The ratio of the actual moment of inertia with respect to the thin walled assumption calculation was found to be 1.024, making this the resultant weight penalty.

WSTR-ST 02 Verifying neglecting of drag force
To test this, the ratio of I_{xx}/I_{yy} over was computed, and considered valid if it was $<5\,\%$. The result was $3.21\,\%$, making the assumption valid.

WSTR-ST 03 Verifying neglecting of wing weight
To test this, the ratio of $W_w/L(z)$ was computed, and considered valid if it was $<5\,\%$. The result was $3.83\,\%$, making the assumption valid.

WSTR-UT 01 Zero test
An input of zero was provided for the load factor, where the expected result was that all loading diagrams and following stress calculations equaled zero. This was the case, passing the test.

WSTR-UT 02 Resultant internal shear flow
In this test the shear flow distribution of a simple vertical shear force is computed and integrated. The test was passed as the resultant internal shear force equaled the shear load.

WSTR-UT 03 Resultant internal torque
Given that the load acted at $0.25c$ there was an internal torque. To check that the resultant shear flow calculation was correct, the internal torque based on the shear flow was computed. The test was passed as the resultant shear flow caused a torque equal to that of the shear force.

Validation of the wingbox is not within the scope of this project, given that it requires a comparison to robust models such as Finite Element Modeling (FEM) or experimental data. It is however, recommended for further study.

12. Fuselage Design

Any aircraft must provide ample volume to contain the mission payload. A conventional aircraft design utilizes the fuselage to fulfill this role, and as such, this chapter will cover the design of the fuselage. As the aircraft in question will be carrying 1 pilot and 2 passengers, as stipulated by **REQ-WS-FLPE-PAY-01**, and thus must be large enough to accommodate this. However, the fuselage can not be infinitely large, as it must be both lightweight and aerodynamically efficient. Section 12.1 will cover the sizing of the internal cabin, and provide justification for the chosen layout, and dimensions. The fuselage design, which is explained in Section 12.2, covers how the fuselage is shaped to remain streamlined while ensuring adequate room for other elements such as the floats, empennage, and powerplant. The requirements relevant for the design of the fuselage can be seen in Table 12.1. All the requirements in this table have the identifier **REQ-WS-FLPE-PAY** with only the numbers varying. These are seen in the table in the 'ID' column.

Table 12.1: Fuselage requirements

ID	Requirement
01	The WS shall perform its mission with an occupancy of 2 passengers and 1 pilot
05	The WS shall have a passenger cabin that accommodates a passenger height of $2.00\,\mathrm{m}$
06	The WS shall have a passenger cabin that accommodates a passenger weight of $100\,\mathrm{kg}$
07	The WS shall have a passenger cabin that accommodates a passenger shoulder width of $0.55\,\mathrm{m}$
08	The WS shall have a passenger cabin that accommodates a passenger hip width of $0.55\,\mathrm{m}$
13	The WS cabin will provide a passenger headroom of $10\,\mathrm{cm}$

12.1. Sizing of cabin

Given the aircraft mission of carrying two passengers and a pilot for sightseeing flights, the cabin will not require any room for cargo or luggage. Therefore, the first order of the cabin sizing was based on the chosen configuration. To ensure the fuselage remains streamlined a 1-2 configuration was chose. This implies the pilot sits in a central seat in the front of the aircraft, while the passengers are seated beside one another on the second row.

To determine the size of the cabin, it requires the sizing of the chairs. Given the expected market of the sightseeing flights, dimensions of Dutch males aged 20-30 were evaluated. Dutch males were chosen as statistically, they are some of the tallest people in the world, and therefore, this would ensure the cabin is large enough to accommodate almost all potential customers.

Using the DINED tool from TU Delft, the dimensions of a Dutch male aged 20-30 in the 99^{th} percentile were assessed. This corresponds to a height of $194\,\mathrm{cm}$.[1] Furthermore, it was assumed that the human body could be split into relative head-height ratios, where the torso is approximately 3:1, the thighs 2:1 and calves also 2:1. Using these proportions, the seat dimensions could be approximated.

In accordance with **REQ-WS-FLPE-PAY-07** and **-08**, the seat width was determined to be $0.55\,\mathrm{m}$. This would provide the average person ample room to sit comfortably throughout the flight.

It was chosen to seat the pilot in a more reclined position, in comparison to the passengers. This allows the passengers to look forward as well as sideways. Furthermore, the seating position of the pilot was designed such to be comparable to existing sailplane's and in-line with diagrams provided by the CS-22 regulations [3]. As can be seen in Figure 12.1, the pilot seat length will be $1.30\,\mathrm{m}$ with an overall height of $0.80\,\mathrm{m}$.

The passenger seats were chosen to be more upright to provide more comfort, as well as better opportunity for sightseeing throughout the flight. As can be seen in Figure 12.1, the seat length was $1.10\,\mathrm{m}$ with a height of $1.15\,\mathrm{m}$. To minimize the overall footprint of the cabin size, some overlap was built into the seating arrangement, as the feet of the passengers could be positioned underneath the seat of the pilot. The floor height of the passengers is also positioned slightly lower than the floor height of the pilot, to ensure adequate legroom, while also trying to ensure the configuration is beneficial to the fuselage aerodynamics.

To maximize the aerodynamic efficiency of the fuselage, the fuselage was shaped in such a way that the cross-sectional dimensions would be tight to the cabin, minimizing excess space. For structural efficiency, it was assumed the fuselage would consist of elliptical cross-sections. The tallest and widest point of the fuselage, represented by cross-section **C ||—|| C** in Figure 12.1, is the point where the passengers are seated, where the addition of the $10\,\mathrm{cm}$ headroom is built in as stipulated by **REQ-WS-FLPE-PAY-13**.

[1] https://dined.io.tudelft.nl/en/database/tool [Accessed: 22 Dec 2021]

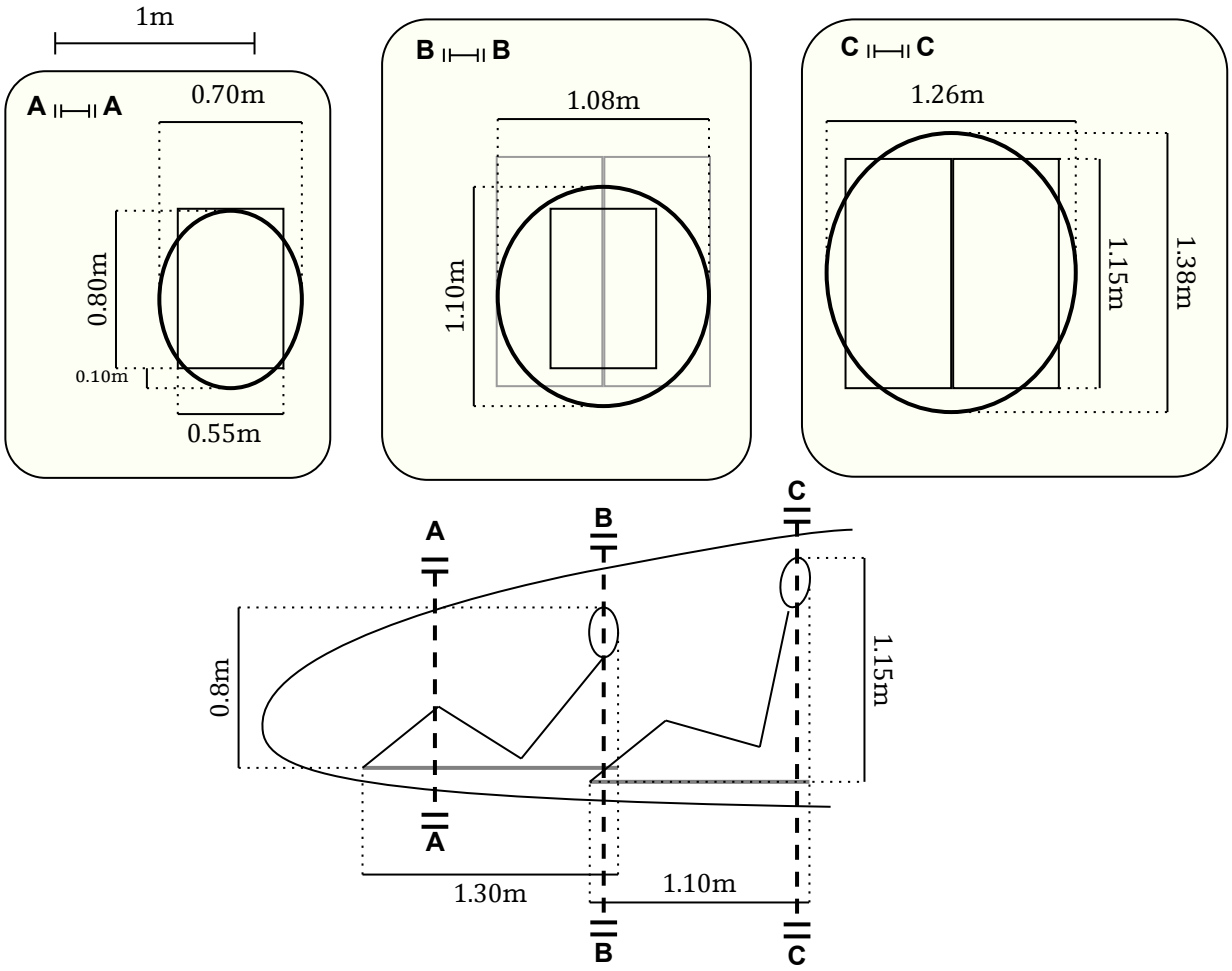

Figure 12.1: Fuselage dimensions based on the seat sizes for the passenger and pilot seats

12.2. Sizing of Fuselage

Based on the dimensions of the cabin, the rest of the fuselage could be sized. Note that the fuselage sizing was done based a sketch, and thus dimensions were determined purely to accommodate the cabin. Note that the tail length was determined based on a preliminary positioning of the floats, to ensure an adequate pitch angle during take-off or landing. Furthermore, the overall shape was made to ensure air flow remained attached, to prevent unnecessary drag increases.

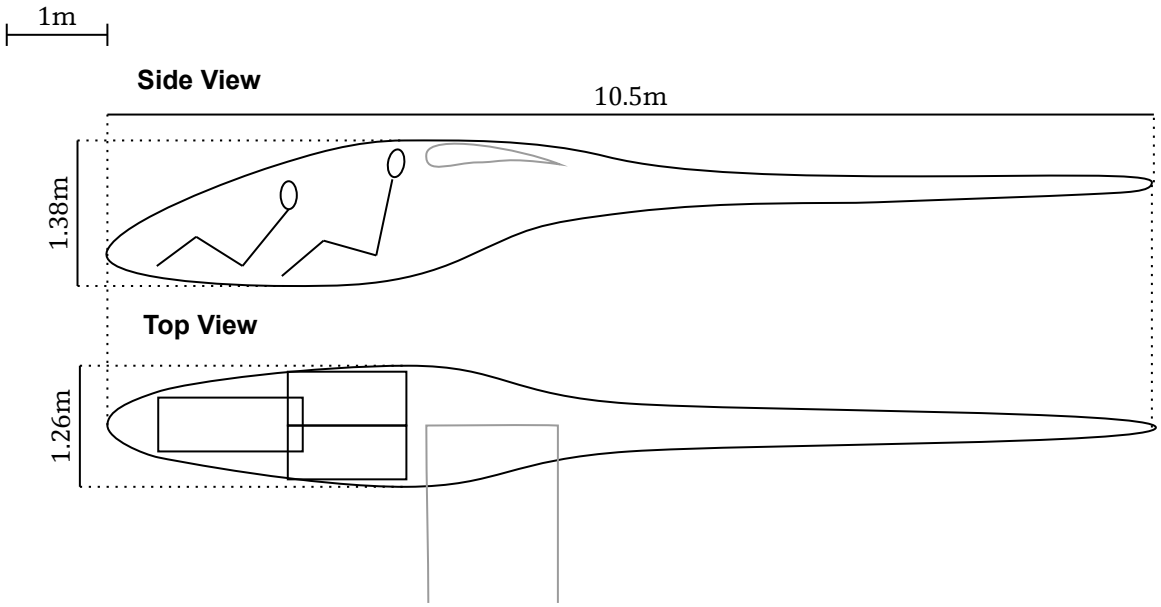

Figure 12.2: Final fuselage dimensions

12.3. Winch Connection

As mentioned in Section 5.5 the water sailplane must have an connection for a winch or aerotow launch. This connection need to be in the symmetry line of the plane in to make sure the plane is pulled straight forward and does not go into a turn. The nose is the most straight forward location as putting this connection in the struts cause very large stresses in these long and slender struts.

13. Empennage Design

The requirements relevant for the empennage can be seen in Table 13.1

Table 13.1: Empennage requirements

Identifier	Requirement
REQ-WS-FLPE-STB-01	The WS shall have a $C_{m_\alpha} < 0$ (longitudinal stability)
REQ-WS-FLPE-CON-06	The WS shall be controllable at V_S to ensure safe recovery
REQ-WS-FLPE-PAY-11	The WS shall have a $c.g.$ range of 3% of the fuselage length

13.1. Initial Sizing

To obtain an initial sizing of the vertical and horizontal tail, the concept of the tail volume coefficient is used, as defined by Roskam [30]. The tail volume coefficient is split among the vertical and horizontal tail, and is a function of the aircraft wing dimensions, tail surface area and tail arm. By rearranging these formulas, it is possible to find a relation for the vertical and horizontal tail surface areas, as can be seen in Equations (13.1) and (13.2) based on the main wing's dimensions.

$$S_h = \frac{\bar{V}_h S_w \bar{c}}{x_h} \tag{13.1}$$

$$S_v = \frac{\bar{V}_v S_w b}{x_v} \tag{13.2}$$

To use Equations (13.1) and (13.2), the tail volume coefficients must be obtained. According to Raymer, the $\bar{V}_v$ is equal to 0.02 for sailplanes, however, with a T-Tail configuration a 5% decrease can be applied due to the end-plate effect which increases the effectiveness of the vertical tail [13, 31]. Furthermore, Raymer has found that $\bar{V}_h$ equals 0.50 for sailplanes. A 5% decrease is also applicable for the horizontal tail for a T-Tail configuration as the horizontal tail receives clean air, however, due to the possible placement of the propulsion system in front of the empennage, it was assumed that this 5% decrease would not be applied.

With an assumed c.g. location, it was possible to estimate an initial tail arm length. Based on an assumed c.g. location approximately in line with quarter chord point of the mean geometric chord, a vertical tail arm of $6\,\mathrm{m}$ was assumed with a horizontal tail arm of $6.5\,\mathrm{m}$.

While Equations (13.1) and (13.2) provide the surface area, an aspect ratio must be assumed to obtain further dimensions. From Raymer, typical sailplane aspect ratios are obtained [13]. A vertical tail aspect ratio of $A_v = 1.5$ and horizontal tail aspect ratio of $A_h = 6$ were used.

By applying these parameters to Equations (13.1) to (13.2) the horizontal and vertical tails could be sized. The initial sizes are provided in

Table 13.2: Initial dimensions of the vertical and horizontal tail

Horizontal Tail			Vertical Tail		
A_h	$-$	6	A_v	$-$	1.5
x_h	m	6.5	x_v	m	6.0
S_h	m^2	2.57	S_v	m^2	2.66
b_h	m	3.92	b_v	m	2.00
$\bar{c}_h$	m	0.65	$\bar{c}_v$	m	1.33

13.2. Scissor Plot

To obtain a more detailed sizing of the horizontal tail, the longitudinal stability and controllability of the water sailplane is analyzed. The aircraft is statically stable if a disturbance is counteracted by an opposite moment to restore the equilibrium. The aircraft is said to be controllable when it can be trimmed for all flight conditions. The total moment at trimmed conditions must be zero. The aircraft's center of gravity location is essential for the stability and controllability. When it is located too far forward, the horizontal tail cannot provide enough negative lift to trim the aircraft. If it is located too far rearward, the aircraft becomes unstable. The find the allowable center of gravity range, a scissor plot is constructed. This plots the center of gravity location on the x-axis and the ratio between the horizontal tail and main wing surface area on the y-axis. This plot shows the stable region as well as the controllable region of the aircraft. Where these regions coincide, the aircraft is stable and controllable. The assumptions and simplifications used in the analysis are stated below:

SP 01: The aerodynamic moment coefficient C_{m_h} was neglected for the horizontal tail.

SP 02: Small changes in the angle of attack were assumed. This lead to the assumption that the C_{L_α} could be approximated to be constant.

SP 03: Neglected the contribution of drag and the vertical placement of the wing and horizontal tail to the stability and control analysis.

SP 04: The effect of propulsion was not included in the stability analysis. AeroDelft was consulted for a better insight in the effects of propulsion to stability. AeroDelft has build a scale model with a similar propulsion location. Their experience, the propulsion has a positive contribution to the stability, since it will reflect the flow downwards with an increase in angle of attack and vice versa. From their experience, not taking the propulsion into account for stability will be lead to a conservative design.

SP 05: Due to the low velocities of the water sailplane, the airflow is assumed to be incompressible.

SP 06: Aeroelasticity has not been taken into account during the stability and control analysis of the water sailplane.

SP 07: Since no accurate approximation of the effect of floats to the aircraft stability was available, the floats have been modeled as nacelles.

SP 08: Clean wing surfaces are assumed. This introduces a certain limitation to the results. The water sailplane will operate in seawater conditions, so the chances are high that the wing skin will be less smooth then anticipated. The effects of this must be taken into account in the more detailed design phase.

13.2.1. Stability

The aircraft must be stable for all allowable speeds. In normal flying conditions, the maximum speed is most critical for stability. This is mostly caused by the aerodynamic center of the wing moving forward at increasing speeds, which has a destabilizing effect. The stability behavior in stall and during maneuvering should be investigated in more detail in the future. In this report, the static stability longitudinal stability in stick-fixed condition is analyzed. A moment equation around the center of gravity is derived using the free body diagram below:

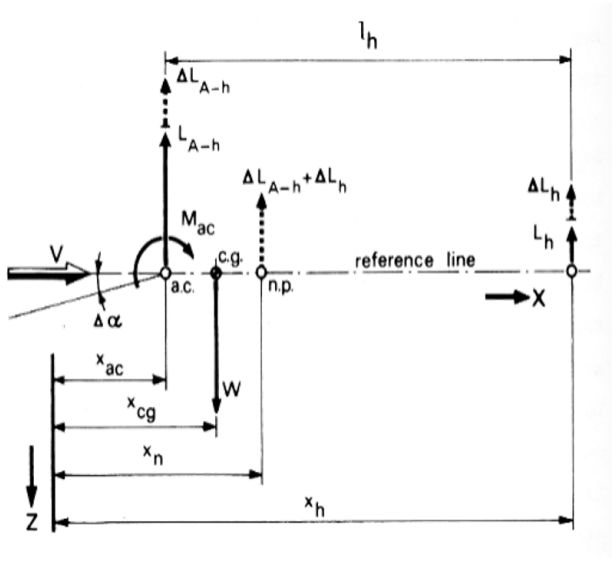

Figure 13.1: Free Body Diagram for longitudinal stability [32]

$$C_m = C_{m_{ac}} + C_{L_{A-h}} \cdot (\bar{x}_{CG} - \bar{x}_{ac}) - C_{L_h} \cdot \frac{S_h}{S} \left(\frac{V_h}{V}\right)^2 (\bar{x}_h - \bar{x}_{CG}) \tag{13.3}$$

The bar above the X locations indicate the the location is relative to the mean aerodynamic chord of the main wing. As mentioned above, a disturbance (change in angle of attack) must be counteracted by an opposite moment. Thus, the moment derivative with respect to the angle of attack must be negative, this also follows from **REQ-WS-FLPE-STB-01**. If the derivative is zero, the aircraft is neutrally stable, and the C.G. is located at the neutral point of the aircraft. With $(\bar{x}_h - \bar{x}_{CG}) = l_h$ and some rearrangement of Equation (13.3), the location of the neutral point can be found:

$$\bar{x}_{np} = \bar{x}_{ac} + \frac{C_{L\alpha_h}}{C_{L\alpha_{A-h}}} \left(1 - \frac{d\varepsilon}{d\alpha}\right) \frac{S_h l_h}{S\bar{c}} \left(\frac{V_h}{V}\right)^2 \tag{13.4}$$

The C.G. must be in front of the neutral point for stability. The equation above can thus be used to find the most aft allowable C.G. location for a given horizontal tail surface. To take into account the fact that these calculations assume a stick fixed condition and inaccuracies of the calculation, a stability margin of 10% is applied. The most aft allowable C.G. location then becomes:

$$\bar{x}_{cg} = \bar{x}_{ac} + \frac{C_{L\alpha_h}}{C_{L\alpha_{A-h}}} \left(1 - \frac{d\varepsilon}{d\alpha}\right) \frac{S_h l_h}{S\bar{c}} \left(\frac{V_h}{V}\right)^2 - S.M. \tag{13.5}$$

Which was rewritten to plot the $\frac{S_h}{S}$:

$$\frac{S_h}{S} = \frac{1}{\frac{C_{L\alpha_h}}{C_{L\alpha_{A-h}}} \left(1 - \frac{d\varepsilon}{d\alpha}\right) \frac{l_h}{\bar{c}} \left(\frac{V_h}{V}\right)^2} \bar{x}_{cg} - \frac{\bar{x}_{ac} - 0.05}{\frac{C_{L\alpha_h}}{C_{L\alpha_{A-h}}} \left(1 - \frac{d\varepsilon}{d\alpha}\right) \frac{l_h}{\bar{c}} \left(\frac{V_h}{V}\right)^2} \tag{13.6}$$

Below, a description on how the value was from Equation (13.5) were found will be given.

$\bar{x}_{ac}$, The aerodynamic center location of the aircraft without tail w.r.t. the MAC

The aircrafts aerodynamic center consist of four contributions [32]: The wings aerodynamic center, two fuselage contributions and, usually, a contribution of the nacelle. The water sailplane, however, has no big engine nacelles. Since there is no good approximation of the (de)stabilizing effect of the floats, the floats contribution is modeled with the same method as how it would be calculated for the nacelle. The wings aerodynamic center was estimated at 25% of the MAC.

$$\text{Fuselage contribution 1} = -\frac{1.8}{C_{L\alpha_{A-h}}} \frac{b_f h_f l_{fn}}{S\bar{c}} \tag{13.7}$$

$$\text{Fuselage contribution 2} = \frac{0.273}{1+\lambda}\frac{b_f c_g \left(b - b_f\right)}{\bar{c}^2 \left(b + 2.15 b_f\right)} \tan \Lambda_{1/4} \tag{13.8}$$

$$\text{Floats contribution} = 2 \cdot k_n \cdot \frac{{b_n}^2 l_n}{S\bar{c} C_{L\alpha_{A-h}}} \tag{13.9}$$

Where k_n is equal to -2.5[32].

C_{L_h}, The slope of the $C_L - \alpha$ curve of the horizontal stabilizer

The DATCOM method [26] is used to compute the $C_{L\alpha_h}$:

$$C_{L\alpha_h} = \frac{2\pi A_h}{2 + \sqrt{4 + \left(\frac{A_h \beta}{\eta}\right)^2 \left(1 + \frac{\tan^2 \Lambda_{0.5c_h}}{\beta^2}\right)}} \tag{13.10}$$

$C_{L_{A-h}}$, The slope of the $C_L - \alpha$ curve of the aircraft without tail

With the DATCOM method, the $C_{L\alpha_{A-h}}$ can be estimated. The $C_{L\alpha_w}$ can be approximated with Equation (13.10).

$$C_{L_{\alpha_{A-h}}} = C_{L_{\alpha_w}} \left(1 + 2.15\frac{b_f}{b}\right)\frac{S_{net}}{S} + \frac{\pi}{2}\frac{b_f^2}{S} \tag{13.11}$$

$\frac{d\varepsilon}{d\alpha}$, The wing downwash effect on the tail

The downwash on the tail is approximated using the equations below [33]:

$$\begin{aligned}\frac{d\varepsilon}{d\alpha} = &\frac{K_{\varepsilon_\Lambda}}{K_{\varepsilon_{\Lambda=0}}}\left(\frac{r}{r^2 + {m_{tv}}^2}\frac{0.4876}{\sqrt{r^2 + 0.6319 + {m_{tv}}^2}} + \right. \\ &\left.\left[1 + \left(\frac{r^2}{r^2 + 0.7915 + 5.0734{m_{tv}}^2}\right)^{0.3113}\right]\left\{1 - \sqrt{\frac{{m_{tv}}^2}{1 + {m_{tv}}^2}}\right\}\right)\frac{C_{L_{\alpha_w}}}{\pi \mathrm{A}}\end{aligned} \tag{13.12}$$

Where:

$$K_{\varepsilon_\Lambda} = \frac{0.1124 + 0.1265\Lambda + 0.1766\Lambda^2}{r^2} + \frac{0.1024}{r} + 2 \tag{13.13}$$

$$K_{\varepsilon_{\Lambda=0}} = \frac{0.1124}{r^2} + \frac{0.1024}{r} + 2 \tag{13.14}$$

$\frac{V_h}{V}$, The speed ratio of the horizontal tail w.r.t. the main wing

The water sailplane is designed with a T-tail to minimize the interference of the main wing with the tail. Therefore, $\frac{V_h}{V}$ is assumed to equal 1 during cruise.

S.M., The Stability Margin

The stability margin takes into account inaccuracies of the stability calculations. Contributions to the inaccuracies are the stick-free stability. The current method analyzes stability in stick-fixed condition. A more detailed analysis of the horizontal tail and elevator is required to perform stick-free stability analysis. To be on the safe side, a stability margin of 0.1 was chosen. This means that the C.G. is located 10% of the mean aerodynamic chord in front of the neutral point of the aircraft.

13.2.2. Verification of Stability Analysis

To verify the stability analysis of the water sailplane, multiple tests were performed: Three unit tests were performed, two zero tests and a compile test. Table 13.4.

Table 13.3: Verification of stability calculations

ID	Parameter	Input	Pass Condition	Test Result	Pass or Fail	Comments
UT 00	$C_{L\alpha_h}$	0	error - divide by zero	error - divide by zero	Pass	-
UT 00	$C_{L\alpha_{A-h}}$	0	error - divide by zero	error - divide by zero	Pass	-
UT 01	-	-	No compiling error	No compiling error	Pass	-
ST 03	l_h	decrease	smaller stability region	smaller stability region	Pass	-
ST 03	$\frac{V_h}{V}$	$2 \cdot \frac{V_h}{V}$	Larger stability region	Larger stability region	Pass	-
ST 03	$C_{L\alpha_h}$	$2 \cdot C_{L\alpha_h}$	Larger stability region	Larger stability region	Pass	-

13.2.3. Controllability In Landing

For controllability, the critical condition is the stall speed in landing configuration, which also follows from **REQ-WS-FLPE-CON-06**. In this situation, the highest negative lift is required of the horizontal tail. Similarly to Section 13.2.1, only the flying condition is analyzed and further research should be done to analyze the controllability in for example stall conditions. In a trimmed situation, all moments should equate to zero. This will result in the equation below. The left part represents the moment of the aircraft's aerodynamic center and the moment of the aircraft without tail. The right part represents the moment caused by the tail.

$$C_{m_{ac}} + C_{L_{a-h}}\left(\frac{x_{cg} - x_{ac}}{\bar{c}}\right) = \frac{C_{L_h} S_h l_h}{S\bar{c}}\left(\frac{V_h}{V}\right)^2 \tag{13.15}$$

The equation can then be rewritten to find the C.G. location:

$$\bar{x}_{cg} = \bar{x}_{ac} - \frac{C_{m_{ac}}}{C_{L_{A-h}}} + \frac{C_{L_h}}{C_{L_{A-h}}}\frac{S_h l_h}{S\bar{c}}\left(\frac{V_h}{V}\right)^2 \tag{13.16}$$

The list below defines each new variable of Equation (13.16). Then a description on how the value was found will be given.

$C_{m_{ac}}$, The moment coefficient of the aircraft around its aerodynamic center

The moment coefficient if the aircraft around its aerodynamic center can be found using the following calculation:

$$C_{m_{ac}} = C_{m_{ac_w}} + \Delta f C_{m_{ac}} + \Delta f us C_{m_{ac}} \tag{13.17}$$

Where $C_{m_{ac_w}}$ is the aerodynamic center of the main wing. $\Delta f C_{m_{ac}}$ is the the contribution of the flaps. $\Delta f us C_{m_{ac}}$ is the contribution of the fuselage to the moment coefficient. These coefficients were found using the following equations [32]:

$$C_{m_{ac_w}} = Cm_{0\text{airfoil}}\left(\text{Acos}^2\,\Lambda/(A + 2\cos\Lambda)\right) \tag{13.18}$$

$$\Delta f C_{m_{ac}} = \mu_2\left\{-\mu_1 \Delta C_{l_{\max}}\frac{c'}{c} - \left[C_L + \Delta C_{l_{\max}}\left(1 - \frac{Swf}{S}\right)\right]\frac{1}{8}\frac{c'}{c}\left(\frac{c'}{c} - 1\right)\right\} + 0.7\frac{A}{1 + 2/A}\mu_3 \Delta C_{l_{\max}} \tan\Lambda_{1/4} \tag{13.19}$$

$$\Delta f us C_{m_{ac}} = -1.8\left(1 - \frac{2.5 b_f}{l_f}\right)\frac{\pi b_f h_f l_f}{4S\bar{c}}\frac{C_{L_0}}{C_{L_{\alpha_{A-h}}}} \tag{13.20}$$

μ_1, μ_2 and μ_3 from Equation (13.19) where found using the empirical relations described by Torenbeek [32].

$C_{L_{A-h}}$, The lift coefficient of the aircraft without tail

It was assumed that the aircrafts most dominant lift contribution would come from the main wing. Therefor, the $C_{L_{A-h}}$ was set equal to the C_{L_max} of the wing in landing configuration.

C_{L_h}, The lift coefficient of the horizontal stabilizer

The maximum desirable negative lift coefficient was approximated using the following equation:

$$C_{Lh} = -0.35A_h^{1/3} \tag{13.21}$$

13.2.4. Controllability In Climb

In climb, two things change for the controllability analysis: The engine is operating and, as a consequence of the engine, the speed over the horizontal tail is increased. The first creates a nose down moment, which is not beneficial for the controllability, especially since the engine is located in the horizontal stabilizer, increasing its moment arm. The latter creates an increase in controllability, since the speed ratio is increased. Therefor, the controllability during climb is analyzed to see if this condition is more critical then cruise conditions. To take into account the moment caused by the propeller, Equation (13.16) was rewritten to:

$$\bar{x}_{cg} = \bar{x}_{ac} - \frac{C_{m_{ac}}}{C_{L_{A-h}}} + \frac{C_{L_h}}{C_{L_{A-h}}}\frac{S_h l_h}{S\bar{c}}\left(\frac{V_h}{V}\right)^2_{climb} + \frac{1}{C_{L_{A-h}}}\frac{T_{climb}\left(z_{CG} - z_{eng}\right)}{0.5\rho V_{climb}^2 S\bar{c}} \tag{13.22}$$

As mentioned above, the $\left(\frac{V_h}{V}\right)_{climb}$ must analyzed to get the proper ratio. The equation below [14] is used to calculate the velocity after the propeller:

$$V_h = V_\infty + 2w \tag{13.23}$$

$$w = \frac{1}{2}\left[-V_\infty + \sqrt{V_\infty^2 + 2T/\left(\rho A_P\right)}\right] \tag{13.24}$$

13.2.5. Controllability In Take-Off

During take-off, it is essential that the water sailplane can rotate to the floats step to reduce its water drag. This case is analyzed to make sure the horizontal tail is sized to make sure it can provide the required negative lift for this rotation. The following moment equation is derived:

$$S_h = \left(M_{lift} + M_{ac} - M_{floation} - M_{drag_{floats}}\right) / \left(0.5\rho V_{step}^2 C_{Lh} l_h\right) \tag{13.25}$$

Moment caused by aircrafts lift:

$$M_{lift} = 0.5\rho V_{step}^2 S C_{L_{A-h}} \tag{13.26}$$

Moment caused by aircrafts aerodynamic center:

$$M_{ac} = C_{m_{ac}} 0.5\rho V_{step}^2 S\bar{c} \tag{13.27}$$

Moment caused by flotation force of floats:

$$M_{floation} = F_{floatation}\left(x_{boyancy} - x_{CG}\right) \tag{13.28}$$

Moment caused by drag of floats:

$$M_{drag_{floats}} = D_{float}\left(z_{float - z_{CG}}\right) \tag{13.29}$$

Equation (13.5), Equation (13.16) and Equation (13.22) can both be plotted in a scissor plot. Combining the scissor plot with a C.G. range of the aircraft, the required $\frac{S_h}{S}$ can be found. This must then be compared with the result of Equation (13.25) to find the minimum required horizontal tail surface area.

13.2.6. Verification of Controllability Analysis

To verify the controllability analysis of the water sailplane, multiple tests were performed: Three unit tests were performed, two zero tests and a compile test. To test the system, two relation tests were performed.

Table 13.4: Verification of controllability calculations

ID	Parameter	Input	Pass Condition	Test Result	Pass or Fail	Comments
UT 00	$C_{L\alpha_h}$	0	error - divide by zero	error - divide by zero	Pass	-
UT 00	$C_{L\alpha_{A-h}}$	0	error - divide by zero	error - divide by zero	Pass	-
UT 01	-	-	No compiling error	No compiling error	Pass	-
ST 03	l_h	decrease	smaller stability region	smaller stability region	Pass	-
ST 03	$\frac{V_h}{V}$	$2 \cdot \frac{V_h}{V}$	Larger stability region	Larger stability region	Pass	-

13.3. Center Of Gravity Range

The C.G. range of the aircraft must be analyzed for the stability and controllability. The center of gravity location is analyzed along the x-axis and the z-axis, where the x-axis runs through the nose towards the tail and the z-axis points downwards from the x-axis. It was assumed that the aircraft is symmetric in the xz plane, so the C.G. would lay on the y-axis. A basic moment equation was used to find the center of gravity location:

$$x_{CG} = \frac{\sum x_i \cdot W_i}{\sum W_i} \tag{13.30}$$

$$z_{CG} = \frac{\sum z_i \cdot W_i}{\sum W_i} \tag{13.31}$$

The following assumptions and simplifications were made:

CG 01: The fuselage, passenger, pilot, avionics, batteries C.G. location were assumed to be located on the z-axis.

CG 02: A constant pilot weight was used to analyze the C.G. range. It is likely that a pilot has a weight lower than this constant. For a complete C.G. range, this should be taken into account.

The components used in the center of gravity analysis are:

- Fuselage
- Floats
- Passengers
- Pilot
- Avionics
- Batteries
- Horizontal tail
- Vertical tail
- Engine

The C.G. position was analyzed for two conditions: a loading of a pilot and two passengers and loading of only a pilot, without passengers. This resulted in an aft and forward C.G. location. The C.G. range must be located such that it fits within the scissor plot. During the initial sizing of the aircraft, it became evident that the C.G. had the tendency to be located far in front of the mean aerodynamic chord. After the engine was located at the tail, this was no longer the case as the C.G. shifted more towards the tail. The design freedom with regards to the C.G. position mainly comes from the battery placement. The forward location is constraint by the passenger seats, and the aft position of the battery is constrained by the limited tail diameter.

13.3.1. Verification of center of gravity Location Analysis

To verify the C.G. location, multiple unit and system tests were performed. The moment arm of various components were increased to see if the center of gravity would shift in in that direction.

Table 13.5: Verification of center of gravity locations anlysis

ID	Parameter	Input	Pass Condition	Test Result	Pass or Fail
UT 01	-	0	no compiling error	no compiling error	Pass
ST 03	z	$z \cdot 2$	C.G. shift towards component	C.G. shift towards component	Pass
ST 03	x	$x \cdot 2$	C.G. shift towards component	C.G. shift towards component	Pass

13.4. Elevator sizing

The Equation (13.21) is used to analyze the required elevator to chord ratio and deflection angle. Javafoil was used to analyze the horizontal tail. The C_{L_h} was calculated to be $-0.635\,99$. It was assumed that the airfoil C_{l_h} was $\frac{C_{L_h}}{0.9} = -0.7067$. In Javafoil, the flap to chord ratio was iterated in combination with the deflection angle of the elevator to find the combination that would provide the minimum lift coefficient with as little drag as possible. The following assumptions and simplifications were made:

ES 01: $C_{l_h} = \frac{C_{L_h}}{0.9}$. A more detailed analysis should be performed to correctly relate the 2D lift coefficient to a 3D lift coefficient

ES 02: A symmetric airfoil was selected to simplify the lift and drag estimations.

14. Floats Design

This chapter covers the design of the water sailplane floats and the struts connecting the floats to the fuselage of the aircraft.

The floats have multiple functions and requirements. First, the floats should provide enough buoyancy to allow the water sailplane to float on the water, with extra support. Next, the floats should provide adequate hydrostatic stability. The floats have to be designed to allow for fast take-off, and should thus not create to much hydrodynamic resistance. Finally the floats and the connecting struts should be able to withstand landing loads. The requirements can be seen in Table 14.1

Table 14.1: Floats requirements

Requirement ID	Description
REQ-WS-WATO-01	The WS shall have a total buoyancy force of $80\,\%$ greater than the MTOW
REQ-WS-WATO-05	The WS shall be able to land with a wave height of $0.3\,\mathrm{m}$
REQ-WS-WATO-09	The WS shall have a turn radius of $10\,\mathrm{m}$ on the water
REQ-WS-WATO-16	The WS shall have a metacentric height $GM > 0$ at MTOW

14.1. Float Sizing

This section covers the design and sizing of the floats shapes and dimensions, based on hydrostatic stability and buoyancy volume.

14.1.1. General shape

The general shape of the floats has a significant impact on the hydrodynamic resistance of the aircraft, and thus its take-off performance. While theoretically a lot of shapes are possible, the most commonly used shape is the step float, or planing-tail float [34]. During a take-off with step floats the aircraft is trimmed so that the forebody of the floats are rotated out of the water, and only the step makes contact with the water. This process

is referred to as 'getting on the step', and significantly reduces the hydrodynamic resistance during take-off, allowing the aircraft to accelerate and take-off faster [12]. Since the step is a discontinuity in the bottom surface of the float, this design has the downside of added aerodynamic drag. The take-off performance with a step is so beneficial that the cost of the extra aerodynamic drag is worthwhile. This design was therefore chosen for the floats of the water sailplane.

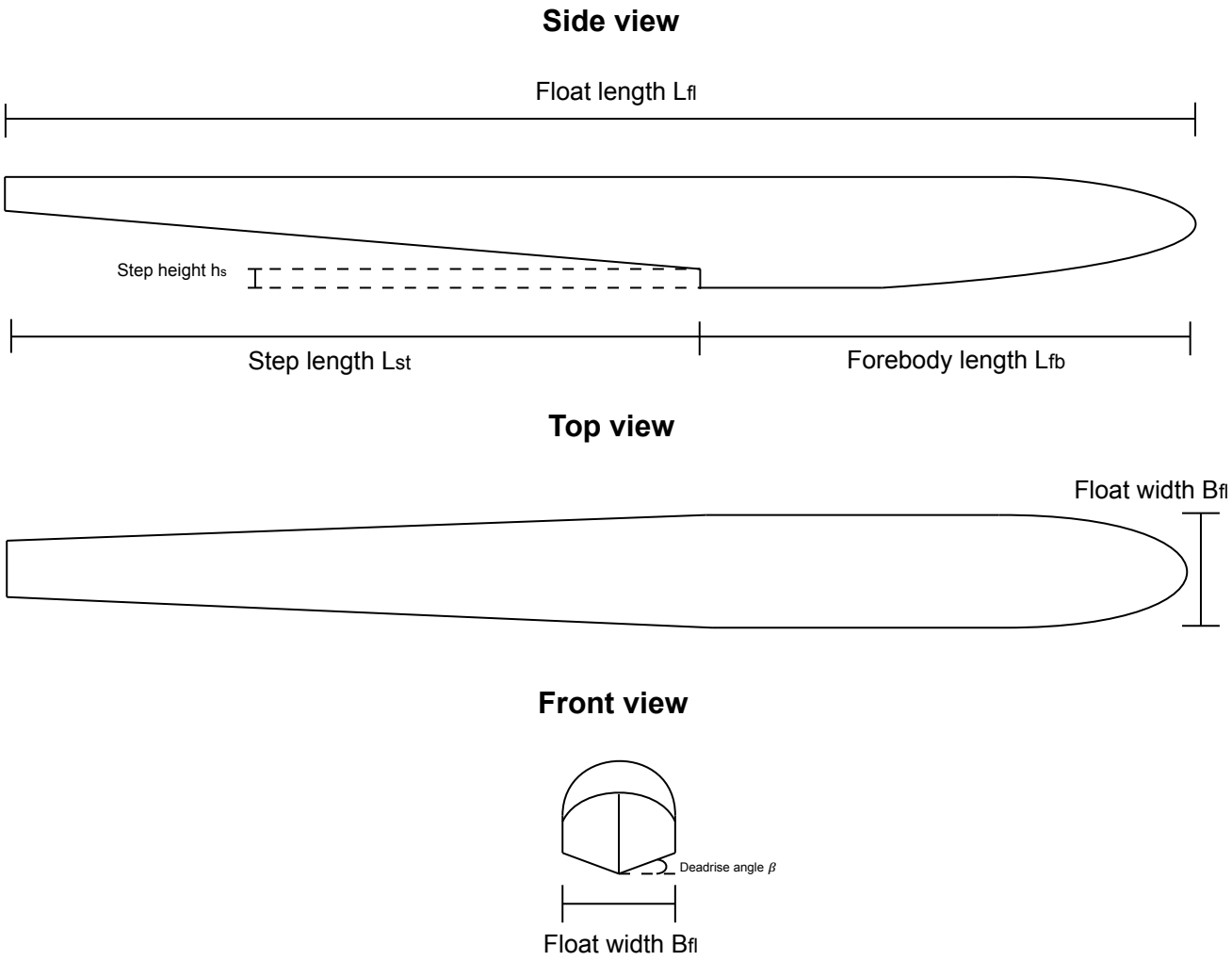

Figure 14.1: Float dimensions

The location of the step is commonly at or slightly behind the longitudinal position of the CG of a seaplane, to allow for easier rotation of the aircraft [14]. From inspection of seaplane floats, this often leads to the step being located between a third and half of the float length from the nose of the float [35].

14.1.2. Hydrostatic Stability

The hydrostatic stability of a body floating in water is defined as the ability to put itself in its original upright resting position, after it has been tipped in the water by a disturbance [14]. As a body is tipped over in the water by a certain angle θ_b, called the heel angle, more volume is pushed under water. This causes both a shift in center of buoyancy (CB), through which the buoyancy force acts, and an increase in the buoyancy force itself. This offset and increase of the buoyancy force results in a restoring moment, which is called the righting moment of the body. This is illustrated in Figure 14.2.

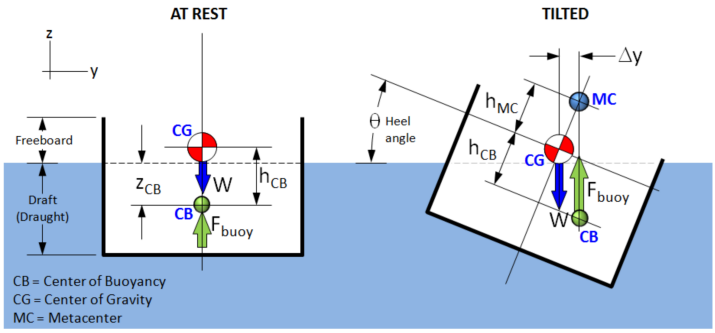

Figure 14.2: Restoring or 'righting' moment of a disturbed body in water [14]

The buoyancy force of a floating body is defined by Equation (14.1):

$$F_{\text{buoy}} = \Delta = \rho_W \cdot g \cdot V_d \tag{14.1}$$

Here ρ_W is the mass density of the displaced fluid, in this case seawater, g is the gravitational acceleration and V_d is the volume of the object displacing the water, which is equal to the volume of water displaced.

An important parameter for hydrostatic stability is the height of the an imaginary point called the metacenter (MC). As seen in Figure 14.2 the MC is the intersection point of the rotated line going through the CG and the vertical line going through the displaced CB. If the MC is above the CG, its height is defined as positive, and the body is called stable, as it will have the tendency to right itself to its at-rest attitude [14]. There is however a limit to the amount of heel angle a body can achieve. At a certain angle the MC will end up below the CG, and the body will become unstable.

According to [14] and [36] satisfactory hydrostatic stability is achieved if the metacentric height is given by Equation (14.2):

$$h_{MC} = K\sqrt[3]{W_0} \tag{14.2}$$

Here K is a constant that depends on the type of seaplane, which is 1.4 for floatplanes with two main floats, and W_0 is the gross weight of the seaplane in lbf.

Furthermore, it is suggested that for twin floatplanes the transverse and longitudinal metacentric heights should be designed to match Equation (14.3) and 14.4:

$$h_{MC_T} = \frac{19.5 B_{fl} L_{fl} s_{fl}^2}{W_0} \tag{14.3}$$

$$h_{MC_L} = \frac{4.20 B_{fl} L_{fl}^3}{W_0} \tag{14.4}$$

Here h_{MC_T} and h_{MC_L} are the transverse and longitudinal metacentric heights, B_{fl} and L_{fl} are the beam or the width and length of a single float respectively, and s_{fl} is the center-to-center spacing between the floats. All parameters are in ft.

Combining Equation (14.2) and 14.3 a recommended float spacing can be estimated, leading to Equation (14.5):

$$s_{fl} = \frac{0.2679 W_0^{2/3}}{\sqrt{L_{fl} B_{fl}}} \tag{14.5}$$

Next to this, Equation (14.2) and 14.4 can be combined to find a recommended float width B_{fl} for a given float length L_{fl}, leading to Equation (14.6):

$$B_{fl} = \frac{0.333 W_0^{4/3}}{L_{fl}^3} \tag{14.6}$$

It was determined that the length of a twin float is typically around 75% of the length of the aircraft, which was used as a base for the float design [37].

14.1.3. Buoyancy Volume

One of the requirements for the floats, REQ-WS-WATO-01, the floats of the water sailplane shall be able to provide a total buoyancy force of $1.8 \cdot MTOW$.

To determine the volume of the floats, a similar method was used to the determination of fuselage wetted area, by breaking up the float in elementary solids. The forebody of the float was assumed to be a paraboloid, and the stepped afterbody to be half a frustum. It was assumed that the end with of the float was half the maximum width of the float B_{fl}. This leads to Equation (14.7) for the volume per float:

$$V_{fl} = V_{fb} + V_{step} = \frac{\pi B_{fl}^2 L_{fb}}{8} + 0.5 \cdot \frac{\pi \cdot L_{step}}{12} \cdot (B_{fl}^2 + \frac{B_{fl}^2}{2} + \frac{B^2}{4}) \tag{14.7}$$

The required volume per float based on REQ-WS-WATO-01 can be calculated by rewriting Equation (14.1) to Equation (14.8):

$$V_{req} = \frac{1.8 \cdot MTOW}{\rho_w \cdot g} \tag{14.8}$$

14.1.4. Float & Wave Height

Another parameter that needs to be determined is the float height, which is defined as the distance between the float center line and the CG of the entire aircraft, as shown in Figure 14.3. Typically the float spacing to height ratio w/h is between 1.4 and 1.7. An w/h ratio of 1.5 was chosen for the initial float design.

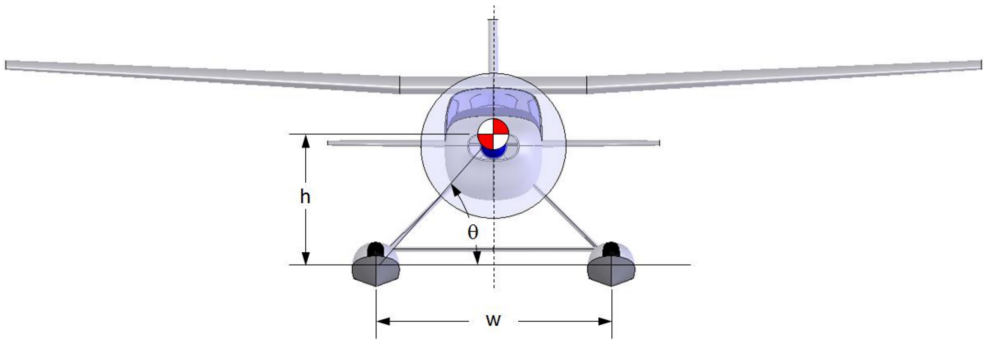

Figure 14.3: Float height & spacing [14]

Lastly an estimate of the maximum wave height a seaplane with a certain weight and thus displacement is given by Equation (14.9) [14]:

$$h_{\text{wave}} \approx 1.25 \ln(W_0) - 8.6414 \tag{14.9}$$

14.1.5. Initial Design

Based on the the following initial aircraft parameters, an initial sizing of the floats was done:

- L_{fuse} = $10.6m$
- $MTOW$ = $962kg \cdot 9.80665 = 9434N$

This lead to a float length L of $7.95m$. With this length, the recommended float width for sufficient hydrostatic stability should be greater than:

$$B_{fl} = \frac{0.333 \cdot (962 \cdot 9.80665 \cdot 0.2248)^{4/3}}{(7.95 \cdot 3.28)^3} = 0.512\text{ft} = 0.16\text{m}$$

This L and B would lead to a float volume of:

$$V_{fl} = \frac{\pi \cdot 0.16^2 \cdot \frac{7.95}{3}}{8} + 0.5 \cdot \frac{\pi \cdot \frac{2 \cdot 7.95}{3}}{12} \cdot (0.16^2 + \frac{0.16^2}{2} + \frac{0.16^2}{4}) = 0.055 m^3$$

The total float volume of the aircraft would then be $0.11 m^3$. The required volume with the initial weight was:

$$V_{req} = \frac{1.8 \cdot 9434}{1026 \cdot 9.80665} = 1.69 m^3$$

Clearly the minimum required B_{fl} for stability does not necessarily lead to floats with enough volume. One other parameter that is of interest for the floats is the slenderness ratio, defined by L/B_{fl}. This ratio is typically around 5 to 9, but can be as large as 15 [14]. The previously calculated float L and B would lead to an L/B_{fl} ratio of 51, which is then extremely high. Therefore the float width should be higher to get a sufficient float volume and a reasonable L/B_{fl} ratio.

Increasing B_{fl} to get a sufficient float buoyancy volume leads to the initial float dimensions given in Table 14.2:

Table 14.2: Initial float parameters

Element	Symbol	Value
Length	L	$7.95\,\mathrm{m}$
Width	B	$0.61\,\mathrm{m}$
Slenderness	L/B	$13.0 -$
Total float volume	V_{fl}	$1.70\,\mathrm{m}^3$
Float spacing	s_{fl}	$3.69\,\mathrm{m}$
Float height	h_{fl}	$2.46\,\mathrm{m}$
Wave height	h_w	$0.28\,\mathrm{m}$

14.2. Structural Design Float struts

After the dimensions of the floats are calculated it is essential to determine how the floats will be secured. As is suspected this will be done with a number of struts between the fuselage and floats as well as struts between the floats themselves. The method via which the properties of these struts is calculated is described in the following sections.

14.2.1. Methodology and Assumptions

In order to perform a structural analysis of the float struts different load cases are identified, these are;

- Taxiing
- Take-off
- Landing
- Flying at a high negative load factor
- Flying at a high positive load factor

To ensure the struts will not fail during operation the cases which have the highest load factor are used to design the struts. The impact during landing will be substantially higher than during take-off or taxiing. Also it is assumed that the high negative load factor will create less compression in the struts than the landing case. Thus the load cases which are used for the structural design are landing and flying with high positive load factor.

The most positive load factor the plane must be able to withstand is 4.4 as was described in Section 9.3.

The load factor during landing is found using the method described by EASA[38]. There are a number of landing cases, namely; step, bow and stern landing cases. These landing cases can either be symmetrical or asymmetrical landings. With asymmetrical landings the pressure of the water on the float is not symmetrical causing, aside from the upward force, an inward force acting towards the other float. With symmetrical landing this water pressure is symmetrical causing only a upward force.

A number of assumptions are made to be able to perform the float strut calculations described in the following sections. The assumptions Item **FS 01** up to and including item **FS 07** is derived from EASA assumptions[38].

FS 01 **Symmetrical step landings** The resultant water load acts through the center of gravity

FS 02 **Symmetrical bow landings** The resultant water load acts at one-fifth of the length from the bow to the step

FS 03 **Symmetrical stern landings** The resultant water load acts at 85% of the length from the step to the stern

FS 04 **Asymmetrical landing** The resultant upward water load is 0.75 and side load $0.25 * \tan\beta$ times the landing load. The side load is direct inboard

FS 05 **Global load factor** The whole plane is subjected to the load factor

FS 06 **No point loads** The loads resulting from the load factors may be distributed over the hull and float surface

FS 07 **Each float is a fictitious plane** For twin float seaplane each float can be seen as an equivalent hull on a fictitious seaplane with a weight of half the twin float plane weight.

FS 08 **Vertical forces** For the calculation of the struts it is assumed the landing forces act vertically, except for bow landing (Section 14.2.3)

FS 09 **Symmetrical step landings** The resultant water force acts through the step

FS 10 **Compression and tensile** It is assumed the critical forces to be either compression or tensile forces.

With the following requirement;

1. **Load factor of** 2.33 **minimal**

Step, Bow and Stern Load Factors
The step, bow and stern load factors are calculated using Equation (14.10).

$$n = \frac{C_1 * V_{stall}^2}{(\tan\beta)^{\frac{2}{3}} W^{\frac{1}{3}}} * \frac{K_1}{(1 + r_x^2)^{\frac{2}{3}}} \tag{14.10}$$

Here, C_1 is and empirical seaplane operation factor equal to 0.012, except if requirement 1 is not met. The angle of dead rise β describes how 'sharp' the float is. An angle of $0°$ would mean a flat bottom and an angle of $80°$ would mean a very sharp bottom. W Is the MTOW since the highest loads occur if the plane is heaviest and due to using batteries in stead of fuel the MTOW is also the maximum landing weight. K_1 is the empirical hull station weighing factor and is found using [38]. Lastly the r_x is the ratio of distance, from the c.g. to the longitudinal location where the load factor is applied to the radius of gyration in pitch of the seaplane. For the step landing the distance between the c.g. and the location where the load factor is applied is 0 thus the second term is removed.

Radius of gyration
The radius of gyration can be calculated using the following equation;

$$k = \sqrt{\frac{I_y}{M}} \tag{14.11}$$

Thus, firstly the I_y has to be calculated, this is done with Equation (14.12). The moment of inertia is the sum of the moment of inertia of all the subsystems, such as the wing and the floats. This resulted in a moment of inertia of $15\,438\,\mathrm{kg/m^2}$. Which resulted in a radius of gyration of $3.83\,\mathrm{m}$.

$$I = \sum_{i=1}^{N} * m_i * r_i^2 \tag{14.12}$$

14.2.2. Strut configuration

For the configuration of the struts the least amount of struts will be used. This means two spreader bars between the floats, one forward and one aft. And a total of three struts between each float and fuselage. One forward, one aft and one diagonal strut. The diagonal strut is oriented in this manner so that in the case that the floats dip under water during landing the diagonal strut will be under tension. Under compression Euler's critical load might be reached in such an situation. In Figure 14.4 the strut configuration can be seen. From the right picture it becomes clear that the aft and forward strut are spaced an equal distance, of $0.75\,\mathrm{m}$ front and aft of the c.g. The spacing is set to this value through comparison to equally sized seaplanes. If the loads become to high the spacing might have to be altered. All the joints are rotational free and transnational fixed. This means the struts can only carry compression and tensile forces as well as torsion. However the struts will not be able to carry moment forces. Though it is assumed that compression and tensile forces are critical (assumption Item **FS 10**).

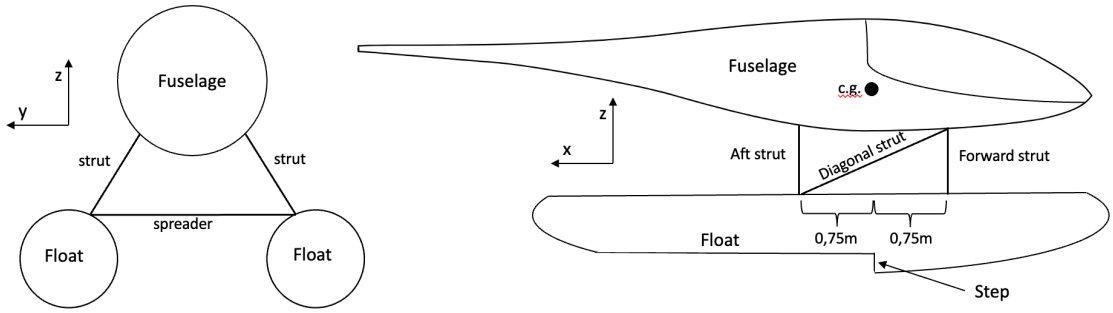

Figure 14.4: Strut configuration, picture on the left is front view, picture on the right is side view

14.2.3. Landings

Each of the different landing cases is calculated. Thus the step, bow and stern landings as well as symmetrical and asymmetrical landings. For all landing cases the force is assumed to be vertical (assumption Item **FS 08**) except for the bow landing. Here two cases are calculated; one with the force oriented vertically and one with the force oriented horizontally. The latter is supposed to analyze the case in which one float hits the water in such a manner that the float dips underwater creating a very high horizontal load on the structure.

14.2.4. Step Landing

For the step landing it is assumed that the force acts on the step (assumption Item **FS 09**. Since the force is directed upward at the step and the struts are equally spaced from the step the force is also equally distributed between the pair of struts.

Symmetrical

Firstly the load factor is calculated using Equation (14.10). The force which the fuselage exerts on the struts is calculated using Equation (14.13). Notice the weight of the floats is subtracted from the total weight as the weight of the floats do not cause forces in the struts during landing.

$$F_f = ((MTOW - W_{float}) * 9.81 * n)/2 \tag{14.13}$$

To identify the forces in each of these two struts the angle between the struts is needed. This is calculated using Equation (14.14). The float height h_{fl} can also be seen as the fuselage height. And is the vertical distance from the center of the fuselage to the center of the float.

$$S_\angle = 2 * \tan^{-1}(0.5 * s_{fl}/h_{fl}) \tag{14.14}$$

Finally the force in the forward strut can be calculated with Equation (14.15). Notice the force multiplied with a half, this is due the forward struts each carrying half of that load. The force in the spreaders is calculated with Equation (14.16).

$$F_{st} = 0.5 * F_f/(\cos(S_\angle/2)) \tag{14.15}$$

$$F_{sp} = F_{st} * \cos(180 - 90 - 0.5 * S_\angle) \tag{14.16}$$

This results can be seen in Table 14.3.

Asymmetrical

With assumption 7 of Section 14.2.1 the load factor can be divided into both an upward and inboard water load. These forces are calculated with the following equations;

$$F_z = 0.75 * n * (((MTOW - W_{float}) * 9.81)/2) \tag{14.17}$$

$$F_y = 0.25 * \tan(\beta) * n * (((MTOW - W_{float}) * 9.81)/2) \tag{14.18}$$

With F_y and F_x the equations Equation (14.19) and Equation (14.20) are calculated.

$$F_{st} = F_z/\cos(0.5 * S_\angle) \tag{14.19}$$

$$F_{sp} = F_y - \sin(0.5 * S_\angle) * F_{st} \tag{14.20}$$

The results can be seen in Table 14.3.

Table 14.3: Loads in struts during step landing, positive is tension, negative is compression, all forces are in Newtons

Load case	Forward Strut	Aft Strut	Forward Spreader	Aft Spreader
Symmetrical	-11143	-11143	1982	1982
Asymmetrical	-8357	-8357	-4203	-4203

14.2.5. Bow Landing

The calculation for the bow landings follows the same steps as with the step landing. However because the force acts in front of the struts an arm is created which increases the loads on the struts. Also the horizontal load case will be investigated which mainly calculates the required strength of the diagonal strut.

Symmetrical

Again Equation (14.15) is used to calculate the force on one float. Notice the force on one float is half the value of F_f. The distance between the struts and the applied force were calculated with the following equations. Equation (14.21) calculates the location where the load is applied. This location is 1/5 of the length from the bow to the step removed from the bow. With the distance from the bow to the step equal to 1/3 of the float length.

$$x_F = 1/3 * 1/5 * L_{fl} \tag{14.21}$$

The location of the forward and aft struts are calculated using the following equations.

$$x_{st,for} = L_{fl} * 1/3 - 0.75 \qquad x_{st,aft} = L_{fl} * 1/3 + 0.75 \tag{14.22}$$

The distance between the applied force and the forward strut is calculated using the following equation.

$$x_{F,st} = x_{st,for} - x_F \tag{14.23}$$

Finally, with basic statics the vertical force of the aft struts and the vertical force of the forward struts are calculated using Equation (14.24)

$$F_{aft} = -F_f * x_{F,st}/x_{fl} \qquad F_{for} = -F_{aft} + F_{fl} \tag{14.24}$$

The force in the struts and spreaders are again calculated using Equation (14.15) and Equation (14.16) respectively. The results can be seen in Table 14.4.

Asymmetrical

The following equations are used to calculate the upward and inward forces.

$$F_z = 0.75 * F_{aft} \qquad F_y = 0.25 * \tan(\mathrm{B}) * F_{aft} \tag{14.25}$$

Then the aft strut and spreader forces are calculated with Equation (14.19) and Equation (14.20). The forward forces are calculated with the same equations however in Equation (14.25) the F_{aft} is changed to F_{for}. The results can be seen in Table 14.4.

Lastly the forces for the diagonal strut are calculated. For this calculation it is assumed that the load acts horizontally. This means the load will have to be carried completely by the diagonal strut. Such a situation might occur when the floats dips underwater, stopping the aircraft quickly with high horizontal forces as a consequence. To calculate the force in the strut firstly the angle between the diagonal strut and the float was calculated using Equation (14.26). With this angle and Equation (14.27) the force in the diagonal strut is calculated. Notice the F_{fl} is multiplied with two, this is done to identify the largest force which happens if only one float dips in the water and the load of the whole aircraft acts on the diagonal strut.

$$\angle_{dia} = \tan^{-1}(h_{fl}/x_{fl}) \tag{14.26}$$

$$F_{dia} = 2 * F_{fl}/\cos(\angle_{dia}) \tag{14.27}$$

The result can be seen in Table 14.4. Notice the force in the diagonal strut is put under the symmetrical load case. This is because the load acts in one direction; horizontal. And for the asymmetrical load case the load is divided into two directions.

Table 14.4: Loads in struts during bow landing, positive is tension, negative is compression, all forces are in Newtons

Load case	Forward Strut	Aft Strut	Forward Spreader	Aft Spreader	Diagonal Strut
Symmetrical	-42645	20200	25587	-12120	68491
Asymmetrical	-31984	15150	16086	-7619	-

14.2.6. Stern Landing

The stern landing case is very similar to the bow landing case however some values are different. Mainly the distance between the struts and the location of the load. Since the load is applied aft the struts instead of forward the struts.

Symmetrical

The distance between the aft strut and the applied load is calculated using Equation (14.28). The force on the float is again calculated with Equation (14.13). However the load factor n is now different.

$$x_F = 2/3 * L_{fl} - 0.5 * x_{fl} \tag{14.28}$$

With some basic statics the forces on the struts are calculated. The vertical force acting on the struts is calculated with Equation (14.24). However the terms F_{aft} and F_{for} are switched because the force acts behind the struts instead of in front of it. The force in the struts and spreaders are again calculated using Equation (14.15) and Equation (14.16) respectively. The results can be seen in Table 14.5.

Asymmetrical

The force created by the load is split into an upward and inward force. These are calculated with Equation (14.25). The aft strut and spreader forces are then calculated with Equation (14.19) and Equation (14.20). The forward forces are calculated in the same manner however F_{aft} is changed to F_{for} in the equations. he results can be seen in Table 14.5.

Table 14.5: Loads in struts during stern landing, positive is tesnion, negative is compression, all forces are in Newtons

Load case	Forward Strut	Aft Strut	Forward Spreader	Aft Spreader
Symmetrical	30195	-40260	-18117	24156
Asymmetrical	22646	-30195	-11390	15186

14.2.7. Maneuvering load

Due to the positive maneuvering load the weight of the floats creates forces in the struts which have to analyzed. The force acting on one pair of struts is calculated with Equation (14.29).

$$F_f = ((W_{float}) * 9.81 * n)/2 \tag{14.29}$$

The force in one strut is calculated with Equation (14.30). The result can be seen in Table 14.6.

$$F_{st} = 0.5 * F_f/(\cos(S_\angle/2)) \tag{14.30}$$

The force in the spreader is calculated with Equation (14.31). The result can be seen in Table 14.6.

$$F_{sp} = F_{st} * \cos(180 - 90 - 0.5 * S_\angle) \tag{14.31}$$

Table 14.6: Loads in struts during stern landing, positive is tension, negative is compression, all forces are in Newtons

Load case	Struts	Spreaders
Maneuvering positive load factor	-989	176

It is clear form Table 14.6 the maneuvering will not create the critical load. Thus only the landing will be used to identify the critical load.

14.2.8. Euler's Critical Load

Due to the slender struts and the high compression forces in the struts the chance on Euler's critical load being reached is large. Euler's critical load is calculated with Equation (14.32). The unsupported length, L, is fixed. As is the K, the column effective length factor, which is 1 for an column which is clamped. The Young's modulus, E, is a material property and is $63\,\mathrm{Gpa}$ for high modulus carbon. Aluminum might also be a suited material for these struts, however it is essential the weight is kept down. Thus because of this reason high modulus carbon is most suited for this job. Lastly to calculate the moment of inertia, I, the dimensions of the struts have to be known.

$$P_{cr} = \frac{\pi^2 EI}{(KL)^2} \tag{14.32}$$

The moment of inertia is found by rewriting Equation (14.32) and setting P_{cr} to the highest compression load found in the previous sections. Only for the diagonal strut this is not possible as the strut is not exposed to compression forces. For these struts the area is simply calculated by Equation (14.33). The safety margin, s_m, is set to 1.7 as is standard for composites.

$$S_{dia} = -F_{dia} * s_m/\sigma_{ult,com} \tag{14.33}$$

Round

The struts have a round shape because this shape is most easy and also cheap to produce. The aerodynamics can easily be improved by adding some sort of sleeve in the shape of an symmetrical airfoil, around the strut. Figure 14.5.

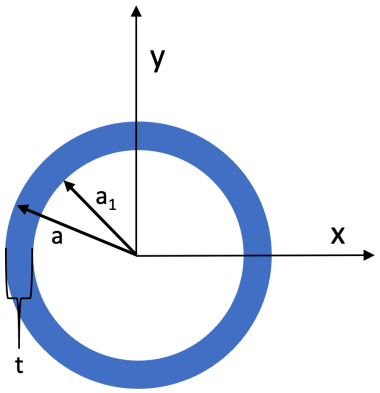

Figure 14.5: Elliptical dimension names

The area of the hollow tube is calculated with Equation (14.34) and the moment of inertia around the x-axis is calculated with Equation (14.35). It is decided that the struts will have an constant thickness. This makes it easier to calculate as well as fabricate. The outer diameter is set to a realistic value such that the only variable in Equation (14.35) and Equation (14.34) is thickness t.

$$A = \frac{\pi}{4}(a - a_1) \tag{14.34}$$

$$I_x = \frac{\pi}{64}(a^4 - a_1^4) \tag{14.35}$$

Lastly, the unsupported length of the struts is calculated. Previously the length from center of the float or fuselage to center of the float or fuselage was used. The unsupported length is simply found by subtracting the diameter of the floats and fuselage from the previous lengths. Since the length of the spreader struts is much higher than the struts they will be calculated separately with different outer diameters.

Strut lengths

Firstly the outer radius a of the tube is set to $0.04\,\mathrm{m}$. This value is found through an iterative process. For the spreaders this value is $0.06\,\mathrm{m}$ due to the long length and thus lower buckling stress. The length of the struts, spreaders and diagonal struts are calculated with Equation (14.36).

$$\begin{aligned} L_{st} &= (\cos(0.5 * S_\angle) * h_{fl}) - (B_{fl}/2) - (D_{fus}/2) \\ L_{sp} &= s_{fl} - B_{fl} \\ L_{dia} &= \sqrt{1.5^2 + L_{st}^2} \end{aligned} \tag{14.36}$$

With these length the moment needed moment of inertia is calculated using Equation (14.32). After which the thickness is found using Equation (14.35). With the length, area and density known the weight is also calculated. The density of high modulus carbon is $1.6\,\mathrm{kg/dm^3}$. With the cost of $116\,€/\mathrm{kg}$. The results can be seen in Table 14.7.

Table 14.7: Dimensions of the different struts

Property	Forward Strut	Aft Strut	Forward Spreader	Aft Spreader	Diagonal Strut	Total
a [mm]	20	20	30	30	20	-
t [mm]	9.22	7.86	7.84	4.40	1.67	-
Area [mm^2]	512	445	690	399	200	-
Length [m]	0.993	0.993	3.00	3.00	1.41	-
Weight [kg]	1.416	0.708	3.317	1.919	0.4527	19.9
Price [€]	164	82	384	223	52	2309

14.2.9. Verification & Validation

The verification and validation is performed in accordance with Chapter 8. The design tool used for the calculation of the struts is python and has to be verified and validated to ensure correctness and usefulness of the tools. Firstly the verification is performed in Section 14.2.9 where after the validation is performed in Section 14.2.9.

Verification

For the verification of the code a number of unit and system tests are presented in Chapter 8. Aside from the code verification the assumptions made in Section 14.2.1 are also verified in this section. However the first seven assumptions are derived from EASA[38] thus these are assumed to be verified. The results of the verification of the code and assumptions is presented below, with a summery in Table 14.8.

- **Unit tests** All unit tests from **UT00-UT06** are passed thus no irregulars were found in the code. The results can be seen in Table 14.8. No discretization error is calculated because no discretizations have been made in the python code.
- **System tests** A number of assumption testing can be seen bellow. Also an analytical comparison is added Table 14.8. For this comparison the F_st was used to calculate the dimensions of the strut and compared to the dimensions which resulted from the code.

Assumption testing:

- **Validity of vertical forces (Item FS 08)** If the forces created by the landing would act diagonally the stresses created are not higher than the maximum stress created by either only vertical or only horizontal forces. For the calculation for the struts the stresses are simply multiplied with a factor of $\cos 45 = \frac{\sqrt{2}}{2} = 0.71$ when the force is acting diagonally, $45\,\text{degrees}$. Every possible angle would result in a factor smaller or equal to 1 which would results in lower or the same stresses. Thus the assumption is valid.
- **Symmetrical step landings (Item FS 09)** To check this the stress in the struts is examined for the case when the resultant water force acts in front of the step. This would create higher compression stress in the forward strut. If the resultant force is located at the struts even twice as much, $22\,286\,\text{newton}$ in stead of $11\,143\,\text{newton}$. This assumption is not valid. However since the forces in the struts do not exceed the maximum forces from the different landing cases the dimensions of the struts are still correct.
- **Compression and tensile (Item FS 10)** To check if the compression and tensile stresses are indeed critical the shear stress has to be examined. The highest shear stresses occur if the reaction force of the water is oriented horizontal. This calculation was used to calculate the diagonal struts. These diagonal struts carry these horizontal loads resulting in only tensile or compression force in these struts. Thus the assumption is valid.

Table 14.8: Unit and system tests for the struts

ID	Parameter	Input	Pass Condition	Test Result	Pass or Fail	Comments
UT 00	V_{stall}	0	Total weight struts = 0	0	Pass	-
UT 02	V_{stall}	$-$	$+$	$+$	Pass	-
UT 02	V_{stall}	$+$	$+$	$+$	Pass	-
UT 03	V_{stall}	$/2$	$F_{st}/4$	$F_{st}/4$	Pass	-
UT 05	V_{knots}	1	$1.94\,\text{m/s}$	1.94	Pass	-
UT 06	F_{st}		N	$kgms^{-1}$	Pass	-
ST 08	t_{st}	$42\,645\,\text{newton}$	$t = 9.2\,\text{mm}$	9.2	Pass	-

Validation
Due to the limited time no validation has been performed.

15. Drag Estimation

In order to evaluate the performance of the water sailplane, firstly, the drag had to be analyzed. The drag plays a big role in the design's success as it determines whether the concept is feasible. Therefore, a drag estimation was performed on the aircraft. In this analysis, both the zero-lift drag coefficient and the drag coefficient at $C_{L_{des}}$ were calculated.

Section 15.1 describes the general approach that was followed as well as the assumptions that were made. Thereafter, the method of approximating the C_{D_0} of the wing, empennage and the struts are presented in Section 15.2. The analysis on the drag of the fuselage and floats is shown in Section 15.3. Section 15.4 presents how the induced drag was calculated. Furthermore, the method to obtain the total drag coefficient can be found in Section 15.5. And finally, Section 15.6 presents the verification of the drag analysis.

The results coming from this drag analysis are presented in Chapter 20.

15.1. Assumptions

The total drag of an aircraft is a summation of the various drag components experienced by the aircraft, which are shown in Equation (15.1). Before the analysis on the drag was initiated, assumptions were established, which simplified the evaluation of the drag coefficients. These are shown below.

$$C_D = C_{D_o} + C_{D_f} + C_{D_i} + C_{D_W} + C_{D_{misc}} \tag{15.1}$$

DE 01: Incompressible flow. This implies that the density of the flow of the wing is assumed to be constant.

DE 02: Wave drag omitted. This simplifies Equation (15.1).

DE 03: Pressure drag incorporated through form and interference factors. This implies that the pressure drag coefficients were taken into account using form and interference factors with the skin friction drag coefficient.

DE 04: Floats have the same drag behavior as the fuselage. The floats have a similar shape to a fuselage body. Therefore, the floats were evaluated as a fuselage.

DE 05: 'Hoerner ratio'. The floats will not behave completely as fuselages due to the float step. Therefore, a 'Hoerner ratio' was established as a sophisticated correction factor for the floats. This ratio was obtained through the comparison of the investigated drag behavior of fuselages and floats by Hoerner [39].

DE 06: Struts have the same drag behavior as wings. The cylindrical struts will be covered by an airfoil shape so that the drag behavior of the struts is improved. Due to the wing-shaped struts, these were evaluated as wings.

Because of **DE 02** and **DE 03** Equation (15.1) was simplified to Equation (15.2).

$$C_D = C_{D_f} \cdot FF \cdot IF + C_{D_{misc}} + C_{D_i} = C_{D_0} + C_{D_i} \tag{15.2}$$

15.2. Wing, Empennage and Strut Zero-Lift Drag

The zero-lift drag coefficient of the wing, empennage and the struts were estimated with the same approach due to their wing similarities. This method relied on calculating the skin friction drag coefficient to obtain the total C_{D_0}. To do so the skin friction coefficients for each component were determined as well as their wetted areas. This is shown in Equation (15.3).

$$C_{D_f} = C_f \cdot \frac{S_{wet}}{S} \tag{15.3}$$

The skin friction coefficient was calculated using Equation (15.4). However, to use this equation, the transition point and fictitious location from laminar to turbulent flow on the airfoil had to be determined. By using Javafoil, the transition point from laminar to turbulent flow was obtained for the airfoil of each component. These values were then inputted into Equation (15.5) to find the fictitious locations of the turbulent boundary layer. For the asymmetrical airfoil, the transition points were found for both the upper and lower surfaces of the airfoil. The transition points for each component are shown in Table 15.1. Accordingly, the skin friction coefficients were calculated for the root and tip chords. The average of the value for the root and tip was used as the final value per component. As the wing consists of multiple panels, this procedure was repeated for each of these. The weighted average of the skin friction coefficients for the panels was taken as the total skin friction coefficient for the wing. [14]

$$C_f = \frac{0.074}{Re^{0.2}} \cdot (1 - (\frac{X_{tr}}{C} - \frac{X_0}{C}))^{0.8} \quad (15.4) \qquad \frac{X_0}{C} = 36.9 \cdot (\frac{X_{tr}}{C})^{0.625} \cdot (\frac{1}{Re})^{0.375} \quad (15.5)$$

Table 15.1: Transition points per component

Component	Airfoil	$X_{tr_{upper}}$	$X_{tr_{lower}}$
Wing	FX 62-K-153/20	0.67	0.53
Empennage	NACA 0012	0.50	0.50
Struts	NACA 0012	0.50	0.50

To obtain the skin friction drag coefficients of the wing, empennage and struts, their wetted areas were calculated. This was done by estimating the airfoil circumference through geometric shapes. The circumference was converted into a ratio by dividing by the chord so that the wetted area became a simple multiplication of the reference area with this ratio.

As mentioned at the beginning of Section 15.1 the zero-lift drag was estimated by incorporating the FF and IF for the various components. The FF was determined using Equation (15.6), which is based on the maximum thickness-to-chord ratio of the corresponding airfoil. The IF's were obtained from literature. [14] Eventually, the zero-lift drag coefficient for each component relative to the aircraft was calculated via Equation (15.7).

$$FF = 1 + 2.7\frac{t}{c} + 100\frac{t}{c}^4 \quad (15.6) \qquad C_{D_0} = \frac{1}{S} \cdot \sum C_{D_f} \cdot FF \cdot IF \cdot S_{wet} \quad (15.7)$$

15.3. Fuselage and Floats Zero-Lift Drag

The fuselage and floats were also evaluated with a similar approach regarding their drag coefficients. In principle, the same method was used as in Section 15.2. However, the skin friction coefficient was determined differently. Furthermore, a miscellaneous drag component was taken into account for the fuselage and floats.

As opposed to the wing, empennage and struts, the boundary layer of the fuselage and floats was divided into a laminar and turbulent part. The location of the transition point between these two types of flow decided its contribution to the skin friction coefficient, as can be seen in Equation (15.8). The skin friction coefficients for laminar and turbulent flow were obtained through Equation (15.9) and Equation (15.10), respectively. [14]

$$C_f = X_{tr} \cdot C_{f_{laminar}} + (1 - X_{tr}) \cdot C_{f_{turbulent}} \quad (15.8)$$

$$C_{f_{laminar}} = \frac{1.328}{\sqrt{Re}} \quad (15.9) \qquad C_{f_{turbulent}} = \frac{0.455}{(\log Re)^{2.58} \cdot (1 + 0.144 \cdot M^2)^{0.65}} \quad (15.10)$$

The wetted areas of both the fuselage and floats were estimated by dividing the complex shape into several simpler parts, such as paraboloids, cylinders and frustums.

Due to the upsweep and rough ends of both the fuselage and the floats, an additional drag component needed to be calculated, called the miscellaneous drag. This coefficient consists of additive drag due to the upsweep and the base drag. Their contributions were calculated through the following: Equation (15.11) and Equation (15.12).

$$C_{D_{additive}} = 3.83 \cdot u^{2.5} \cdot A_{max} \quad (15.11) \qquad C_{D_{base}} = (0.139 + 0.419 \cdot (M - 0.161)^2) \cdot A_{base} \quad (15.12)$$

For the floats, it was noted that due to the step, essentially two contributions to the base drag exist. Therefore the base drag of the floats was calculated for both the step and the end of the float. However, due to the rapid flow separation at the step, the flow behavior after the step is already very much disturbed, which increases the drag even more. To take this effect into account, a correction factor was established based on the research performed by Dr. Ir. S.F. Hoerner in his book Fluid-Dynamic Drag [39].

Again the FF was estimated through an equation, Equation (15.13), and the IF was obtained from literature [14]. The C_{D_0} of the fuselage and floats were then calculated through Equation (15.14).

$$FF = 1 + \frac{60}{f^3} + \frac{f}{400} \quad (15.13) \qquad C_{D_0} = \frac{1}{S} \cdot \sum C_{D_f} \cdot FF \cdot IF \cdot S_{wet} + C_{D_{misc}} \quad (15.14)$$

15.4. Induced Drag

The lift-induced drag was the last component that was being looked at during the drag analysis of the wing. The design lift coefficient was used to obtain the value for the induced drag coefficient during 'cruise', which was calculated using Section 15.4.

$$C_{D_i} = \frac{C_{L_{des}}^2}{\pi \cdot AR \cdot e}$$

15.5. Total Drag

The total drag was determined through the summation of all the above described drag coefficients for each aircraft component, which can be seen in Equation (15.15).

$$C_{D_0} = \frac{1}{S} \cdot \sum C_{D_{f_{component}}} \cdot FF_{component} \cdot IFcomponent \cdot S_{wet_{component}} + C_{D_{misc_{component}}} + C_{D_i} \quad (15.15)$$

15.6. Verification

To increase the credibility of the results of the drag estimation, verification was performed. Besides code verification, the made assumptions were verified, which showed that the usage of these was deemed valid.

15.6.1. Assumption Verification

Item **DE 01:** stated that incompressible flow was assumed for the drag calculations. This assumption is deemed valid for Mach numbers lower than 0.3 M [28]. Item **DE 02:** assumed the omittance of the wave drag. The norm for this assumption is also valid for low subsonic Mach numbers [14]. Thus, in order to verify both of these assumptions, it must be proven that the Mach number with the water sailplane will be flown is lower than 0.3 M.

Equation (15.16) was used to calculate the Mach number of the water sailplane, where γ represents the adiabatic index, R the specific gas constant and T the ISA temperature at sea level. A Mach number of 0.08 was obtained, proving the validity of both assumptions.

$$M = \frac{V_{cruise}}{c} = \frac{V_{cruise}}{\sqrt{\gamma \cdot R \cdot T}} = \frac{27.8}{\sqrt{1.4 \cdot 287 \cdot 288.15}} = 0.08 \quad (15.16)$$

15.6.2. Code Verification

Since the drag aircraft was estimated by using a numerical code, code verification was performed. By verifying the used code, possible errors could be identified and accordingly solved. Several unit tests from Chapter 8 were used to verify the system of codes, for which the results can be seen in Table 15.2.

Table 15.2: Unit test results for the numerical code of the drag estimation.

Unit test	Number of errors	Result
UT 00	0	PASS
UT 01	0	PASS
UT 03	0	PASS

16. Propulsion and Power Design

The design of the propulsion is done for a water sailplane capable of self-launch. Thus, the function of the propulsion system is to provide enough power and thrust to perform take-off and climb, while making use of electric propulsion. This section entails the description of tools used for the design and analysis of the propulsion system capable of such tasks. First, a power supply trade-off is shown in Section 16.1. Then, an analysis and selection of the electric motor, battery, and propeller can be seen in Section 16.3, Section 16.4, and Section 16.5 respectively. Section 16.6 presents the calculation and optimization of the propulsion subsystem mass. The verification and validation of the propulsion subsystem in presented in Section 16.7. The requirements relevant for the propulsion system can be seen in Table 16.1:

Table 16.1: Propulsion and power requirements

Identifier	Requirement
REQ-WS-FLPE-POW-08	Battery cycle life shall be at least 5000 cycles
REQ-WS-SUST-01	The WS shall produce no carbon emissions during operations
REQ-WS-COMF-01	The WS shall have an interior noise level of $70\,\mathrm{dB}$

16.1. Power Supply Trade-off

This section will present the method and rationale for the power supply trade-off. A trade-off was done by analyzing power supply's alternatives for the following four criteria.

- Energy density 25%
- Safety 25%
- Operational Feasibility 25%
- Sustainability 25%

These criteria were all deemed to be of equal importance. Therefore, the weight of each criterion was uniformly distributed. The scoring of each criterion is done by comparing the characteristics of both power supply systems for a defined criterion. The alternative that is able to achieve the criterion to the highest extent is then awarded a point. To conclude, the power supply method with the most points will be chosen. The alternatives to be analyzed for the trade-off will now be presented and briefly highlighted. Note that, requirement **REQ-WS-SUST-01** limits the trade-off to power supplementation methods to non carbon producing methods.

A battery stores energy in the form of chemical energy. Through a chemical reaction, the battery turns the chemical energy into electrical energy. In brief, the chemical reaction entails a flow of electrons from the anode to the cathode, which in turn provides electric current allowing for work to be done. A fuel cell, on the other hand, generates electricity through a chemical reaction of its fuel. Generally, an electric current occurs through releasing hydrogen from the anode and oxygen from the cathode.

Other Alternatives Alternatives of power supplementation that have not been taken into account during the trade-off include hybrid systems, solar cells, and beamed energy. Hybrid systems make use of batteries in combination with fuel cells. Solar cells generate electricity with the use of the photo-voltaic effect. The method of beamed energy makes use of beaming energy through microwaves into the aircraft. The argumentation of not including them in the trade-off will now be presented.

Hybrid systems are an option in the design of the propulsion system. However, their implementation lies in the functionality of a backup power system, to be used for emergencies or other situations that might require an extra impulse of power. The trade-off currently done is for the primary form of power supply. Hence a hybrid system is not an applicable alternative for this process.

The drawback of solar cells as a form of power supply is that it does not also provide power storage. Whereas, power supply alternatives such as batteries and fuel cells supply and store power. Moreover, the supplementation of power is dependent on the occurrence of sunlight. Although there is an abundant presence of sunlight in the Maldives, the occurrence of it can still be seen as a stochastic process. Therefore, the use of solar cells automatically implies the use of a power storage unit in case sunlight is not present during the mission. The weight penalty obtained from having both solar panels and a power storage unit onboard the aircraft was regarded too high to be seen as a viable option. Another, reasoning for the disregard of solar cells is that they are not formed to the desired airfoil contour, affecting the airflow in a negative way. Lastly, the power generated by a solar panel per square meter is too low for it to be sufficient with respect to the average surface area of gliders [13].

The use of beamed energy as a power supply alternative was disregarded due to the technological immaturity of the method. Power reception is currently limited to line of sight of the ground transmitting station. [13]

16.1.1. Safety

A detailed analysis of the safety and risk considerations for batteries and fuel cells can be found in this section. The definition of safety was determined to be the following:

The minimization of risk

The major risks of using batteries in an aircraft is twofold. The first is heat-related, known as thermal runaway. This occurs when the heat generated by the battery exceeds the heat dissipated by the battery. The origin of it can be due to, but is not limited by, mishandling by the crew, overcharging of the battery, or inaccuracies during production. The phenomenon is extremely propagating, as adjoining cells could also be heated to the point of thermal runaway. The FAA has noted 158 accidents involving batteries as of 2015.[1] To mitigate such risks, a battery management system must be used to monitor the temperature and performance of the battery pack during flight and charging. The second is the partial or complete loss of safety–critical power supply. Issues in terms of loss of power supply originate from degradation during operations and affect parameters such as capacity fade, power fade, internal short circuits and increased internal resistance [40]. To mitigate these risks, it is critical to have insight into the health of the batteries. With the use of big data obtained from TMA's fleet, empirical models can be made against relatively low cost to obtain insight on these parameters through battery lifetime. Furthermore, there is current legislation to address the airworthiness of the batteries, such as the DO-311A documentation. A clear framework of requirements lowers the probability of the occurrence of unforeseen risks, as these legislation documentation are often built on previous accidents.[2]

The risks of fuel cells as a power supply method are again twofold. The first being, the risk of flammability of the fuel, the gas is flammable under a wide concentration. Therefore, the smallest leak of the pressurized hydrogen causes a risk. There is no current legislative framework for fuel cell powered aviation.[3] The second risk is that a lot of the fuel cell technology is currently in the prototype stage. This technological immaturity means that the method has not been through the extensive testing that allows for verification and validation.

Although both methods of power supplementation have two substantial risks, the power supply method of the battery does have a legislative framework for the verification and the validation of the airworthiness of it. This makes it more desirable as the risks and their mitigations will be more known and formalized. To conclude, the battery is thus awarded a point for the safety criterion.

16.1.2. Energy density

Energy density is the amount of energy that can be stored in a given system per unit mass. The higher the energy density of a system, the less mass is required for the aircraft to perform its mission. Therefore it is a

[1] https://safetyfirst.airbus.com/lithium-batteries-safe-to-fly/ [Accessed: 23 Dec 2021]

[2] https://www.easa.europa.eu/download/etso/ETSO-C179b.pdf [Accessed: 23 Dec 2021]

[3] https://dps.mn.gov/divisions/sfm/programs-services/Documents/Responder%20Safety/Alternative%20Fuels/FuelCellHydrogenFuelVehicleSafety.pdf [Accessed: 23 Dec 2021]

crucial parameter in the design of an aircraft. Thus, a point is awarded to the alternative with the highest energy density

The highest energy density of commercially found batteries, applicable in aerospace, was found to be $500\,\mathrm{Wh/kg}$.[4] Commercially found fuel cells, also being applicable of aerospace, have an energy density of $960\,\mathrm{Wh/kg}$, where the main component of weight comes from the high-pressure tanks.[5] Hence a point is awarded to the fuel cell for the energy density criterion.

16.1.3. Operational Feasibility

Operational feasibility is an important aspect of the determination of the power supply method, as a power supply method may be the most suitable for a single mission but it cannot be provided on a basis to have the mission also be commercially viable. A power supply alternative should be available as much as possible to increase the amount of flight time and thus the revenue generated by the aircraft. Therefore, the operational feasibility was defined to be the following:

The minimization of downtime

The recharging of batteries could be done without the aircraft leaving the water and requires less precision than the removal and placement of new fuel cells. The amount of downtime between flights can be minimized if charging stations comparable to the electric vehicle industry are used during the operation. The newest version of electric vehicle chargers can provide up to $350\,\mathrm{kW}$.[6]

While a battery stores energy, a fuel cell generates it by converting an available fuel. Fuel, such as hydrogen, would need to be shipped from other countries to the Maldives, as there is no current infrastructure to support the supply of hydrogen. To then again be distributed to one of the individual resorts. This is undesirable as it allows for the probability of downtime, due to issues in the supply chain or regulatory safety requirements of the transportation of hydrogen. Furthermore, replacing empty fuel cells is a task that should be done with a lot of care and precision, and is thus not suited for open sea. This would mean that the aircraft would to be beached or brought into a hangar for refueling. Therefore a point is awarded to the batteries.

16.1.4. Sustainability

Although the production of batteries is not environment friendly, the charging of it can be done with the use of sustainable methods such as locally generated solar or hydropower.

Hydrogen energy is a renewable energy source that does not produce any harmful emissions during use. However, the supplementation of the fuel cells will be done through the use of maritime transport which runs on fossil fuels. Furthermore, fossil fuels are still used by hydrogen gas producers to separate it from oxygen. It cannot be guaranteed that the supplier of the fuel cells will choose to do this process without the emission of carbon gases. Whereas the generation of energy for the batteries can be done within the control of the client. Therefore, the battery obtains the final point for this trade-off

16.1.5. Trade-off results

To conclude, the battery alternative was determined to be safer, more operationally feasible and sustainable. Thus, the battery obtained 3 of out 4 points, whereas the fuel cell obtained 1 out of 4, due to its higher energy density. As the winner of the trade-off, the battery has been used as the method of power supplementation for the detailed design phase. A more detailed selection and sizing of the battery will be presented in Section 16.4.

Table 16.2: Trade-off results for the power supplementation method

Criterion	Battery	Fuel cell
Energy density	0	1
Safety	1	0
Operational feasibility	1	0
Sustainability	1	0
Total	3	1

[4] https://sionpower.com/ [Accessed: 22 Dec 2021]
[5] https://www.aviationtoday.com/2020/04/16/will-hydrogen-fuel-cells-play-a-role-in-the-vtol-revolution/ [Accessed: 22 Dec 2021]
[6] https://tritiumcharging.com/product/pk-350/ [Accessed: 2 Jan 2022]

16.2. Sizing of the Propulsion System

This section will present the design choices, and the rationale behind them, for the elements within the propulsion system. The design choices are based on their compliance with the requirements in relation to the presented mission profile and wing power loading diagram from Chapter 9.

16.3. Electric Motor Selection

This section entails the selection procedure of the electric motor. Although, power supplying methods weigh more than their carbon emitting equivalents, electric motors weigh less than their piston complements. In brief, an electric motor consists of a stator and rotor. Where the stator is a non-moving magnetic object and a rotor is a magnetic object configured to move, as seen in Figure 16.1. Movement is generated by the attraction of opposite magnetic poles from the rotor and stator. To continue movement as the poles move towards their opposite, the polarity of the magnet is switched. Hence, either the rotor or stator has to be an electromagnet so poles can be changed through the change of electric current. Thus, either the rotor or stator must have wiring with a current running through it. Therefore, the use of a DC motor requires a commutator, which switches the direction of the electric current. The switching is either done with the use of electronic circuits that register the rotor position or mechanical brushes that are pressed against the rotor.

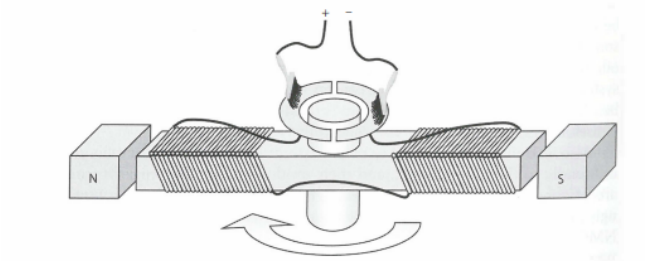

Figure 16.1: A simplified schematic of an electric motor[13]

The use of brushes lowers the efficiency of an electric motor and introduces a risk of sparking. Sparking is the breaking of electrical connections made by the brushes between the windings. Hence, the electric motor selected was chosen to be a brushless DC permanent magnet motor (BLDC). Literature showed that this is the best choice due to its superior efficiency and weight. [13]

The goal of designing a proof of concept water sailplane is to show the viability of it. Therefore, it is essential to use a commercially available motor for the design of the water sailplane. Hence, a comparison of market available aerospace applicable BLDC motors was made. This lead to the selection of the MGM COMPRO 80 kW Electric motor - REB 90.[7] The selection of the electric motor was based on the ability to meet the required brake power, of $64\,491.303\,42\,\mathrm{W}$ determined in Section 9.2, for a minimal mass. The REB 90 delivers a continuous power of $70\,\mathrm{kW}$, with a peak power of $80\,\mathrm{kW}$, at a weight of $22\,\mathrm{kg}$.

16.4. Battery Requirements

For the selection of the battery, a selection of market available secondary batteries must be made. The choice for a secondary battery is logical, as the sustainability of using primary batteries is significantly lower. For the selection of batteries, the following parameters are of importance.

Energy Density The higher the energy density, $\mathrm{Wh/kg}$, of the battery, the more energy it can carry per unit of weight. This in turn lowers the depth of discharge required for the same weight, increasing the lifetime and sustainability of the batteries. The lower the depth of discharge, the higher the cycle life.

Dimensional Concerns The availability of space for the placement of batteries is limited by the dimensional constraints with respect to the aerodynamic performance of the aircraft. Thus, it is preferable that a battery with shape-able characteristics is selected, so that the placement of the battery module can be done, whilst the aerodynamic, stability and controllability performance is penalized as little as possible. Furthermore, the higher the volumetric energy density, $\mathrm{Wh/L}$, the less space the battery pack requires and thus the less shape-able the battery has to be.

[7] https://www.mgm-compro.com/electric-motor/80-kw-electric-motor/ [Accessed: 10 Jan 2022]

Discharge rate The discharge and charge rate of a battery is determined by the C-rate of the battery. As the rate of discharge of a battery increases, its capacity decreases. Which is also known as Peukert's law. The C-rate directly relates to the power the battery is able to deliver to the motor. By multiplying the C rate of the battery with the amount of Ampere hour, the current can be found, and the power then calculated by Equation (16.2):

$$I = C_{rate} \cdot Electric\ charge \qquad (16.1) \qquad P = I \cdot V \qquad (16.2)$$

The selected motor can deliver a peak power of $70\,\mathrm{kW}$ at a maximum voltage of $800\,\mathrm{V}$. It is assumed that the terminal voltage of the battery remains constant during flight, further discussion of this assumption can be found in Section 16.7. Thus, with the use of Equation (16.2) and taking the efficiencies of the components in between the battery into account leads to a maximum required current of $91.11\,\mathrm{A}$. For the calculation of the required charge to deliver this current, it is assumed that the energy density of the battery can be divided by its nominal charge to determine a value for the electric charge per kilogram, $\mathrm{Ah/kg}$. So, once a final weight has been determined, as done in Section 16.6, it can be seen whether the charge of the battery in combination with its C-rating is able to meet the required current of $91.11\,\mathrm{A}$. It should be noted that, the batteries with the highest energy density are commonly used in space appliances where discharge requirements are significantly lower.

Environmental and Mission Concerns As stated previously, the design of the water sailplane is a proof of concept. Therefore, a commercially available battery must be sought to determine the viability of the concept. Thus, it is critical that the selection of batteries is done only for those designed for aerospace applications. These batteries are verified and validated for that intended use and have a higher standard of reliability. A higher level of reliability allows handling in a larger envelope of loads, movements and environmental conditions. To phrase this reasoning more pragmatically, commercially available battery modules from the EV industry have been left out of the selection as their safety requirements are less confining.

16.4.1. Selected Battery

Literature showed that the use of lithium polymer batteries is beneficial for aircraft appliances. Lithium polymer batteries with a solid-state allow for a higher level of shape ability. Furthermore, the batteries have the highest level of energy density of currently available batteries applicable in aviation, whilst also having high levels of discharge [13].

A consideration of Sion Power Licerion batteries was made due to the considerable specific energy of $480\,\mathrm{Wh/kg}$. However, the discharge rate of 5C revealed that the battery pack could not deliver the current required by the engine.[8]

The final selected battery pack is LI-POL Battery System developed by MGM-COMPRO.[9] The battery system has an energy density of $267\,\mathrm{Wh/kg}$, a maximum pack voltage of $800\,\mathrm{V}$ with a max C-rating of $30\,\mathrm{C}$. The pack includes cooling and a battery management system and is used for aerospace appliances.

Section 16.4 calculated that the current required from the battery is $91.11\,\mathrm{A}$. As stated previously, it is assumed that the capacity can be found by dividing the specific energy by the nominal voltage. Which leads to a value of $0.333\,75\,\mathrm{Ah/kg}$, Section 16.6 present a value of $128.31\,\mathrm{kg}$ of battery need for energy requirements. Resulting in a capacity of $42.82\,\mathrm{Ah}$. With a C-rating of 30, Equation (16.1) shows that a maximum theoretical current of $1284.6\,\mathrm{A}$ could be produced, for and is thus able to meet the required current of $91.11\,\mathrm{A}$. Note that, if a new battery is selected the procedure discussed would be repeated again.

16.5. Propeller design choices

It is common for aircraft to have a variable pitch propeller. The ability to vary the pitch allows keeping the blades at an optimal angle of attack during a wide range of speed in flight. This in turn allows for the motor to be kept at constant RPM, increasing efficiency and performance. An electric motor has a larger efficient RPM range than a traditional combustion engine. Hence, the benefit of using variable pitch is not required and would only increase the weight and complexity of the propeller. Therefore, this design choice was abandoned.

[8] https://sionpower.com/files/Company-Brochure-21B.pdf [Accessed: 10 Jan 2022]
[9] https://www.mgm-compro.com/battery/li-pol-battery-system/ [Accessed: 9 Jan 2022]

For a preliminary estimation of the propeller pitch, Figure 16.2 is used as an indication obtained from literature [14], where a propeller efficiency of 0.8 is assumed.

		INTENDED CRUISING AIRSPEED in KTAS (η_P = 0.80)														
		50	60	70	80	90	100	110	120	130	140	150	160	170	180	190
RPM	2000	39	47	55	63	70	78	86	94	102	109	117	125	133	141	149
	2100	37	45	52	60	67	74	82	89	97	104	112	119	127	134	142
	2200	36	43	50	57	64	71	78	85	92	100	107	114	121	128	135
	2300	34	41	48	54	61	68	75	82	88	95	102	109	116	122	129
	2400	33	39	46	52	59	65	72	78	85	91	98	104	111	117	124
	2500	31	38	44	50	56	63	69	75	81	88	94	100	106	113	119
	2600	30	36	42	48	54	60	66	72	78	84	90	96	102	108	114
	2700	29	35	41	46	52	58	64	**70**	75	81	87	93	98	104	110
	2800	28	34	39	45	50	56	61	67	73	78	84	89	95	101	106
	2900	27	32	38	43	49	54	59	65	70	76	81	86	92	97	102
	3000	26	31	36	42	47	52	57	63	68	73	78	83	89	94	99
	3100	25	30	35	40	45	50	56	61	66	71	76	81	86	91	96
	3200	24	29	34	39	44	49	54	59	64	68	73	78	83	88	93
	3300	24	28	33	38	43	47	52	57	62	66	71	76	81	85	90
	3400	23	28	32	37	41	46	51	55	60	64	69	74	78	83	87
	3500	22	27	31	36	40	45	49	54	58	63	67	72	76	80	85

Figure 16.2: Relation between RPM, propeller pitch and airspeed at 70% of the radius [14].

With a cruise speed of $54\,\mathrm{KTAS}$ and a rotational speed of $3000\,\mathrm{RPM}$, Figure 16.2 shows a propeller pitch of $26°$ to $31°$ Where a middle value of $29°$ was chosen.

16.5.1. Sizing of propeller

For the sizing of the propeller two approaches are used. Firstly, the diameter of the propeller is determined on its relation with tip speed. The tip speed of the propeller should be kept below trans-sonic speed to avoid shocks. Then, the diameter of the propeller was determined with the use of a statistical approach.

With respect to the tip speed, the propeller velocity $V_{tip_{helical}}$ should not exceed a tip speed of $290\,\mathrm{m/s}$ [13] for metal propellers to avoid shocks on the tips. With the use of this constraint and a maximum design speed of $57.99\,\mathrm{m/s}$, Equation (16.3) leads to a static tip propeller speed of $284.14\,\mathrm{m/s}$.

$$V_{tip_{helical}} = \sqrt{V_{tip}^2 + V^2} \tag{16.3}$$

With the obtained static tip propeller speed, the diameter of the propeller D can be determined, using Equation (16.4). Where n_{rot} is the number of rotations per second (RPS), the manufacturer's site of the selected motor states that the motor operates at an RPM range of $1500\,\mathrm{RPM}$ to $4000\,\mathrm{RPM}$. The engine will be operating at continuous power, not peak power. Therefore a value of $3000\,\mathrm{RPM}$ is used for the preliminary calculation. Which resulted in a propeller diameter of $1.808\,\mathrm{m}$

$$V_{tip_{static}} = \pi \cdot n_{rot} \cdot D_{prop} \tag{16.4}$$

Equation (16.5) is a statistical relation between propeller diameter and power can also be found from literature. The engine selected in Section 16.3 has a continuous power of $70\,\mathrm{kW}$. The propeller resulting from Equation (16.5), where K_p is a dimensionless constant of 0.56 obtained from literature for two bladed propellers [13], has a calculated diameter of $1.619\,\mathrm{m}$.

$$D_{prop} = K_p \cdot \sqrt[4]{P_{mot}} \tag{16.5}$$

The propeller diameter found from the statistical approach was found to be $1.808\,\mathrm{m}$, whereas the noise constraints determined a lower diameter of $1.619\,\mathrm{m}$. Thus, the lower value will be used for the iterative design. With the given diameter the propeller would account for an additional weight of $3.3\,\mathrm{kg}$ when compared to the weight of a similar propeller.[10]

[10] https://www.pipistrel-aircraft.com/ [Accessed: 14 Jan 2022]

16.5.2. Propeller Performance

To determine the performance of the propeller, an estimation of the propeller efficiency is calculated. The propeller efficiency is determined with the use of the momentum theory method [14], which will now be presented. The calculation is commenced by calculating the thrust for an initial propeller efficiency of $0.65\eta_p$ and the continuous power generated by the motor P_{mot}, with the use of Equation (16.6).

$$Thrust = \frac{\eta_p * P_{mot}}{V} \tag{16.6}$$

With the determined thrust, the induced airspeed w is calculated, as seen in Equation (16.7). Where A_{prop} is the area of the propeller determined in Section 16.5.1 and ρ is the standard ISA sea-level density.

$$w = \frac{-V + \sqrt{V^2 + \frac{2 \cdot T}{\rho \cdot A_{prop}}}}{2} \tag{16.7}$$

With the use of the induced airspeed and Equation (16.8), the ideal efficiency η_i can be calculated.

$$\eta_i = \frac{1}{1 + \frac{w}{V}} \tag{16.8}$$

Now, with the use of Equation (16.9), a new propeller efficiency can be calculated by taking the product of the ideal and viscous profile efficiencies, where η_v is the viscous profile efficiency assumed to be 0.85 in accordance with literature [14].

$$\eta_{p_{new}} = \eta_v \cdot \eta_i \tag{16.9}$$

Finally, Equation (16.10) is used to determine the difference between the last and second to last propulsive efficiencies. So that if the difference reaches a required accuracy, the iteration is stopped. Further discussion of the required accuracy can be found in Section 16.7.

$$\delta = \eta_p - \eta_{p_{new}} \tag{16.10}$$

This iteration was done for all the airspeeds until V_d, the maximum design speed of the aircraft. This relation can be seen in Figure 16.3.

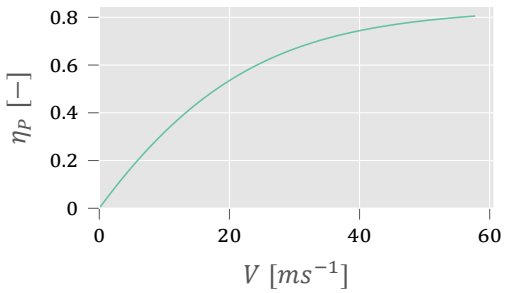

Figure 16.3: Relation of the propeller efficiency and airspeed for a given propeller diameter and engine power [14]

The generated list of propeller efficiency for a given airspeed was also implemented in Equation (16.11), to determine the thrust for all airspeeds for a given propeller diameter and engine power.

$$T = \frac{P_{br} \cdot \eta_p(V)}{V} \tag{16.11}$$

It is cardinal to further analyze the thrust generated by the propeller at low speeds. To gain more insight into the performance during take-off and climb, the analysis of the propeller performance is done with the use of the quadratic interpolation method [14], which revolves around the assumption that propeller thrust varies from the static thrust at zero speed, to the thrust at the maximum design speed V_D. Allowing for interpolation with the use of the general quadratic equation where the thrust is a function of airspeed. Where the static thrust was found with the use of Equation (16.12), and the quadratic interpolation is done with Equation (16.13).

$$T_{static} = 0.85 * P_{br}^{2/3} (2\rho A_p)^{1/3} \left(1 - \frac{A_{sp}}{A_p}\right) \tag{16.12}$$

$$T(V) = \left(\frac{T_{static} - 2T_{V_{max}}}{V_{max}^2}\right) V^2 + \frac{3T_{V_{max}} - 2T_{static}}{V_{max}} V + T_{static} \tag{16.13}$$

$$T(V) = \frac{\eta_p P_{br}}{V} \tag{16.14}$$

Figure 16.4a shows the values of thrust determined with the use of the quadratic interpolation method, propeller efficiency from momentum theory and basic thrust equation. This is then compared to drag estimated with the use of the standard drag equation, where C_{d0} is determined in Chapter 15 and C_L is determined with the use of Equation (16.15). It can be concluded from the graph that the engine and propeller combination are able to generate enough thrust for the airspeed in which it operates, the stall speed V_s and maximum design speed V_d.

$$C_L = \frac{W}{S} \cdot \frac{2}{\rho} \cdot \frac{1}{V^2} \tag{16.15}$$

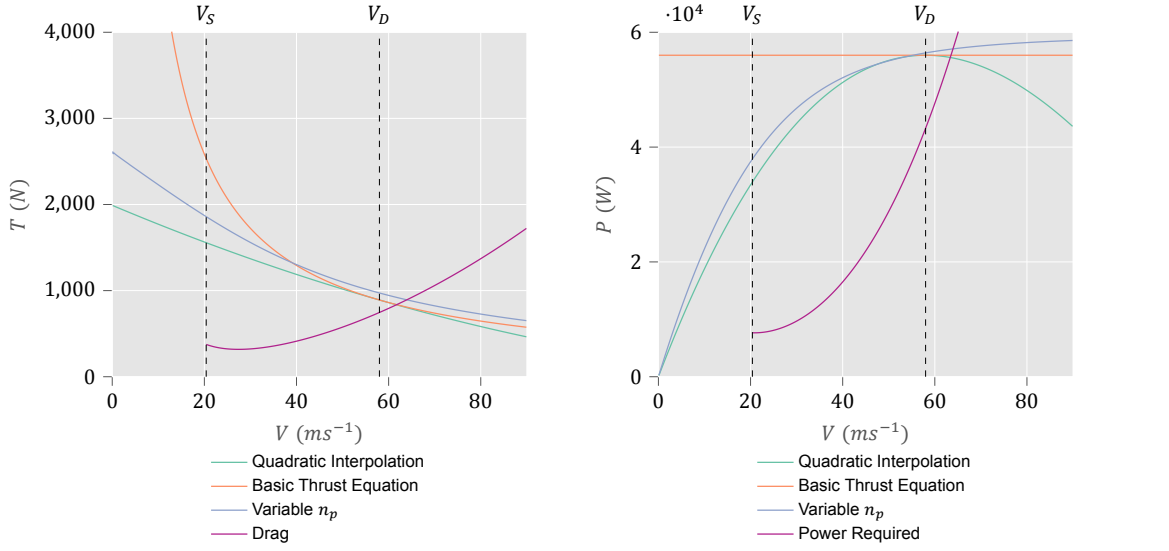

(a) Comparison between quadratic and basic thrust equations

(b) Power available based on the quadratic and basic thrust equations

Figure 16.4

Multiplication of the calculated thrust and drag with the airspeed allows for the plotting of the available versus required power, as seen in Figure 16.4. From the graph, it can be deduced that within the airspeed envelope of the aircraft, sufficient excess power is generated.

16.5.3. Propeller Speed Reduction Unit and Controller Implementation

In order to avoid the propeller tips reaching trans sonic velocities a propeller speed reduction unit (PSRU) is required. This ensures that the motor is still capable of delivering its maximum power, while the propeller still spins at an acceptable RPM. The chosen motor has a maximum deliverable RPM of 4000, while the propeller has a maximum operational RPM of 3000. Therefore the propeller speed reduction unit would require a gear ratio of 4:3. Typically such units have an efficiency loss of $2\,\%$ [13]. The weight penalty of the unit is assumed to be $10\,\mathrm{kg}$ based on the weight of a PSRU from EPI Inc. and rubberizing it to the motor torque and gear ratio.[11] Additionally, an electric motor always requires a motor controller that controls the rotational speed of the motor.

[11] http://www.epi-eng.com/gearbox_products/mark-15_gearbox.htm [Accessed: 14 Jan 2022]

However this comes with an efficiency and additional weight penalty. According to Raymer a motor controller typically is $15\,\%$ of the motor weight, and results in an efficiency loss of $2\,\%$ [13].

Table 16.3: Weight and efficiency penalties of additional engine components

Component	Weight penalty	Efficiency
Propeller	$3.3\,\mathrm{kg}$	$80\,\%$
PSRU	$10\,\mathrm{kg}$	$98\,\%$
Motor controller	$0.15\ W_{mot}$	$98\,\%$

16.6. Optimization of the Propulsion System

The optimization of the propulsion system is done for the batteries, as this is the most mass intense element of the propulsion system. The optimization is done as follows, from the previously determined continuous motor power and propeller sizing, a Python script determines the time required to reach a height of $15\,\mathrm{m}$ during take-off and a height of $1050\,\mathrm{m}$ during climb. The energy required for these two phases are the largest components of the energy required. Once the required energy is determined, a battery mass can be calculated. Based on the energy density of the battery selected in Section 16.4.1. The calculated battery mass will in turn update the weight estimation. With the new weight, a new estimation of the time duration of take-off and climb can be done. Note that, the loop has the following constraining factors. A similar runway length as the Twin Otter is a constraining factor to make sure that the water sailplane is operable in every location TMA operates.

To determine the energy required during take-off, the following calculation is done. The power setting during the first fifteen seconds of take-off is increased with the use of a linear ramp function to the maximum continuous power of $70\,\mathrm{kW}$ of the electric motor selected in Section 16.3. The implementation of the ramp function was done to approximate the pilot slowly increasing the thrust setting. If the pilot were to apply a maximum thrust setting suddenly, then the force would cause a large nose-down moment, which would cause the unproductive result of the floats to dig into the water.

To go from the power required by the engine during the first ten seconds to the energy required from the batteries, the efficiency of the motor, motor controller, battery and battery controller have to be taken into account. To then finally, sum the required power for these first fifteen seconds.

Then, with the use of the python script described in Section 17.5, the time for the remaining take-off phase was determined. This leads to the relation seen in Equation (16.16), where the final energy was determined to be $479.26\,\mathrm{Wh}$.

$$E_{takeoff} = \frac{\sum_{10}^{t_{takeoff}} P_{mot} \cdot \eta_{mot} \cdot \eta_{motcon} \cdot \eta_{bat}}{3600} = 445.418Wh \tag{16.16}$$

The calculation for the energy required during the climb phase is as follows, for simplicity the constant power setting is used during climb. The power setting used during climb is the P_{br} of $64\,491.303\,42\,\mathrm{W}$ again determined from the power loading diagram in Section 9.2 is used. With the use of the Python script detailed in Section 17.2 the climb duration for the first and the second climb is determined, in compliance with the mission profile determined in Section 9.1. Leading to a required energy of $12\,977.62\,\mathrm{Wh}$

$$E_{climb} = \frac{\sum_{t_takeoff}^{t_{glide1}} P_{br}}{3600} + \frac{\sum_{t_glide1}^{t_{climb2}} P_{br}}{3600} = 12977.62\ Wh$$

The energy required from the batteries is also influenced by a number of other smaller factors which are listed below.

- Energy required during taxi
- Depth of Discharge

The calculation for these factors will now be presented.

Taxi Another part of the mission that requires energy is the taxiing from the area the airlift landed to the raft from which the passengers are picked up. Furthermore, the aircraft has to return to the beach to recharge the batteries of the aircraft when empty. For these movements energy for a distance of $8\,\mathrm{km}$ is reserved. A speed of $6.0\,\mathrm{kts}$ to $8.0\,\mathrm{kts}$, or $2.05\,\mathrm{m/s}$ to $4.11\,\mathrm{m/s}$, is obtained by seaplanes during the taxi phase, as else water spray will be picked up by the propeller [41]. This in turn causes erosion, lowering the lifetime of the propeller. The total drag experienced by the aircraft at a velocity of $4\,\mathrm{m/s}$ is $78\,\mathrm{N}$. Note that, the drag estimated by the Python script is equal to the thrust, as the taxiing is done at constant velocity. Therefore the power required and available can be estimated with the use of Equation (16.17). Where η is a corrective factor with a value of 0.85 for the inefficiencies for transferring power from the electric motor to the propeller, rho is the density of air in the Maldives, S is the surface area of the propeller and P is the power delivered by the engine.

Filling in the required thrust of $78\,\mathrm{N}$ in Equation (16.17) solving for P_{mot} leads to a value of $393.95\,\mathrm{W}$. Correcting this number for the efficiencies of the battery and battery management system leads to a value of $445.41\,\mathrm{W}$. To find the energy, the power is finally multiplied with the time spent taxiing, which then dividend by 3600 to determine the watt-hours needed.

$$\text{Thrust} = \eta \cdot P_{mot}^{\frac{2}{3}} \cdot \sqrt[\frac{1}{3}]{2 \cdot \rho \cdot S} \tag{16.17}$$

$$\text{Energy} = \frac{P_{mot} \cdot t_{taxi} \cdot \eta_{mot} \cdot \eta_{motcon} \cdot \eta_{bat}}{3600} = \frac{8738.68 \cdot \frac{8000}{4}}{3600} = 247.45\ Wh$$

Battery degradation The number of cycles before the performance of the battery is impacted is dependent on the depth of discharge. The higher the depth of discharge, the less mass is required. However, the sooner the battery needs to be replaced due to performance degradation. This relation is illustrated in Figure 16.5, showing the cycle life versus depth of discharge of general Lithium-ion battery cells based on a relation found from data.

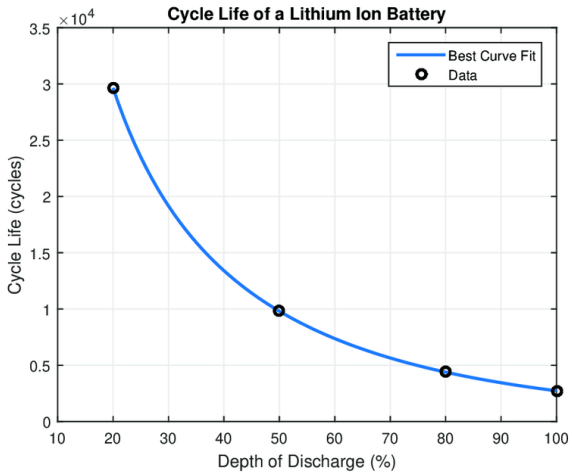

Figure 16.5: Cycle life of a general Li-ion cell [42]

It was decided that a requirement on the lifetime of the battery must be set, as the mining operations for the gathering of the lithium in the batteries leave a large carbon footprint. Thus, it was determined that the life required from a battery would be set as, **REQ-WS-FLPE-POW-08**: Battery cycle life shall be at least 5000 cycles, leading to a depth of discharge of 80%.

Reserve battery capacity Note that, reserve energy is not included in the design of the power supplementation system as the water sailplane is designed to land without the ability of a go-around Furthermore, a conservative $8\,\mathrm{km}$ of taxi distance is included in the design, thus providing a sufficient buffer.

The summation of the required energy for all flight phases leads to a value of $17\,130.41\,\mathrm{Wh}$, with an energy density of $267\,\mathrm{Wh}$ leads to a battery weight of $66.65\,\mathrm{kg}$ for a single repetition of the mission profile. From an operational point of view, the number of times the aircraft is able to perform its mission on a single charge should be as high as possible. Previous iterations showed that battery weight around $120\,\mathrm{kg}$ would still result in an MTOW that was within the estimated budget presented in Chapter 24. Thus, the battery was doubled in size leading to a final mass of $133.31\,\mathrm{kg}$. The calculated mass is then used as input for the weight estimation.

The new required weight leads to new values time for take-off and climb. Thus, restarting the loop allowing for a new calculation of battery mass.

16.6.1. Charging module

A detailed design of the charging module was not feasible due to time constraints. However, an estimate of charge time can be made if the charge rate is assumed to be ideal. The total amount of capacity in the batteries was calculated to be $42.82\,\mathrm{Ah}$. A commercially available charger, produced by the same manufacturer as the battery, is capable of delivering currents up to $100\,\mathrm{A}$.[12]

$$\text{Charging time} = \frac{Capacity}{Current} = \frac{42.82}{100} = 0.428\ hour \tag{16.18}$$

Thus, as seen in Equation (16.18), the idealized time of charging would $0.428\,\mathrm{hrs}$ or approximately 30 minutes. This could be handled by the batteries as their max C-rating is 30C, whereas the charge is done with a C-rating of just over two. Note that, the manufacturer was contacted with the request for data or graphs on the discharge and cycle characteristics but no reply was received.

16.7. Verification of Propulsion System

As the selected motor and battery are commercially available products suited for aviation, the verification and validation of them as standalone products have already been done. Special interest should lie in the verification and validation of these components as an integrated design, which will be presented in the following sections.

16.7.1. Verification of the Battery Modeling

The excel used to optimize the battery mass passed unit tests **UT00 - UT06** without any point of significance.

For the calculation of the power the battery can deliver, it was assumed that the terminal voltage of the battery remains constant during flight, this implies that the effective capacity remains constant during discharge. System test, **ST-07**, is done to verify the assumption. Research into the discharging character of lithium polymer batteries used for aerospace appliances at different discharge rates and power shows that deviation of the battery capacity is no more than 0.5% [43]. Moreover, the power available during all flight phases exceeds the power required, as seen in Figure 16.4b and Figure 17.11 , to an extent that the design is robust enough to neglect the effect. It should be noted that the neglecting of these effects overestimates the effective capacity of the battery.

ST-07 is also done to verify that, it is assumed that the energy density of the battery can be divided by its nominal charge to determine a value capacity per kilogram. Research based on data collected from Ace Battery has shown that the capacity of the battery can be approximated as a function of its weight [43]. The regression model in the research shows a coefficient of determination of 0.9948, verifying the the reliability of the model.

16.7.2. Verification of the Propeller Modeling

The code used to calculate the propeller efficiency for the airspeed envelope of the aircraft passed unit tests **UT00 - UT06** without any point of significance. **UT04**, was done by changing the required accuracy δ to a smaller quantity, from 0.001 to 0.0001. The absolute difference found for values of propeller efficiency for this change are in the order 10^{-4}. SO it was concluded that a required accuracy of 0.001 does not cause discretization errors of a significant level.

17. Flight Performance Analysis

This chapter discusses the methodology for analyzing the water sailplane's performance. The flight phases that are assessed include the climb performance (Section 17.2), the glide performance (Section 17.3), the turning performance (Section 17.4), and finally the take-off performance (Section 17.5). The relevant requirements for flight performance analysis can be seen in Table 17.1.

[12] https://www.mgm-compro.com/other-products/chargers/ [Accessed: 18 Jan]

Table 17.1: Flight performance analysis requirements

Identifier	Requirement
REQ-WS-FLPE-AER-03	The WS shall have a descent rate of $1.4\,\mathrm{m\,s^{-1}}$ at MTOW
REQ-WS-FLPE-END-01	The WS shall glide for $30\,\mathrm{min}$ during cruise at MTOW

17.1. Equations of Motion for Symmetric Flight

To assess the aircraft's flight performance at this point in the design stage, some assumptions must be made about the dynamics of the aircraft during flight. Therefore, a simplified model is used whereby it is assumed the aircraft is in symmetric flight. This implies that the aircraft is experiencing no net lateral forces and flies along a curved flight path. Note that this is not valid for turning flight, as will be further elaborated on in Section 17.4.

It is assumed that the aircraft acts as a rigid body and experiences the forces as shown in Figure 17.1 from the center of gravity [11]. This eliminates any moments created and simplifies the analysis. As the final design is not complete, this level of detail is sufficient for this stage in the design process.

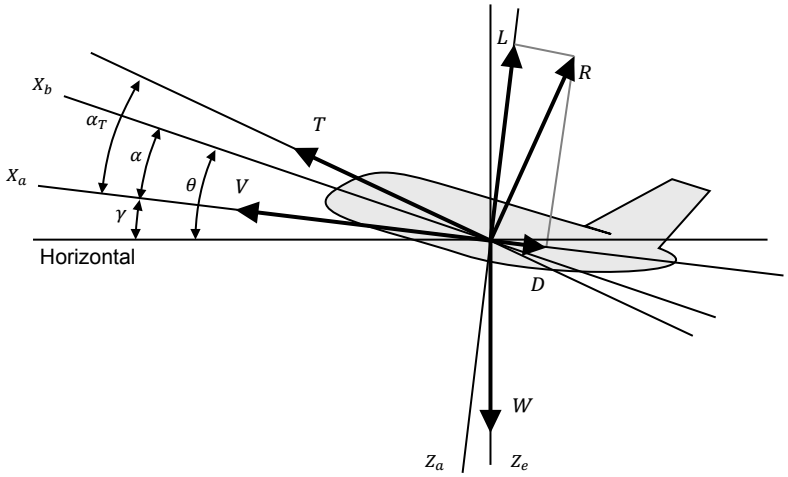

Figure 17.1: Diagram of an airplane in symmetric flight

Analyzing the aircraft forces along the aerodynamic X_a and Z_a axes, and applying Newton's second law of motion, yields two principle equations of motion. The sum of forces along the X_a axis, which is represented by Equation (17.1), must equal the net acceleration force experienced by the aircraft. Similarly, the sum of forces along the Z_a axis, represented by Equation (17.2), must equal the centrifugal force experienced by the aircraft due to the curved flight path.

$$\frac{W}{g}\frac{dV}{dt} = T\cos\alpha_T - D - W\sin\gamma \tag{17.1}$$

$$\frac{W}{g}V\frac{d\gamma}{dt} = T\sin\alpha_T + L - W\cos\gamma \tag{17.2}$$

17.2. Climb Performance

To analyze the aircraft's climb performance, several additional assumptions are made. These assumptions are specific to the analysis of the climb performance and are as follows:

CP 01: Steady flight assumption. This implies that the aircraft's flight path and velocity are constant. This is due to the climb rate typically being maximized around a specific velocity, and thus the climb procedure maintains a relatively constant velocity and flight path. Therefore the acceleration term dV/dt evaluates to zero, and similarly, the flight path gradient $d\gamma/dt$ also evaluates to zero.

CP 02: Zero thrust angle of attack. This assumes the thrust vector coincides with the velocity vector, and thus α_T is reduced to zero.

CP 03: Small-angle approximation for the flight path. This assumes that throughout the climb phase of the flight, the flight path angle (γ) is relatively small such that $\cos\gamma \approx 1$.

By applying these assumptions to the equations of motion (Equations (17.1) and (17.2)) it is possible to simplify the equations into the simplified equations of motion for steady symmetric flight. This results in Equations (17.3) and (17.4).

$$0 = T - D - W\sin\gamma \tag{17.3}$$

$$0 = L - W \tag{17.4}$$

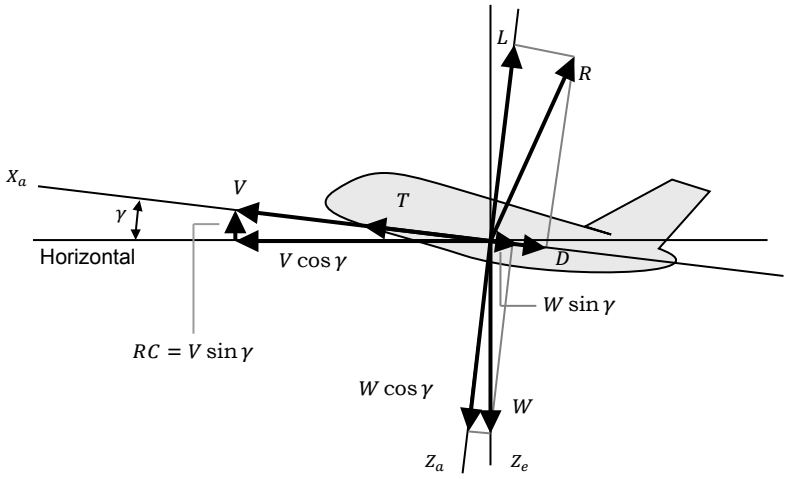

Figure 17.2: Diagram of an airplane in steady symmetric flight

As shown by Figure 17.2, the rate-of-climb is equivalent to the vertical component of the velocity vector, and thus is defined as $RC = V\sin\gamma$. By multiplying velocity with Equation (17.3), it's possible to relate the rate-of-climb with the dynamics of the aircraft, resulting in Equation (17.6).

$$TV - DV - WV\sin\gamma = 0 \tag{17.5}$$

$$RC = \frac{P_a - P_r}{W} \tag{17.6}$$

Therefore, RC is a function of the excess power $P_a - P_r$.

Power Available Curve

The power available of the aircraft is defined as the total power the aircraft is able to deliver, and is a product of the thrust and the velocity. To approximate the power available curve of the aircraft, the quadratic approximation of thrust (Equation (16.13)) is used where T_{static} is defined by Equation (16.12). Note that T_{max} and V_{max} were chosen to correspond to a velocity of $30\,\mathrm{m\,s^{-1}}$, as climb is the only prolonged power intensive phase, and thus it would be beneficial for the thrust to be optimized for lower speeds. This yields Equation (17.8).

$$P_a = TV \tag{17.7}$$

$$P_a = \frac{T_{static} - 2T_{max}}{V_{max}^2}V^3 + \frac{3T_{max}}{V_{max}}V^2 + T_{static}V \tag{17.8}$$

Power Required Curve

The power required of the aircraft is defined as the power required by the aircraft to overcome the drag force during flight and is, therefore, a product of the drag and the velocity. By applying the parabolic drag polar to approximate the drag coefficient, it can be split into the zero-lift drag coefficient (C_{D_0}) and the induced drag term, which is a function of C_L. As both the drag coefficient and lift coefficient are functions of angle-of-attack, equation Equation (17.4) is utilized to approximate the lift coefficient through the weight of the aircraft. This eliminates the dependency on α and yields Equation (17.9), where the power required is purely a function of velocity.

$$P_r = DV$$

$$DV = C_D\frac{1}{2}\rho V^3 S$$

$$P_r = f(V) = C_{D_0}\frac{1}{2}\rho V^3 S + \frac{2W^2}{\pi Ae\rho VS} \tag{17.9}$$

With expressions for both P_a and P_r as functions of velocity, it is possible to plot the two as curves and subsequently compute the rate-of-climb at each velocity. Note that the velocity domain is restricted by the stall speed, as the P_r curve would reach C_L values greater than $C_{L_{max}}$ at lower velocities.

Rate-of-Climb Curves

By using the previous functions, the rate-of-climb is implicitly a function of velocity. As can be seen in Figure 17.3, the maximum rate-of-climb can easily be found with its corresponding velocity. Additional information such as V_{stall} and V_{max} can also readily be read off the graph.

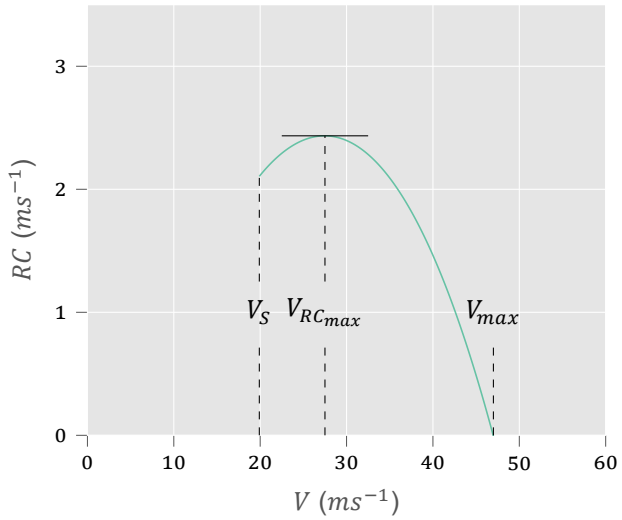

Figure 17.3: Typical rate-of-climb curve

Effect of Altitude

In reality, the rate-of-climb is not steady throughout the climb phase due to altitude effects. As the altitude increases, the air density decreases. This affects the drag as well as the thrust and therefore P_a and P_r. Analytically, it can be seen by Equation (17.9), the air density is a component in both the zero-lift drag term and the induced drag term. The overall effect is a slight upward and rightward shift. This increases the stall speed, however, also decreases the relative drag at higher velocities.

Unfortunately, however, the lower air density also means the propulsion system has a lower mass flow at the same velocity, and thus the power available also decreases. According to Ruijgrok, Equation (17.10) describes the variation of power available as a function of air density [11]. The subscript 0 indicates the sea-level condition. The power n is given to be less than 1 when flying in the troposphere. As no specific value range was provided, this exponent was assumed to be equal to 0.9.

$$P_a = P_{a,0}\left(\frac{\rho}{\rho_0}\right)^n \tag{17.10}$$

The overall effect is that the RC curve shifts down and to the right. Therefore, RC_{max} decreases with altitude, and the optimum climb velocity increases. This increase in the resultant velocity violates assumption **CP 01** as there must be a resultant acceleration given that the velocity does not stay constant.

17.2.1. Verifying Steady Flight Assumption

Unsteady Quasi-Rectilinear Climb

In order to factor the net acceleration, Equation (17.1) must be used. Note that quasi-rectilinear flight assumes the flight path angle remains relatively unchanged and thus, Equation (17.4) is still valid. The same procedure can be followed as before and the equation can be multiplied by V. The velocity derivative can be expanded and this results in Equation (17.11). The relations $dh/dt = V\sin\gamma = RC$, $TV = P_a$, and $DV = P_r$ can then be used to yield Equation (17.12). Note that the subscript s denotes the previously assumed steady-state rate-of-climb.

$$\frac{W}{g}V\frac{dV}{dh}\frac{dh}{dt} = TV - DV - WV\sin\gamma \tag{17.11}$$

$$RC\left[1 + \frac{V}{g}\frac{dV}{dh}\right] = \frac{P_a - P_r}{W} = RC_s \tag{17.12}$$

Rearranging Equation (17.12) allows for the computation of the new rate-of-climb based on the previous value and a so-called *kinetic energy correction factor*. Applying formulae derived from the International Standard Atmosphere (ISA), it is possible to compute the *kinetic energy correction factor* and subsequently compute the true rate-of-climb.

$$RC = \frac{RC_s}{1 + \frac{V}{g_0}\frac{dV}{dH}} \tag{17.13}$$

$$\frac{dV}{dH} = V_{EAS}\frac{d(\rho_0/\rho)}{dH}$$

$$\frac{d(\rho_0/\rho)}{dH} = \frac{\lambda}{T_0}\left(\frac{g_0}{2R\lambda} + 0.5\right)\left(1 + \lambda\frac{H}{T_0}\right)^{\left[\frac{g_0}{2R\lambda} - 0.5\right]}$$

By comparing RC with RC_s, the steady climb assumption can be tested. To test the most extreme case, the highest altitude was taken, as this provided a larger air density ratio gradient and thus would yield the largest difference. At the highest altitude of $1050\,\mathrm{m}$ the ratio of $\frac{RC_{max}}{RC_{s_{max}}}$ was found to be 0.99615. This corresponds to an absolute percentage error of $0.386\,\%$. This was deemed sufficiently small to verify the steady flight assumption for the purposes of estimating the climb performance of the water sailplane.

17.2.2. Optimum Climb

To estimate the time to climb to the target altitude the *energy-state approximation*, described by Ruijgrok is used [11]. Considering the true rate-of-climb value, the total energy of the aircraft can be expressed by Equation (17.14), where the first term is the potential energy and the second term the kinetic energy. Dividing the equation by the airplane weight results in a term called the *energy height* denoted by H_e, which is equivalent to the total energy per unit weight.

$$E = WH + \frac{1}{2}\frac{W}{g_0}V^2 \tag{17.14}$$

$$\frac{E}{W} = H_e = H + \frac{V^2}{2g_0} \tag{17.15}$$

By differentiating Equation (17.15), it is possible to relate the derivative to the steady rate-of-climb RC_s. Using this relation, it is possible to calculate the time to climb with the energy height by Equation (17.16).

$$t = \int_{H_{e_1}}^{H_{e_2}} \frac{1}{RC_s} dH_e \tag{17.16}$$

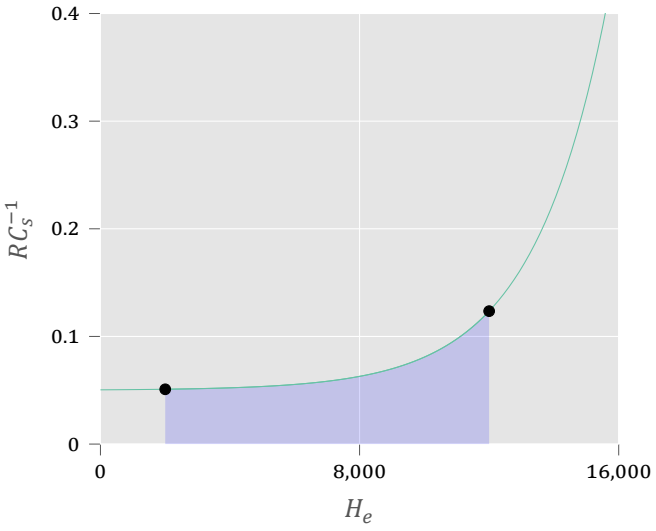

Figure 17.4: Example of a H_e-RC_s^{-1} curve with the shaded area representing the time to climb between the two black points [11, p.277]

17.3. Glide Performance

As the steady flight assumption was verified through the *kinetic energy correction factor*, the equations of motion for steady flight could be used (Equations (17.3) and (17.4)). By definition, gliding flight involves zero thrust and thus by setting $T = 0$ yields the equations of motion for quasi-steady glide, as can be seen by Equations (17.17) and (17.18).

GP 01: Quasi-steady flight assumption. This has been verified to yield negligible differences, which, at this stage of the design, are within acceptable margins. See **CP 01**

GP 02: Small angle approximation for the flight path. This assumes that throughout the glide phase of the flight, the flight path angle (γ) is relatively small such that $\cos\gamma \approx 1$.

GP 03: Steady weather conditions. During the glide phase, it is assumed that there is no presence of gusts, thermals or wind gradients.

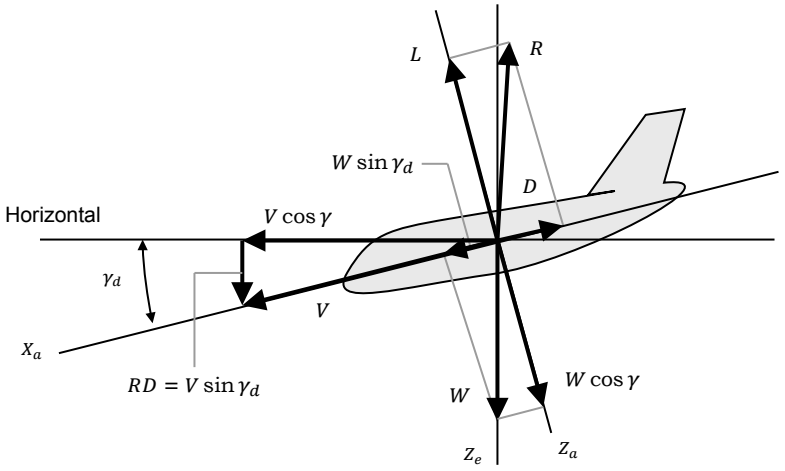

Figure 17.5: Diagram of an airplane in steady symmetric gliding flight

$$0 = -D - W\sin\gamma \qquad (17.17) \qquad\qquad 0 = L - W \qquad (17.18)$$

Minimum Rate-of-Descent

As the mission profile is a sightseeing flight, the maximum glide time is of greater importance than the maximum glide distance. Therefore, the minimum descent rate is analyzed. As the glide phase involves descending flight, the glide angle is defined as $\gamma_d = -\gamma$, and thus rate-of-descent $RD = -RC$ as can be seen in Figure 17.5. Thus by definition, the rate-of-descent is defined as Equation (17.19).

$$RD = V\sin\gamma_d \qquad (17.19)$$

To obtain an expression for RD, an expression for both V and $\sin\gamma_d$ must be obtained. Using Equation (17.17) and using the fact that $L \approx W$, an expression can be found for $\sin\gamma_d$. Similarly, using Equation (17.18) an expression for V can be found.

$$\sin\gamma_d = \frac{D}{W} = \frac{D}{L} = \frac{C_D}{C_L} \qquad\qquad L = W = C_L\frac{1}{2}\rho V^2 S$$

$$\sin\gamma_d = \frac{C_D}{C_L} \qquad\qquad V = \sqrt{\frac{W}{S}\frac{2}{\rho}\frac{1}{C_L}}$$

Applying these expressions for $\sin\gamma_d$ and V yields Equation (17.20).

$$RD = \sqrt{\frac{W}{S}\frac{2}{\rho}\frac{C_D^2}{C_L^3}} \qquad (17.20)$$

As can be seen in Equation (17.20), the RD is at a minimum when the C_D^2/C_L^3 ratio is at a minimum, or conversely, when C_L^3/C_D^2 is at its maximum. Furthermore, by plotting RD against V, a plot called the *hodograph* can be constructed. From this graph, the minimum rate-of-descent can be found, as well as the minimum glide angle for maximum range.

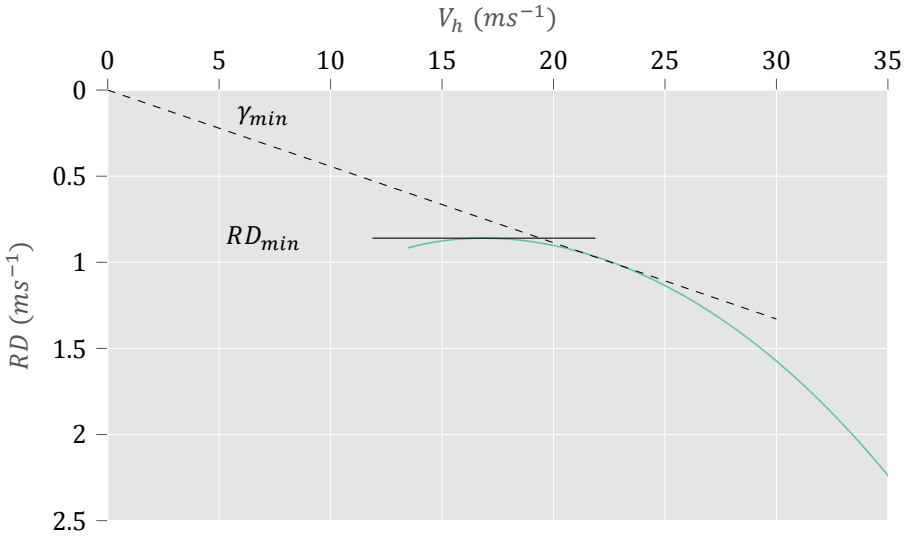

Figure 17.6: Example of a hodograph showing the rate of descent as a function of velocity

17.4. Turning Performance

Any flight will never be only straight, and thus it is necessary to evaluate the turning performance of the aircraft. This section will cover four types of turning performance. The first three will concern powered, steady curvilinear, coordinated turns. Therefore, the following assumptions were made.

TP 01: Coordinated turn assumption. A coordinated turn involves no rudder input, and thus there is no yawing motion.

TP 02: No sideslipping flight. The absence of any sideslip means there is no sideforce, and thus laterally, the equilibrium condition is only comprised of the centrifugal force and the lateral weight component.

TP 03: Zero thrust angle-of-attack. As with **CP 02**, the thrust vector is assumed to coincide with the longitudinal aerodynamic axis X_a.

TP 04: Turning reference frame. The coordinate system used, denoted by subscript t, contains the following properties. X_t coincides with the aerodynamic axis X_a and velocity vector. The lateral axis Y_t is horizontal and coincides with the radius of curvature. The vertical axis Z_t is thus orthogonal to the aforementioned axes.

TP 05: Instantaneous level flight. This assumes that at any given instant, the flight path angle γ is approximately equal to zero. This simplifies the analysis and allows for the analysis to be applicable to turning performance in climb and descent as well as during level turns. This also implies that the aerodynamic roll angle μ is equal to the angle of bank Φ.

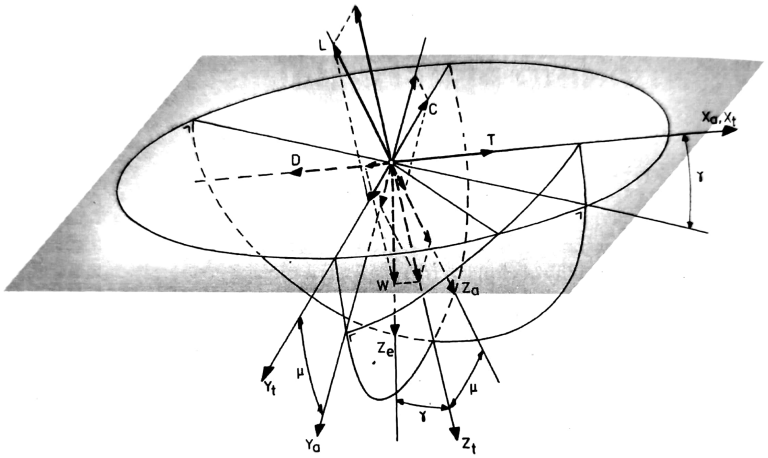

Figure 17.7: Diagram of an aircraft performing a coordinated turn [11, p.232]

Utilizing the above assumptions, then the forces can be visualized with the help of Figure 17.7. Furthermore, the centrifugal force C can be defined as $C = \frac{W}{g}\frac{V^2}{R}$, where R is the radius of the turn. Thus the full equations of motions can be written as Equations (17.21) to (17.23).

$$0 = T - D \qquad (17.21) \qquad 0 = L\sin\Phi - \frac{W}{g}\frac{V^2}{R} \qquad (17.22) \qquad 0 = -L\cos\Phi + W \qquad (17.23)$$

17.4.1. Steepest Turn

The steepest possible turn the aircraft can perform while maintaining constant altitude corresponds with the largest possible bank angle (Φ_{max}). When analyzing the vertical and lateral equations, the bank angle can directly be related to the load factor by Equation (17.24). Furthermore, combining the relations from Equations (17.23) and (17.24) yields Equation (17.25) for the drag as a function of the load factor and implicitly a function of the bank angle.

Combining this equation with the thrust curve from Equation (16.13), it is possible to evaluate the velocities where $T = nD$ at various load factors. Thus, the load factor and the bank angle can be expressed as a function velocity and conversely as a function of the turn radius through Equation (17.26).

$$n = \frac{L}{W} = \frac{1}{\cos\Phi} \qquad (17.24) \qquad D = nW\frac{C_D}{C_L} = W\frac{C_D}{C_L}\frac{1}{\cos\Phi} \qquad (17.25)$$

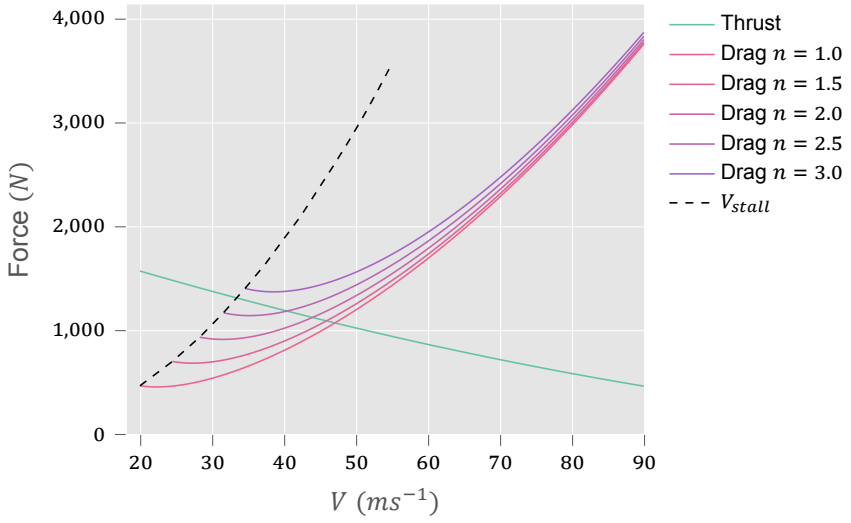

Figure 17.8: Example of Thrust vs Drag at different load factors

17.4.2. Verification of Step Size

As the determination of the maximum load factor is an iterative process whereby various steps of n are tested, it is important to very the step size is adequately small to simulate a continuous variation of n. Hence a discretization test was performed, whereby the true value was assumed to be the value with a step size of n and V equal to 10^{-4}. Step sizes ranging between 10^{0} and 10^{-4} were tested and the absolute percentage error (APE) in both n_{max} and correspondingly $V_{n_{max}}$.

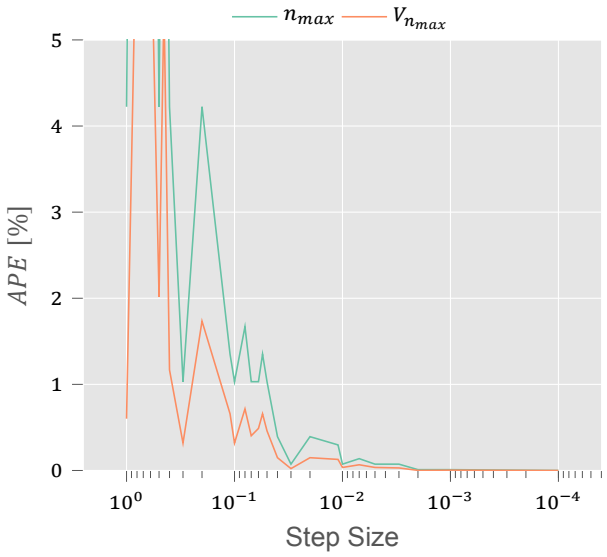

Figure 17.9: Discretization error of the maximum load factor and corresponding velocity for various step sizes

As can be seen in Figure 17.9, the APE is quite volatile at larger step sizes, however, beyond a step size of 10^{-3}, the values converge to the true value with much less volatility. As each smaller step size increased processing time, a step size of 10^{-3} was deemed sufficiently small.

17.4.3. Tightest Turn

The tightest possible turn corresponds to the smallest possible turn radius. By processing the function $n(V)$ in Equation (17.26), the turn radius can be computed as a function of velocity.

$$R = \frac{V^2}{g_0\sqrt{n^2 - 1}} \tag{17.26}$$

17.4.4. Fastest Turn

Knowing the range of turn radii and corresponding velocities, it is possible to compute the fastest turn. A tighter turn must be flown at a lower velocity and thus these turns do not occur at the same velocity or turn radius. A slightly wider turn can be flown at a higher speed and thus be completed in less time. The time to complete a $180°$ turn is given by Equation (17.27).

$$T_\pi = \frac{\pi R}{V} \tag{17.27}$$

17.4.5. Gliding Turn

As the glide phase is the primary flight phase in terms of duration, it is important to evaluate the turning performance during glide. Unlike the three previous turns, the altitude does not remain constant. Returning to the previous expression for RD, it is possible to relate both velocity and the sine of the descent angle to the bank angle.

$$\sin\gamma_d = \frac{D}{W}\frac{1}{\cos\Phi} = \frac{C_D}{C_L}\frac{1}{\cos\Phi} \qquad L = \frac{W}{\cos\Phi} = C_L\frac{1}{2}\rho V^2 S\frac{1}{\cos\Phi}$$

$$\sin\gamma_d = \frac{C_D}{C_L}\frac{1}{\cos\Phi} \qquad V = \sqrt{\frac{W}{S}\frac{2}{\rho}\frac{1}{C_L}\frac{1}{\cos\Phi}}$$

Thus, the rate-of-descent can now be expressed as a function of bank angle as can be seen in Equation (17.28).

$$RD = \sqrt{\frac{W}{S}\frac{2}{\rho}\frac{C_D^2}{C_L^3}\frac{1}{\cos^3 \Phi}} \tag{17.28}$$

The rate-of-descent can also be related to the turn radius. By combining and rearranging Equations (17.24), (17.26) and (17.28) it is possible to eliminate the bank angle and obtain Equation (17.29) [11].

$$RD = \sqrt{\frac{W}{S}\frac{2}{\rho}\left[\frac{C_D^2}{\left[C_L^2 - \left(\frac{W}{S}\frac{2}{\rho}\frac{1}{g_0}\frac{1}{R}\right)^2\right]^{3/2}}\right]} \tag{17.29}$$

17.5. Take-Off Performance

In this section the method of analyzing the take-off performance of the water sailplane is presented.

17.5.1. Base Equations

The take-off performance was analyzed using a numerical model based on methods from Gudmundsson [14]. This model calculated all the forces acting on the aircraft during take-off per time interval, and the net forward force. The model then calculated the acceleration according to Newton's second law of motion, given by Equation (17.30):

$$a = \frac{T_{net}}{m} \tag{17.30}$$

Since the water sailplane will be performing take-offs from water, it will be experiencing both hydrodynamic resistance as aerodynamic drag. The aerodynamic drag was calculated with the typical equation for drag and the drag coefficient, Equations (17.31) and (17.32):

$$D = \frac{1}{2}\rho C_D V^2 S_w \tag{17.31}$$

$$C_D = C_{D_0} + \frac{C_L^2}{\pi A e} \tag{17.32}$$

Furthermore, lift was calculated by Equation (17.33):

$$L = \frac{1}{2}\rho C_L V^2 S_w \tag{17.33}$$

Thrust was approximated by the same interpolated thrust equations from Chapter 16, given by Equations (17.34) to (17.36)

$$T(V) = \left(\frac{T_{static} - 2T_{V_{max}}}{V_{max}^2}\right)V^2 + \frac{3T_{V_{max}} - 2T_{static}}{V_{max}}V + T_{static} \tag{17.34}$$

$$T_{max} = \frac{\eta_p P_{br}}{V_{max}} \tag{17.35}$$

$$T_{\text{static}} = \eta_p P_{br_a}^{2/3} (2\rho A_2)^{1/3}\left(1 - \frac{A_{\text{spinner}}}{A_2}\right) \tag{17.36}$$

At the start of the take-off, the thrust is not immediately at the maximum value it can attain. Rather, the power and throttle slowly increase from zero to the break power available. To account for this, a ramp function was implemented to the break power available. For a conservative estimate, it was assumed that it takes 15 seconds to increase the power fully, leading to the ramp function given by Equations (17.37) and (17.38):

$$P_{br_a} = r \cdot P_{br} \tag{17.37}$$

$$r = \begin{cases} \frac{t}{15} & \text{if t} < 15\text{sec} \\ 1 & \text{if t} \geq 15\text{sec} \end{cases} \tag{17.38}$$

17.5.2. Hydrodynamic Resistance Estimation

The hydrodynamic resistance of floats is difficult to estimate without performing tank tow tests. Gudmundsson presents a method based on towing tests of hull shapes [14]. This method was used to estimate the hydrodynamic resistance during the take-off of the water sailplane, and is explained in this subsection.

First, several coefficients have to be defined. The first is the buoyancy force or load coefficient C_Δ given by Equation (17.39), where B is the width of one float:

$$C_\Delta = \frac{F_{\text{buoy}}}{\rho_W B^3} = \frac{\Delta}{\rho_W B^3} \tag{17.39}$$

As the water sailplane will generate lift during take-off, it is slowly lifted out of the water, thus decreasing the buoyancy force on the aircraft and thus the load coefficient to 0 at lift-off. This also has an effect on the hydrodynamic resistance, which will be elaborated upon later in this section. This changing buoyancy is calculated by subtracting the lift from the weight in Equation (17.40)

$$\Delta = W - L \tag{17.40}$$

Similar to aerodynamic drag, the hydrodynamic resistance is dependent on a resistance coefficient C_R. This coefficient depends on the geometry of the float and must be determined by water tank towing tests and Equation (17.41):

$$C_R = \frac{R}{\rho_W B^3} \tag{17.41}$$

Naturally, if the resistance coefficient for a certain float geometry is known, the resistance can be determined by Equation (17.42):

$$R = \rho_w B^3 C_R \tag{17.42}$$

The last coefficient to be introduced is the speed coefficient C_V given by Equation (17.43):

$$C_V = \frac{V}{\sqrt{gB}} \tag{17.43}$$

Towing tests with seaplane floats have been performed for different float shapes, and a relation for the resistance coefficient C_R of a planing-tail float as a function of C_V is given by Equation (17.44) [14]:

$$C_R = 0.0011C_V^3 - 0.0221C_V^2 + 0.1062C_V - 0.0149 \tag{17.44}$$

This relation is shown in Figure 17.10. The graph's peak corresponds to the so-called 'hull speed' of the floats, which is the maximum speed a body moving through water can attain. For this reason, it is standard seaplane operation that the pilot trims the aircraft around this speed to rotate the floats out of the water and get the aircraft on the step. Because the floats get rotated out of the water, the float hydrodynamic resistance decreases as the aircraft accelerates further.

Figure 17.10: Frictional resistance curve

However, by getting on the step, an extra resistance parameter is acted on the floats, called the step or hydroplaning resistance. This resistance can be estimated by the Froude frictional resistance equation in Equation (17.45).

$$R_{fr} = f S_{wet_{step}} \left(\frac{V}{1.688} \right)^2 \tag{17.45}$$

This equation is in imperial units, with R_{fr} the Froude resistance in $\mathrm{lb_f}$, $S_{wet_{step}}$ the step wetted area in ft and V in $\mathrm{ft\,s^{-1}}$. The term f is a coefficient representing surface quality. For smooth surfaces it can be taken to be equal to 0.012 [14]. After the resistance was calculated it was converted from $\mathrm{lb_f}$ to N.

As mentioned previously, as the aircraft generates lift and is lifted out of the water, less of the float is moving through the water, decreasing the hydrodynamic resistance on the float. This effect was taken into account by calculating the effective resistance coefficient $C_{R\Delta}$ in Equation (17.46):

$$C_{R\Delta} = C_R \frac{C_\Delta}{C_{\Delta_0}} \tag{17.46}$$

For a certain aircraft velocity the effective C_R was calculated based on the initial load coefficient C_{Δ_0}. The actual hydrodynamic resistance of the aircraft could then be calculated by Equation (17.47)

$$R = \rho_w B^3 C_{R_\Delta} \tag{17.47}$$

17.5.3. Numerical Model

With all forces acting on the aircraft during take-off calculated, the net force was calculated using Equation (17.48):

$$T_{net} = T - D - R - R_{fr} \tag{17.48}$$

For each time step the increase in velocity was calculated by Equation (17.49). The distance traveled during take-off was also calculated, shown by Equation (17.50)

$$V_i = V_{i-1} + a_{i-1} \cdot \Delta t \tag{17.49}$$

$$s_i = s_{i-1} + V_i \cdot \Delta t + a_i \Delta t^2 \tag{17.50}$$

The model then plots the hydrodynamic resistance R, planing resistance R_{fr}, aerodynamic drag D and the total resistance R_{tot}, given by Equation (17.51), against the aircraft airspeed V. It then outputs the total estimated take-off distance, including the $15\,\mathrm{m}$ height clearance and the total time it takes to lift off from the water and reaches this clearance.

$$R_{tot} = R + R_{fr} + D \tag{17.51}$$

17.5.4. Model Verification

Since the numerical model estimated the take-off performance, it was important to check that the model code was written correctly and that no errors were present. This was done by performing the unit tests described in Chapter 8 to each individual module of code, and the system tests to larger parts and the complete model. Below a summary is given of which parts did not pass a test, what the error causing this was, and how this error was solved to lead to the passing of a test.

- **UT/ST 05:** Initially all forces were calculated in $\mathrm{lb_f}$, and afterwards converted to N. This required multiple unit conversions throughout the code. When manually calculating the values of these forces for different velocity values, it was found that these unit conversions were not all correctly performed throughout the code, leading to erroneous results. This issue was solved by calculating all forces in N directly, except for the planning resistance. Now only two unit conversions were necessary, which both passed the test.
- **ST 04:** Since a time step was used in the take-off performance calculations, it was important to verify that the time step used produced results of high enough accuracy and thus investigate the discretization error of the calculations. The discretization error was analyzed by calculating the estimated take-off distance for the different timesteps. The results are shown in Table 17.2. As the results seemed to converge to a take-off distance of $396\,\mathrm{m}$, this value was used to calculate the absolute and relative error for the different timesteps. Results with a relative error of less than 0.1 % were deemed accurate enough. Therefore the model was concluded to produce accurate results for the take-off distance, as long as a time step of $0.01\,\mathrm{s}$ or smaller was used.

Time step dt s	**Take-off time** s	**Take-off Distance** m	**Absolute error** m	**Relative error** $\%$
1	29	380.6	15.4	3.8
0.1	29.5	395.24	0.76	0.19
0.01	29.52	395.81	0.19	0.048
0.001	29.524	395.92	0.08	0.02

Table 17.2: Discretization error of take-off distance calculation

17.5.5. Results Verification

With the numerical code model verified, it was also important to verify that the results from the model accurately represented the take-off performance of the water sailplane. Otherwise, there would be no use in using these results for the design of the aircraft, as this would lead to a wrong design.

The first aspect that was looked at were the P_a and P_r curves of the take-off. For a good take-off estimate, there should continuously be more power available than required. Figure 17.11 shows the P_a and P_r curves from the take-off model. As can be seen, throughout the entire take-off, the power available is indeed always higher than the power required for take-off.

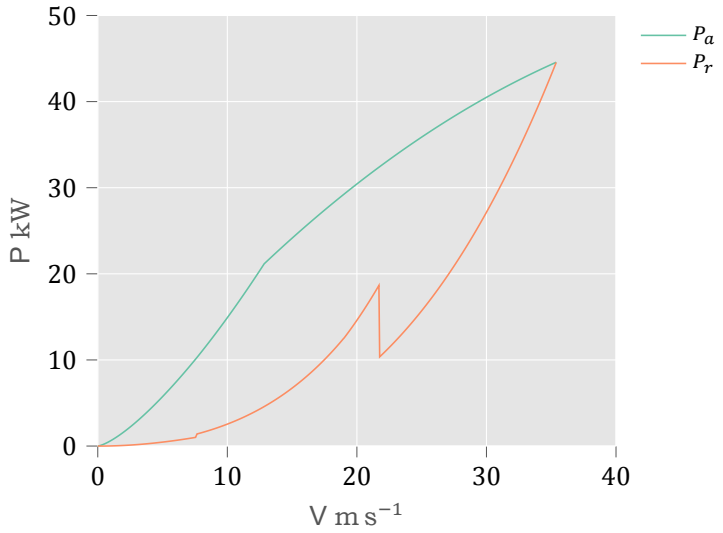

Figure 17.11: Take-off P_a and P_r curves

Another way the results could be verified was by comparing the results to the results of the model it was based on, the model from Gudmundsson [14]. This model used the same equations and assumptions to estimate the take-off performance of a larger flying boat. The results are shown in Figure 17.12 below:

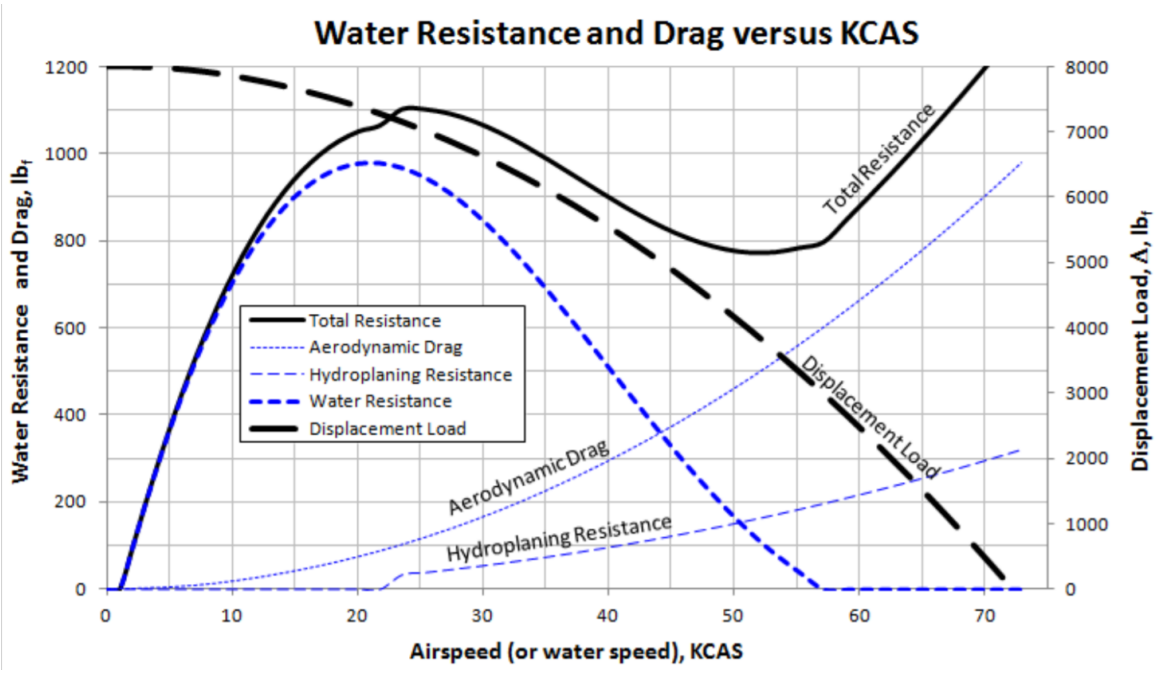

Figure 17.12: Take-off performance of example seaplane [14]. M = 3630 kg, S = 34.8 m^2, AR = 6.41, B = 1.52 m, C_{D_0} = 0.06

This graph is compared with the results for the take-off performance of an early design of the water sailplane, shown in Figure 17.13:

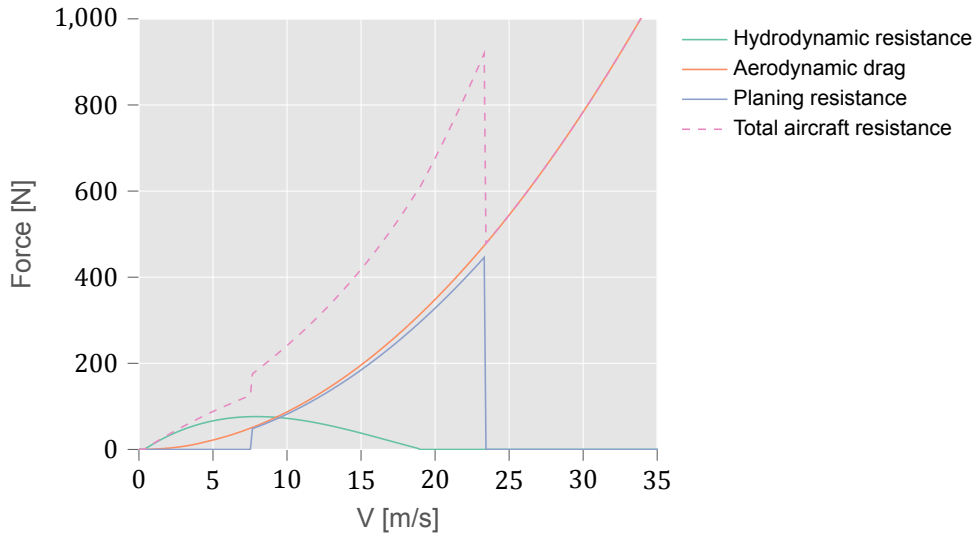

Figure 17.13: Take-off performance of early water sailplane design. M = 962 kg, S = 20.8 m^2, AR = 25.2, B = 0.65 m, C_{D_0} = 0.032

The two graphs clearly have similarities but also significant differences. It was important to check if these differences made physical sense, and thus the model take-off performance results could be used for the design of the water sailplane. The differences are explained below:

- **Hydrodynamic resistance:** One major difference between the water sailplane model results and those from Gudmundsson is the curve of the hydrodynamic resistance. The maximum hydrodynamic resistance for the water sailplane is less than 100 N, while for the Gudmundsson aircraft, this is around 900 lb_f, which is around 4000 N. This can be explained by 2 aspects. The first is that the water sailplane is a lot lighter, while still having a relatively high wing surface area. This means the water sailplane is lifted out of the water relatively fast compared to the other aircraft, thus decreasing the total hydrodynamic resistance.

  Next to this, the water sailplane has floats with lower B, so for the same C_V each float has a lower resistance. While the total resistance of the water sailplane floats has to be doubled to account for the two floats, the Gudmundsson aircraft still has a higher B, accounting for the higher hydrodynamic resistance.

- **Planing resistance:** While the hydrodynamic resistance of the water sailplane is a lot lower, the planing resistance is comparatively higher than that of the Gudmundsson aircraft. For the latter, the planing resistance stays below its aerodynamic drag, for the water sailplane, the two are almost equal in value. This can also be explained by two aspects. Firstly, the Gudmundsson aircraft has a C_{D_0} of 0.06, and an AR of 6.41, while the water sailplane has a C_{D_0} that is nearly half that of the other aircraft, and a significantly larger AR. This means that relatively the water sailplane would generate a lot less aerodynamic drag than the Gudmundsson aircraft.

  Secondly, while the floats of the water sailplane have a lower B, they are quite long, leading to a high step wetted area per float. This increases the planing resistance of each float, which is then doubled to account for the fact that the water sailplane has two floats. This means the water sailplane would have a relatively high planing resistance compared to its hydrodynamic resistance and the other aircraft, which can be seen in the graphs.

The results of the water sailplane take-off performance thus are accurate when viewed from a physical standpoint and compared to the model results of Gudmundsson.

Another verification method would have been to model the same aircraft used in the Gudmundsson example and check that these results matched up. Due to time constraints, this could not be performed however.

17.5.6. Validation

The results from the take-off performance modeled for take-off distance were compared to that of the Twin Otter [44] and the Pipistrel Taurus Electro electric-powered glider[1], to see the if estimated take-off distance would have been a reasonable result. It was expected that the take-off distance would be larger than that of both the Twin Otter and the Pipistrel Taurus Electro. This is because the Twin Otter has comparatively more powerful engines than the water sailplane, thus allowing it to accelerate to lift-off speed faster and having a

[1] https://www.pipistrel-aircraft.com/aircraft/electric-flight/taurus-electro/tab-id-2 [Accessed: 19 January 2022]

shorter take-off distance. The Pipistrel Taurus Electro on the other hand takes off from land, which offers less resistance than water, allowing it to take-off in a shorter distance.

Aircraft	Take-off distance [m]
Twin Otter	685
Pipistrel Taurus Electro	245
Water Sailplane	395

Table 17.3: Take-off distances to $15\,\mathrm{m}$ clearance.

While the estimated take-off distance of the water sailplane was indeed longer than that of the Pipistrel Taurus Electro, it is lower than that of the Twin Otter. This can be explained by the fact that the Twin Otter is heavier and thus has a higher take-off speed. This means that while it might take less time to reach a clearance height of $15\,\mathrm{m}$, the distance traveled in this time would be higher, thus leading to a longer overall take-off distance. Thus the results of the take-off performance are validated.

Another method to validate the take-off results would have been to model the Twin Otter in the take-off model and see if the model would have produced similar results to the known take-off performance of the Twin Otter. Due to time constraints, this was not performed however.

18. Class II Weight Estimation

Having defined the geometry of the preliminary aircraft design, a more sophisticated weight estimation may be performed. In this chapter the Class II weight estimation is presented, where semi-empirical formulas make use of the aircraft's geometry as inputs. Raymer's Class II weight estimation for General Aviation aircraft was chosen [13]. The exception for this was the weight of the propulsion group - split into motor and battery weight. These were sized in Chapter 16 with the motor having a weight of $22\,\mathrm{kg}$ and the batteries a weight of $128.32\,\mathrm{kg}$.

With this weight estimation method, the structural weight was categorized into the wing, horizontal tail, vertical tail, fuselage, propulsion, flight controls, avionics, electronics, and furnishings. For the floats, the same weight estimation method as used in the *Midterm Report* was used, by statistical regression of float planes weights [7]. Additional fudge factors were added to account for the aircraft being made of composites. The equations for all categories listed above are provided below, with the meaning of each symbol provided at the beginning of the report in the list of abbreviations:

$$W_w = 0.036 S_W^{0.758} W_{fw}^{0.0035} \left(\frac{A}{cos^2\Lambda}\right)^{0.6} q_{cr}^{0.006} \lambda^{0.04} \left(\frac{100t/c}{cos\Lambda}\right)^{-0.3} (N_z W_{dg})^{0.49} \tag{18.1}$$

$$W_{ht} = 0.016 (N_z W_{dg})^{0.414} q_{cr}^{0.168} S_{ht}^{0.896} \left(\frac{100t/c}{cos\Lambda}\right)^{-0.12} \left(\frac{A}{cos^2\Lambda_{ht}}\right)^{0.043} \lambda_h^{-0.02} \tag{18.2}$$

$$W_{vt} = 0.0876 (N_z W_{dg})^{0.376} q_{cr}^{0.122} S_{vt}^{0.873} \left(\frac{100t/c}{cos\Lambda_{vt}}\right)^{-0.49} \left(\frac{A}{cos^2\Lambda_{vt}}\right)^{0.357} \lambda_{vt}^{0.039} \tag{18.3}$$

$$W_{fus} = 0.052 S_f^{1.086} (N_z W_{dg})^{0.177} L_t^{-0.051} (L_{fus}/D_{fus})^{-0.072} q_{cr}^{0.241} \tag{18.4}$$

$$W_{fctrl} = 0.053 L_{fus}^{1.536} b_w^{0.371} (N_z W_{dg} \times 10^{-4})^{0.8} \tag{18.5}$$

$$W_{hydraulics} = 0.05 W_{dg}^{0.8} M^{0.5} \tag{18.6}$$

$$W_{avionics} = 40 + 0.008 W_{dg} \tag{18.7}$$

$$W_{elec} = 12.57 W_{avionics}^{0.51} \tag{18.8}$$

$$W_{furn} = 15 \cdot \frac{\mathrm{lb}}{\mathrm{kg}} \tag{18.9}$$

$$W_{floats} = 0.00727 W_{dg} \tag{18.10}$$

$$W_{mot} = 128.32 \cdot \frac{\text{lb}}{\text{kg}} \quad (18.11)$$

$$W_{mc} = 4.2 \cdot \frac{\text{lb}}{\text{kg}} \quad (18.12)$$

$$W_{bat} = 22 \cdot \frac{\text{lb}}{\text{kg}} \quad (18.13)$$

$$W_{gb} = 10 \cdot \frac{\text{lb}}{\text{kg}} \quad (18.14)$$

$$W_{prop} = 3.3 \cdot \frac{\text{lb}}{\text{kg}} \quad (18.15)$$

$$W_{prop} = W_{mot} + W_{mc} + W_{bat} + W_{gb} + W_{prop} \quad (18.16)$$

$$W_{pay} = 300 \cdot \frac{\text{kg}}{\text{lb}} \quad (18.17)$$

$$W_{dg} = W_w + W_{ht} + W_{vt} + W_{fus} + W_{prop} + W_{fctrl} + W_{hydraulics} + W_{avionics} + W_{elec} + W_{furn} + W_{floats} + W_{pay} \quad (18.18)$$

Note that the method is iterative, with W_{dg} being a dependent variable for multiple structural weight groups. Therefore, a Python script was written to iterate the calculations until the difference between the new weight and the previous was less than $1\,\%$. Additionally, the inputs into the equations all were required to be in imperial units, needing the following transformations from SI units to imperial:

$$\frac{\text{lb}}{\text{kg}} = 2.20462 \qquad \frac{\text{ft}}{\text{m}} = 3.28084$$

18.1. Verification and Validation

To verify the results of the Raymer estimation method they were compared with the Torenbeek method [32]. Additionally, the weight of components as a percentage of MTOW was compared to literature for such aircraft. A final validation check consisted of comparing the weight estimation results to the actual weight of similar aircraft.

Torenbeek provides a similar iterative set of equations depending on the aircraft geometry. For brevity, the equations were not included in the report. Similar to when computing the Raymer method, the propulsion group, and furnishing weight were fixed values determined by the design, and the floats were estimated by a statistical regression. Additionally, in the Torenbeek method the empennage is estimated as a group weight rather than broken down into the horizontal and vertical tail. Therefore these four components were not compared in weight as they would be the same. Comparing the results provided the following deviations:

Table 18.1: Verification of Raymer weight estimation with respect to Torenbeek method

Element	**Raymer results** kg	**Torenbeek results** kg	**Deviation w.r.t Raymer** $\%$
Wing	266	235	-11.65
Fuselage	121	143	18.18
Flight controls	15	18	20
Hydraulics	6	1	-83.33
Avionics	18	33	83.33
Electronics	18	51	183.33
MTOW	1071	1057	-1.31

From the verification it shows that there are clear discrepancies within the individual weight components. However the overall MTOW deviates by only $-1.31\,\%$. Given the small percentage discrepancy, the estimation of the overall MTOW is verified.

Given a limitation of data available for the weight breakdown of similar aircraft only certain parameters will be evaluated. These are the wing weight, fuselage plus vertical tail weight, and horizontal stabilizer weight. These components were validated with respect to sailplanes and normalized with respect to the MTOW, given that the aircraft dimensions are comparable. Results are shown in Table 18.2:

Table 18.2: Validation of wing, fuselage and vertical wing, and horizontal wing weights with respect to MTOW [24]

Aircraft	$MTOW$	$W_w/MTOW$	$(W_{fus}+W_{vt})/MTOW$	$W_{ht}/MTOW$
Nimbus 4 T	800	0.39	0.25	0.010
ASW 22BL	750	0.41	0.18	0.011
ASW 22 B	750	0.41	0.18	0.011
ASW 22	650	0.41	0.21	0.012
Kestrel 604	650	0.45	0.24	0.012
SPEAR	1071	0.25	0.11	0.009

Despite the verification of the Class II weight estimation being consisted with another weight estimation, the validation from Table 18.2 shows clear discrepancies. Wing, and fuselage plus vertical tail weights are significantly lower in proportion to the MTOW compared to the reference aircraft. Only the horizontal tail has a reasonable fractional weight of the MTOW, despite also being lower than the reference aircraft. As a result, the Class II weight estimation shows limitations in its results, and in a more detailed design analysis the structural weight could better be estimated with more sophisticated models such as FEM.

III

Final Design

19. Design Overview

This chapter elaborates on the iterations of the water sailplane design leading to the final design and presents a main overview of the final water sailplane design.

19.1. Iteration Process

In Part II all the methods and tools that were used for the design of the water sailplane were explained and verified. When (most of) these tools were completed, several design iterations were performed, with the goal to at the end of the project converge to a final design. The challenge with these iterations was that most tool inputs were dependent on outputs of other tools. A systems engineering approach was used to ensure a smooth operation of design iterations, under responsibility of the System Engineer.

To aid the process of design iterations an N2 chart was made that contains all the different design tools, their inputs and their outputs. This chart made it easy for all group members to see which tools were dependent on the tools they were working on, and also visualized the process of iterating. The N2 chart is shown by Figure 19.1. Tool outputs are placed horizontally in the same row as the tool that outputs them, and tool inputs are placed vertically in the same column that has these inputs.

In general the iterations were performed in the following order:

1. Estimate the MTOW with current design parameters
2. Determine the design point in the W/S-W/P diagram
3. Size the wing
4. Analyze the wing lift
5. Size the floats
6. Perform stability & controllability analysis
7. Size the empennage
8. Analyze the aircraft drag
9. Analyze aircraft performance
10. Size power & propulsion system
11. Perform structural analyses
12. Perform weight estimation
13. Repeat until convergence

Output →

Requirements & Environment	• V_stall • ρ • μ			• V_cr		• K	• V_h • V_v		• ρ(h) • V_cr • V_stall	• ρ • ρ_w	• A • V_cr • V_land		• E • σ_ult • τ_ult • G • ρ_m	• V_stall • K_1 • C_1	• ρ • V_cr		
Class I Weight Estimation	• EW • PW • MTOW	MTOW	• MTOW			• MTOW			• MTOW	• MTOW			• MTOW	• MTOW	• MTOW		
	Design Diagrams (W/S-W/P V-N)	• W/S						• W/P • P_br	• V_A • V_D • P_br • n_max	• P_br • V_D			• n_max				
	• S • AR • B • MGC	Wing Design (Airfoil + Planform)	• S • AR • b • λ • C_1-3 • MGC • Cl_max	• AR • b • C_1-3 • S • tc			• b • MGC		• S • AR • e	• S • AR • e	• MGC • X_LE • λ • AR • ε		• b		• S • AR • b • λ • tc		
	• e • CL_max • CL_alpha	• CL_alpha • CL_des	Lift Analysis	• CL_des • e					• CLmax • CL_alpha •	• CL0 • CL_alpha							
	• CD0 • CD_min			Drag Estimation					• CD0	• CD0						• CD_i_w • CD_fw • FF • CD	
				• D_fus • L_fus • L_1-4 • d_1-2 • S_f	Fuselage Sizing						• S_W_net • L_fus				• L_fus • D_fus • S_f		
				• L_fl • B_fl • S_fl • V_fl		Float Sizing				• L_fl • B_fl				• s_fl • h_fl • β_dr			• h_w
				• S_ht • S_vt			Empennage Sizing				• S_ht • S_vt • b_ht • b_vt					• AR_ht • AR_vt	
	• η_p							Propulsion Design	• η_p • battery capacity	• η_p • D_prop • P_cont • P_peak •					• W_batt • W_eng • W_bms		
	• h		• h • L/D	• L/D				• L/D • P_cl • t_cl	Flight Performance (Climb, Glide, Turn)	• RC • γ_cl	• RC • RD • RT • γ_d	• r_t_min • v_t_opt • t_t_min		• V_stall • V_cr	• V_cr	• L/D • RC • RD • RT	• V_stall • V_cr • γ_d • P_cl
								• T_max • t_TO • D_TO	• s_TO • T_max • V_TO	Take-off Performance							
					• L_t		• S_ht/S • np				Stability Analysis	• L_t • cg-range					
			• CL_δe									Controllability Analysis					
													Wing Structural Analysis		• t_sk • t_sp • t_str • n_str	• n_str_u • n_str_l • x_centroid • I • σ_z_max_u • σ_z_max_l	
• W_struts													• I	Floats Structural Analysis	• b_st • L_st	• N_w_h • N_w_v	
	• MTOW	• MTOW	• MTOW			• MTOW			• MTOW	• MTOW	• X_cg • Y_cg • Z_cg • W_comp		• MTOW	• MTOW	Class II Weight Estimation		
																Final Design	Final Design

Input ↑

Input ↓

← Output

Figure 19.1: Design N2 Chart

19.2. Iteration Overview

An overview of the design iterations and the corresponding changes in major design parameters is given in Table 19.1.

Table 19.1: Overview of the design iterations

Parameter	It1	It2	It3	It4	It5	It6	It7	It8	It9	It10	It11	It12
$MTOW$ [kg]	962	962	962	962	962	962	962	1265	1133	1070	1051	1065
$V_{stall_{clean}}$ [m s^{-1}]	22.22	22.22	22.22	16.67	16.52	20.83	19.69	21.43	18.35	22.29	22.10	22.24
S_w [m^2]	20.79	20.79	21.92	35.42	34.79	39.03	24.43	30.38	37.09	23.74	23.74	23.74
b_w [m]	21.87	24.98	25.65	32.60	32.30	28.22	24.81	27.67	30.57	24.46	24.46	24.46

19.3. Final Design Overview

A final overview of the design parameters found after the final iteration are presented per group. The top, front and side view of the water sailplane with final values of the design parameters are shown in fig. 19.2.

Table 19.2: Final design performance

Parameter	Value	[Unit]
MTOW	1071	[kg]
Pax. weight	300	[kg]
Lift to drag ratio	22.7	[–]
Stall speed clean	22.3	[ms^{-1}]
Stall speed hld	19.95	[ms^{-1}]
Cruise speed	27	[ms^{-1}]
Design maximum speed	64.85	[ms^{-1}]
Descent rate	1.26	[ms^{-1}]
Rate of climb	3.95	[ms^{-1}]

Table 19.3: Final design of the power and propulsion group

Parameter	Value	[Unit]
Max. continuous power	70	[kW]
Power loading	0.17	[N m^{-2}]
Propeller diameter	1.61	[m]
Spinner diameter	0.26	[m]
Motor weight	22	[kg]
Motor efficiency	0.95	[–]
Motor controller weight	4.2	[kg]
Motor controller efficiency	0.98	[–]
Battery weight	168	[kg]
Battery efficiency	0.95	[–]
Propeller weight	3.3	[kg]

Table 19.4: Final design of floats

Parameter	Value	[Unit]
Float spacing	3.65	[m]
Float height	2.43	[m]
Float length	7.87	[m]
Float weight	73	[kg]
Total weight struts	19.9	[kg]
Length diagonal strut	1.41	[m]

Table 19.5: Final design wing group

Parameter	Value	[Unit]
Weight	269	[kg]
Average taper ratio	0.514	[−]
Aspect ratio	25.2	[−]
Span	24.45	[m]
Surface area	23.73	[m^2]
Ultimate negative load factor	−2.65	[−]
Ultimate positive load factor	4.4	[−]
Thickness to chord ratio	0.153	[−]
Average chord	1.09	[m]
Root chord	1.15	[m]
Tip chord	0.44	[m]
Wing loading	434	[$N\,m^{-2}$]
Mean aerodynamic chord	0.8	[m]

Table 19.6: Final design of the empennage group

Parameter	Value	[Unit]
Weight		[kg]
Weight horizontal wing	15	[kg]
Weight vertical wing	24	[kg]
Root chord vertical tail	1.45	[m]
Tip chord vertical tail	0.764	[m]
Root chord horizontal tail	0.764	[m]
tip chord horizontal tail	0.691	[m]
Horizontal tail thickness/chord	0.12	[−]
Vertical tail thickness/chord	0.12	[−]
Surface area horizontal tail	3.2	[m^2]
Surface area vertical tail	1.83	[m^2]
Vertical tail span	1.66	[m]
Horizontal tail span	4.4	[m]

Table 19.7: Final design of fuselage

Parameter	Value	[Unit]
Fuselage weight	121	[kg]
Fuselage diameter		[m]
Fuselage length		[m]
Fuselage wetted area		[m^2]
Avionics weight	18	[kg]
Flight control weight	15	[kg]
Electric systems group weigh	18	[kg]
Hydraulic weight	6	[kg]

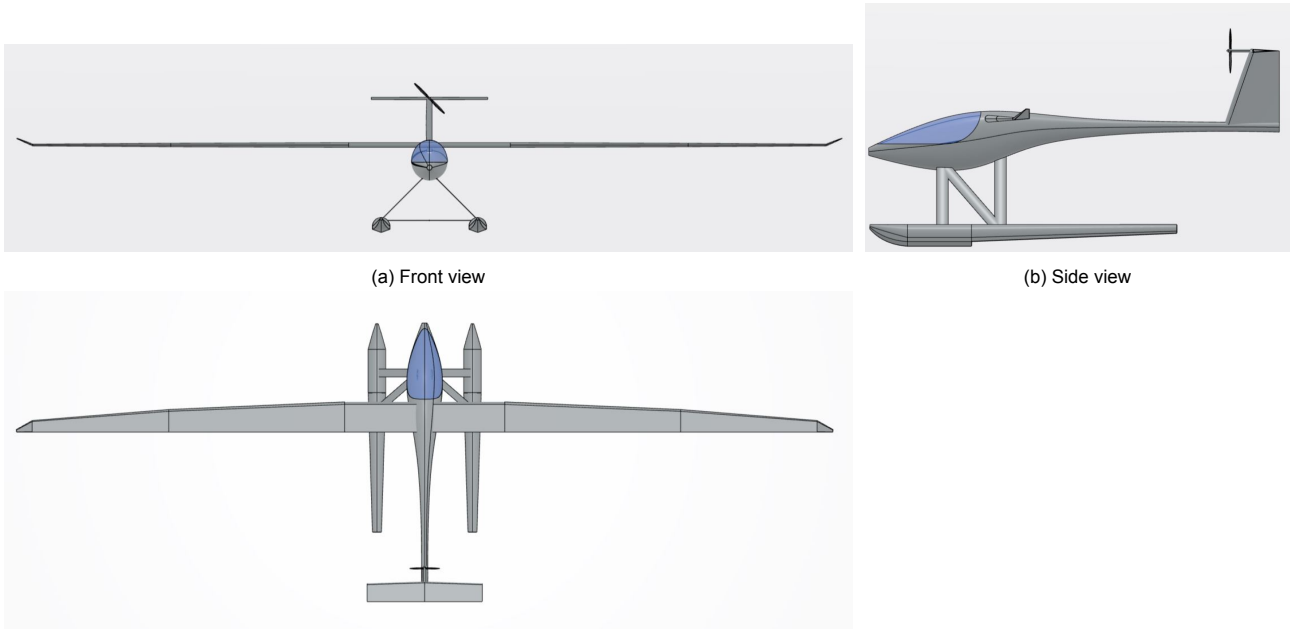

(a) Front view

(b) Side view

(c) Top view

Figure 19.2

20. Aerodynamic Characteristics

The results of the performed analyses in Chapter 17, Chapter 11 and Chapter 15 are presented in this chapter. These results describe the aerodynamic characteristics of the water sailplane. Firstly, the results are presented in Section 20.1. Furthermore, to make sure that the results are reliable a validation procedure was performed, which can be seen in Section 20.2.

20.1. Aerodynamic Results

The outcomes of the analyses are presented in this section. An overview of the numerical results from Section 11.3 and Chapter 15 is provided in Table 20.1. Figure 20.1, Figure 20.2a, Figure 20.2b and Figure 20.2c show the plotted results.

Table 20.1: Numerical results from the aerodynamic lift and drag analyses.

Parameter	Value	Unit	Parameter	Value	Unit
$C_{L\alpha_{wing}}$	0.114	$[\frac{1}{\circ}]$	$C_{D0_{horizontaltail}}$	0.0008	[-]
$C_{Lmax_{clean}}$	1.45	[-]	$C_{D0_{verticaltail}}$	0.0007	[-]
$C_{Lmax_{HLD}}$	1.81	[-]	$C_{D0_{struts}}$	0.0023	[-]
$C_{D0_{total}}$	0.0319	[-]	$C_{D0_{fuselage}}$	0.0098	[-]
$C_{D_{des}}$	0.0472	[-]	$C_{D0_{floats}}$	0.0099	[-]
$C_{D0_{wing}}$	0.0085	[-]			

The Lift Curve

Figure 20.1 shows the lift curve that was obtained through Section 11.3. The green curve describes the lift of the wing in clean configuration, where the dashed line is the result of the wing with a flap deflection of $30°$. Note that for these lift curves solely the lift of the wing was taken into account. Therefore, the lift curves for the total aircraft would have a lower C_{L_α} and $C_{L_{max}}$ than illustrated in this plot. Also note that if the wing becomes contaminated with salt water the lift generation will decrease. This was not analyzed, but is mentioned in Chapter 31 to be investigated in a later phase.

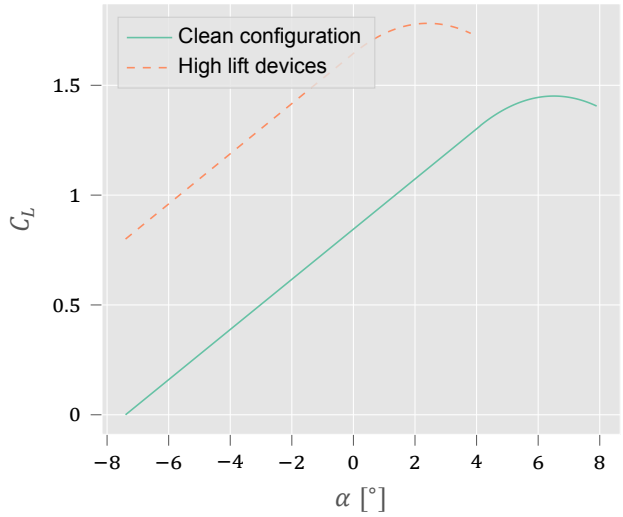

Figure 20.1: C_L-α curve in clean configuration and with high lift devices

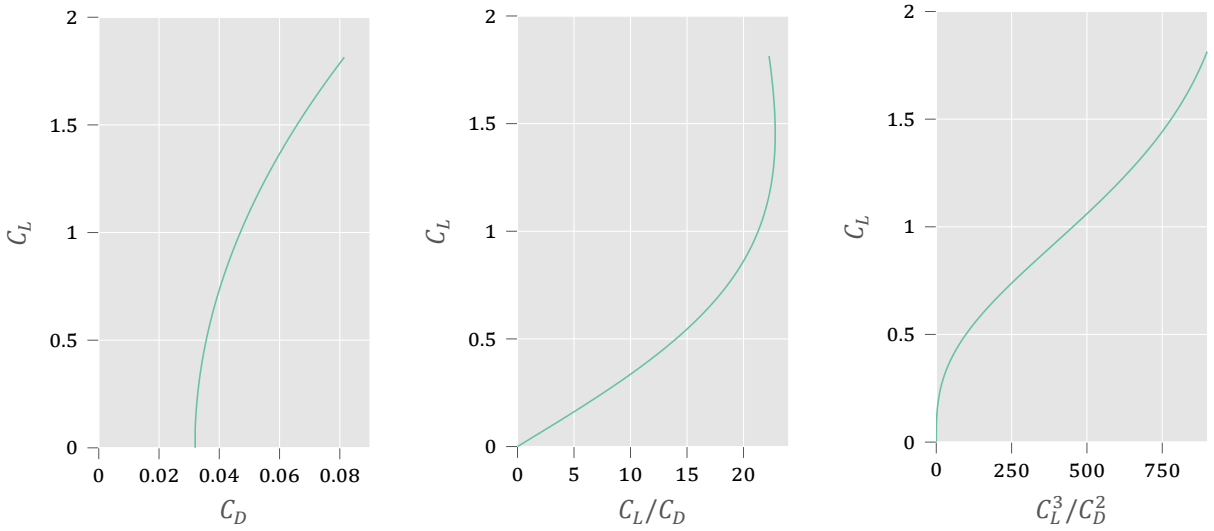

(a) Parabolic lift-drag polar

(b) Lift-to-Drag ratio

(c) Optimum lift-drag for RD

Figure 20.2: Various lift-drag ratios

20.2. Validation of the Results

As mentioned validation was needed to prove the reliability and validity of the obtained results. Both the numerical results and the plots were validated, which is described in Section 20.2.1 and Section 20.2.2 respectively.

20.2.1. Numerical Validation

This validation for the numerical results was performed through comparison a DHC-6 Twin Otter. This aircraft was chosen for the validation procedure, because the seaplane variant of this aircraft is used by TMA. Table 20.2 provides a comparison of the values of the water sailplane and of the Twin Otter, obtained from literature [45].

Table 20.2: Validation of the aerodynamic numerical results.

Parameter	WS	DHC-6 Twin Otter	Unit
$C_{L\alpha}$	0.114	0.086	$[\frac{1}{\circ}]$
$C_{Lmax_{clean}}$	1.45	0.9	[-]
$C_{D0_{total}}$	0.0319	0.036	[-]

Lift Parameters

When looking at the values of the lift slope and the maximum lift coefficient a significant difference is noticed. However, this was as expected based on two factors. Firstly, the numerical values were calculated for the wing only, which result in an overestimation of the lift behavior of the total aircraft. The second factor was the fact that the Twin Otter is a transport aircraft [45], not designed for optimal glide performance. The comparison of these values indicate that the numerical results are in the expected range, thus the lift parameters were validated.

Zero-lift Drag Coefficient

Regarding the parasitic drag coefficient, the values relatively close, which at first glance might seem odd as the water sailplane was optimized for performance. However, the Twin Otter discussed is not a seaplane. Therefore, the contribution of floats is not included in the C_{D_0}. With this in mind the result for the water sailplane became more reliable. Hence, also this value was validated, since it was expected that zero-lift drag coefficient of the water sailplane should be significantly lower than that of the Twin Otter seaplane.

20.2.2. Plot Validation

Analyzing the various lift-drag curves in Figure 20.2, the deficiencies of the parabolic approximation become apparent. The parabolic curve follows the shape of a parabola and thus will continuously increase in the C_D as the C_L increases. However, at high values of C_L, the true behavior of the drag coefficient should start to dramatically increase and deviate from the parabola due to flow separation effects [13, 46]. This also explains why the maximum C_L^3/C_D^2 occurs at the stall condition as can be seen in Figure 20.2c. This implies that the plots are not valid for high values of C_L, and thorougher methods such as CFD or wind tunnel tests are required to obtain a better prediction of the aerodynamic behavior approaching stall.

Furthermore, the chosen airfoil contains a laminar drag bucket, which is beneficial for minimizing drag at optimal C_L conditions. However, this was not factored into the drag estimation and thus is also not visible in Figure 20.2a. Therefore, the final results of Figure 20.2 must be taken with skepticism and can not be relied upon to provide an accurate prediction.

21. Structural Characteristics

This chapter presents the final structural characteristics of the aircraft. In Section 21.1 the final wingbox geometry is presented based on the methodology described in Section 11.4. Section 21.2 shows the final design of the struts connecting the floats to the fuselage based on the methodology from Section 14.2.

21.1. Wingbox design

With the iteration steps presented in Section 11.4.3 the final cross sectional design was determined. As mentioned above the number of stringers along the span changed due to a decreasing chord and normal stress. The chosen stringer shape was an L-stringer with equal height and width given the ease of manufacturing such a shape. The spar and skin thickness, however, were assumed to be constant along the entire span. This simplified the production of these parts, particularly the skin. A summary of the wingbox's cross-sectional geometry is provided in Table 21.1 and the number of stringers across the percentage of the half span in Table 21.2:

Table 21.1: Wingbox geometry

Part	Dimension
Skin thickness	2.7 mm
Spar thickness	5 mm
Stringer height and width	3 cm
Stringer thickness	5 mm

Table 21.2: Number of stringers along the half-wing span

Percentage of half-wing span:	0 %	10 %	20 %	30 %	40 %	50 %	60 %	70 %	80 %	90 %
Number of stringers on top	9	8	7	6	5	4	3	2	2	0
Number of stringers on bottom	8	7	6	5	4	4	3	2	1	0

Furthermore, the wingbox had to be compliant with the maximum positive and negative load factor with an additional safety factor of 1.5 over the load factor. The most critical failure analyzed was skin buckling of the top skin for the positive load factor, and the bottom skin for the negative load factor. The results are presented in Figure 21.1

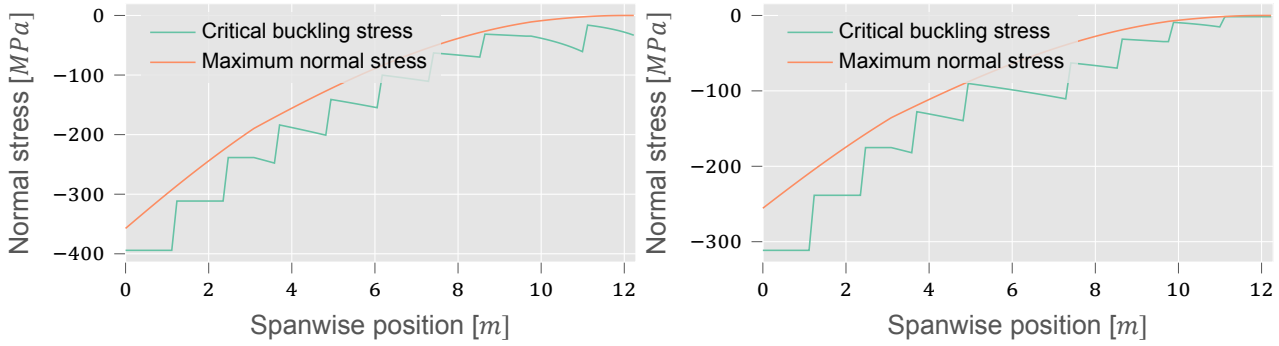

(a) Top skin

(b) Bottom skin

Figure 21.1: Critical buckling load of the top and bottom skin with respect to the maximum normal stress of each respective side

Another additional stress that was critical to the wingbox design was shear. This was as a result of the shear force and torque, as lift acted at $0.25c$. Figure 21.2 shows the maximum shear stress along the half span of the wing, with the highest shear occurring in the front spar at the root with a value of $72.5\,\mathrm{MPa}$.

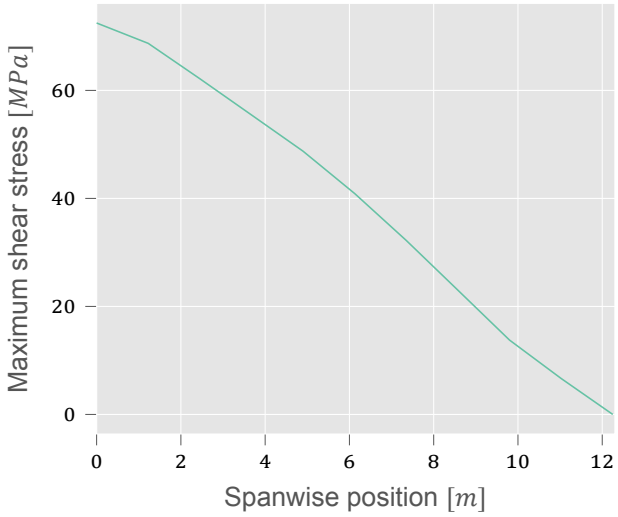

Figure 21.2: Maximum shear stress along the half span of the wing

21.2. Strut design

With the iteration steps presented in Section 11.4.3 the final dimensions of the struts were determined. The shape of the struts is circular with a hole in the middle to reduce weight. To make the struts more aerodynamic a sleeve with a symmetrical airfoil shape is put around the struts. The dimensions of the struts can be seen in Table 21.3. There are a total of two forward struts, two aft struts, two diagonal struts and one aft spreader and forward spreader.

Table 21.3: Dimensions of the different struts

Property	Forward Strut	Aft Strut	Forward Spreader	Aft Spreader	Diagonal Strut	Total
a [mm]	20	20	30	30	20	-
t [mm]	9.22	7.86	7.84	4.40	1.67	-
Area [mm^2]	512	445	690	399	200	-
Length [m]	0.993	0.993	3.00	3.00	1.41	-
Weight [kg]	1.416	0.708	3.317	1.919	0.4527	19.9
Price [€]	164	82	384	223	52	2309

22. Performance Characteristics

The upcoming chapter presents the performance characteristics of the final design determined with the use of tools described in part two of the report. First, the characteristics of the propulsion system will be presented in Section 22.1. Then, the aircraft's stability and control characteristics are presented in Section 22.2. Finally, the overall flight performance characteristics are presented in Section 22.3.

22.1. Propulsion System

This section will present the system characteristics of the propulsion system. First, the engine characteristics will be presented, this will be followed by the battery characteristics and finally the characteristics of the propeller and other components will be shown.

22.1.1. Electric Motor Characteristics

The brake power seen in tab. 22.1 is based on the wing power loading diagram explained in sec. 9.2. All other characteristics are established by the electric motor manufacturer.

Table 22.1

Parameter	Value	Unit
Peak power	80	kW
Max continuous power	70	kW
Brake power	65	kW
Maximum rotational speed	4000	rpm
Electric motor weight	22	kg
Electric motor efficiency	0.95	-
Electric motor controller weight	4.2	kg
Electric motor controller efficiency	0.98	-

22.1.2. Battery Characteristics

The battery mass seem is calculated with the use of the optimization process explained in sec. 16.6, as the total deliverable energy was dependent on the mass of the battery. The final mass of the battery pack was determined to be $128.31\,\mathrm{kg}$ Furthermore, the capacity of the battery was determined with the approximation of dividing the energy density by the nominal voltage of the battery. Further specifications seen in the table are specified by the manufacturer.

Table 22.2

Parameter	Value	Unit
Battery weight	128.31	kg
Battery efficiency	0.95	-
Energy density	267	Wh/kg
Max discharge rate	30	C
Max Pack voltage	800	V
Capacity	42.82	Ah
Ideal charge time	25.68	min

Validation of Battery

For a calculation of the charge time, it was assumed that the charge rate was ideal. To make an accurate estimation of the charge time required for the selected batteries, the discharge and charge curves were requested from the manufacturer for the first and final choice of batteries. However, no response was received. It is known that as the battery is charged, the voltage increases. So the charge rate slows down. Therefore, as stated in the calculation, the real charge time is lower than estimated. For further study, it is recommended to obtain these curves by testing the selected batteries.

22.1.3. Propeller Characteristics

The characteristics of the propeller with particular interest will now be highlighted. The propeller diameter has been approximated with the use of a limiting tip propeller velocity due to considerable drag from transsonic speeds and statistical approach for which the lower bound is taken. The propeller efficiency was determined with as a function of airspeed with the use of momentum theory as described in sec. 16.5.2, where the highest efficiency achieved is shown in the table below.

Table 22.3

Parameter	Value	Unit
Propeller weight	3.3	kg
Propeller efficiency	0.8058	-
Maximum rotational speed	3000	RPM
Number of propeller blades	2	-
Propeller diameter	1.619	m
Propeller pitch	29	deg
Spinner diameter	0.2688	m
Weight gearbox	10	kg

Validation of the Propeller modeling

For the calculation of thrust with the use of the quadratic interpolation, it was assumed that the propeller efficiency, η_p, is equal to 0.8. This is only justifiable for a higher speed range [14]. As the team was aware of this caveat another method of estimating thrust for low airspeeds was done. This is done by determining the propeller efficiency with the use of the momentum theory method as seen in fig. 16.4 However, the results showed even higher values for thrust at lower airspeeds. Thus, it is recommended for further study that a more accurate model of low thrust is analyzed, as current modeling overestimates it.

22.2. Stability and Control

For stability and control, three things were analyzed: The longitudinal stability and controllability, the elevator sizing and the center of gravity range.

22.2.1. Tail sizing

From the calculations in Section 13.2, the Scissor plot in Figure 22.1 was constructed. As can be observed in the graph, the landing condition is limiting for controllability.

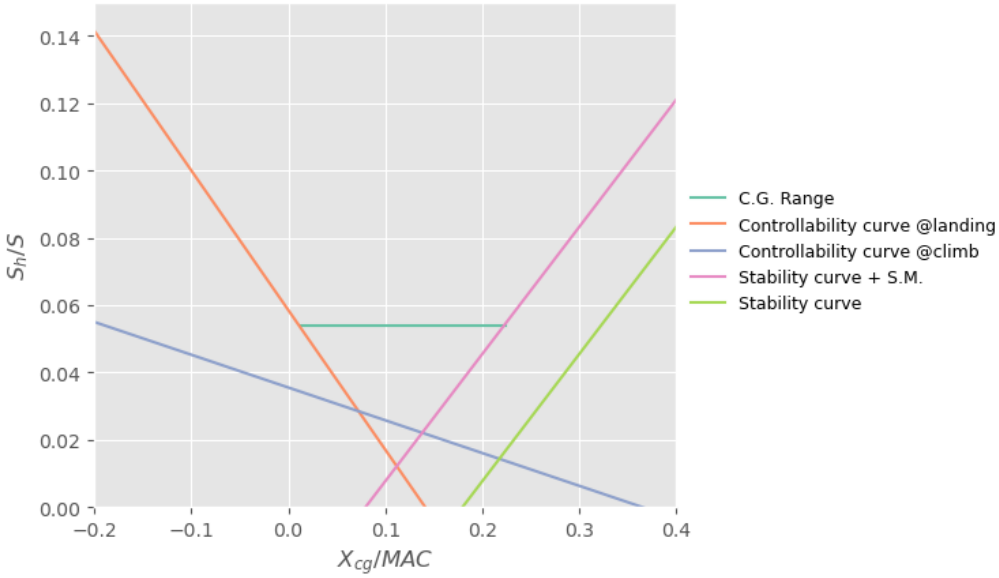

Figure 22.1: Scissor plot with controllability analyzed or cruise and climb conditions. S.M. = 0.1

After the scissor plot was constructed, the C.G. range was iterated until it fitted within the controllability and stability curves. As mentioned in Section 13.3, the battery position was mainly used to change the C.G. range. Table 22.5 shows all components and their respective C.G. location, as well as the total aircraft C.G. locations. Using Figure 22.1, a $\frac{S_h}{S}$ of 0.053 was found. Combining this ratio with the main wing area from Section 19.3, a horizontal tail area of $1.258\,\mathrm{m}^2$ was found. From the calculations in Section 13.2.5, where the rotation onto the step of the floats was analyzed, a horizontal tail surface area of $3.18\,\mathrm{m}^2$ was found. Thus, this shows that the take-off phase is critical for the sizing of the horizontal tail surface. This would result the C.G. range in Figure 22.1 to move upwards, which gives the horizontal tail more stability and controllability margin during flight. Using the aspect ratio and the vertical tail sizing from Section 13.1, the following horizontal and vertical tail dimensions were found:

Table 22.4: Horizontal and vertical tail dimensions

Horizontal Tail			**Vertical Tail**		
Area	m^2	3.18	Area	m^2	2.66
Root chord	m	0.764	Root chord	m	1.45
Tip chord	m	0.691	Tip chord	m	0.764

22.2.2. Elevator sizing

As mentioned in Section 13.4, the elevator is sized by iterating the elevator to chord ratio and the deflection angle to minimize drag. This resulted in in the elevator to be **25%** of the root chord of the horizontal tail.

22.2.3. Center Of Gravity Range

The following C.G. locations were used to calculate the C.G. range. As mentioned before, mainly the location of the battery was used to make the C.G. range fit within the Scissor plot, Figure 22.1

Table 22.5: Aircraft components and their C.G. position

Component	X-location [m]	Z-location [m]
Fuselage	3.6	0
Floats	3.5	3
Passengers	2.7	0
Pilot	1.35	0
Avionics	0.3	0
Batteries	3.7	0
Horizontal tail	9.28	-1.66
Vertical tail	9.28	-0.83
Engine	9.2	-1.66
Total C.G.	**3.59 - 3.81**	**0.0033**

22.2.4. Discussion of Stability and Control

As can be seen in Section 22.2.1, the required horizontal tail surface area during flight is $1.258\,\mathrm{m}^2$. For the rotation during take-off, a horizontal tail area of $3.18\,\mathrm{m}^2$ is required. After consulting with an experienced float plane pilot, it became evident that the controllability during water operations is much more limiting then during flight. This increases confidence in the result that the minimum required horizontal tail surface area is limited by the rotation during take-off.

The center of gravity range was only computed for a fixed passenger and pilot weight of $100\,\mathrm{kg}$. It would, however, not be unlikely that the passengers and pilot are much lighter than this. This would result in a more aft center of gravity than currently calculated. It is expected that this will not influence the design too much: Since the aircraft already has a big stability controllability margin during flight, because the horizontal tail is sized for rotation, the center of gravity will most likely remain inside the stable and controllable region.

22.3. Flight Performance Characteristics

This section presents the various flight performance characteristics of the final design. This includes climb, glide, turning and take-off performance.

22.3.1. Climb Performance

The aircraft climb performance is described in Figure 22.2, given that the thrust is optimized for maximum efficiency at $V = 30\mathrm{m\,s}^{-1}$. The associated parameters for the climb performance are listed in Table 22.6. The curves follow the expected behavior and, as described in Chapter 17, have been verified for their assumptions. The true performance of the propulsion system thrust, however, is still uncertain and this carries over into the climb performance.

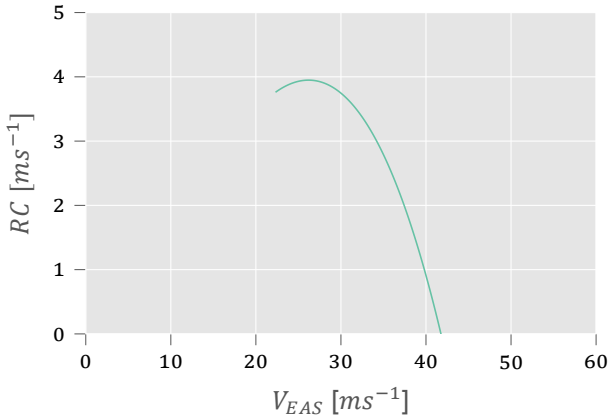

Figure 22.2: Rate-of-climb curve for the final design with $P_{br} = 70kW$ at sea level conditions and in clean configuration

Table 22.6: Climb Performance Parameters

Parameter	Value	Units
RC_{max}	3.95	$\mathrm{m\,s^{-1}}$
$V_{RC_{max}}$	26.2	$\mathrm{m\,s^{-1}}$
$t_{climb,1}$	266.3	s
$t_{climb,2}$	228.2	s
E_{climb}	9615	Wh

22.3.2. Glide Performance

Due to the method of estimation for C_L and C_D as discussed in Section 20.2.2, the values become unreliable when approaching stall conditions. As can be seen in Figure 22.3, this causes the minimum RD to coincide with the stall speed point. In reality, the curve should slope down as the drag coefficient becomes severely underestimated at low speeds. Therefore, some margin was built in when choosing the minimum allowable glide velocity. A 1.2 margin was chosen relative to the stall condition with flaps up. This is represented by the black dot in Figure 22.3 and provides the values in Table 22.7.

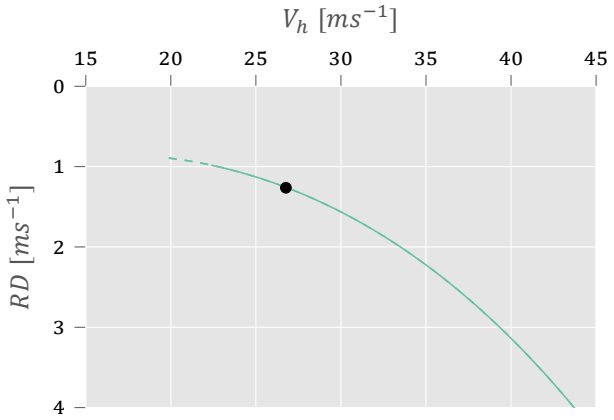

Figure 22.3: Hodograph for the final design showing minimum rate of descent with and without flaps deployed and the chosen descent rate at $1.2V_S$

Table 22.7: Glide Performance Parameters

Parameter	Value	Units
RD_{glide}	1.26	$\mathrm{m\,s^{-1}}$
$C_{L_{glide}}$	1.008	
$V_{RD_{glide}}$	26.7	$\mathrm{m\,s^{-1}}$
$t_{glide,1}$	714	s
$t_{glide,2}$	821	s
$t_{glide,tot}$	25	min

22.3.3. Turning Performance

Turning performance was divided into powered, level flight and gliding flight.

Level Flight

According to Ruijgrok, $V_{R_{min}} < V_{T_{\pi,min}} < V_{n_{max}}$, however, as can be seen in Table 22.8, the velocities are equal to each other. This is likely due to the method for the thrust approximation. The minimum turn radius and turn time follow from the maximum load factor calculation. Due to the quadratic thrust approximation, the thrust curve reduces quite quickly as it is optimized for a single propeller pitch angle. Therefore, the left half of the load factor curve coincides with the stall speed, resulting in a pointed top in comparison to the more bell-shaped curves seen in Ruijgrok [11]. Therefore, the validity of the results may be questionable and further analysis is required.

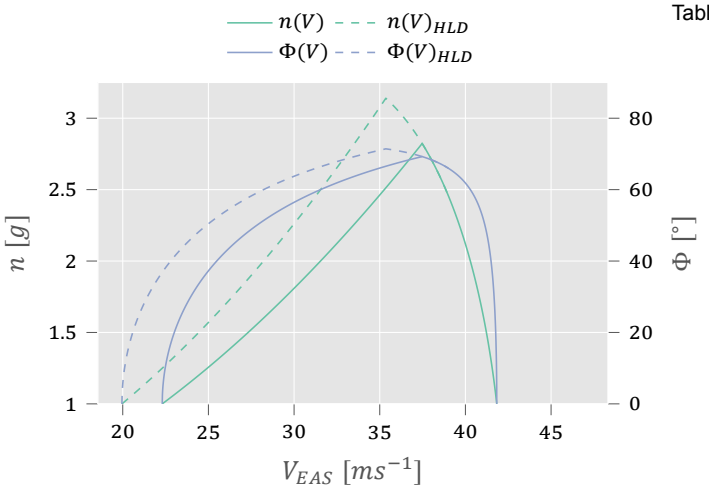

Figure 22.4: Maximum load factor (n) and corresponding bank angle (Φ) at different turning velocities in equivalent air speed

Table 22.8: Turning performance parameters for level flight

Parameter	Value		Units
	Clean	HLD	
n_{max}	2.82	3.13	g
Φ_{max}	69.2	71.4	°
R_{min}	54	43	m
$T_{\pi,min}$	4.6	3.8	s
V_{turn}	37.4	35.3	$m\,s^{-1}$

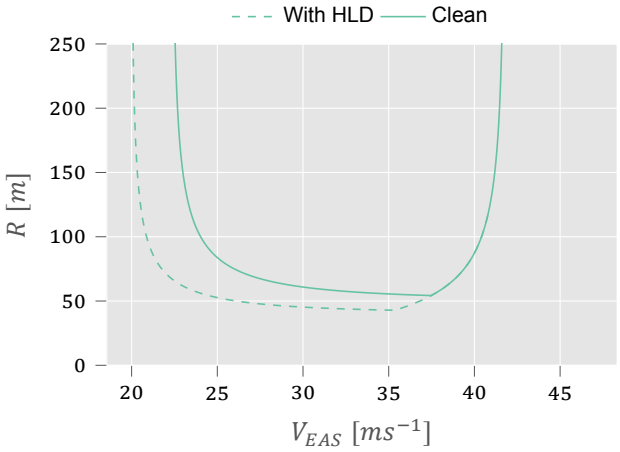

Figure 22.5: Turn radius at different turning velocities in equivalent air speed

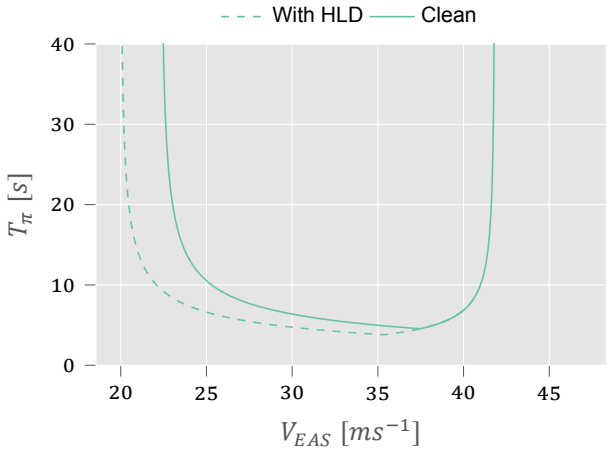

Figure 22.6: Turn time for a 180°heading change at different turning velocities in equivalent air speed

Gliding Flight

While no specific values were of interest for the gliding flight, it is interesting to observe the general expected behavior of turning and its impact on RD. By comparing Figure 22.5 with Figure 22.7, it can be seen that the tightest turns between $50\,\mathrm{m}$ to $100\,\mathrm{m}$ result in a very high descent rate as the curve dramatically dips down. Therefore, to maintain a reasonable descent rate during the glide phase, R should be kept above $100\,\mathrm{m}$, corresponding to a Φ of $45°$ or less, at the desired $C_{L_{glide}}$. Conversely, increasing the bank angle forces a speed increase as the stall speed creeps, as can be seen in Figure 22.8.

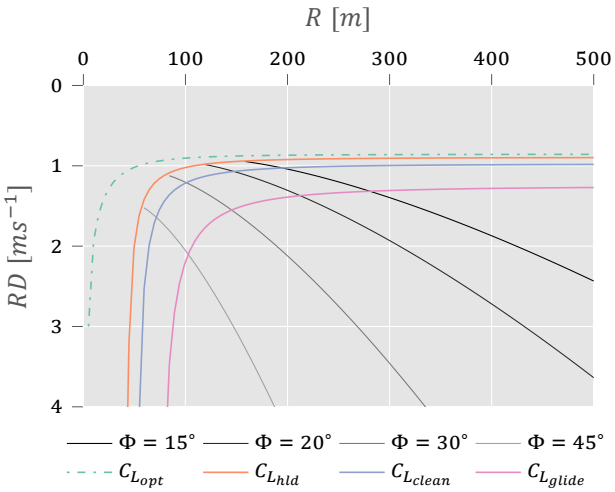

Figure 22.7: Variation of rate-of-descent as a function of turning radius with lines of constant C_L and lines of constant bank angle (Φ)

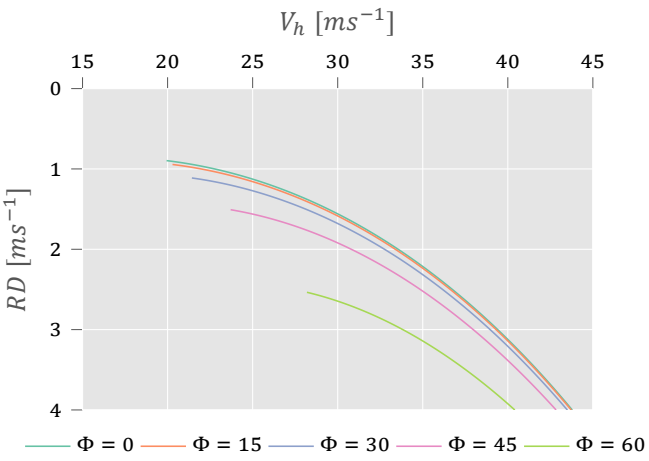

Figure 22.8: Variation of hodograph with different bank angles

22.3.4. Take-Off Performance

The take-off resistances of the final design of the water sailplane is shown in Figure 22.9. Table 22.9 summarizes the take-off distances to lift-off from water and to 15.2 m height clearance, and the total time to achieve both.

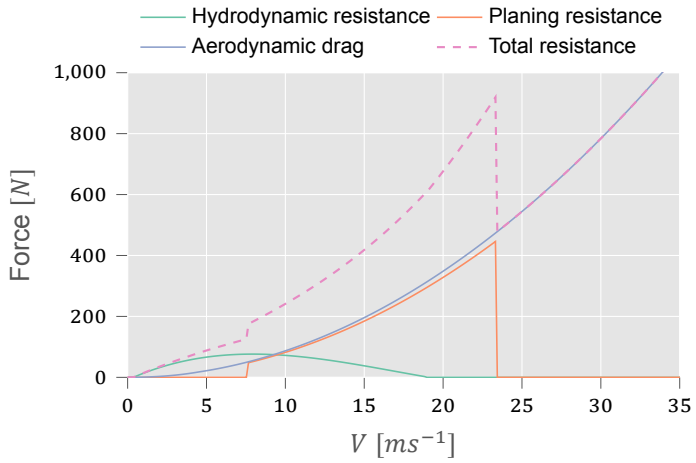

Figure 22.9: Take-off resistance curves of final design

Table 22.9: Take-off distances and times of the water sailplane final design

Parameter	Value
Distance to water lift-off	188.0 m
Time to water lift-off	19.92 s
Distance to take-off clearance	294.0 m
Time to take-off clearance	24.1 s
Take-off speed	23.3 m s^{-1}

23. RAMS

In this chapter the RAMS analysis is presented. RAMS stands for Reliability, Availability, Maintainability and Safety and these characteristics were evaluated for the water sailplane. Through the performance of this analysis the steps can be laid out that need to be fulfilled in order to keep operating the water sailplane in a safe manner. Firstly, the critical systems were identified that could lead to unsafe situations in Section 23.1. Then in Section 23.2 the redundancy philosophy is presented which contributes to the avoidance of these critical consequences. Thereafter, the maintenance that should be performed on the water sailplane to ensure its safety can be found in Section 23.3. Consequently, the reliability was evaluated, which is presented in Section 23.4. And finally, the availability of the aircraft is shown in Section 23.5.

23.1. Safety Critical Systems

In this section the safety of the water sailplane was analyzed based on the systems that could cause critical situations. If these situations occur, they would cause operational failure of the aircraft, which could harm the passengers, the water sailplane itself or both. To make sure these severe consequences are avoided, the safety critical functions were identified. This was done through creating an operational failure tree. Figure 23.1 gives a clear overview of the possible failures that might occur both before and during flight, and their causes. From this the critical systems were determined, which can be seen below:

- The floats
- The wing
- The empennage
- The control surfaces
- The material
- The electric motor
- The battery
- The flight controls
- The gearbox

With these safety critical functions in mind solutions were established through which the safety of the water sailplane could be improved. These solutions involved mostly the incorporated redundancy philosophy and the maintainability of the aircraft.

23.2. Redundancy Philosophy

The redundancy philosophy entails a safety net for the water sailplane, which ensures that some systems and/or subsystems can fail without having a critical impact on the operations of the aircraft as well as on the safety of passengers. This was done through the implementation of backups. The chance of failure of systems and subsystems is substantial due to the humid, hot and salty environment of the Maldives. Two forms of redundancy were adopted in the philosophy of the design team. These included the both dissimilar and division redundancy. Below it is explained how these forms were implemented in the design.

Dissimilar Redundancy

Dissimilar redundancy refers to the addition of an extra piece of the particular system or subsystem so that the impact of failure of that type does not directly harm the water sailplane. The philosophy behind this is that two systems from other manufacturers are unlikely to contain the same flaws. However, it must be checked that the systems are validated and do not give different results when working properly. A number of redundant systems can be included in the water sailplane:

- Flight control instruments
- Control surface actuators
- Batteries

Division Redundancy

Division redundancy refers to having a system that is divided into multiple parts, so that if one fails not the whole system falls apart. There are a few ways in which this philosophy could be implemented in the water sailplane

- A float consisting of multiple compartments, so that if one contains a leak not the entire float fills with water.
- Connecting the electrical systems in parallel instead of in series.

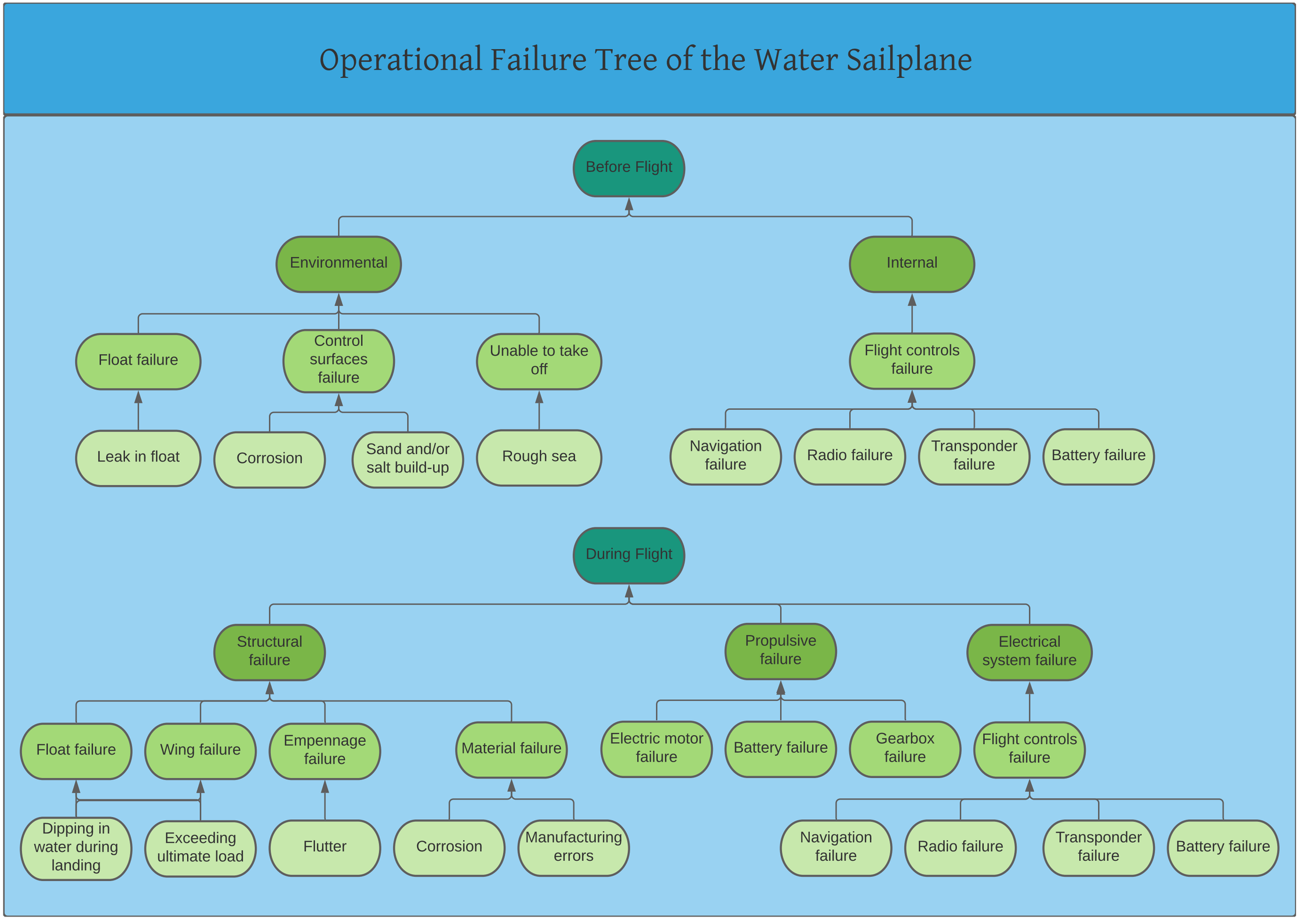

Figure 23.1: The Operational Failure Tree of the water sailplane.

23.3. Maintainability

Maintainability is the ability of the aircraft to meet its operational mission with a minimum expenditure of maintenance effort under the operational and environmental conditions, which minimizes the downtime of the aircraft [47]. For the maintenance the following problems were considered: corrosion, inspection, leakage, sand and/or salt build-up and algae growth. The checks are based on the method described by National Aviation Academy.[1] Here maintenance is divided into multiple types: Line maintenance (LM) and 'A', 'B', 'C' and 'D' checks. The line maintenance occurs daily. 'A' checks are performed every 400-600 flight hours. 'B' checks are performed every 6-8 months. 'C' checks are performed every year. Finally, 'D' checks are performed every 5-10 years. The requirements relevant for the maintainability can be seen in tab. 23.1.

Table 23.1: Maintainability Requirements

Identifier	Requirement
REQ-WS-RELI-02	The WS shall not require maintenance more than once every 8 weeks
REQ-WS-RELI-01	The WS shall have a lifespan of 30 years

Table 23.2: Maintenance Checks

Name	Interval	Duration	Performed by	Description
LM1	Every flight	0.5 hours	Pilot	1. Check battery charge
LM2	Every day	2 hours	Pilot	1. Clean algae from floats 2. Clean skin from sand, salt, etc. 3. Pump water out of floats 4. Visual check on structure, propeller, cracks and deformations
A	Every 2 months or 100 flights	10 hours	TMA Crew	1. Add lubrication to all moving elements 2. Check interior and exterior for evidence of damage, deformation, corrosion or missing parts
C	Every 12 months	100 hours	TMA Crew	1. Check for fluid leakage 2. Check electric systems 3. Check propellers efficiency 4. Test load carrying structures to verify integrity 5. In depth lubrication of all fittings and cables
D	every 5 years or 5000 cycles	400 hours	TMA Crew	1. Strip the complete aircraft and refurbish and upgrade the interior and exterior 2. Replace battery

Besides the scheduled maintenance, unscheduled maintenance might be needed as well. The same holds for damage repairs. The interval, duration and the person performing the maintenance depends on the severity of the maintenance or repair. If the component or system is beyond saving, a new component will have to be made.

23.4. Reliability

Reliability is the probability that the required operation can be performed under given conditions during a given time interval. A different way of interpreting reliability is the opposite of the probability of failure. For example, if the probability of failure is low, the reliability is high and vice versa. In Chapter 5 the risks are identified, and the probability and impact are minimized. However, risks still remain present, thus the reliability can not be 100%. In a broader sense, the reliability can be determined in two ways: analytically for each component, or historically by utilizing experience. However, both methods bring some complexities.

[1] www.naa.edu/types-of-aviation-maintenance-checks [Accessed: 19 Jan 2022]

Because a lot of systems were designed for this water sailplane, it was not possible to determine the reliability of each component. The components used from different concepts, such as the propulsion system, were also challenging for estimating the reliability, because the use case might differ. For example, the propulsion system might not have been tested in an environment of high humidity with salt water.

The historical reliability of a water sailplane was also difficult to define. As close to none have been made. However, the reliability of seaplanes and sailplanes can be combined to find the reliability. The most amount of crashes with sailplanes occur due to 'collision with hill'[48]. Most TMA seaplane crashes were caused due to the float dipping into the water.[2] The possibility of hill collision was ruled out since none are present in the Maldives. Although, the float dipping underwater is a significant risk, the struts were designed for such an impact. Thus, a reliability is expected closely to that the de Havilland Twin Otter used by TMA.

23.5. Availability

Availability is an essential aspect since a higher availability means the sailplane can produce more revenue as more flights can be performed. The water sailplane is unavailable when it is undergoing maintenance, repair, or when being charged. In a broader sense, the availability also relates to the availability on the market and the availability of parts. However, as a interested client is present the focus lays on the availability of the water sailplane regarding the operational side.

Aside from regular maintenance of the water sailplane, the availability of the water sailplane is dependent on the amount of charging that needs to be performed. By minimizing the charge time and/or the amount of charges the availability of the aircraft grows. In Section 16.6.1 the charging time was estimated to be $0.428\,\mathrm{hours}$, which comes down to about $26\,\mathrm{min}$. Assuming that after each flight the battery will have to be charged again, the downtime would equal the sum of the charging time, the inspection time and the briefing time of the passengers.

24. Technical Resource Tracking

This chapter covers the budgets of crucial design parameters, and the progression of these parameters throughout the design project. Section 24.1 gives a breakdown of the technical resource budgets of the final water sailplane design. In Section 24.2 the progression of the water sailplane MTOW value is shown. Section 24.3 then shows the progression of the landing configuration stall speed value, Section 24.4 the progression of the descent rate, and finally Section 24.5 shows the progression of the break power.

24.1. Budget Breakdown

Engineering design projects are characterized by uncertainties. As the design enters new and more detailed design phases, these uncertainties decrease, but only become zero when the design is actually produced and tested. The challenge of the engineers is to account for these uncertainties during the different design phases, to not be surprised when actual results differ from analysis and simulations. While uncertainties decrease as the design furthers, parameters like aircraft mass and required power tend to increase. For this reason budgets were set to these parameters, that in principle cannot be exceeded during any design phase. To account for the uncertainties of these parameters, contingencies were also determined per design phase from Roskam [10], anticipating the possible changes in parameter values.

Throughout the project several crucial parameters were tracked, in order to ensure no parameters exceeded their budget. If this were the case, the System Engineer sat down with the relevant engineers to find a solution to keep the design within the budget, or in the most unfavorable case change the budget. Table 24.1 shows the parameters parameters for which budgets were set, the values of the initial budgets and if applicable the changed budgets. The following sections go into detail about the variation of the different parameters throughout the project.

[2] avherald.com/ [Accessed: 18 Jan 2022]

Table 24.1: Budget breakdown of the final water sailplane conceptual design

Parameter	Budget	Cont. %	Cont. Value	Design Value	Design Value + Cont.
MTOW [kg]	1250	15%	187.5	1071	1258.5
Stall Speed LC [$\mathrm{m\,s^{-1}}$]	22.22	10%	2.2	20	22.2
Descent Rate [$\mathrm{m\,s^{-1}}$]	$1.4\,\mathrm{m\,s^{-1}}$	10%	0.14	1.26	1.4
Power [kW]	70	0%	0	70	70

For all parameters the following four values were tracked:

- **Specification Value** - Value following from requirement, also the parameter budget
- **Target Value** - The specification value minus the pre-planned contingency
- **Actual Value** - The actual value of the design parameter
- **Current Value** - The actual value including the contingency, reflecting the actual status of the design

The idea behind these values is to ensure all values stay below the specification value, but with decreasing differences as the design becomes more detailed and more confidence arises in the correctness of values, and thus contingencies decrease. As the DSE project ends with a conceptual design, there should still be a margin between the final actual value and the specification value. Only when an aircraft would be produced and tested would the uncertainty and therefore contingencies become zero.

24.2. Maximum Take-Off Mass

One of the most important parameters that was tracked was the MTOW of the water sailplane, as this parameter had direct and substantial influence on all other design parameters and aircraft performance. The progression of the MTOW is shown in Figure 24.1:

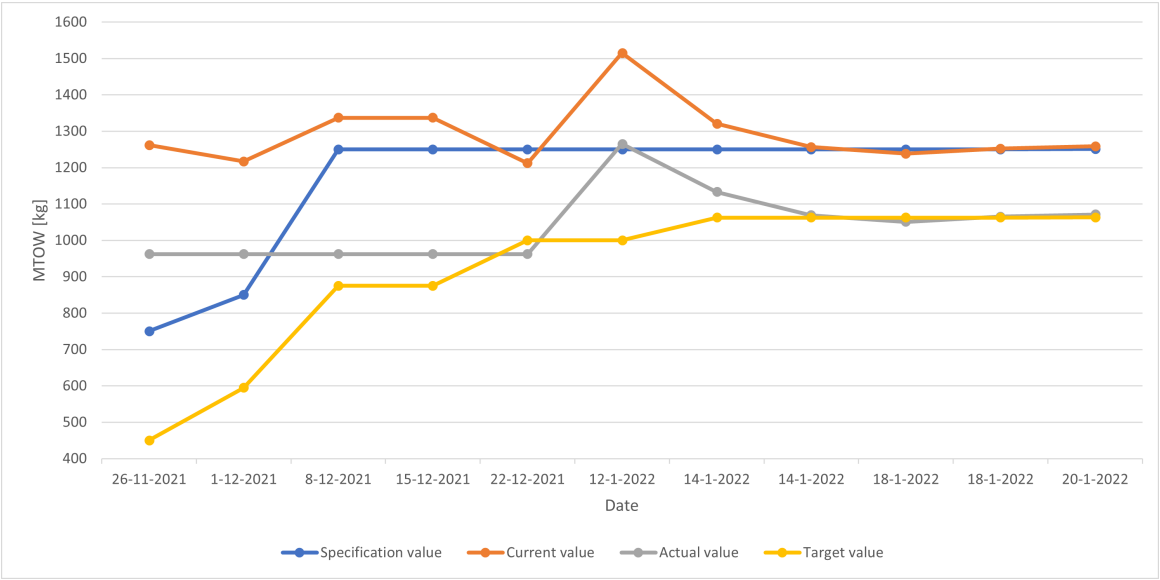

Figure 24.1: Progression of MTOW

As can be seen in the graph, initially the estimate for the MTOW exceeded the specification value. Initially the specification value was $750\,\mathrm{kg}$, as this was the maximum allowable MTOW from CS22 for unpowered sailplanes. This was increased to the higher allowable MTOW for powered sailplanes of $850\,\mathrm{kg}$. The actual value of the design MTOW still exceeded this however. The reason for this was that the CS22 specified MTOW applied to 2-seater powered sailplanes. The water sailplane was designed for three passengers and for water operations, which would naturally lead to a higher weight. The requirement, and budget, were therefore increased to $1250\,\mathrm{kg}$.

At 12-01-2022 another mass estimation was performed, which determined the actual value at that stage to be slightly higher than the specification value, and the current value therefore even higher. The System

Engineer and the Performance Engineers had a meeting to discuss solve this issue. It was concluded that the requirement and budget for V_{stall} landing configuration was unrealistic for the design, and this was increased, as explained in Section 24.3. This resulted in the actual and current value of the MTOW to decrease.

The graph shows that in the end the both the actual and target value matched up, as well as the specification and current value, which is the desired situation. This way there is still sufficient margin between the MTOW of the final conceptual design of the water sailplane and the specification value.

24.3. Stall Speed Landing Configuration

Another important parameter that was tracked throughout the design process was the stall speed in landing configuration. The progression of this parameter is shown in Figure 24.2:

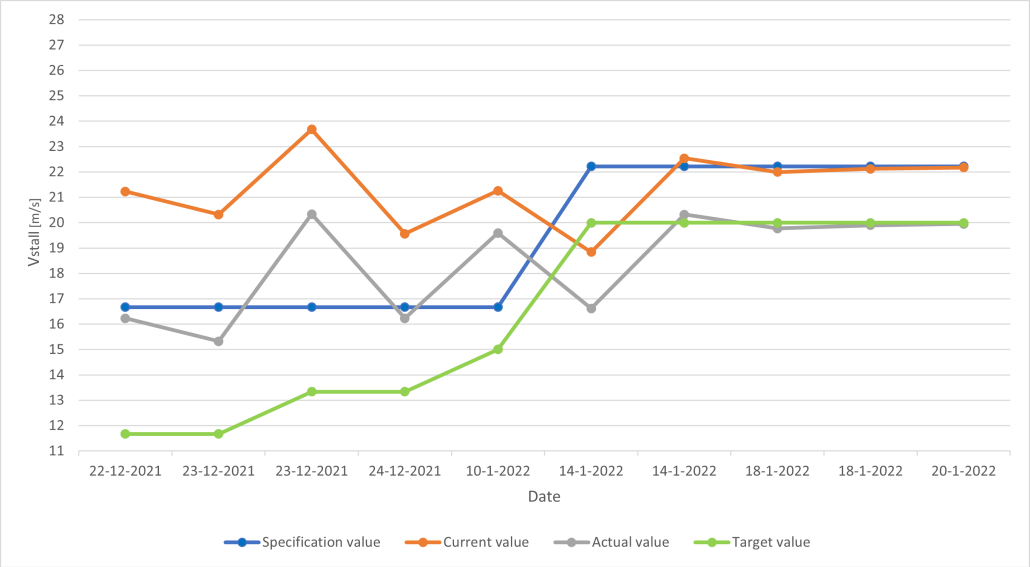

Figure 24.2: Progression of V_{stall} landing configuration

As mentioned in the previous section, this parameter requirement of $60\,\mathrm{km\,h^{-1}}$ proved to be very constricting for the design. According to the CS22 regulations, this parameter was allowed to be $80\,\mathrm{km\,h^{-1}}$. Therefore the budget was changed accordingly. In the end this resulted in a V_{stall} in landing configuration of $72\,\mathrm{km\,h^{-1}}$ or $20\,\mathrm{m\,s^{-1}}$. As seen in the graph, this provided a sufficient margin between the actual value of the water sailplane design and the specification value.

24.4. Descent Rate

As the main mission of the water sailplane is to perform gliding scenic flights around the Maldives, the descent rate was also an important parameter to keep track of throughout the design. The progression is shown in Figure 24.3:

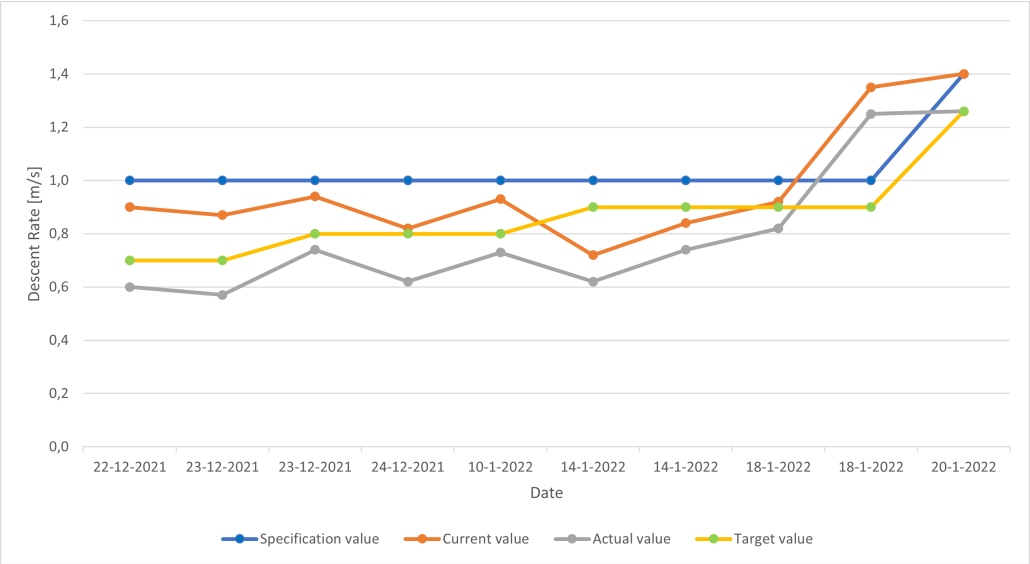

Figure 24.3: Progression of RD

While an RD of $1.0\,\mathrm{m\,s^{-1}}$ is considered a bad glide performance for a sailplane, it was initially assumed that this would be a realistic requirement for the water sailplane, as it was expected that the addition of floats and the accompanying drag would negatively affect the glide performance of the water sailplane. Throughout most of the design the value of the RD for the water sailplane was estimated to be below the requirement value. However, at the end of the design phase it turned out the drag contribution of the floats had be underestimated. This estimation was reevaluated, which resulted in the total aircraft drag increasing. This lead to a significant drop in RD and thus glide performance. However, since the water sailplane was designed for a total glide time exceeding the wishes of the client, this drop in glide performance was accepted, and the budget increased to $1.4\,\mathrm{m\,s^{-1}}$. In the end the final design also had sufficient margin between the actual value of the RD and the increased specification value.

24.5. Power

The last parameter that was tracked was the engine break power. The progression is shown in Figure 24.4:

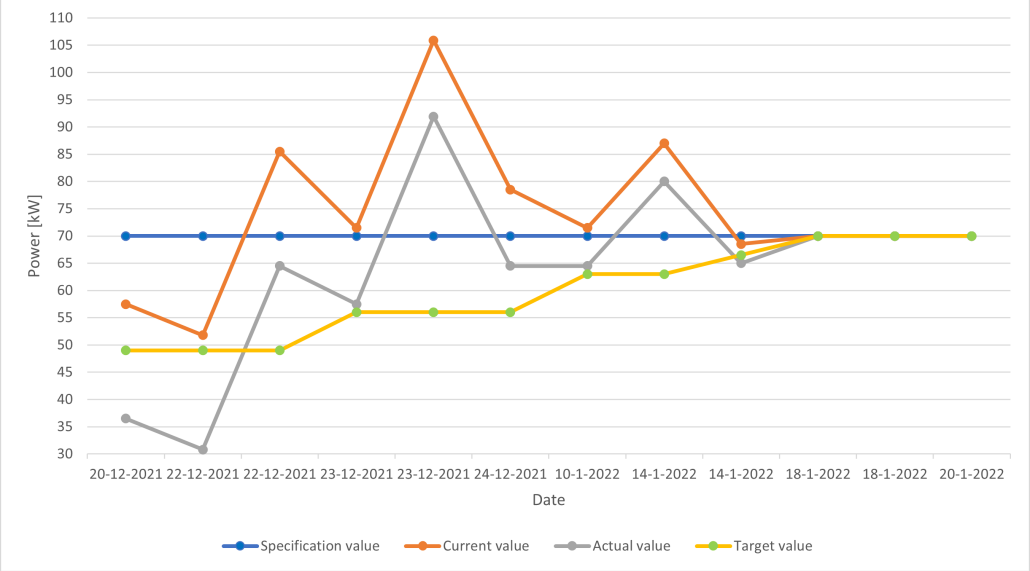

Figure 24.4: Progression of P_{br}

While there were several spikes in the break power required for the water sailplane, in the end it was possible to get this value to below the specification value. There is no margin between the actual value and the specification value, which is explained by the fact that a commercially available engine was selected for the water sailplane, thus there was no contingency necessary for this parameter for the conceptual design.

25. Sensitivity Analysis

The final design of the water sailplane is a conceptual design. This means there is uncertainty in the actual values of design parameters, due to the limits of the tools and methods used up to this stage in the design. As shown in Chapter 24, there is a margin between the parameter values of the final design and the requirements. It is however important to analyze what happens to these margins when the unfavorable case of the uncertainties are taken into account. This could have an impact on the design of the water sailplane and its ability to meet the requirements. For that reason a sensitivity analysis was performed. Section 25.1 highlights the requirements to which the impact of the design uncertainties were analyzed. In Section 25.2 the impact of the uncertainty in MTOW estimation is analyzed. Section 25.3 then explores what the consequences of underestimated aircraft drag could be, while Section 25.4 covers the implications of overestimating the design lift characteristics. Lastly, Section 25.5 explains what the impact on the design would be if the battery energy density would be lower than specified.

25.1. Requirements Analyzed

In the sensitivity analysis the impact of parameter uncertainty was analyzed on the requirements given in Table 25.1:

Table 25.1: Requirements analyzed in sensitivity analysis

Requirement	Description
REQ-WS-FLPE-OPL-01	The WS shall have a V_{stall} of $80\,\mathrm{km\,h^{-1}}$ in landing configuration
REQ-WS-WATO-07	The WS shall have a water take-off distance of $400\,\mathrm{m}$
REQ-WS-FLPE-AER-03	The WS shall have a descent rate of $1.4\,\mathrm{m\,s^{-1}}$ at MTOW

Furthermore, the impact on the total energy required for take-off and climb is analyzed, since the batteries have a limited power capacity that the water sailplane can use for operations. The current values of the final design for the analyzed requirements and the total energy required are given in Table 25.2:

Parameter	Current design value	Margin to requirement
V_{stall}	$19.95\,\mathrm{m\,s^{-1}}$	+11.4%
s_{TO}	$294.0\,\mathrm{m}$	+36.1%
RD_{min}	$1.26\,\mathrm{m\,s^{-1}}$	+11.1%
E_{tot}	$10239\,\mathrm{W\,h}$	+31.4%

Table 25.2: Current design values of requirement parameters, and their margin to the requirement value

25.2. MTOW Uncertainty

The first parameter to which the sensitivity was analyzed was the MTOW of the aircraft. At this stage of the design, there is a 15 % uncertainty between the current value of $1071\,\mathrm{kg}$ and the requirement value of $1250\,\mathrm{kg}$. Therefore it was analyzed what the impact was on the design if the MTOW was increased by 5, 10 and 15 %. The results are show in Table 25.3:

Table 25.3: Sensitivity of crucial parameters with 5, 10 and 15% increases in MTOW

Parameter	+5%	+10%	+15%
V_{stall}	$+2.5\%$	$+4.9\%$	$+7.3\%$
s_{TO}	$+9.6\%$	$+21.2\%$	$+32.9\%$
RD_{min}	$+2.4\%$	$+5.6\%$	$+7.1\%$
E_{tot}	$+6.3\%$	$+12.6\%$	$+19.4\%$

As can be seen from the results, the most sensitive parameters to an increase in MTOW are the take-off distance and the total energy required. Both parameters would still comply with the requirements however. It can thus be concluded that the current design margins for these parameters are sufficient for the uncertainty in MTOW.

25.3. Drag Underestimation

The next parameter of which the impact of uncertainty was analyzed was the drag, and more specifically the total aircraft C_{D_0}. It was analyzed what the effect on the requirement parameters was for an increase in the total C_{D_0}. There are two aspects that could lead to the actual C_{D_0} of the aircraft being higher than the value used in the design calculations. The first is that relative simple methods were used to estimate the C_{D_0} of the floats. However, due to the fact that the step of the floats contribute to a discontinuity in the surface, the actual drag of the floats could be higher than estimated.

Secondly, for the lift and drag estimations of the aircraft it was assumed that no surfaces were contaminated. However, since the water sailplane would operate on seawater, it is very likely that some of the surfaces would be covered with seawater droplets, or dried up salt deposits. This would lead to a higher drag of the aircraft. The results of the analysis are given in Table 25.4:

Table 25.4: Sensitivity of important parameters with 10, 15 and 20% increases in aircraft C_{D_0}

Parameter	+10%	+15%	+20%
s_{TO}	$+1.6\%$	$+1.6\%$	$+3.2\%$
RD_{min}	$+7.1\%$	$+10.3\%$	$+13.5\%$
E_{tot}	$+1.9\%$	$+2.9\%$	$+3.9\%$

It was concluded that the descent rate was most sensitive to an increase in aircraft drag, and this could even lead to non-compliance of the descent rate requirement, which is a highly undesirable situation. The drag characteristics of the water sailplane would therefore be a highly important aspect to analyze and optimize in more detail in the further design stages.

25.4. Lift Overestimation

Similar to the drag calculations, the contamination of the wing surface was not taken into account in design calculations. These contaminations could lead to a worse lift characteristic of the aircraft. Therefore the impact of a decreased C_L was analyzed for the requirements, and the results are shown in Table 25.5:

Table 25.5: Sensitivity of important parameters with 5, 10 and 15% decreases in C_L

Parameter	-5%	-10%	-15%
V_{stall}	$+2.6\%$	$+5.4\%$	$+8.5\%$
s_{TO}	$+4.1\%$	$+10.1\%$	$+15.3\%$
RD_{min}	$+4.8\%$	$+10.3\%$	$+16.7\%$

Similar to the impact of increased drag, decreased lift characteristics have a high impact on the descent rate, and could lead to the water sailplane not meeting this requirement. It would therefore be paramount that the contaminated lift characteristics are analyzed and optimized in further design stages, in parallel with the drag characteristics.

25.5. Energy Density Overestimation

Lastly the energy density was analyzed. While the batteries selected for the design are commercially available batteries that have a specified energy density of $267\,\mathrm{Wh\,kg^{-1}}$, in reality the actual energy density could be lower than this. The effects of this are analyzed in this section.

In principle, the batteries at the current energy density have an available energy capacity of $27\,408\,\mathrm{Wh}$, taking the designed depth of discharge from Chapter 16 into account, while the total energy required at this stage in the design is $20\,500\,\mathrm{Wh}$. This means that if the energy density of the batteries were to go down for the same battery weight of $128\,\mathrm{kg}$, the aircraft would still have enough energy to perform the mission it was designed for. The limit for this was determined to be a decrease in energy density of 25 %, which corresponds to an energy density of $200\,\mathrm{Wh\,kg^{-1}}$.

If the energy density would be below this limit however, the battery weight would have to increase to supply enough energy for the aircraft to perform its mission. Using the Class II weight estimation from Chapter 18 the MTOW increase due to the battery weight increase was then calculated, assuming all other design parameters remained the same. In Figure 25.1 the estimated MTOW for different battery energy densities U is plotted. Also shown is the limit line of the MTOW of $1250\,\mathrm{kg}$, and the point where the two lines intersect.

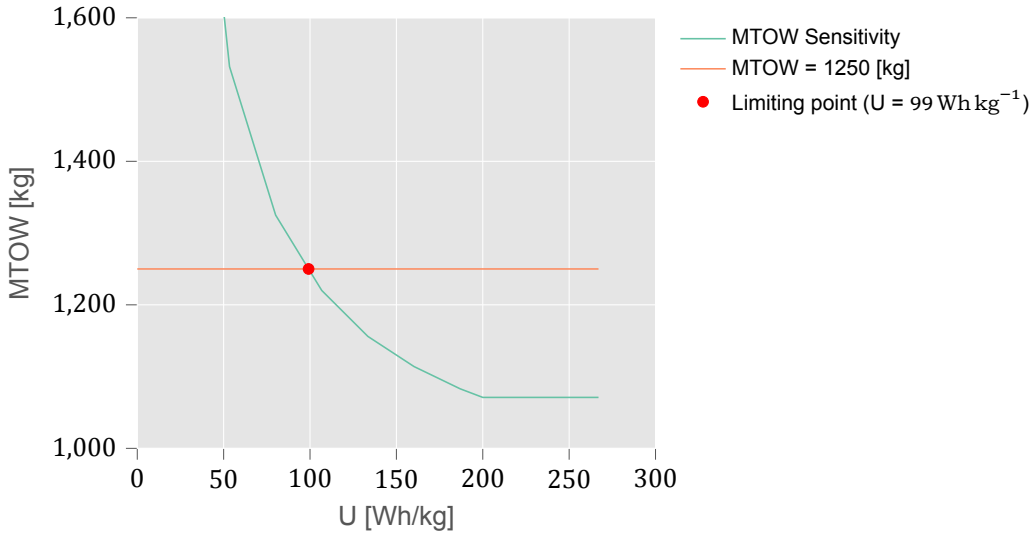

Figure 25.1: Change in MTOW for different battery energy densities U

As can be seen from the graph, the battery energy density of the water sailplane could reduce up to $99\,\mathrm{Wh\,kg^{-1}}$, where the MTOW would reach the limit of $1250\,\mathrm{kg}$. This corresponds to a decrease of 63 % in energy density compared to the value that was used for the design calculations of the water sailplane. This means there is quite a sufficient margin to account for a reduction in actual battery energy density. Note that this MTOW increase would have the performance decreases from Section 25.2 as a consequence. Furthermore, the effect of the increased battery weight on the stability and controllability of the water sailplane would have to be analyzed in further design phases, and could require a shift in battery placement to ensure sufficient stability and controllability.

26. Requirement Compliance

The requirement compliance is performed with a requirement compliance matrix (RCM). This is done for a number of reasons. Firstly, it shows if the design is fully compliant. Secondly it packs important information together. And lastly it can easily be seen if the requirements are met. The RCM can be seen in Section 26.1 and the rationale why the design does not meet some of the requirements or the modifications which would make the requirement compliant can be seen in Section 26.2.

26.1. Requirements Compliance Matrix

The RCM can be seen in Table 26.1. In this table all the requirements can be seen, with their requirement ID in the first column. The second column shows the value, if there is any. Then in the third column it can be seen if the requirement is compliant or not. This compliance is dividend into ratings which are the following; Compliant, non-compliant and to be determined (TBD). For the latter two a rationale is given why the design does not meet the requirements and which possible modifications of the design would make the requirements compliant. This rational is explained in Section 26.2. In the fourth column the table is given where the requirement is described. The last column gives the section where the result of the requirement is described.

Table 26.1: Requirements comliance matrix

Requirement ID	WS Value	Compliance	Origin	Result
Water Operations				
REQ-WS-WATO-01	181% MTOW	Compliant	Table 14.1	Section 14.1.3
REQ-WS-WATO-05	$0.32\,\mathrm{m}$	Compliant	Table 14.1	Section 14.1.4
REQ-WS-WATO-07	$294\,\mathrm{m}$	Compliant	Table 9.2	Section 22.3.4
REQ-WS-WATO-08	-	TBD	Table 9.2	-
REQ-WS-WATO-13	$1.17 \cdot V_{stall}\mathrm{m\,s^{-1}}$	Non-compliant	Table 9.2	Section 22.3.4
REQ-WS-WATO-14	-	TBD	Table 9.2	-
REQ-WS-WATO-16	-	TBD	Table 14.1	-
Aerodynamics				
REQ-WS-FLPE-AER-01	$3.95\,\mathrm{m\,s^{-1}}$	Non-compliant	Table 9.2	Section 22.3
REQ-WS-FLPE-AER-03	$1.26\,\mathrm{m\,s^{-1}}$	Compliant	Table 17.1	Section 22.3
REQ-WS-FLPE-AER-04	FL35	Compliant	Table 9.1	Section 9.1
Operational Limits				
REQ-WS-FLPE-OPL-01	$72\,\mathrm{km\,h^{-1}}$	Compliant	Table 9.2	Section 22.3
REQ-WS-FLPE-OPL-08	$15\,\mathrm{m\,s^{-1}}$	Compliant	Table 9.5	Section 9.3
REQ-WS-FLPE-OPL-09	$7.5\,\mathrm{m\,s^{-1}}$	Compliant	Table 9.5	Section 9.3
Stability				
REQ-WS-FLPE-STB-01	-	Compliant	Table 13.1	Section 22.2
Controllability				
REQ-WS-FLPE-CON-06	-	TBD	Table 13.1	-
Endurance				
REQ-WS-FLPE-END-01	25 minutes	Non-compliant	Table 17.1	Section 22.3.2
Payload				
REQ-WS-FLPE-PAY-01	-	Compliant	Table 12.1	Section 12.1
REQ-WS-FLPE-PAY-05	-	Compliant	Table 12.1	Section 12.1
REQ-WS-FLPE-PAY-06	-	Compliant	Table 12.1	Chapter 12
REQ-WS-FLPE-PAY-07	-	Compliant	Table 12.1	Section 12.1
REQ-WS-FLPE-PAY-08	-	Compliant	Table 12.1	Section 12.1
REQ-WS-FLPE-PAY-11	2.1%	Compliant	Table 13.1	Section 22.2.3
REQ-WS-FLPE-PAY-12	$1071\,\mathrm{kg}$	Compliant	Table 9.2	Section 24.2
REQ-WS-FLPE-PAY-13	-	Compliant	Table 12.1	Chapter 12
Aerobatics				
REQ-WS-FLPE-PAB-01	-	TBD	Table 9.5	-
Power				

Table 26.1 continued from previous page

Requirement ID	WS Value	Compliance	Origin	Result
REQ-WS-FLPE-POW-08	5000	Compliant	Table 16.1	Section 16.6
Structures				
REQ-WS-STRC-03	-	TBD	Table 10.1	-
REQ-WS-STRC-13	$4.4\,\mathrm{g}$	Compliant	Table 11.6	Section 11.4
REQ-WS-STRC-14	$-2.65\,\mathrm{g}$	Compliant	Table 11.6	Section 11.4
Reliability				
REQ-WS-RELI-01	-	TBD	Table 23.1	-
REQ-WS-RELI-02	8 weeks	Compliant	Table 23.1	Section 23.3
Regulations				
REQ-WS-REGS-01	-	Non-compliant	Table 9.5	Section 9.3
REQ-WS-REGS-03	-	Compliant	Table 9.5	Section 9.3
Sustainability				
REQ-WS-SUST-01	-	Compliant	Table 16.1	Chapter 16
REQ-WS-SUST-05	67%	Non-compliant	Table 10.1	Section 10.3
Comfort				
REQ-WS-COMF-01	-	TBD	Table 16.1	-

26.2. Feasibility Analysis

In this section the feasibility of the water sailplane design is analyzed, based on the compliance of the system requirements.

Non-Compliant Requirements

- **REQ-WS-WATO-13**: At this stage the take-off speed is slightly below the requirement of 1.2 times V_{stall}. However, the take-off distance is currently below the requirement of $400\,\mathrm{m}$ by quite a margin. This means the take-off speed could be increased to meet the requirement, while the take-off distance requirement would still be met.
- **REQ-WS-FLPE-AER-01**: The climb rate requirement of $4\,\mathrm{m\,s^{-1}}$ is not met by a very small margin. By optimizing the propellers for climb in a further design stage it could be possible to meet this requirement.
- **REQ-WS-FLPE-END-01**: Due to the drag being higher than initially estimated, the descent rate of the water sailplane ended up being less then ideal. Therefore the glide time requirement of 30 minutes was not met. However, the client wished to have a glide time of 15 minutes, so currently the design does exceed this expectation. As stated in Chapter 25, the descent rate has a high negative sensitivity to a further increase of drag and a decrease in lift. If the lift and drag characteristics of the water sailplane design turn out to be worse then currently estimated, the descent rate could further increase, and the glide time of the aircraft could become less than 15 minutes, which would lead to a failed design. So while there is still margin, the glide time could be a crucial parameter to determine the succes or failure of the water sailplane.
- **REQ-WS-REGS-01**: The CS22 regulations do not accommodate 3-seater sailplanes, as well as sea-planes that perform water operations. Therefore the water sailplane was non-compliant with this requirement from the start. However, these regulations were followed as much as possible for design aspect where they were applicable, mostly with regard to the saillane specific aspects.
- **REQ-WS-SUST-05**: From the end of life analysis in Section 10.3 it was determined only 67% of the total aircraft weight is recyclable, thus not complying to the requirement. However, in this analysis the re-purposing or recycling of components other than structural elements was not investigated. If these components are investigated further, it could be possible to meet the requirement of 80% of the aircraft being recyclable.

To Be Determined Requirements

- **REQ-WS-WATO-08:** In order to determine if the water sailplane would meet this requirement, the landing performance would have to be investigated.
- **REQ-WS-WATO-14:** Similar to the previous requirement, the landing performance would have to be investigated to determine the compliance of this requirement.
- **REQ-WS-WATO-16:** The exact height of the water sailplane metacentric height was not determined, and therefore the compliance to this requirement can not be determined. However, the equations used to size the floats in Chapter 14 were based on limits for hydrostatic stability, which the floats were shown to exceed. Therefore it is expected the water sailplane has sufficient hydrostatic stability, and thus GM > 0.
- **REQ-WS-FLPE-CON-06:** The controllability of the water sailplane was not investigated for the stall condition. It can thus not be concluded if the design is compliant to this requirement. Further investigation would determine this compliance.
- **REQ-WS-FLPE-PAB-01:** No analysis of aerobatic performance of the design was performed, therefore the compliance to this requirement can not be concluded. While it is expected that the water sailplane will be able to perform some simple aerobatic manouevers, like the lazy eight, further analysis is needed to determine this.
- **REQ-WS-STRC-03:** Although composites do not rust or corrode the corrosion resistance of carbon has not been investigated. Therefor the compliance of the requirement is to be determined.
- **REQ-WS-RELI-01:** Except for the battery no analysis of aircraft lifespan was performed, and it could not be concluded if the design is compliant without further investigation.
- **REQ-WS-COMF-01:** It is very difficult to determine the interior noise level of the cabin without acoustic testing, and since these tests could not be performed, it could not be concluded if the design was compliant to this requirement.

IV

Operations

27. Financial Analysis

To determine whether the detailed design is feasible in the broadest sense of the word, it is essential to analyze whether the found technical solution for the mission does so within the determined financial requirements of the client. This chapter provides a financial analysis of the costs to be considered for the product. This includes everything from the first line drawn on paper for the concept, to the final delivery to the client. Section 27.1 presents the financial requirements established with the client. A breakdown of all costs incurred is shown in Section 27.2. Based on these costs it is possible to calculate a return on investment and breakeven point, which can be seen in Section 27.3.

27.1. Financial Requirements

During client meetings, a list price and operational costs of the water sailplane were decided. These requirements and whether they comply will be presented below. Also the section where the results can be found can be seen in the last column.

Table 27.1: List of requirements relevant to cost

Identifier	Requirement	Compliance	Value	Section
REQ-WS-COST-01	The WS unit price shall be 400 000 $	Non-compliant	414 419 $	Chapter 27
REQ-WS-COST-02	The WS training package costs shall be 100 000 $	Compliant	961.7 $	Section 27.2.2
REQ-WS-COST-03	The WS operating cost shall be 25 000 $ per month	Non-compliant	41 493 $	Section 27.2.3

27.2. Cost Breakdown

The Life Cycle Cost (LCC) of an aircraft is broken down into three main components: the program cost - from research and development to production and certification - the fixed operational costs, and variable operational costs. This section presents the three components where the first is relevant for the return on investment for the manufacturer, and the latter two for the aircraft operator.

27.2.1. Program Costs

Estimating the cost of an aircraft program is inherently difficult as private corporations generally do not share this data. The most common method is the DAPCA IV model, which uses program cost data from the U.S. Department of Defense. The model splits the program cost into eight components: engineering, tooling, manufacturing labor, quality control, material cost, development support, flight test operations, and engine production. However the model has a clear caveat of overestimating costs for general aviation aircraft as it relies on data from military aircraft. Yet, modifications to the model exist that provide more accurate estimates for general aviation aircraft. For the financial analysis the Eastlake modification for a Cessna 172 was used [49].

A Cessna 172 is a comparable in empty weight to the aircraft being designed, making this set of Cost Estimation Relationships (CER) most suitable to estimate the aircraft's cost. The modification makes use of fudge factors applied to the tooling, manufacturing, quality control, and material costs. Equation (27.1) - 27.7 provides the list of CERs used:

$$H_E = 0.0396\, W_{af}^{0.791}\, V^{1.526}\, Q^{0.183} \tag{27.1}$$

$$H_T = 5.99\, W_{af}^{0.777}\, V^{0.696}\, Q^{0.263} \cdot 0.25 \tag{27.2}$$

$$H_M = 7.37\, W_{af}^{0.82}\, V^{0.484}\, Q^{0.641} \cdot 0.33 \tag{27.3}$$

$$C_Q = 0.13\, C_M \cdot 0.33 \tag{27.4}$$

$$C_D = 91.3\, W_{af}^{0.630}\, V^{1.3} \tag{27.5}$$

$$C_F = 1947\, W_{af}^{0.325}\, V^{0.822}\, FTA^{1.21} \tag{27.6}$$

$$C_M = 31.2\, W_{af}^{0.921}\, V^{0.621}\, Q^{0.799} \cdot 0.125 \tag{27.7}$$

Where W_{af} is the airframe weight (empty weight minus propulsion, furnishing, and avionics) in lbs, V the maximum velocity in kts, Q the number of aircraft produced in 5 years, and FTA the number of flight test aircraft. Note that the propulsion system cost is excluded as this is an off-the-shelf component with its price presented later in the section. Additionally the cost of avionics must be included. These typically cost $6000\,\$$ according to Gudmundsson [14].

Note that the first three equations provide an output of hours of work. Therefore to find the cost they must be multiplied by the hourly rates of workers for such activities. Typical hourly rates for engineering are $92\,\$/\mathrm{hr}$, $61\,\$/\mathrm{hr}$ for tooling, and $53\,\$/\mathrm{hr}$ for manufacturing labor in June 2012 [14]. The hourly rates were adjusted with the Consumer Price Index (CPI) of 2021 with respect to 2012, resulting in an increase of rates by 1.21:[1]

Table 27.2: Inflation adjusted hourly rates for December 2021

Job	Symbol	Hourly rate
Engineer	R_E	$110.4\,\$/\mathrm{hr}$
Tooling labor	R_T	$73.2\,\$/\mathrm{hr}$
Manufacturing labor	R_M	$63.6\,\$/\mathrm{hr}$

The cost breakdown of these seven components are presented in in Table 27.3. Note that the costs are split between fixed and variable costs. Fixed costs consist of engineering, development support, flight test operations, and tooling costs. Variable costs consist of manufacturing labor, quality control, and material cost. It is assumed that 60 aircraft can be produced in 5 years, as determined by the Market Analysis:

Table 27.3: Program costs of SPEAR for 60 aircraft produced in 5 years

Activity	Total cost $	Cost per unit $
Engineering	3 360 720	56 012
Tooling labor	2 097 657	34 961
Development support	3 653 300	60 888
Flight test and certification	5 042 203	84 037
Total fixed costs:	14 153 879	235 898
Manufacturing labor	6 925 525	115 425
Material costs	1 301 074	21 685
Quality control	303 961	5066
Total variable costs:	8 530 561	142 176
Total costs:	18 663 131	378 074

Note that Table 27.3 does not include the costs of the propulsion group, the avionics, and pilot training in the cost per unit. Pilot training was agreed to be included within the list price of the aircraft in a client meeting. These will be presented in the subsection below. Additionally, given that the CERs account for the learning curve effect - where the cost per unit aircraft decreases as the number of aircraft produced increases - the

[1] https://www.bls.gov/data/inflation_calculator.htm [Accessed: 17 Jan 2022]

number of aircraft produced in five years is optimized to achieve the required list price. This is also presented later in the section.

27.2.2. Propulsion Group, Avionics, and Pilot Training Costs

As the propulsion group and avionics are bought as off-the-shelf components they contribute a fixed cost per unit aircraft. As mentioned previously in the section, the cost of avionics was assumed to be $6000\,\$$. Pilot training is also assumed to be such a fixed cost, where one pilot is trained per unit aircraft produced. It will be assumed that there is no learning curve for these cost contributions.

The cost of the propulsion and power group consist of the propeller group, motor group, battery group, and charger. The propeller group consists of the following elements: the propeller itself, the spinner, and the mounting plate. The cost of a two blade composite propeller with a diameter of $1.6\,\mathrm{m}$ was found to be $1891\,\$$. The costs of a spinner and mounting blade with the appropriate radii, from the same manufacturer, cost $367\,\$$ and $235\,\$$ respectively.[2] The motor group consist of the electric motor and its controller. The motor selected in Chapter 16, is commercially available and can be bought for a price of $13.700\,\$$.[3] The battery group consist of a battery pack that includes a battery controller. Contact regarding the list price with the manufacturer of the battery group was initiated, however no response was received. Hence, an estimate is made by comparing the price of battery packs with similar energy storage levels as the selected battery is chosen. The price of Pipistrel's battery packs, used in their electric self launching gliders, are $11.480\,\$$ for the battery pack with an energy storage of $30\,\mathrm{kWh}$.[4] For an indication of the charger price that would be congruent with the selected battery, the charger of the same manufacturer as the battery group used. The charger can be found online for a list price of $1710\,\$$.[5] Note that, the cost of power generation machines has not been included in the cost analysis. As it is expected that the aircraft will only be operable at locations where a power grid already exists.

For the calculation of the training cost it is assumed that all pilots that will be trained for use of the water sailplane already have acquired a commercial pilot license. In discussion with the client it was determined that 3 days of 6 hours of transition training would be required given the design footprint of the sailplane to the Twin Otter. An additional day is allocated to train the pilot in basic maintenance. The cost breakdown of the training therefore consists of: pilot and instructor salary for the duration of training, and the operational cost of the aircraft during the training. A pilot and instructor salary in the Maldives was estimated at $14\,\$$ per hour, and confirmed to be a reasonable estimate by the client. Operational costs are the electricity and maintenance costs for the training time (detailed explanation of how these were calculated are presented in Section 27.2.3). This provided the following costs:

$$\text{Training cost} = n_{hours}(S_{pilot} + S_{instructor}) + C_{op} = 32 \cdot 28 + 65.7 = 961.7 \tag{27.8}$$

A summary of all additional costs per unit aircraft is provided in Table 27.4:

Table 27.4: Additional fixed costs per unit

Component	**Cost** $
Propeller	1891
Spinner	367
Mounting blade	235
Motor	13 700
Battery packs	11 480
Charger	1710
Avionics	6000
Pilot training	961.7
Total additional costs:	36 345

[2] http://www.duc-helices.com/produit.php?id_produit=130&id_rubrique=37 [Accessed: 16 Jan 2022]
[3] https://www.aeroexpo.online/prod/mgm-compro/product-171210-63386.html [Accessed: 15 Jan 2022]
[4] https://sustainableskies.org/total-operating-costs-batteries-included/ [Accessed: 15 Jan 2022]
[5] https://www.aeroexpo.online/prod/mgm-compro/product-171210-35264.html [Accessed: 16 Jan 2022]

Adding the additional costs per unit of the aircraft to the program costs per unit results in a total cost per unit of $414\,419\,\$$. All costs of the aircraft are visualized in the cost breakdown structure presented in Figure 27.1:

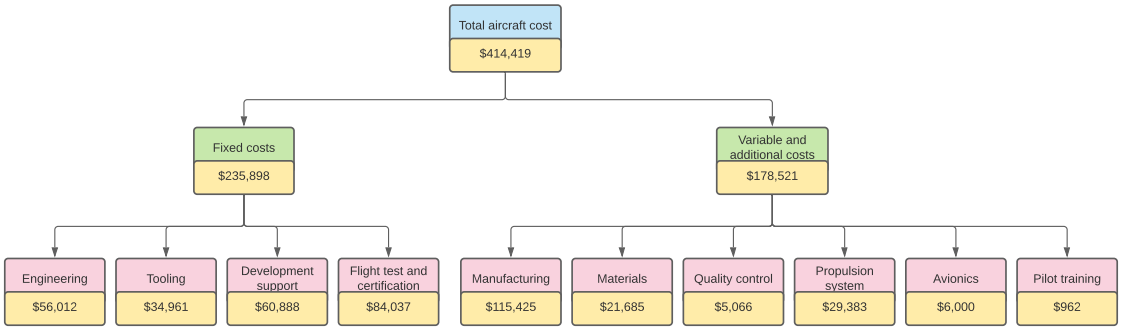

Figure 27.1: Cost breakdown structure per aircraft

27.2.3. Operational Costs

Operational costs are the costs of ownership of the aircraft, and therefore only relevant for the client. Those considered from what could be reasonably estimated were maintenance and inspection, electricity, crew, insurance, and loan payment costs.

Maintenance costs of the aircraft are estimated with a method from Gudmundsson [14]. It is an equation depending on three variables: the ratio of maintenance work hours to flight hours, the hourly rate of a mechanic, and the number of flight hours per year. Typically ratios of maintenance work hours to flight hours is 0.3. Assuming that the aircraft flies three times per day with a flight duration of 30 minutes and is only serviced half of the year, given that this is the duration of the tourist season, the aircraft has 274 flight hours per year. A mechanic in the Maldives was estimated to earn $1\,\$$ per hour, an estimate confirmed by the client, resulting in an annual maintenance cost of $82.2\,\$$.

In addition to the maintenance costs there are daily inspection and operation costs. This consists of pumping water from the floats and washing the aircraft down to remove algae and salt residue. It is estimated that this occurs once a day and occurs every day of the year, and requires an hour of work. With the same salary estimate this results in an inspection cost of $578\,\$$, totaling inspection and maintenance to $660.2\,\$$ per year.

Given that the aircraft is electric the fuel costs derive by the price of electricity in the Maldives. This costs around 40 US$ cents per kilo Watt-hour [50]. With the mission profile specified in Section 9.1, a total energy of $17.13\,\mathrm{kWh}$ as determined in Section 16.6 was required to perform one flight. With 548 annual flights this results in an estimated electricity cost of $3755\,\$$.

The cost of crew is determined by taking considering the amount of time the crew is required to operate the aircraft for a mission by the hourly salary of a pilot. It was assumed that along with the 30 minute mission profile the pilot spends an additional 30 minutes to perform flight checks and inspections after the flight. The hourly wage was estimated to be $14\,\$$ per hour, a value confirmed by the client to be reasonable. Therefore the crew cost is $8092\,\$$ per year.

Annual insurance costs of the aircraft are estimated by the following equation [14]:

$$C_{INS} = 500 + 0.015\ C_{AC} \tag{27.9}$$

Where C_{AC} is amounts to the purchase price of the aircraft. The purchase price of the aircraft was assumed to be the list price by the client, $500\,000\,\$$. With this, the annual insurance cost of the aircraft are estimated at $8000\,\$$ per year.

The final cost considered is the annual loan payment for an aircraft. Typical down payment percentages of an aircraft price are $15\,\%$, with a loan duration of 20 years at $5.15\,\%$ interest.[6] Given the aircraft list price of $500\,000\,\$$ the principle loan amount is $425\,000\,\$$. As a result annual loan payments are estimated with the following equation:

$$C_{loan} = \frac{12\ P_i}{1 - 1/(1+i)^n} \tag{27.10}$$

Where P_i is the principle amount, i the interest rate, and n the number of pay periods in months. This results in an annual loan cost of $21\,887\,\$$. A summary of all operational costs is provided in Table 27.5:

[6] https://finance.aopa.org/resources/2016/july/12/sample-aircraft-loan-rates [Accessed: 18 Jan 2022]

Table 27.5: Summary of operational costs

Operation	Cost $
Maintenance and inspection	660.2
Electricity	3755
Crew	8092
Insurance	8000
Loan payments	21 887
Total costs:	41 493

27.3. Breakeven Point and Return on Investment

Following the cost breakdown for the aircraft manufacturer the breakeven point and return on investment may be determined. The breakeven point is the number of aircraft required to be produced in five years such that the total production costs equal the list price cost. The breakeven point was determined by plotting the production cost per unit aircraft with respect to the number of aircraft produced and the list price. The intersection of this curve indicates the number of aircraft required to produce for breakeven. Figure 27.2 presents the respective curves and the breakeven point:

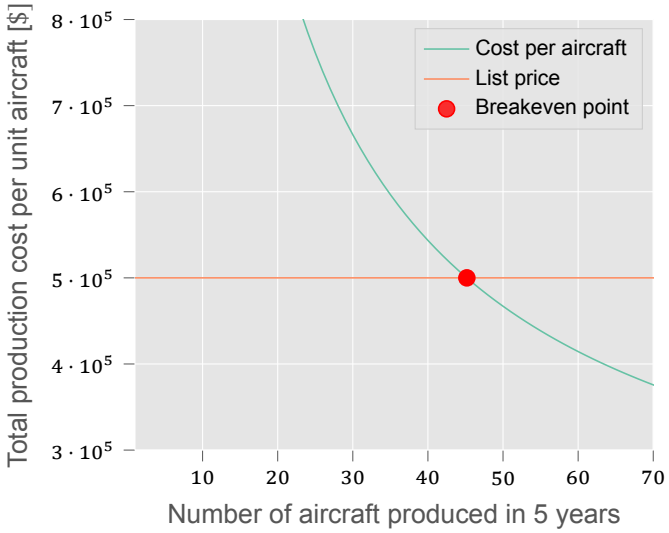

Figure 27.2: Breakeven point of aircraft production with a list price of 500 000 $

Rounding up, the project requires 42 aircraft to be produced over 5 years to reach a breakeven point. Following the market analysis it was determined that 20 amount of aircraft could be sold to the market in the Maldives. Assuming this could be replicated in two other markets, such as the United Arab Emirates and Caribbean a total of 60 aircraft could be sold. Given this amount, the cost of production per unit becomes 414 419 $, including the additional cost of the propulsion system and pilot training, providing a net profit of 85 581 $ per aircraft. The return of investment in this situation is calculated with:

$$\text{ROI} = \frac{\text{Total program revenue} - \text{Total program cost}}{\text{Total program cost}} 100 = 17\,\% \tag{27.11}$$

27.4. List Price Scenarios

The list price of the aircraft varies with respect to when the client wishes to receive the aircraft, how many he wishes over a spread amount of time, and the financing of payments. The financing of payments referring to whether all costs are paid up front, or if they are amortized. In a discussion with the client three scenarios for the purchase of 20 aircraft were demanded so that they could make a decision on what was most preferable to them:

1. Immediate delivery of all all 20 aircraft after the lead time of engineering design and certification hours, with immediate payment.
2. Delivery of 10 aircraft after the lead time of engineering design and certification hours with the other 10 aircraft delivered over the production time after the initial 10. Lease construction of $50\,\%$ upfront, and the remaining $50\,\%$ paid over the lead time of the whole order until the final aircraft.
3. Delivery of 10 aircraft after lead time of engineering and certification hours, with the other 10 aircraft delivered over the production time after the initial 10. Lease construction of $50\,\%$ up front and the remaining $50\,\%$ paid over the lead time of the whole order until the final aircraft. However TMA has exclusive rights for 3 years, forbidding the manufacturer to sell to another customer in this time.

Cost estimations from the manufacturer side were completed in the same manner as presented in Section 27.2.1. It was assumed that 60 aircraft would be produced in 5 years time, and that all development phases have been completed. This meant that only the lead time of production remained. Further, it was assumed that one factory could produced an aircraft per month, or 10 per year with vacation days accounted for. Scaling of an additional factory would be assumed to double the variable costs. Finally, it was also assumed that a $10\,\%$ profit margin is included in the list price. This provided the following results:

- **Scenario 1:** Variable costs double, resulting in a cost of production price of $612\,000\,\$$ per aircraft, or $12.2\,\$$ million for the whole order.
- **Scenario 2:** Cost of production per aircraft is $456\,000\,\$$. Therefore there is an upfront payment of $4.56\,\$$ million, with monthly payments of $200\,000\,\$$. The lease is assumed to have a duration of 24 months, with an interest rate of $5\,\%$ over the principle of $4.56\,\$$ million. Contract breakdown cost is $468\,000\,\$$ per aircraft.
- **Scenario 3:** If the aircraft cannot be sold for three years results in an opportunity cost of 30 aircraft not being able to be sold. This is a dollar amount of $13.7\,\$$ million and is paid $50\,\%$ up front, and $50\,\%$ over the 24 month loan. Cost of aircraft production per aircraft is $456\,000\,\$$, meaning that the total upfront payment is $11.41\,\$$ million. Lease with $5\,\%$ interest of principle of $11.41\,\$$ million results in monthly payments of $500\,000\,\$$. Contract breakdown cost is $1.17\,\$$ per aircraft.

Having presented the list price scenarios to the client, they agreed to the first option with renewal every year for five years to keep increasing the fleet size. Additionally there would be five year exclusivity rights as the orders are filled in this time by TMA.

28. Operations and Logistics

This chapter describes how the concept would fit into the current infrastructure of the Maldives. The following three phases is elaborated upon in this section: pre-flight, flight, and post-flight phase, in respectively Section 28.1, Section 28.2 and Section 28.3. These are also visualized in Figure 28.1.

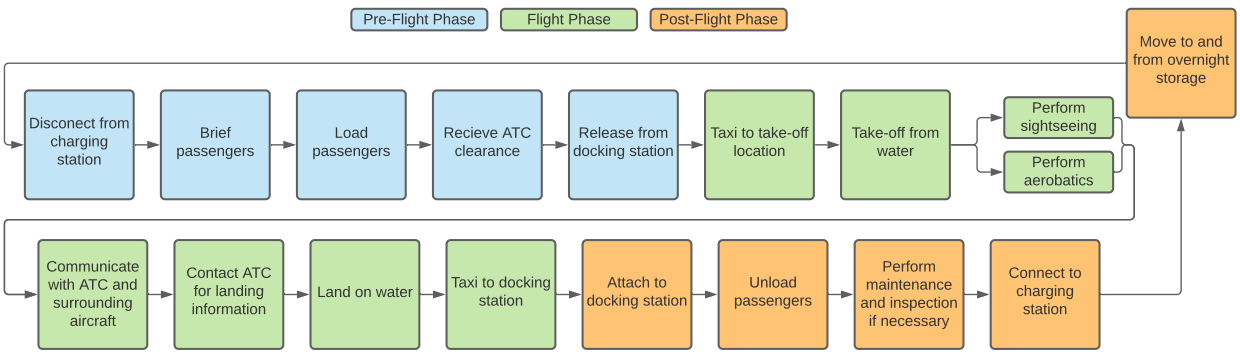

Figure 28.1: Operations and Logistics flow diagram

28.1. Pre-Flight Phase

The pre-flight phase covers all the operations that need to be performed before the actual mission can start. These operations are described in this section.

- **Disconnect from Charging Station:** Since the water sailplane operates on electrical energy stored in batteries, it is required to install a charging infrastructure. Section 16.1.3 described that the charging of the aircraft could be done without the aircraft leaving the water, minimizing the downtime. For safety purpose, the charger should be disconnected before the passengers enter the aircraft. Before disconnecting the charger, the battery level should be checked to make sure they are charged enough to perform its mission.
- **Passenger Briefing:** Before the passengers enter the aircraft, they should be thoroughly briefed about the mission, what can be expected and the most relevant safety procedures. An additional briefing should be held if the mission includes aerobatics. The passengers can be briefed while the airplane is still charging. After the briefing is completed, the pilot and passengers can move to the aircraft and the charger is disconnected.
- **Board Passengers:** Once seated, the passengers will be checked on proper fastening of their seat belts and whether they are comfortable. Thereafter, the last briefing will be held. The pilot will then get seated and perform the pre-flight checks, after which the canopy will be closed.
- **Receive Air Traffic Control Clearance:** The pilot will communicate with the ATC to receive clearance to taxi to the take-off location and to take-off.
- **Release from Docking Station:** When the clearance is granted, the aircraft can be released from its docking station and start its mission.

28.2. Flight Phase

The flight phase includes all operations during the actual mission. These are described below:

- **Taxi to Take-Off Location:** Once the aircraft is released from its docking station, it can begin to taxi to the take-off location. After arriving at the take-off location, the aircraft must be lined up correctly for take-off. The water sailplanes engine will be used to propel the aircraft during taxiing.
- **Take-Off from Water:** The pilot will gradually increase the thrust setting to accelerate and take-off. After lift-off, the pilot will fly at the speed and attitude for optimal climb until the desired altitude is reached. The motor will then be turned off and the gliding phase can begin.
- **Perform Sightseeing:** If the mission is to perform sightseeing, the pilot will fly with the minimum rate of decent to optimally let the passengers enjoy the experience. The pilot will regularly check whether the passengers are still comfortable.
- **Perform Aerobatics:** If the mission is to perform aerobatics, the pilot will fly the designed aerobatic maneuvers. Especially during aerobatics, the conditions of the passengers must be monitored by the pilot.
- **Communicate with ATC and Surrounding Aircraft:** During the entire flying phase, the pilot will keep in touch with the ATC and other surrounding aircraft if necessary.
- **Contact ATC for Landing Information:** As soon as the flight comes to an end, the pilot will inform the ATC when he will initiate the landing procedures. Information will be requested on the most recent weather conditions.
- **Land on Water:** The pilot will set the aircraft to landing configuration and land the aircraft as safely and comfortably as possible.
- **Taxi to Docking Station:** After landing the pilot shall start the engine again and taxi to the docking station.

28.3. Post-Flight Phase

The flight phase covers all operations during the post-flight phase. These are described below.

- **Attach to Docking Station:** After taxiing to the docking station, the water sailplane will be re-attached to it.
- **Unboard Passengers:** The canopy will be opened up and the pilot will leave the aircraft firstly. He will then assist the passengers while getting out of the plane.

- **Perform Maintenance and Inspection:** If necessary, maintenance and inspection shall be performed on the aircraft. The maintenance was elaborated upon in more detail in Section 23.3.
- **Connect to Charging Station:** After docking and possibly maintenace and inspection, the aircraft shall be re-connected to the charger, so that a new mission can start with full batteries.
- **Overnight Storage:**At night, the aircraft will be moved to its overnight storage location. In the morning, the aircraft will be moved back from the storage location to the docking station. After this, the operation will start again at the beginning of the pre-flight phase, and the cycle is complete.

29. Project Development Logic

The Project Design & Development Logic (PD&D) shows all steps that need to be taken in the post-DSE phase in a logical order. This concerns a more detailed design phase and certification, to the final production and sales of the aircraft. A visualization of the PD&D is given in Figure 29.1:

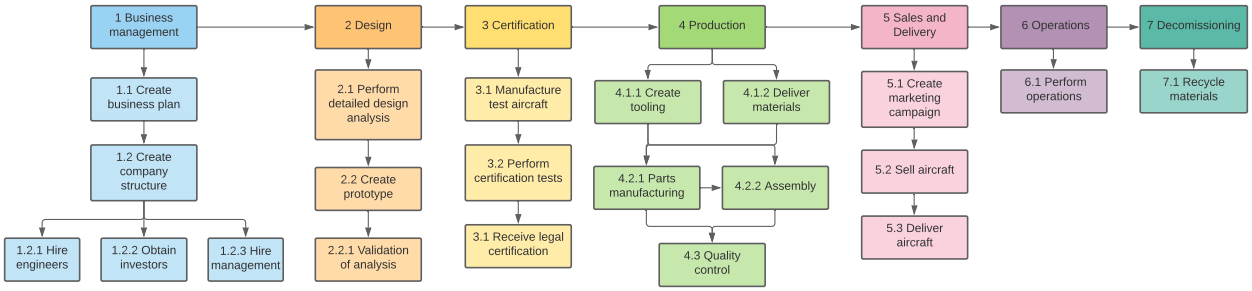

Figure 29.1: Project Design & Development Logic flow diagram

The PD&D diagram shows that there are seven main steps following the post-DSE phase. They will be touched upon in brief below, describing more detail on the activities then what is present in the diagrams. Figure 29.2 displays the Post-DSE Gantt Chart corresponding to Figure 29.1

Business Management Phase

During the business management phase a detailed business plan would be made to evaluate the definitive reasoning why the product is necessary. In this step a more detailed market analysis would be performed, which could include activities such as interviewing tourists in the Maldives to determine the enthusiasm for such a product. Following this, a company structure would be determined and the first set of personnel hired. As the phases following the business phase require large sums of money, as presented in the Chapter 27, investors should be attracted. Once funding is sorted, the design phase can begin.

Design Phase

The hired engineers would work on the design phase, engaging in more detail than what was presented in this report. Examples of such activities would include wind tunnel tests of a prototype to determine more precise aerodynamic characteristics. Structural detail would increase as well in this phase, to the final point of designing the location and size of every bolt and rivet. In preparation for the following step of certification, where test aircraft are manufactured, manufacturing tools and assembly jigs are designed. All design decisions are made with respect to the certification requirements set by the relevant legal body.

Certification Phase

Prior to certifying the aircraft, a number of test aircraft must be manufactured. Multiple are necessary, as in certain tests such as the wing loading the aircraft is tested until destruction. Structural tests are the first to be completed in order to receive clearance for the first test flight. Once received, numerous hours of flight testing are performed to demonstrate that the necessary maneuvers, flight speeds, and altitudes are reachable. Flight tests also demonstrate the fatigue limit of the aircraft. With the completion of all tests to the level required, a legal airworthiness certificate is given to the aircraft, allowing it to be replicated in a scaled production phase and sold to customers.

Production Phase

Having designed the tooling during the design phase, they are now manufactured. As the sailplane is largely made of composites examples of such tooling are molds and machinery to trim parts. This is done alongside the delivery of raw material that is processed by the tooling. Part manufacturing can begin, and alongside this the assembly of sub-assemblies. Orders for the off-the-shelf components, such as the propulsion unit and avionics, must also be placed that they arrive on time for the final assembly. During the entire production phase quality control checks are completed.

Sales and Delivery Phase

Sales and marketing occurs at the same time as the production phase to avoid the loss of capital of a complete aircraft waiting in storage prior to being sold. Orders are placed by customers, and financing agreements are set in place. Following the completion of the product it may be delivered to the eventual customer. In the delivery phase ground checks are completed, which includes activities such as painting the aircraft in the livery desired by the client. Once all final checks are completed, the aircraft is ready to enter the operational phase.

Operations and Decommissioning phase

Upon delivery, the aircraft is ready for operation. From the customer side additional steps are required beforehand, such as training the pilots to fly the water sailplane. More specific details of operations have already been described in Chapter 28. Once the aircraft has completed its lifetime it is decommissioned. During this phase the aircraft is deconstructed, and recyclable materials sorted and sent to the relevant recycling plants.

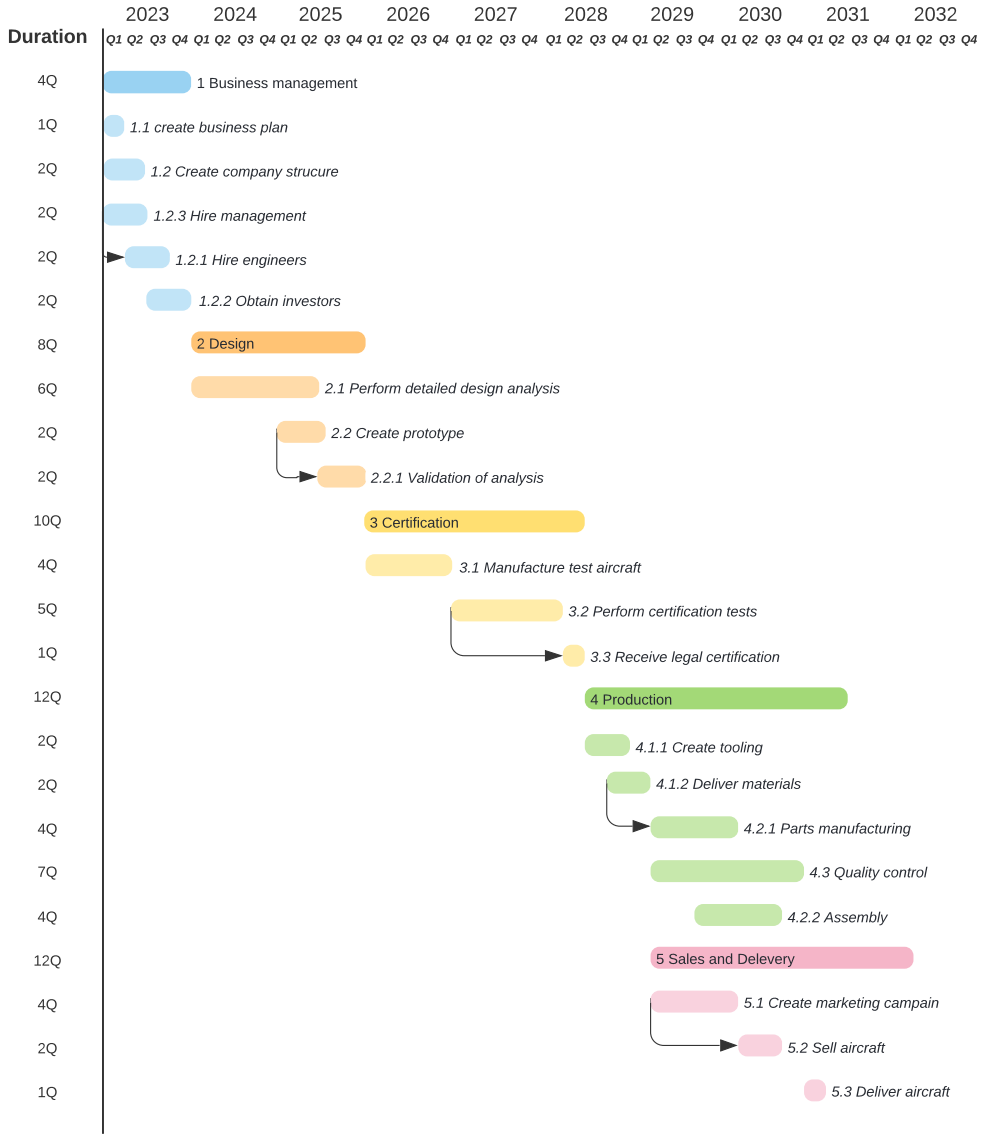

Figure 29.2: Gantt Chart of post-DSE activities

30. Conclusion

The team was tasked by Trans Maldivian Airways to investigate the possibility of designing a water sailplane that could provide tourists scenic flights of the islands and resorts of the Maldives. This task was formulated in the following Mission Need Statement:

Conceptualize and design a sustainable, emission-free sailplane capable of taking off from and landing on water.

Applying knowledge and tools obtained during the Bachelor program of Aerospace Engineering at the Delft University of Technology, the team investigated whether it would be possible to design such a water sailplane, and analyzed what its performance characteristics would be, given certain design requirements. When necessary, experts were consulted to extend the team's knowledge on the design aspects of a water sailplane. The results of this investigation were presented in this report.

It was concluded that, on a conceptual level, it would be possible to design a sailplane fulfilling the Mission Need Statement. While the performance estimated resulted in a performance below the expected standard, it was determined that a water sailplane would still provide adequate performance of gliding scenic flights, with a glide time exceeding 15 minutes per flight, while conforming relevant EASA CS22 and CS23 regulation specifications.

This conclusion comes with certain limitations however. As the water sailplane that was designed was still only a conceptual design, there is an uncertainty present in the results from the analysis, arising from the limitations of the design tools and methods used in this stage of design. From a sensitivity and feasibility analysis it was determined that small changes lift and drag characteristics have a big impact on gliding performance, and are thus crucial aspects that could severely limit the performance of a water sailplane.

Further investigation and design is therefore needed to more accurately determine what the performance would be of a water sailplane, in order to establish whether this would be a viable product to be used by Trans Maldivian Airways to offer tourists emission-free scenic flights of the Maldives. Recommendations by the team on where the focus of a further investigation and design of a water sailplane should lie are given in the next section.

31. Recommendations

To improve the design of a water sailplane, several recommendations are given below. They are based on the deficiencies of the current analyses.

Stall Behavior

Throughout the analysis, the stall characteristics of the aircraft were not thoroughly assessed. The stall behavior assumed steady symmetric flight assumptions and thus the condition that lift equals weight. This analysis is rudimentary at best. The effect of flow separation is not taken into account with regards to the drag analysis and this has knock-on effects on the performance analysis casting doubt over the validity of the results [46]. Furthermore, the aerodynamic behavior of stall different based on entry rate and aircraft configuration and is quite unpredictable regarding main wing-empennage interactions [11]. Therefore, it is recommended to further investigate the stall behavior of the aircraft on an aerodynamic basis, as well as on a controllability front, to better predict the aircraft's performance.

Contamination of surfaces

Although the airfoil of the main wing was chosen such that the influence of contamination was limited, the influence of contamination has not been taken into account during the aerodynamic analysis. Contamination on the main wing is expected to mostly influence the drag and lift characteristics. The effect on airflow separation due to a contaminated wing should also be investigated in more detail. The contamination of the other surfaces will mainly influence the drag of the aircraft. From the sensitivity analysis in Chapter 25, it showed that the

performance is very sensitive to an increase in drag. This justifies the recommendation to investigate the effect of contamination. At last, it is unknown how contamination would effect the stability and controllability of the aircraft. Therefore, this should also be analyzed in more detail.

Rough water conditions

One of the aspects that was not investigated in the design of the water sailplane was the impact of rough water conditions on the take-off & landing performance. During several meetings with the client it was mentioned that the water conditions are never perfect, and that in the recent decade the weather has proved to be volatile at times, resulting in weather conditions changing from calm to stormy in a matter of minutes. Therefore the client expressed the wish for the water sailplane to be able to land in changed conditions to a certain limit. While a rough estimate of the wave height was possible in the conceptual design stage, a further investigation of the landing limits of the water sailplane, would therefore be necessary.

Furthermore, the take-off performance of the water sailplane was only analyzed for smooth water conditions. Since the water in the Maldives is practically never smooth, the impact of rough water conditions on the take-off time and distance would have to be analyzed, in order to determine the operational capabilities and limits of the water sailplane.

Optimization of float design

A crucial aspect of the water sailplane are the floats. The floats were designed to provide adequate buoyancy and hydrostatic stability, as described in Chapter 14. Next to this, minimization of both aerodynamic drag and hydrodynamic resistance are paramount to achieve optimal performance of the water sailplane. The analyses of both characteristics were very limited in the conceptual design stage however, and thus a more detailed analysis of both the aero- and hydrodynamic characteristics would be necessary, in order to optimize the size and shape of the floats for performance.

Next to this, further structural analyses on the floats and the struts connecting these to the fuselage would be necessary to determine the overall safety of the water sailplane. The client has expressed that safety of customers is of high priority for a sailplane flying around tourists, as well as high reliability. Through more detailed structural analyses of critical scenarios, like emergancy landings and accidents, the limits of structural integrity of the water sailplane could be determined, and therefore its safety limits.

Detailed optimization of propeller design

The design of the propeller and accompanying propulsion and power subsystems were designed using basic approximations and empirical formulas. This only yielded a propeller diameter with an assumed thrust behavior. More in-depth design methods such as Finite Blade Element Theory could be used in future to provide more detailed sizing and characteristics of the propeller design, providing pitch angle and thereby a more accurate approximation for the efficiency and generated thrust. This would also make performance calculations such as take-off and climb performance more reliable. Furthermore, optimization of the propeller could be done due to the unconventional operations of the water sailplane. As only take-off and climb are the powered flight phases, the propeller should be optimized for these phases and not for cruise, which the empirical methods used in Chapter 16 make use of.

In addition, the interaction of the propeller with the empennage and the effect of this on controllability could be further analyzed to assess the impact on controllability and take-off procedures. The current design does not factor the imbalance of airflow over the horizontal stabilizer and how the local differences in dynamic pressure may affect the controllability. Therefore, it is advised to go into more detail with regards to the propeller design and optimizing the integrated design aspects with regards to the current placement on the empennage.

Aerobatic performance

One of the requirements of the customer was that the aircraft shall be able to perform aerobatic maneuvers. The aerobatic performance has not yet been analyzed at this stage of the design. Therefore it is currently unknown whether the aircraft is capable of performing any aerobatic maneuvers. To meet the requirements, a performance analysis on the aerodynamic capabilities must be made.

Bibliography

[1] A. M. Didi, I. Nizam, and S. Hamza, *The determinants of customer satisfaction and the intention to return: A study on tourism sector of maldives,* International Journal of Accounting and Business Management 4 (2016), 10.24924/ijabm/2016.11/v4.iss2/179.205.

[2] R. Stojanov, B. Duží, D. Němec, and D. Procházka, *Slow Onset Climate Change Impacts in Maldives and Population Movement from Islanders' Perspective Brain*, KNOMAD Working Paper 20 (KNOMAD, 2017).

[3] *Certification Specifications, Acceptable Means of Compliance and Guidance Material for Sailplanes and Powered Sailplanes (CS-22)*, European Union Aviation Safety Agency (EASA), Köln, Germany (2021), Amendment 3.

[4] *Certification Specifications for Normal, Utility, Aerobatic, and Commuter Category Aeroplanes (CS-23)*, European Union Aviation Safety Agency (EASA), Brussels, Belgium (2003), Amendment 3.

[5] S. R. Hirshorn, *System design processes,* in *NASA Systems Engineering Handbook* (Books Express Publishing, 2017) Chap. 4, 2nd ed.

[6] M. S. Reed, A. Graves, N. Dandy, H. Posthumus, K. Hubacek, J. Morris, C. Prell, C. H. Quinn, and L. C. Stringer, *Who's in and why? A typology of stakeholder analysis methods for natural resource management,* Journal of Environmental Management 90, 1993 (2009).

[7] P. N. Albert, S. L. J. de Vries, D. A. Hartong, J. P. Q. Hoyng, A. C. C. van den Heiligenberg, J. J. A. van der Toorn, and W. R. Verbeek, *Midterm Report*, Tech. Rep. (TU Delft, Delft, South Holland, Netherlands, 2021) unpublished.

[8] R. F. Aziz and S. M. Hafez, *Applying lean thinking in construction and performance improvement,* Alexandria Engineering Journal **52(4)**, 679 (2013).

[9] P. Kench, R. Brander, K. Parnell, and J. O'Callaghan, *Seasonal variations in wave characteristics around a coral reef island, South Maalhosmadulu atoll, Maldives,* Marine Geology **262(1)**, 116 (2009).

[10] J. Roskam, *Preliminary Sizing of Airplanes*, 1st ed., Airplane Design Part 1 (DARcorporation, Lawrence, Kansas, U.S.A., 1986).

[11] G. J. J. Ruijgrok, *Elements of airplane performance*, 2nd ed. (Delft Academic Press, Delft, The Netherlands, 2009).

[12] B. Mees, *Notes of a Seaplane Instructor: An Instructional Guide to Seaplane Flying*, 2nd ed. (Aviation Supplies & Academics, Inc., 2005).

[13] D. P. Raymer, *Aircraft Design: A Conceptual Approach*, 6th ed. (American Institute of Aeronautics and Astronautics, Reston, V.A., U.S.A., 2018).

[14] S. Gudmundsson, *General Aviation Aircraft Design: Applied Methods and Procedures*, 2nd ed. (Butterworth-Heinemann, Oxford, U.K., 2021).

[15] M. D. Maughmer, *The evolution of sailplane wing design,* AIAA International Air and Space Symposium and Exposition: The Next 100 Years (2003), 10.2514/6.2003-2777.

[16] M. Kutz and C. Zweben, *Composite materials,* in *Mechanical Engineers' Handbook, Volume 1: Materials and Engineering Mechanics, 4th Edition*, Vol. 1 (Wiley, 2015) Chap. 10, 4th ed.

[17] D. Plappert, G. C. Ganzenmüller, M. May, and S. Beisel, *Mechanical properties of a unidirectional basalt-fiber/epoxy composite,* Journal of Composites Science **4(3)** (2020), 10.3390/jcs4030101.

[18] M. F. Ashby, *Materials Selection in Mechanical Design*, 2nd ed., Vol. 2 (Butterworth-Heinemann, 1999).

[19] A. Rahimizadeh, J. Kalman, K. Fayazbakhsh, and L. Lessard, *Recycling of fiberglass wind turbine blades into reinforced filaments for use in additive manufacturing,* Composites Part B: Engineering 175 (2019).

[20] A. Dehghan, K. Peterson, and A. Shvarzman, *Recycled glass fiber reinforced polymer additions to portland cement concrete,* Construction and Building Materials 146, 238 (2017).

[21] H. Sun, G. Guo, S. A. Memon, W. Xu, Q. Zhang, J.-H. Zhu, and F. Xing, *Recycling of carbon fibers from carbon fiber reinforced polymer using electrochemical method,* Composites Part A: Applied Science and Manufacturing 78, 10 (2015).

[22] A. K. Bledzki, H. Seidlitz, J. Krenz, K. Goracy, M. Urbaniak, and J. J. Rösch, *Recycling of carbon fiber reinforced composite polymers—review—part 2: Recovery and application of recycled carbon fibers,* Polymers **12(12)** (2020).

[23] L. M. Nicolai and G. E. Carichner, *Fundamentals of Aircraft and Airship Design, Volume I - Aircraft Design*, Vol. 1 (American Institute of Aeronautics and Astronautics (AIAA), 2010).

[24] F. Thomas, *Fundamentals of Sailplane Design*, 3rd ed., edited by J. Milgram (College Park Press, College Park, M.D., U.S.A., 1999).

[25] J. G. Lowry and E. C. Polhamus, *A Method For Predicting Lift Increments Due To Flap Deflection At Low Angles Of Attack In Incompressible Flow*, Tech. Rep. Technical Note 3911 (National Advisory Committee for Aeronautics, Langley, Va., United States of America, 1957).

[26] R. D. Finck, *USAF stability and control DATCOM*, Tech. Rep. AFWAL-TR-83-3048 (Air Force Wright Aeronautical Laboratories, Wright-Patterson AFB, O.H., U.S.A., 1978).

[27] R. Eppler, *The effect of disturbances on a wing,* in *Science and Technology of Low Speed and Motorless Flight* (National Aeronautics and Space Administration, Hampton, Virginia, United States of America, 1979) Chap. 4, 1st ed.

[28] G. A. Flandro, H. M. McMahon, and R. L. Roach, *Basic Aerodynamics: Incompressible Flow*, Cambridge Aerospace Series (Cambridge University Press, 2011).

[29] J. Ainsworth, C. Collier, P. Yarrington, R. Lucking, and J. Locke, *Airframe wingbox preliminary design and weight prediction,* (2010).

[30] J. Roskam, *Preliminary Configuration Design and Integration of the Propulsion System*, 1st ed., Airplane Design Part 2 (DARcorporation, Lawrence, Kansas, U.S.A., 1986).

[31] D. Scholz, *Empennage general design,* in *Aircraft Design* (Hamburg Open Online University, 2016) Chap. 9.

[32] E. Torenbeek, *Synthesis of Subsonic Airplane Design: An introduction to the preliminary design of subsonic general aviation and transport aircraft, with emphasis on layout, aerodynamic design, propulsion and performance* (Springer Netherlands, Dordrecht, Netherlands, 1982).

[33] E. Garcia, A. van Nispen, and R. Slingerland, *Downwash at the tail of swept-wing transports with high-lift devices,* in *1st AIAA, Aircraft, Technology Integration, and Operations Forum*, AIAA20015237 (Los Angeles, C.A., U.S.A., 2001).

[34] W. Nelson, *Seaplane Design*, 1st ed. (McGraw-Hill Book Company, Inc., New York, N.Y., U.S.A., 1934).

[35] J. Frey, *How to fly floats*, 21st ed. (Kenmore Air EDO Floats L.L.C., Kenmore, USA, 2005).

[36] W. Diehl, *Static stability of seaplane floats and hulls,* (1924).

[37] M. Langley, *Seaplane Float & Hull Design* (Sir Isaac Pitman & Sons, Ltd., London, United Kingdom, 1935).

[38] *SPECIAL CONDITION, Water Load Conditions*, European Union Aviation Safety Agency (EASA) (2009), 03 (Structure).

[39] S. F. Hoerner, *Fluid-Dynamic Drag*, 1st ed. (Hoerner Fluid Dynamics, United States of America, 1965).

[40] S. Sripad, A. Bills, and V. Viswanathan, *A review of safety considerations for batteries in aircraft with electric propulsion,* MRS Bulletin 46, 435–442 (2021).

[41] S. Chinvorarat, B. Watjatrakul, P. Nimdum, T. Sangpet, and P. Valliku, *Water takeoff performance calculation method for amphibious aircraft based on digital virtual flight,* IOP Conference Series: Materials Science and Engineering **1137(1)**, (2021).

[42] K. Mallon, F. Assadian, and B. Fu, *Analysis of on-board photovoltaics for a battery electric bus and their impact on battery lifespan,* Energies 10, 943 (2017).

[43] T. Chang and H. Yu, *Improving electric powered uavs' endurance by incorporating battery dumping concept,* Procedia Engineering 99 (2015), 10.1016/j.proeng.2014.12.522.

[44] *Aircraft floats,* in *Jane's All the World's Aircraft: Development & Production 19/20* (Jane's, United Kingdom, 2020).

[45] A. B. A. Muta'ali, R. E. M. Nasir, W. Wisnoe, and W. Kuntjoro, *Aerodynamic performance of a tailless blended wing-body small transport aircraft,* Journal of Advanced Research in Fluid Mechanics and Thermal Sciences **(66)**, 16 (2020).

[46] O. Gur, W. H. Mason, and J. A. Schetz, *Full-configuration drag estimation,* Journal of Aircraft **47(4)**, 1356 (2010).

[47] B. S. M. Augustine, B. R. Ramesh Bapu, K. V. Narayanan, and S. Kolanjiappan, *Evaluation of aircraft maintainability and aircraft maintenance,* in *Proceedings of International Conference and Exhibition on Emerging Challenges in Design and Manufacturing Technologies (ECHDEM 2007)* (Sathyabama University, Chennai, India, 2007).

[48] *Annual Safety Review 2021*, Tech. Rep. TO-AA-21-001-EN-N (EASA, Köln, Germany, 2021).

[49] C. N. Eastlake and H. W. Blackwell, *Cost estimating software for general aviation aircraft design,* (2002).

[50] *Small Islands ASPIRE Supplement*, PROJECT INFORMATION DOCUMENT 20 (Worldbank, 2015).